

# Improvement of a mobile platform for plant phenotyping

A Thesis Submitted

Submitted to the College of Graduate and Postdoctoral Studies

In Partially Fulfillment of the Requirements

For the Degree of Master of Science

In the Department of Mechanical Engineering

University of Saskatchewan

Saskatoon, Saskatchewan, Canada

By

**Majid Khak Pour**

© Copyright Majid Khak Pour, May, 2020. All rights reserved

## **Permission to use**

In presenting this thesis/dissertation in partial fulfillment of the requirements for a Postgraduate degree from the University of Saskatchewan, I agree that the Libraries of this University may make it freely available for inspection. I further agree that permission for copying of this thesis/dissertation in any manner, in whole or in part, for scholarly purposes may be granted by the professor (Prof. Reza Fotouhi) who supervised my thesis/dissertation work or, in his absence, by the Head of the Department or the Dean of the College in which my thesis work was done. It is understood that any copying or publication or use of this thesis/dissertation or parts thereof for financial gain shall not be allowed without my written permission. It is also understood that due recognition shall be given to me and to the University of Saskatchewan in any scholarly use which may be made of any material in my thesis/dissertation.

Requests for permission to copy or to make other uses of materials in this thesis/dissertation in whole or part should be addressed to:

Head of the Department of Mechanical Engineering  
University of Saskatchewan, College of Engineering  
3B48 Engineering Building, 57 Campus Drive  
Saskatoon, Saskatchewan, S7N 5A9, Canada

OR

Dean  
College of Graduate and Postdoctoral Studies  
University of Saskatchewan  
116 Thorvaldson Building, 110 Science Place  
Saskatoon, Saskatchewan S7N 5C9, Canada



## Abstract

Plant phenotyping refers to monitoring traits (physical characteristics) of plants. Crop scientists/breeders, are interested to find relations between phenotypes and genotypes, which improves yields and ultimately may address issue of food insecurity. Manual measurement currently is the primary method for phenotyping. However, this method has several limitations, including intensive labor requirement and human errors in monitoring. Therefore, a field-based mobile platform for autonomous crop monitoring is considered a better option for crop monitoring.

An intensive literature search was carried out to understand state of development around the globe for different field-based High-Throughput Phenotyping Platforms (HTPP). In this study, existing farm vehicles, such as a Swather and/or a Tractor, were used for carrying a mechanical boom that all of the measuring devices were attached to them.

By selecting and adding other electrical equipment and devices to the existing HTPP, features of plots can be measured to provide necessary information to crop scientists. Targeted traits were selected as plant height, temperature, NDVI (Normalized Difference Vegetation Index), RGB (Red-Green-Blue)/multispectral images, and ambient temperature/humidity.

User-friendly and automated software programs were developed for mapping breeding field, data acquisition, visualization, sorting, and post-processing. In this research MATLAB was used as the main programming language for developing software. Moreover, another programming language (*CRBasic*) was used for data acquisition program.

To validate the effectiveness and reliability of the developed HTPP with new parts and programs, different types of nurseries like canola and wheat, with different numbers of plots were studied. In this way, a valuable phenotypic database was gathered for the crop scientists/breeders. For providing this database standards of the breeding business are followed. Several verification tests were applied to verify the efficiency and accuracy of developed HTPP.

In this study, I contribute mainly in designing and installation of electrical architecture, development of user-friendly and modular software package, evaluating operation of both hardware and software parts, conducting several field tests, analyzing collected data/images and examining reliability and accuracy of developed HTPP.

## Acknowledgements

I would like to express my sincere gratitude to the people who contributed to a successful completion of this work. I would like to acknowledge my supervisor, Prof. Reza Fotouhi, for his continuous advice, support and encouragement throughout this research. My gratitude also goes to my advisory committee, Prof. Chris Zhang and Prof. Anh Dinh, for their valuable suggestions and comments.

I would also like to acknowledge Natural Sciences and Engineering Research Council of Canada (NSERC) for funding this research through The Global Institute for Food Security - Plant Phenotyping and Imaging Research Centre (GIFS-P2IRC) and Cargill Canada Ltd. for providing equipment, test field, and support for performing field tests.

I would like to acknowledge plant scientist's role, Dr. Katy Navabi, Dr. Pierre Hucl, Mr. Karsten Nielsen and Mr. Michael Grieman for their assistance and support. Moreover, I want to thank my colleagues at Robotics laboratory, especially, Dr. Rahim Oraji, Mr. Tyler Zhang, Mr. Mostafa Bayati, Mr. Joshua Cote, Mr. Mohammad Amir Khozeimeh, Miss. Hedieh Badkoobehhezaveh, Mr. Keegan Wegner, Mr. Haoyu Wu, Mr. Colbly Neald and Mr. Toyin Famure, for their continues help during this project.

Lastly, lots of thanks to all the department technicians, office support staff, other graduate students and especially my very supportive friends for their support.

# Table of Contents

Permission to use .....	i
Acknowledgements .....	iii
Abstract .....	ii
Table of Contents .....	iv
List of Figures .....	x
List of Tables .....	xxiii
List of Abbreviations .....	xxvi
List of Symbols .....	xxviii
CHAPTER 1- Introduction .....	1
1.1. Motivation .....	1
1.2. Background .....	1
1.3. Research objectives and scopes.....	3
1.4. Methodology .....	4
1.5. Different plant phenotyping systems (Literature review) .....	4
1.6. Outline of the Thesis .....	9
CHAPTER 2- Infrastructure of the platform .....	10
2.1. Introduction .....	10
2.2. Canopy's height measurement methods.....	10
2.2.1. Height measurement method for 2018 data collections .....	13
2.2.2. Height measurement method for 2019 data collections .....	17
2.3. Canopy's temperature measurement methods.....	20
2.3.1. Plant's temperature measurement system used .....	22
2.4. Ambient temperature and humidity measurements.....	25
2.4.1. The ambient and humidity measurement methods used.....	26

2.5. The NDVI measurement methods.....	27
2.5.1. The NDVI measurement method used .....	29
2.6. RGB Image acquisition system .....	34
2.7. GPS setup used.....	37
2.8. Data storage system.....	40
2.9. The hardware system for HTTP .....	42
2.10. Summary .....	44
CHAPTER 3- Software developed for the platform.....	45
3.1. Introduction .....	45
3.2. Mapping programs .....	46
3.2.1. Mapping program- Version 2018 .....	47
3.2.2. Mapping program- Version 2019 .....	49
3.3. Data acquisition program .....	52
3.4. Image acquisition programs .....	55
3.4.1. Image acquisition program for RGB camera.....	55
3.4.2. Image acquisition program for multispectral camera .....	59
3.5. Multispectral images post processing program .....	61
3.6. Data visualization programs.....	64
3.6.1. Data visualization program- Version 2018.....	66
3.6.2. Data visualization program- Version 2019.....	69
3.7. Sorting program for data and images .....	71
3.8. Summary .....	74
CHAPTER 4- Experimental results .....	75
4.1. Introduction .....	75
4.2. Monitored Canola fields.....	75

4.2.1. Analyzing growth of plots for canola field in 2018.....	77
4.2.2. Analyzing growth of plots for canola field in 2019.....	85
4.3. Monitored Wheat fields.....	89
4.3.1. Analyzing growth of plots for wheat field in 2018 .....	91
4.3.2. Analyzing growth of plots for wheat field in 2019 .....	94
4.4. Mapping programs’ performance.....	98
4.4.1. Performance of mapping program-version 2018.....	98
4.4.2. Performance of mapping program-version 2019 (Pheno-VISDM3).....	100
4.5. Verifying geo-referencing reliability for canola and wheat fields .....	103
4.6. Comparing manual and ultrasonic height measurements.....	105
4.7. Comparing manual and IRT measurements.....	111
4.8. Comparing weather stations (HTPP vs. Local).....	118
4.9. Comparing Crop Circle and multispectral camera.....	122
4.10. Summary .....	126
CHAPTER 5- Conclusions and future works .....	127
5.1. Conclusions .....	127
5.2. Future works.....	128
References.....	131
APENDIX A- Datasheets of utilized equipment .....	135
A1- Honeywell Ultrasonic Distance Sensor (943-F4Y-2D-1D0-180E) [26] .....	135
A2- Sick Ultrasonic Sensor (UM30-21_113)[27] .....	138
A3- Apogee SI-131 IR Thermometer[28] .....	140
A4- Visala HMP60 Temperature and Relative Humidity Probe[29] .....	142
A5- Crop Circle Sensor ACS-430 [31] .....	144
A6- Campbell Scientific CR3000 Data Logger [39].....	145

APPENDIX B- The source code to find correlation of a point 2 according to the latitude and longitude of point 1 .....	148
APPENDIX C- Manuals for the developed programs.....	149
C1- Manual for the using mapping module of Pheno-VISDM3 .....	149
C2- Manual for the using Data Logger .....	149
C3- Manual for the using data visualization program-Version 2018.....	149
C4- Manual for the using data visualization program-Version 2019.....	149
C5- Manual for the using data and image sorting of Pheno-VISDM3.....	149
APPENDIX D- The location of studied nurseries .....	150
APPENDIX E- Summary of conducted field trials .....	152
E1- Preparation and test dates for the studied canola field on 2018 .....	152
E2- Preparation and test dates for the studied canola field on 2019 .....	153
E3- Preparation and test dates for the studied wheat field on 2018 .....	154
E4- Preparation and test dates for the studied wheat field on 2019 .....	155
APPENDIX F- Analyzing growth of canola plots over summer 2018.....	156
F1. Analyzing growth of the plot #11.12 (Selected randomly from HP7 genotype) .....	156
F1.1. Summary of captured data for plot # 11.12 during summer 2018 .....	157
F2. Analyzing growth of the plot #9.18 (Selected randomly from HP5 genotype) .....	159
F2.1. Summary of captured data for plot # 9.18 during summer 2018 .....	160
F3. Analyzing growth of the plot #17.46(Selected randomly from HA2 rep1 genotype) .....	162
F3.1. Summary of captured data for plot # 17.46 during summer 2018 .....	163
F4. Analyzing growth of the plot #14.44 (Selected randomly from HA2 rep2 genotype) .....	165
F4.1. Summary of captured data for plot # 14.44 during summer 2018 .....	166
F5. Analyzing growth of the plot #30.77 (Selected randomly from TC8 genotype) .....	168
F5.1. Summary of captured data for plot # 30.77 during summer 2018 .....	170

APPENDIX G- Analyzing growth of canola plots over summer 2019 .....	172
G1. Analyzing growth of the plot #3.7 (Selected randomly from HA01 genotype).....	172
G1.1. Summary of captured data for plot # 3.7 during summer 2019 .....	174
G2. Analyzing the growth of plot #7.20 (Selected randomly from HA02 genotype).....	176
G2.1. Summary of captured data for plot # 7.20 during summer 2019 .....	178
G3. Analyzing the growth of the plot #10.3 (Selected randomly from HA03 genotype) .....	180
G3.1. Summary of captured data for plot # 10.3 during summer 2019 .....	182
G4. Analyzing the growth of the plot #14.30 (Selected randomly from PR-RST genotype) .	184
G4.1. Summary of captured data for plot # 14.30 during summer 2019 .....	186
G5. Analyzing the growth of the plot #16.2 (Selected randomly from PR-RST Extra) .....	188
G5.1. Summary of captured data for plot # 16.2 during summer 2019 .....	190
G6. Analyzing the growth of the plot #18.18 (Selected randomly from IM-RST genotype) .	192
G6.1. Summary of captured data for plot # 16.2 during summer 2019 .....	194
APPENDIX H- Analyzing growth of wheat plots over summer 2018 .....	196
H1. Analyzing growth of the plot #108 (Selected randomly from genotype 18).....	196
H1.1. Summary of captured data for plot # 108 during summer 2018 .....	198
H2. Analyzing growth of the plot #112 (Selected randomly from genotype 8).....	199
H2.1. Summary of captured data for plot # 112 during summer 2018 .....	201
H3. Analyzing growth of the plot #175 (Selected randomly from genotype 45).....	203
H3.1. Summary of captured data for plot # 175 during summer 2018 .....	205
H4. Analyzing growth of the plot #260 (Selected randomly from genotype 31).....	206
H4.1. Summary of captured data for plot # 260 during summer 2018 .....	208
H5. Analyzing growth of the plot #333 (Selected randomly from genotype 51).....	210
H5. Summary of captured data for plot # 333 during summer 2018 .....	212
H6. Analyzing growth of the plot #373 (Selected randomly from genotype 72).....	213

H6.1. Summary of captured data for plot # 373 during summer 2018 .....	215
APPENDIX I- Analyzing growth of wheat plots over summer 2019 .....	217
I1. Analyzing growth of the plot #104 (Selected randomly from genotype 44) .....	217
I1.1. Summary of captured data for plot # 104 during summer 2019 .....	219
I2. Analyzing growth of the plot #169 (Selected randomly from genotype 63) .....	220
I2.1. Summary of captured data for plot # 169 during summer 2019 .....	222
I3. Analyzing growth of the plot #225 (Selected randomly from genotype 81) .....	224
I3.1. Summary of captured data for plot # 225 during summer 2019 .....	226
I4. Analyzing growth of the plot #264 (Selected randomly from genotype 11) .....	227
I4.1. Summary of captured data for plot # 264 during summer 2019 .....	229
I5. Analyzing growth of the plot #321 (Selected randomly from genotype 27) .....	231
I5. Summary of captured data for plot # 325 during summer 2019 .....	233
I6. Analyzing growth of the plot #376 (Selected randomly from genotype 3) .....	234
I6.1. Summary of captured data for plot # 376 during summer 2019 .....	236



## List of Figures

Figure 1- 1: The schematic view of fields and phenotyping platform (HTPP) .....	3
Figure 1- 2: A field-based-high-throughput plant phenotyping platform with foldable boom developed by U of S [25] .....	8
Figure 2- 1: The schematic of a plot (green rectangular) and sensor's measurements (red dots). 10	
Figure 2- 2: The schematic of laser sensor for distance measurement .....	11
Figure 2- 3: The schematic of ultrasonic sensor for distance measurement .....	12
Figure 2- 4: Ultrasonic sensor's calibration graph .....	14
Figure 2- 5: Honeywell ultrasonic sensor (model: 943-F4Y-2D-1D0-180E) and its wiring.....	15
Figure 2- 6: Sick ultrasonic sensor (model: UM30-214113) and its wiring .....	16
Figure 2- 7: The schematic of mechanical boom with four ultrasonic sensors (US) for 2018 data collections .....	17
Figure 2- 8: Utilized ultrasonic sensors (US) on the developed HTPP for canola data collections during 2018 .....	17
Figure 2- 9: height measurement based on measuring distance (2019 season) .....	18
Figure 2- 10: The schematic of mechanical boom with five Ultrasonic Sensors (US) for 2019 data collections .....	19
Figure 2- 11: Utilized ultrasonic sensors (US) on the developed HTPP for wheat data collections during 2019 .....	19
Figure 2- 12: The schematic of contact temperature measurement sensor .....	20
Figure 2- 13: A portable thermal camera for taking thermal images from plants .....	21
Figure 2- 14: A sample thermal image from a plant and different random point's temperature... 21	
Figure 2- 15: The schematic of non-contact IRT sensor for temperature measurement .....	22
Figure 2- 16: Apogee IRT sensor (model: SI-131).....	23
Figure 2- 17: Internal circuit diagram of IRT .....	24
Figure 2- 18: The schematic of mechanical boom with two Inferred Thermometer sensors (IRT) for 2018-2019 data collections.....	25
Figure 2- 19: Utilized Inferred Thermometer sensors (IRT) on the developed HTPP for canola data collections during 2018-2019 .....	25
Figure 2- 20: Temperature and relative humidity probe with 6 plate solar radiation shield and its wire function .....	26

Figure 2- 21: The schematic of mechanical boom with an ambient temperature/humidity sensor for 2018-2019 data collections.....	27
Figure 2- 22: Utilized ambient temperature/humidity sensor on the developed HTPP for wheat data collections during 2018-2019 .....	27
Figure 2- 23: Linear relationship between the NDVI equations (-1 to 1 and 0 to 1 ranges) .....	29
Figure 2- 24: Utilized Crop Circle sensor (a) and its wirings (b) .....	30
Figure 2- 25: Utilized multispectral camera .....	30
Figure 2- 26: An example of multispectral image with four bands .....	31
Figure 2- 27: Calculating projected area of multispectral camera and crop circle sensor .....	32
Figure 2- 28: The schematic of mechanical boom with two multispectral cameras and two Crop Circle sensors for 2018-2019 data collections .....	33
Figure 2- 29: Utilized devices on the developed HTPP for canola data collections to measure NDVI value of crops during 2018-2019 .....	33
Figure 2- 30: Selected cameras a) Logitech C920, b) Logitech BRIO, and c) Canon 70D.....	34
Figure 2- 31: The setup for testing camera's operation.....	34
Figure 2- 32: Test images captured by two webcams a) Logitech C920 and b) Logitech BRIO .	35
Figure 2- 33: Image histogram for the captured images by Logitech a) C920 and b) BRIO ) .....	36
Figure 2- 34: Utilized cameras on the developed HTPP for the wheat data collections to take RGB images from crops during 2018-2019 .....	37
Figure 2- 35: Existed GPS receiver on the developed HTPP for a) wheat and b) canola data collections during 2018- 2019 .....	38
Figure 2- 36: Top view of the platform, which shows GPS antenna and sensors' location .....	40
Figure 2- 37: Utilized Data Logger and its wirings .....	41
Figure 2- 38: LoggerNet program to communicate with utilized Data Logger.....	41
Figure 2- 39: System's hardware part for 2018 data collections with four ultrasonic sensors, two IRTs, ambient temperature and humidity sensor, two Crop Circle sensors and two BRIO webcams .....	42
Figure 2- 40: System's hardware part for 2019 data collections with five ultrasonic sensors, two IRTs, ambient temperature and humidity sensor, two Crop Circle sensors, two BRIO webcams and two multispectral cameras.....	43

Figure 2- 41: Mounted boom on a Swather and wired with devices for canola data collections a) transportation and b) expanded mode .....	43
Figure 2- 42: Mounted boom on a Tractor and wired with devices for wheat data collections a) transportation and b) expanded mode .....	44
Figure 3- 1: Using GPS receiver to find correlation of unknown point.....	47
Figure 3- 2: Using interpolation to find center of plots from information of the first plot.....	47
Figure 3- 3: A screenshot from part of the generated Excel sheet for plots' center information .	48
Figure 3- 4: A schematic of plot and its four corners .....	48
Figure 3- 5: The flowchart of loading field's map (version 2018) .....	49
Figure 3- 6: Calculating the location of all plots using a starting point to create a map for the studied field .....	50
Figure 3- 7: Mapping module of PHENO-VISDM3 .....	51
Figure 3- 8: Calculator module of Pheno-VISDM3 .....	51
Figure 3- 9: Data acquisition system consists of Data Logger, GPS receiver for geo-tagging, five ultrasonic sensors for height measurement, two IRT for temperature measurement, two Crop Circle sensors for NDVI measurement, and a weather station sensor for measuring ambient temperature/humidity .....	52
Figure 3- 10: Utilizing CRBasic Editor for programming Data Logger by using LoggerNet.....	53
Figure 3- 11: The flowchart for the data acquisition program.....	53
Figure 3- 12: The structure of Excel database to store phenotypic data.....	54
Figure 3- 13: Image acquisition system consists of laptop, GPS receiver for geo-tagging, two webcam for capturing RGB images and two multispectral camera for capturing multispectral images .....	55
Figure 3- 14: The developed GUI for image acquisition program for RGB cameras .....	56
Figure 3- 15: Automatic pause of image acquisition program during the data collection.....	57
Figure 3- 16: The flowchart of developed image acquisition program for RGB cameras .....	58
Figure 3- 17: The developed GUI for image acquisition program for multispectral cameras.....	59
Figure 3- 18: The flowchart of developed image acquisition program for multispectral camera	60
Figure 3- 19: A multispectral image with four bands as 1) 580, 2) 660, 3) 735, and 4) 820 nm .	61
Figure 3- 20: The developed GUI for multispectral image's post-processing program.....	62

Figure 3- 21: Sample of extracted NDVI information via multispectral image's post processing program a) modified multispectral image of 4 bands b) histogram of NDVI pixels c) gray NDVI image d) color NDVI image e) detailed information of NDVI image.....	63
Figure 3- 22: The flowchart of developed multispectral image's post-processing program.....	64
Figure 3- 23: A screenshot of a sample phenotypic database.....	65
Figure 3- 24: Distances of devices in the developed HTTP.....	66
Figure 3- 25: The developed GUI for data visualization program- Version 2018.....	67
Figure 3- 26: Monitoring five sample data points via data visualization program-Version 2018 a) Height b) Temperature c) NDVI d) Boom's height and ambient temperature/humidity e) RGB image.....	67
Figure 3- 27: Flowchart of different functions of developed data visualization program-Version 2018 a) Visualizing collected data b) Visualizing captured images c) Monitoring an available data point d) Monitoring an available image.....	68
Figure 3- 28: The developed GUI for data visualization module of Pheno-VISDM3.....	69
Figure 3- 29: Monitoring four sample data points via developed GUI for data visualization module of Pheno-VISDM3 a) Height b) Temperature c) NDVI d) RGB image.....	70
Figure 3- 30: A screen of generated Excel sheets for a) NDVI b) temperature c) height measurements via the developed data/image sorting module of Pheno-VISDM3 .....	72
Figure 3- 31: A screen of generated images' folders via the developed data/image sorting module of Pheno-VISDM3 .....	73
Figure 3- 32: The sorting data and images window of developed GUI for data and image sorting module of Pheno-VISDM3 .....	73
Figure 4- 1: Dimensions of canola plots on a) 2018 b) 2019 fields.....	76
Figure 4- 2: Studied canola field on 2018 with canola plots and winter canola between them....	77
Figure 4- 3: Plot #30.77 on a) June 19, 2018 (Seedling Status) b) June 29, 2018 (Flowering Status) c) July 18, 2018 (End of Flowering Status) d) August 14, 2018 (Before Harvest Status) .....	79
Figure 4- 4: Variation of NDVI, height, temperature, ambient temperature and humidity of plot #30.77 during summer 2018 .....	80
Figure 4- 5: Kilograms of harvest per hectare variation of different genotypes.....	81
Figure 4- 6: Comparison different genotype's NDVI during different stages .....	81
Figure 4- 7: Comparison different genotype's height during different stages .....	82

Figure 4- 8: Comparison different genotype's temperature during different stages .....	82
Figure 4- 9: Comparison different genotype's images during different stages .....	83
Figure 4- 10: Distribution of NDVI values with considering about edge-effect for around 3000 plots observed on a) June 19 b) June 29 c) July 18 d) August 2 e) August 14.....	84
Figure 4- 11: Average NDVI variation in the entire studied population with considering edge-effect .....	85
Figure 4- 12: Comparison different genotype's temperature during different stages .....	86
Figure 4- 13: Comparison different genotype's NDVI during different stages .....	87
Figure 4- 14: Comparison different genotype's height during different stages .....	87
Figure 4- 15: Comparison different genotype's images during different stages .....	88
Figure 4- 16: Distribution of NDVI values with considering about edge-effect for around 400 plots observed on a) June 26 b) July 11 c) July 31 d) August 15 e) August 28 .....	89
Figure 4- 17: The map of studied wheat field on 2018.....	90
Figure 4- 18: The map of studied wheat field on 2019.....	90
Figure 4- 19: Dimensions of wheat plots on 2018 and 2019 fields .....	91
Figure 4- 20: Comparison different genotype's temperature during different stages .....	92
Figure 4- 21: Comparison different genotype's NDVI during different stages .....	93
Figure 4- 22: Comparison different genotype's height during different stages .....	93
Figure 4- 23: Distribution of NDVI values with considering about edge-effect for around 270 plots observed on a) June 26 b) July 11 c) July 31 d) August 15 e) August 28 .....	94
Figure 4- 24: Comparison different genotype's temperature during different stages .....	95
Figure 4- 25: Comparison different genotype's height during different stages .....	96
Figure 4- 26: Comparison different genotype's NDVI during different stages .....	96
Figure 4- 27: Comparison different genotype's images during different stages .....	97
Figure 4- 28: Distribution of NDVI values for 243 plots observed on a) July 23 b) August 11 c) August 20 d) September 17.....	98
Figure 4- 29: Mapped and loaded map file of studied canola field on 2018 through mapping program- version 2018.....	99
Figure 4- 30: Mapped and loaded map of studied wheat field on 2018 through mapping program- version 2018.....	99

Figure 4- 31: Mapped and loaded map of studied wheat field on 2019 through mapping program-version 2019.....	100
Figure 4- 32: Mapped and loaded map of studied canola field on 2019 through mapping program-version 2019.....	101
Figure 4- 33: A screen shot of generated draft map of studied canola field on 2019 through data mapping module of Pheno-VISDM3 a) based on plot 1.1 b) based on plot 37.38 c) comparing generated maps.....	102
Figure 4- 34: An example of utilized physical signs next to individual plots to verify the accuracy of geo-referencing.....	103
Figure 4- 35: Verifying the accuracy of the geo-referencing using Pheno-VISDM2.....	104
Figure 4- 36: Verifying the accuracy of the geo-referencing using Pheno-VISDM3.....	104
Figure 4- 37: Manual height measurement .....	105
Figure 4- 38: Comparison between manual and ultrasonic sensor's height measurements of different canola plots (with considering edge-effects) on July 31, 2019 .....	107
Figure 4- 39: The spectrum of the correlation coefficient (-1 to +1).....	107
Figure 4- 40: Scatter diagrams (including regression line) between manual and a) average b) maximum ultrasonic height measurements of different canola plots on July 31, 2019.....	109
Figure 4- 41: The height of boom during collecting data from entire and part of the field on August 15, 2019.....	110
Figure 4- 42: Manual temperature measurement by portable a) hand held thermometer b) thermal camera .....	111
Figure 4- 43 Comparison between manual (hand held thermometer) and IR sensor temperature measurements of different canola plot (with considering edge-effects) on August 2, 2018: .....	113
Figure 4- 44: Scatter diagram (including regression line) between hand held thermometer and IRT sensor's temperature measurements of different canola plots on August 2, 2018.....	114
Figure 4- 45: A sample thermal image from a plant and selected different points for reading temperature from thermal camera .....	114
Figure 4- 46: Comparison between the thermal image and IRT sensor temperature measurements of different random canola plots on July 11, 2019 .....	115
Figure 4- 47: Differences between the thermal image and IRT sensor temperature measurements of different random canola plots on July 11, 2019 .....	115

Figure 4- 48: Scatter diagram (including regression line) between TIC and IRT sensor's temperature measurements of different canola plots on July 11, 2019.....	117
Figure 4- 49: HTPP's weather station for canola data collections .....	119
Figure 4- 50: local weather station in the side on 2018 data collections .....	119
Figure 4- 51: Comparison between local and HTPP's weather station measurements for temperature during different times on July 18, 2018.....	120
Figure 4- 52: Comparison between local and HTPP's weather station measurements for humidity during different times on July 18, 2018 .....	120
Figure 4- 53: Scatter diagram (including regression line) between temperature records of local and HTPP's weather station on July 18, 2018.....	121
Figure 4- 54: Scatter diagram (including regression line) between humidity records of local and HTPP's weather station on July 18, 2018.....	121
Figure 4- 55: Extracted NDVI information via multispectral image's post processing program for canola plot #14.30 on July 31, 2019 a) NDVI values within two ranges b) histogram of NDVI pixels c) gray NDVI image d) color NDVI image e) detailed information of NDVI image .....	124
Figure 5- 1: Schematic of a) 5-DOF robot arm b) mounted manipulator to the vehicle .....	129
Figure 5- 2: Examples of captured RGB images that were affected with mechanical boom's shade .....	129
Figure A- 1: Technical information of Honeywell Ultrasonic Distance Sensor.....	135
Figure A- 2: Detection range of Honeywell Ultrasonic Distance Sensor .....	136
Figure A- 3: Dimensions of Honeywell Ultrasonic Distance Sensor .....	136
Figure A- 4: Wiring of Honeywell Ultrasonic Distance Sensor .....	136
Figure A- 5: Tech in procedure of Honeywell Ultrasonic Distance Sensor .....	137
Figure A- 6: Dimensions of Sick Ultrasonic Sensor.....	138
Figure A- 7: Connection type and diagram of Sick Ultrasonic Sensor.....	138
Figure A- 8: Detailed technical information for Sick Ultrasonic Sensor.....	139
Figure A- 9: Detection area of Sick Ultrasonic Sensor.....	140
Figure A- 10: Dimensions of Apogee SI-131 IR Thermometer .....	140
Figure A- 11: Apogee IRT sensor wiring diagram .....	141
Figure A- 12: Spectral response of Apogee SI-131 IR Thermometer .....	141
Figure A- 13: Detailed technical information for Apogee SI-131 IR Thermometer .....	142

Figure A- 14: Exploded view of HMP60 Temperature and Relative Humidity Probe .....	142
Figure A- 15: Dimensions of HMP60 Temperature and Relative Humidity Probe .....	143
Figure A- 16: Detailed technical information of HMP60 Temperature and Relative Humidity Probe .....	143
Figure A- 17: Wiring of HMP60 Temperature and Relative Humidity Probe .....	144
Figure A- 18: Technical information for Crop Circle Sensor ACS-430.....	144
Figure A- 19: Schematic of grounds for Campbell Scientific CR3000 Data Logger .....	145
Figure A- 20: Analog sensor wired to single-ended channel.....	146
Figure A- 21: Analog sensor wired to differential channel .....	146
Figure A- 22: Use of digital I/O and RS-232 when reading RS-232 devices.....	146
Figure A- 23: Pinouts diagram for Campbell Scientific CR3000 Data Logger.....	147
Figure D- 1: Location of studied canola field on 2018 data collections.....	150
Figure D- 2: Location of studied canola field on 2019 data collections.....	150
Figure D- 3: Location of studied wheat fields on 2018 and 2019 data collections .....	151
Figure F- 1: Plot #11.12 on June 19, 2018 (Seedling Status) .....	156
Figure F- 2: Plot #11.12 on June 29, 2018 (Flowering Status).....	156
Figure F- 3: Plot #11.12 on July 18, 2018 (End of Flowering Status).....	157
Figure F- 4: Variation of NDVI, height, temperature, ambient temperature and humidity of plot #11.12 during summer 2018 .....	158
Figure F- 5: Plot #9.18 on June 19, 2018 (Seedling Status) .....	159
Figure F- 6: Plot #9.18 on June 29, 2018 (Flowering Status).....	159
Figure F- 7: Plot #9.18 on July 18 (End of Flowering Status).....	160
Figure F- 8: Variation of NDVI, height, temperature, ambient temperature and humidity of plot #9.18 during summer 2018 .....	161
Figure F- 9: Plot #17.46 on June 19, 2018 (Seedling Status) .....	162
Figure F- 10: Plot #17.46 on June 29, 2018 (Flowering Status).....	162
Figure F- 11: Plot #17.46 on July 18, 2018 (End of Flowering Status).....	163
Figure F- 12: Variation of NDVI, height, temperature, ambient temperature and humidity of plot #17.46 during summer 2018 .....	164
Figure F- 13: Plot #14.44 on June 19, 2018(Seedling Status) .....	165
Figure F- 14: Plot #14.44 on June 29, 2018 (Flowering Status).....	165



Figure F- 15: Plot #14.44 on July 18, 2018 (End of Flowering Status).....	166
Figure F- 16: Variation of NDVI, height, temperature, ambient temperature and humidity of plot #14.44 during summer 2018 .....	167
Figure F- 17: Plot #30.77 on June 19, 2018 (Seedling Status) .....	168
Figure F- 18: Plot #30.77 on June 29, 2018 (Flowering Status).....	168
Figure F- 19: Plot #30.77 on July 18, 2018 (End of Flowering Status).....	169
Figure F- 20: Plot #30.77 on July 18, 2018 (End of Flowering Status).....	169
Figure F- 21: Variation of NDVI, height, temperature, ambient temperature and humidity of plot #30.77 during summer 2018 .....	170
Figure G- 1: Plot #3.7 on June 26, 2019 (Seedling Status) .....	172
Figure G- 2: Plot #3.7 on July 11, 2019 (Start of Flowering Status).....	172
Figure G- 3: Plot #3.7 on July 31, 2019 (End of Flowering Status).....	173
Figure G- 4: Plot #3.7 on August 15, 2019 (Start of Maturity Status) .....	173
Figure G- 5: Plot #3.7 on August 28, 2019 (End of Maturity Status) .....	174
Figure G- 6: Variation of NDVI, height, temperature, ambient temperature and humidity of plot #3.7 during summer 2019 .....	175
Figure G- 7: Plot #7.20 on June 26, 2019 (Seedling Status) .....	176
Figure G- 8: Plot #7.20 on July 11, 2019 (Start of Flowering Status).....	176
Figure G- 9: Plot #7.20 on July 31, 2019 (End of Flowering Status).....	177
Figure G- 10: Plot #7.20 on August 15, 2019 (Start of Maturity Status) .....	177
Figure G- 11: Plot #7.20 on August 28, 2019 (End of Maturity Status).....	178
Figure G- 12: Variation of NDVI, height, temperature, ambient temperature and humidity of plot #7.20 during summer 2019 .....	179
Figure G- 13: Plot #10.3 on June 26, 2019 (Seedling Status) .....	180
Figure G- 14: Plot #10.3 on July 11, 2019 (Start of Flowering Status).....	180
Figure G- 15: Plot #10.3 on July 31, 2019 (End of Flowering Status).....	181
Figure G- 16: Plot #10.3 on August 15, 2019 (Start of Maturity Status) .....	181
Figure G- 17: Plot #10.3 on August 28, 2019 (End of Maturity Status).....	182
Figure G- 18: Variation of NDVI, height, temperature, ambient temperature and humidity of plot #10.3 during summer 2019 .....	183
Figure G- 19: Plot #14.30 on June 26, 2019 (Seedling Status).....	184

Figure G- 20: Plot #14.30 on July 11, 2019 (Start of Flowering Status).....	184
Figure G- 21: Plot #14.30 on July 31, 2019 (End of Flowering Status).....	185
Figure G- 22: Plot #14.30 on August 15, 2019 (Start of Maturity Status) .....	185
Figure G- 23: Plot #14.30 on August 28, 2019 (End of Maturity Status).....	186
Figure G- 24: Variation of NDVI, height, temperature, ambient temperature and humidity of plot #14.30 during summer 2019 .....	187
Figure G- 25: Plot #16.2 on June 26, 2019 (Seedling Status) .....	188
Figure G- 26: Plot #16.2 on July 11, 2019 (Start of Flowering Status).....	188
Figure G- 27: Plot #16.2 on July 31, 2019 (End of Flowering Status).....	189
Figure G- 28: Plot #16.2 on August 15, 2019 (Start of Maturity Status) .....	189
Figure G- 29: Plot #16.2 on August 28, 2019 (End of Maturity Status).....	190
Figure G- 30: Variation of NDVI, height, temperature, ambient temperature and humidity of plot #16.2 during summer .....	191
Figure G- 31: Plot #18.18 on June 26, 2019 (Seedling Status).....	192
Figure G- 32: Plot #18.18 on July 11, 2019 (Start of Flowering Status).....	192
Figure G- 33: Plot #18.18 on July 31, 2019 (End of Flowering Status).....	193
Figure G- 34: Plot #18.18 on August 15, 2019 (Start of Maturity Status) .....	193
Figure G- 35: Plot #18.18 on August 28, 2019 (End of Maturity Status).....	194
Figure G- 36: Variation of NDVI, height, temperature, ambient temperature and humidity of plot #18.18 during summer 2019 .....	195
Figure H- 1: Plot #108 on July 13, 2018 (Flowering Status).....	196
Figure H- 2: Plot #108 on July 26, 2018 (End of Flowering Status).....	196
Figure H- 3: Plot #108 on August 9, 2018 (Before Maturity Status) .....	197
Figure H- 4: Plot #108 on August 23, 2018 (Before Harvest Status).....	197
Figure H- 5: Variation of NDVI, height, temperature, ambient temperature and humidity of plot #108 during summer of 2018.....	198
Figure H- 6: Plot #112 on July 13, 2018 (Flowering Status).....	199
Figure H- 7: Plot #112 on July 26, 2018 (End of Flowering Status).....	200
Figure H- 8: Plot #112 on August 9, 2018 (Before Maturity Status) .....	200
Figure H- 9: Plot #112 on August 2018 (Before Harvest Status).....	201

Figure H- 10: Variation of NDVI, height, temperature, ambient temperature and humidity of plot #112 during summer of 2018.....	202
Figure H- 11: Plot #175 on July 13, 2018 (Flowering Status).....	203
Figure H- 12: Plot #175 on July 26, 2018 (End of Flowering Status).....	203
Figure H- 13: Plot #175 on August 9, 2018 (Before Maturity Status).....	204
Figure H- 14: Plot #175 on August 23, 2018 (Before Harvest Status).....	204
Figure H- 15: Variation of NDVI, height, temperature, ambient temperature and humidity of plot #175 during summer of 2018.....	206
Figure H- 16: Plot #260 on July 13, 2018 (Flowering Status).....	206
Figure H- 17: Plot #260 on July 26, 2018 (End of Flowering Status).....	207
Figure H- 18: Plot #260 on August 9, 2018 (Before Maturity Status) .....	207
Figure H- 19: Plot #260 on August 23, 2018 (Before Harvest Status).....	208
Figure H- 20: Variation of NDVI, height, temperature, ambient temperature and humidity of plot #260 during summer of 2018.....	209
Figure H- 21: Plot #333 on July 13, 2018 (Flowering Status).....	210
Figure H- 22: Plot #333 on July 26, 2018 (End of Flowering Status).....	210
Figure H- 23: Plot #333 on August 9, 2018 (Before Maturity Status) .....	211
Figure H- 24: Plot #333 on August 23, 2018 (Before Harvest Status).....	211
Figure H- 25: Variation of NDVI, height, temperature, ambient temperature and humidity of plot #333 during summer of 2018.....	212
Figure H- 26: Plot #373 on July 13, 2018 (Flowering Status).....	213
Figure H- 27: Plot #373 on July 26, 2018 (End of Flowering Status).....	214
Figure H- 28: Plot #373 on August 9, 2018 (Before Maturity Status) .....	214
Figure H- 29: Plot #373 on August 23, 2018 (Before Harvest Status).....	215
Figure H- 30: Variation of NDVI, height, temperature, ambient temperature and humidity of plot #373 during summer of 2018.....	216
Figure I- 1: Plot #104 on July 23, 2019 (Flowering Status) .....	217
Figure I- 2: Plot #104 on August 1, 2019 (End of Flowering Status).....	217
Figure I- 3: Plot #104 on August 20, 2019 (Before Maturity).....	218
Figure I- 4: Plot #104 on September 17, 2019 (Before Harvest Status).....	218

Figure I- 5: Variation of NDVI, height, temperature, ambient temperature and humidity of plot #104 during summer of 2019 .....	219
Figure I- 6: Plot #169 on July 23, 2019 (Flowering Status) .....	220
Figure I- 7: Plot #169 on August 1, 2019 (End of Flowering Status).....	221
Figure I- 8: Plot #169 on August 20, 2019 (Before Maturity).....	221
Figure I- 9: Plot #169 on September 17, 2019 (Before Harvest Status) .....	222
Figure I- 10: Variation of NDVI, height, temperature, ambient temperature and humidity of plot #169 during summer of 2019.....	223
Figure I- 11: Plot #225 on July 23, 2019 (Flowering Status) .....	224
Figure I- 12: Plot #225 on August 1, 2019 (End of Flowering Status).....	224
Figure I- 13: Plot #225 on August 20, 2019 (Before Maturity).....	225
Figure I- 14: Plot #225 on September 17, 2019 (Before Harvest Status) .....	225
Figure I- 15: Variation of NDVI, height, temperature, ambient temperature and humidity of plot #225 during summer of 2019 .....	226
Figure I- 16: Plot #264 on July 23, 2019 (Flowering Status) .....	227
Figure I- 17: Plot #264 on August 1, 2019 (End of Flowering Status).....	228
Figure I- 18: Plot #264 on August 20, 2019 (Before Maturity).....	228
Figure I- 19: Plot #264 on September 17, 2019 (Before Harvest Status) .....	229
Figure I- 20: Variation of NDVI, height, temperature, ambient temperature and humidity of plot #264 during summer of 2019 .....	230
Figure I- 21: Plot #321 on July 23, 2019 (Flowering Status) .....	231
Figure I- 22: Plot #321 on August 1, 2019 (End of Flowering Status).....	231
Figure I- 23: Plot #321 on August 20, 2019 (Before Maturity).....	232
Figure I- 24: Plot #321 on September 17, 2019 (Before Harvest Status) .....	232
Figure I- 25: Variation of NDVI, height, temperature, ambient temperature and humidity of plot #321 during summer of 2019.....	233
Figure I- 26: Plot #376 on July 23, 2019 (Flowering Status) .....	234
Figure I- 27: Plot #376 on August 1, 2019 (End of Flowering Status).....	235
Figure I- 28: Plot #376 on August 20, 2019 (Before Maturity).....	235
Figure I- 29: Plot #376 on September 17, 2019 (Before Harvest Status) .....	236

Figure I- 30: Variation of NDVI, height, temperature, ambient temperature and humidity of plot #376 during summer of 2019 .....	237
---	-----

## List of Tables

Table 2- 1: Comparison between laser and ultrasonic sensors .....	13
Table 2- 2: Collected data for calibration of ultrasonic sensor for measuring distance .....	14
Table 2- 3: Collected data for calibration of ultrasonic sensor for measuring height.....	14
Table 2- 4: Comparison between Honeywell and Sick ultrasonic sensor.....	16
Table 2- 5: Comparison of Crop Circle and multispectral camera specifications .....	32
Table 3- 1: Spent time for saving RGB images with different resolutions and formats.....	57
Table 3- 2: Comparison between the operation of developed image acquisition program for RGB images with and without auto-pause option for the entire studied wheat field .....	58
Table 4- 1: Stages of data collection on canola 2018 field .....	78
Table 4- 2: Variation of NDVI, height, temperature, ambient temperature and humidity of plot #30.77 during summer 2018 .....	79
Table 4- 3: Stages of data collection on canola 2019 field .....	85
Table 4- 4: Stages of data collection on wheat 2018 field.....	92
Table 4- 5: Stages of data collection on wheat 2019 field.....	95
Table 4- 6: Comparison between manual and ultrasonic sensor's height measurements of different canola plot (with considering edge-effects) on July 31, 2019 .....	106
Table 4- 7: Summary of correlation values between manual and ultrasonic measurements .....	108
Table 4- 8: Comparison between manual (hand held thermometer) and IRT sensor temperature measurements of different canola plot (with considering edge-effects) on August 2, 2018 .....	112
Table 4- 9: Comparison between the thermal image and IR sensor temperature measurements of different random plots on July 11, 2019 .....	116
Table 4- 10: Summary of correlation values between manual and IRT measurements .....	118
Table 4- 11: Comparison between Cargill and HTPP's weather station measurements during different times on July 18, 2018 .....	119
Table 4- 12: Sorted NDVI data for plot #14.30 on July 31, 2019 .....	122
Table 4- 13: Comparison between Crop Circle and Multispectral camera's NDVI measurements of different canola plot on 2019.....	125
Table 4- 14: Advantages and disadvantages of NDVI measurement devices .....	125

Table E- 1: List of conducted field trials during 2018 growing season on canola field .....	152
Table E- 2: List of conducted field trials during 2019 growing season on canola field .....	153
Table E- 3: List of conducted field trials during 2018 growing season on wheat field .....	154
Table E- 4: List of conducted field trials during 2019 growing season on wheat field .....	155
Table F- 1: Variation of NDVI, height, temperature, ambient temperature and humidity of plot #11.12 during summer 2018 .....	157
Table F- 2: Variation of NDVI, height, temperature, ambient temperature and humidity of plot #9.18 during summer 2018 .....	160
Table F- 3: Variation of NDVI, height, temperature, ambient temperature and humidity of plot #17.46 during summer 2018 .....	163
Table F- 4: Variation of NDVI, height, temperature, ambient temperature and humidity of plot #14.44 during summer 2018 .....	166
Table F- 5: Variation of NDVI, height, temperature, ambient temperature and humidity of plot #30.77 during summer 2018 .....	171
Table G- 1: Variation of NDVI, height, temperature, ambient temperature and humidity of plot #3.7 during summer 2019 .....	174
Table G- 2: Variation of NDVI, height, temperature, ambient temperature and humidity of plot #7.20 during summer 2019 .....	178
Table G- 3: Variation of NDVI, height, temperature, ambient temperature and humidity of plot #10.3 during summer 2019 .....	182
Table G- 4: Variation of NDVI, height, temperature, ambient temperature and humidity of plot #14.30 during summer 2019 .....	186
Table G- 5: Variation of NDVI, height, temperature, ambient temperature and humidity of plot #16.2 during summer 2019 .....	190
Table G- 6: Variation of NDVI, height, temperature, ambient temperature and humidity of plot #18.18 during summer 2019 .....	194
Table H- 1: Variation of NDVI, height, temperature, ambient temperature and humidity of plot #108 during summer of 2018 .....	199
Table H- 2: Variation of NDVI, height, temperature, ambient temperature and humidity of plot #112 during summer of 2018 .....	201

Table H- 3: Variation of NDVI, height, temperature, ambient temperature and humidity of plot #175 during summer of 2018.....	206
Table H- 4: Variation of NDVI, height, temperature, ambient temperature and humidity of plot #260 during summer of 2018.....	208
Table H- 5: Variation of NDVI, height, temperature, ambient temperature and humidity of plot #333 during summer of 2018.....	213
Table H- 6: Variation of NDVI, height, temperature, ambient temperature and humidity of plot #373 during summer of 2018.....	215
Table I- 1: Variation of NDVI, height, temperature, ambient temperature and humidity of plot #104 during summer of 2019.....	220
Table I- 2: Variation of NDVI, height, temperature, ambient temperature and humidity of plot #169 during summer of 2019.....	222
Table I- 3: Variation of NDVI, height, temperature, ambient temperature and humidity of plot #225 during summer of 2019.....	227
Table I- 4: Variation of NDVI, height, temperature, ambient temperature and humidity of plot #264 during summer of 2019.....	229
Table I- 5: Variation of NDVI, height, temperature, ambient temperature and humidity of plot #321 during summer of 2019.....	234
Table I- 6: Variation of NDVI, height, temperature, ambient temperature and humidity of plot #376 during summer of 2019.....	236



## List of Abbreviations

<b><i>BpS</i></b>	Bits per Second
<b><i>CC</i></b>	Crop Circle
<b><i>CCD</i></b>	Charge-coupled Device
<b><i>CO<sub>2</sub></i></b>	Carbon Dioxide
<b><i>COM</i></b>	Component Object Model
<b><i>DOF</i></b>	Degree of Freedom
<b><i>DSLR</i></b>	Digital Single –Lens Reflex
<b><i>FOV</i></b>	Field of View
<b><i>GND</i></b>	Ground
<b><i>GNSS</i></b>	Global Navigation Satellite System
<b><i>GPS</i></b>	Global Positioning System
<b><i>GUI</i></b>	Graphical User Interface
<b><i>HTP</i></b>	High Throughput Phenotyping
<b><i>HTPP</i></b>	High-Throughput Phenotyping Platform
<b><i>IRT</i></b>	Infra-Red Thermometer
<b><i>JPG</i></b>	Joint Photographic Graphics
<b><i>LED</i></b>	Light-emitting Diode
<b><i>LiDAR</i></b>	Light Detection and Ranging
<b><i>MFA</i></b>	Multispectral Filter Array
<b><i>MpH</i></b>	Miles per Hour
<b><i>NDVI</i></b>	Normalized Difference Vegetation Index
<b><i>NDYI</i></b>	Normalized Difference Yellow Index
<b><i>NIR</i></b>	Near Infrared
<b><i>NMEA</i></b>	National Marine Electronics Association
<b><i>PNG</i></b>	Portable Network Graphics
<b><i>RE</i></b>	Red Edge
<b><i>RGB</i></b>	Red-Green-Blue
<b><i>RMC</i></b>	Recommended Minimum Sentence C
<b><i>RTK</i></b>	Real-Time Kinematic

<b><i>RTX</i></b>	Real-Time Extended
<b><i>STD</i></b>	Standard Deviation
<b><i>TIC</i></b>	Thermal Imaging Camera
<b><i>US</i></b>	Ultrasonic Sensor
<b><i>UTC</i></b>	Coordinated Universal Time

## List of Symbols

$d$	Distance between the tip of sensor and object
$h$	Height of objects
$R$	Earth's radius
$S$	Traveling speed of sound
$x$	Width of canopy plot
$y$	Length of canopy plot
$v$	Vehicle's speed
$t_{US}$	Traveling time of ultrasonic waves
$X_{US}$	Output of ultrasonic sensor
$Y_{us}$	Distance between the object and sensor
$R_T$	Resistance of the thermistor
$V_{EX}$	Excitation voltage
$V_{OUT}$	Output voltage
$T_k$	Temperature (Kelvin)
$T_c$	Temperature (Celsius)
$T_T$	Target Temperature
$S_D$	Millivolt signal of the detector of Inferred Thermometer
$T_D$	Detector temperature of Inferred Thermometer
$e$	Vapor pressure
$e_s$	Saturation vapor pressure
$\theta$	Vehicle's heading angle
$\beta$	Angular FOV of device
$lat$	Latitude value
$lon$	Longitude value
$Lat_{DD}$	Latitude value in decimal degrees format
$Lon_{DD}$	Longitude value in decimal degrees format
$Lat_{DM}$	Latitude value in degrees minute format
$Lon_{DM}$	Longitude value in degrees minute format
$X_s$	Data sampled per plot

$h_m$ ,	Manual height
$h_u$	Ultrasonic height
$r$	Correlation value
$T_c$	Recorded ambient temperature with Cargill weather station
$H_c$	Recorded ambient humidity with Cargill weather station
$T_p$	Recorded ambient temperature with HTPP weather station
$H_p$	Recorded ambient humidity with HTPP weather station

# CHAPTER 1- Introduction

## 1.1. Motivation

It has been predicted that humanity will need more demand for food and resources in the future. More than 820 million people in the world were suffering hunger in 2018, which is mostly rising in African sub regions, Latin America and Western Asia [1]. This situation can get worse in the coming years. It is clear that not only available resources should be managed for future but also the quality and quantity of food productions should be increased.

Improving breeding techniques is the most important task to prepare enough food resources for next generation. Therefore, crop-breeding should be closely influenced by genetic analysis of plants. Thus, it must be an interaction between crop-breeders and experts who use phenotyping to monitor different features of plants. This way, breeders will be able to improve crop production industry and support more production [2–4]. Genotyping nowadays is fully implemented. However, phenotyping needs more improvements to provide sufficient information about plants. As an example, measuring characteristics of crops such as plant's height, temperature, and vegetation indices are challenging and time consuming. To test different genotypes, breeders should grow crops in large scale fields, where collecting and analyzing of their phenotypic data without any damage to crops is labor-intensive.

Engineers from different areas like mechanical engineering, electrical engineering, and computer scientists are trying to make progress and improvement in the phenotyping research. The major and important efforts that they can do is designing and developing HTP (High Throughput Phenotyping) system by using specific devices [5-6]. HTP platforms have advantages like increasing the accuracy and amount of data, decreasing data collection time and costs for phenotyping. Therefore, it can be said that by using proper HTP, useful and valuable information can be prepared for the breeders by further analyzing of collected data. In next sections, different concepts of this study will be discussed.

## 1.2. Background

Plant phenotyping platforms can be classified as:

- Indoor vs. field-based platforms

- Stationary vs. Mobile platforms
- Destructive vs. non-destructive platforms
- Low-throughput vs. high-throughput platforms
- Aerial vs. Ground-based platforms

In this research project, data collections for actual fields with outdoor configurations was considered. As long as mobile platforms work faster than stationary ones and stationary platforms have fixed structure [7], preference is to use mobile platforms. Moreover, the plan was monitoring canopies during their different stages of growth without damaging them[8]. That's why, non-destructive platforms should be selected, too. By using high-throughput systems, many parameters and characteristics of plants can be measured and stored at the same time, which can prepare more valuable information for breeders [9]. For example canopy's temperature can be compared with the ambient temperature and humidity by using two different sensors in the proposed platform. In addition, aerial platforms are not applicable for large-scale fields because of their batteries' restrictions [5]. Also, they are not able to carry more sensors and instruments [10]. Because of all mentioned reasons, in this study, focus was on field-based, mobile, non-destructive, high-throughput and ground based platforms.

A developed HTPP (High-Throughput Phenotyping Platform) consists of different devices and programs. Most of existing platforms are designed and developed for specific type of plants [11-13]. A new HTPP was developed to be able to monitor different types of plants like canola, wheat or others (i.e. lentils). Furthermore, it is anticipated that the developed HTPP work semi-autonomously for large-scale fields where data collection and labor force is unbearable. Existing farm vehicles, such as a Swather and a Tractor, were used for carrying a mechanical boom that all of the measuring devices were attached to it. Figure 1-1 shows the schematic view of fields and developed HTPP during the data collection. Each side of mechanical boom, which was attached to the farm vehicle has the same sensors. Therefore, proper amount of data could be collected during the data collection (by travelling through the paths).

Several programs were developed for different phases such as data collection, visualization (post-processing) and sorting. The programs work autonomously, feasibly and reliably with an acceptable level of error.

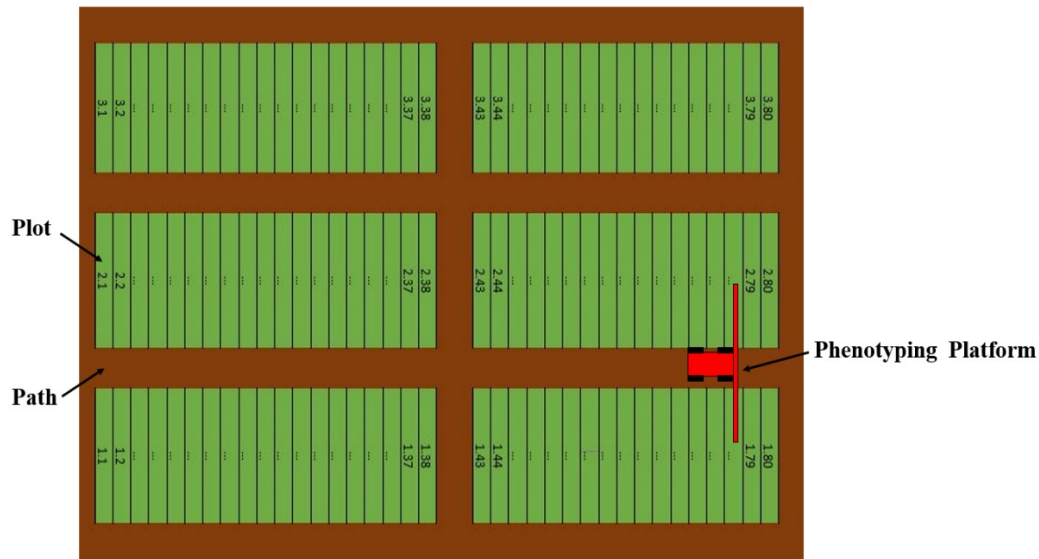


*Figure 1- 1: The schematic view of fields and phenotyping platform (HTPP)*

Further analyzes of collected data by breeders, provide valuable information to find correlation between genotypes and phenotypes, and increased the crops yields.

### 1.3. Research objectives and scopes

The aim of this research is to exploit the automation technologies to record different physical features of a plant. There are five sub objectives of this study as follows:

a) How a field can be mapped?

Each nursery has comprised from rows of plots and we should find their coordination to map them. But, we should find a procedure for this process when the number of plots are more, like 3000.

b) What kind of measurement system (hardware part) do we need for data collection?

By identifying, the demands of an effective field-based plant phenotyping platform and adding electrical equipment and devices to the existing platform features of plots can be measured to prepare more information.

c) Can we develop programs (software part) for data collection and post-processing?

A user-friendly software should be developed for the different phases of this study, which are data/image acquisition, field mapping, data/image visualization, sorting and post processing.

d) Are collected data and images reliable and valuable?

By finding and using different verification strategies, we should verify the efficiency and accuracy of the developed plant phenotyping platform.

e) Can we study the growth of different types of nurseries?

To validate the effectiveness of the developed HTPP with new parts and the software package, different types of nurseries like canola and wheat, with different genotypes and number of plots are going to be analyzed during the plant growth season.

## **1.4. Methodology**

In this research, there were many steps for developing and testing the proposed field-based HTPP platform to study canola and wheat nurseries. To begin with, several meetings and field visits were done by farm technical experts, breeders from industrial partners, Cargill Canada and University of Saskatchewan's plant science department, to define critical needs of breeders and their challenges in the area of plant phenotyping. Based on these issues and by considering the advantages and disadvantages of previous plant phenotyping platforms, new draft model of system was designed and developed. Set of new equipment, which are useful for our research area, was found and purchased from different companies.

Two platforms were developed for monitoring canola (using in Cargill fields) and wheat (using U of S Kernen research farm). For data collection and analysis of the collected data and pictures, several software were developed in house. Developed field-based HTPP were used for several fields with different number of plots (medium, large and mega size fields) and gens in their different stages of growth in Saskatoon, Canada.

Different sources of error were found, and they were eliminated during the data collections. New equipment was added to the HTP and related programs were improved, gradually. Further analysis of collected data prepared a valuable information about each gen in their different stages of growth, which is demand of breeders and agronomist.

## **1.5. Different plant phenotyping systems (Literature review)**

In this section, existing literature on ground-based plant phenotyping platforms are discussed. Some reference publications are going to be introduced for better understanding of the plant phenotyping research and its importance.

Different approaches of genotyping and plant phenotyping firstly have been discussed in [2][13][14]. In addition, the importance of plant phenotyping has been clarified. By using of plant phenotyping, breeders become able to improve agriculture industry and support future agricultural production.



In [15] the genetic basis of complex traits have been considered by relating it to plant phenotyping. Authors are focused on spectral reflectance of crops and Near-infrared spectroscopy on agricultural harvesters. It has been discussed that related sensors can be classified as active and passive. Passive sensor is almost influenced by the environment and it can measure wide spectral range with high spectral resolutions. However, active sensor is the one that is independent from environment conditions and it can measure few wavelengths. It was achieved that using active sensors is more proper for the area of plant phenotyping. Because the data collection can be done in every time of day.

Phenoscope is a HTPP for indoor applications [13]. This platform is equipped with a zenithal imaging system and makes watering automatically. As a result, the expansion rate and plant's different stages during its growth can be analyzed by using captured images. Moreover, breeders can control different condition to recognize stronger genotype.

In [16] two common and contemporary 2D laser scanners, which are low cost, are used to give 3D structure of plants for indoor setting. 2D laser scanners are attached to the dynamic system and by movement of this system a full 3D representation of each row of plants, which represents their structural details.

In [17] an automated high throughput imaging system is developed for indoor setting at the University of Nebraska-Lincoln. This system is able to demonstrate characteristic feature of plant such as growth, water use and leaf water content under two different water treatments. The platform has cameras that they can take RGB pictures and these pictures can be used for estimating projected plant area. In addition, hyperspectral pictures are used to extract plant's leaf structure. Furthermore, information such as plant's fresh weight, dry weight and leaf area can be extracted from the collected data.

Phenocart is a platform that is developed and deployed in the elite wheat field [18]. It is a portable and hand-held phenotyping platform that has a GreenSeeker sensor, an infrared thermometer and a GPS receiver for measuring spectral reflectance (NDVI index), canopy's temperature and geo-tagging collected data, respectively. Also, it is equipped with a webcam to take RGB image of the crops. The data collection is stored in a laptop and are extracted by LabView software.

An autonomous vehicle that equipped with cameras is proposed in [19] for weed detection. All of its four wheels are steered for the orientation and movement. The developed platform is equipped with a GPS receiver that has around 2 cm accuracy, and a gyroscope for measuring vehicle's heading. The position and location of platform can be determined by use of utilized encoders, magnetometer, gyroscope and GPS receiver. The platform is controlled by computer through a wireless communication channel.

The proposed HTPP in [20] is developed for the purpose of measuring spectral and geometric characteristics of canopy plants such as vegetation indices and canopy texture. This platform has a box that is equipped with a CCD (Charge-coupled Device) camera and a LED (Light-emitting Diode) panel that produces nine spectral wavelengths. To take a picture, the box should covers target plant. The purpose of using this box is eliminating sunlight and shutting out wind to have accurate images. By analyzing collected images via developed software, vegetation coverage and NDVI index can be extracted.

A high-throughput plant phenotyping platform which is non-destructive is proposed in [21]. This platform is based on light curtain sensor and spectral reflectance sensor that are mounted on a Tractor. By using of this platform, biomass determination can be compared and combination impact of the calibration data sets can be measured. Moreover, repeatability of biomass determination can be determined.

In [22] a new platform is proposed for measuring height, temperature and data fusion of plots. Crop's physical features like their height and temperature are measured by using ultrasonic sensor and infrared thermometers. Information such as canopy growth, plant structure and the physiological status such as biomass, tissue chlorophyll content and water status or chlorophyll fluorescence can be drawn by using hyperspectral data that comes from the passive bidirectional reflectance sensor system. It was shown that analyzes of collected data from different phase of plant's growth can improve yield models.

Phenobot 1.0 is a ground based, auto steered and self-propelled field based high-throughput phenotyping platform that is developed in [9]. Phenobot 1.0 is designed for tall and densely planted crop species. The developed platform has RGB cameras that are positioned laterally and vertically. This structure of the cameras provides 3D feature of the plants to measure height and stem's

diameter. As some plants are somehow tall, an extension rig was used for capturing the top section of the canopy.

In [23] a field-based, high-throughput phenotyping platform has been developed that is able to measure temperature, height and greenness of plots. The process of measuring these features is achieved by use of two infrared thermometers, one ultrasonic sensor, one Crop Circle and one Green Seeker crop sensing system. The Greenseeker measures NDVI (Normalized Difference Vegetation Index) and Crop Circle calculates and records other vegetative indices. Another sensor that works independently in this platform is laser sensor that measures the height of the mechanical boom from ground. All sensor's output data are geo-tagged by using of two RTK GPS receiver. It is notable that, in this paper it has been showed that the ambient light and temperature can have significant effect on the result's accuracy.

Another multi-sensor platform for high throughput plant phenotyping is proposed in [24]. The platform has 5 pieces as its hardware part: ultrasonic sensor for height measurement, thermal infrared radiometer for measuring temperature, NDVI sensor for measuring greenness index of the plant, portable spectrometer for extracting NDVI and red-edge NDVI spectral indices and RGB cameras. The NDVI sensors are passive-type sensor. That is why, these kind of sensors had both up-looking part and down-looking parts to evaluate respectively down-welling solar radiation and upwelling reflected solar radiation .There are two additional sensors for measuring temperature by solar radiation sensor and humidity of the environment by humidity sensor. There is a GPS device in this platform with pass-to-pass accuracy of 20 cm that is used for geo-referencing purposes.

Recently, an affordable field-based-high-throughput plant phenotyping platform for monitoring Canola plants has been developed by our robotic group of Mechanical Engineering Department of the University of Saskatchewan (Figure 1-2) [8]. This platform has several sensors, which are ultrasonic sensor, LiDAR (Light Detection and Ranging), Inferred Thermometer and Crop Circle. They are used for measuring height (ultrasonic sensor and LiDAR) temperature and greenness of plants. In addition, this platform is equipped with RGB and multispectral cameras that can capture several images from each plot and by using the GPS, pictures and sensor's output data are geo-tagged. Different programs are developed for different phases of research (mapping, data collection, monitoring collected data, data sorting). It is mentionable that none of the previous developed platforms that were reviewed here are not commercialized.



*Figure 1- 2: A field-based-high-throughput plant phenotyping platform with foldable boom developed by U of S [25]*

Developed HTPP consists from hardware and software parts and its specifications can be listed as:

- Using existence agricultural vehicles like Tractor and Swather for carrying developed mechanical boom and wired equipment.
- Ability to utilize developed HTPP for phenotyping of different types of crops such as wheat, canola, etc.
- Collecting canopy plant's traits such as their height, temperature, vegetation index (NDVI) and high quality images, simultaneously.
- Utilizing developed software package, which consist of several modules (mapping, data/image acquisition, visualization, and sorting) and is user-friendly.
- Flexibility of hardware and software part for expansion (adding new devices or removing sensors).
- Ability of system to compare crop's temperature with the ambient temperature/humidity on each record.
- Collecting and labeling data and images based on the GPS information and relating it to the plot level.

- Adjustability for the changing the spacing between the sensor sets
- Reliability and high accuracy of geo-tagged and sorted data.
- Performing data collection for different stages of growth without any damages or bad effects on the canopies.
- Ability to adjust mechanical boom's height to increase quality of data collection in different stages of growth.
- Recording data from different parts of a plot (7-8 record for each plot).
- Fast sampling rates for sensors (250 ms) and cameras (500 ms).
- No delay between the devices and GPS string's reading and saving actions.

## **1.6. Outline of the Thesis**

This thesis has five chapters. Current chapter introduced the background, categories and overview of plant phenotyping platforms. This chapter also discussed motivations, objectives, methodology and a literature review. Chapter 2 covers hardware part of the developed HTPP. Different sensors and equipment parts are discussed in detail. Operation of these devices are also explained in detail. Finally, a hardware configuration of the developed HTPP is proposed. Details of developed programs for different devices and phases of data collection and analysis are described in Chapter 3. Several programs for mapping, data acquisition, (RGB and multispectral) image acquisition, data visualization, sorting and post processing are discussed in detail. Chapter 4 investigates experimental field tests that were performed during summer/spring 2018 and 2019. The performance and reliability of developed HTPP were discussed comprehensively. Finally, Chapter 5 brings the main contribution and concludes the thesis. Also, some suggestions for potential future works are made in this chapter.

## CHAPTER 2- Infrastructure of the platform

### 2.1. Introduction

As discussed in Chapter 1, plant phenotyping platform consists of different parts, such as sensors for measuring, collecting and storing physical or chemical features of plants, reliable and fix mechanical structure for carrying related devices, and programs for data collection and post-processing. Also, it was mentioned that one of main objectives of this study is selecting and using proper devices. By using these apparatus, different physical and chemical characteristics of plots can be recorded.

In this chapter, the infrastructure part of developed HTPP is discussed. Different plant and environmental traits were chosen like plant's height, temperature, ambient temperature and humidity, plant's vegetation index (NDVI), RGB image and multispectral image of plant. It should be mentioned that features of different points in each plot, is recorded by the sensors of HTPP. Figure 2-1 illustrates a plot (green rectangular) and sensor's records (red dots) that measured features of canopy in different locations. Therefore, as sensors and devices are measuring part of canopy, collected information is not in the plant level and is in the canopy level. At the end of this chapter, the proposed hardware of the developed system is listed.

### 2.2. Canopy's height measurement methods

One of the essential characteristic of plant for phenotyping is height measurement. There are several methods to measure plant's height. It is clear that most prevalent and common method is manual measurement.



*Figure 2- 1: The schematic of a plot (green rectangular) and sensor's measurements (red dots)*

However, this method has disadvantages such as being uncertain, ineffective and unbearable, especially for large-scale fields. For example, measuring the height of crops in a field with 3000 plots during the summer's hot weather is an issue.

Different devices and sensors exist for measuring height of objects. Most common sensors are laser and ultrasonic sensors. A laser sensor emits a light from the light emitting element in the transmitter as a straight line and receives the reflected light with its light receiving element (Figure 2-2). By analyzing the reflected signal, height of objects or distance between the tip of sensor and object can be calculated. Laser sensors are usually used for small objects and precise positions. On the other hand, FOV (Field of View) of these kinds of sensor is very low. Also, these types of sensors usually are not proper for the outdoor setups. Because they are extremely sensitive to the ambient light.

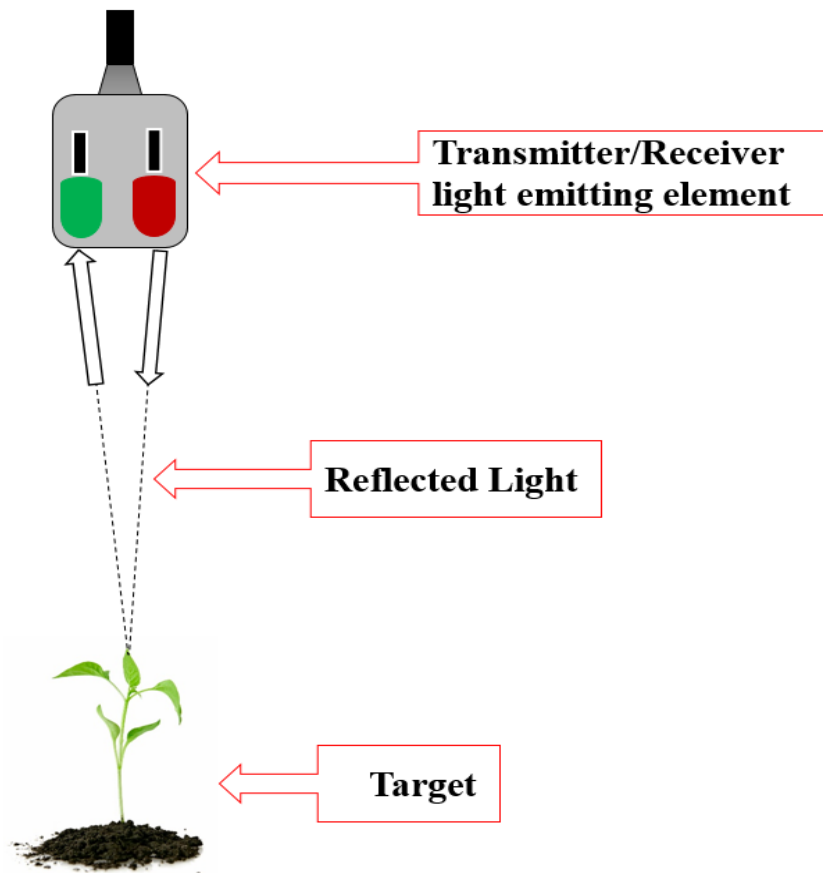


*Figure 2- 2: The schematic of laser sensor for distance measurement*

An ultrasonic sensor is one of the most common sensors for measuring distance of the objects from sensor. This device uses sound waves for the operation. It dispatches sound waves at a specific frequency and listens for that sound wave to bounce back (Figure 2-3). It calculates distance between the sensor and object by using the elapsed time between sound waves' generation and its bouncing back. These kinds of sensors have larger FOV in comparison with the laser sensors. Also, if they are not sensitive to the sunlight, they can be used in the outdoor configurations. It is mentionable that they have less accuracy and slow response speed in comparison to laser sensor. As can be seen in Table 2-1, both laser and ultrasonic sensors have pros and cons.

In this study, FOV of sensor is an important issue. A larger FOV would allow to have reliable and good measurement for a large, uneven surface like crops. Also, as the platform was designing and developing for outdoor configurations, it shouldn't be sensitive to the sunlight. Since, ultrasonic sensor's signal is sound, dust and water do not much effect this sensor's operation. Therefore, ultrasonic sensor was selected for the developed HTPP.

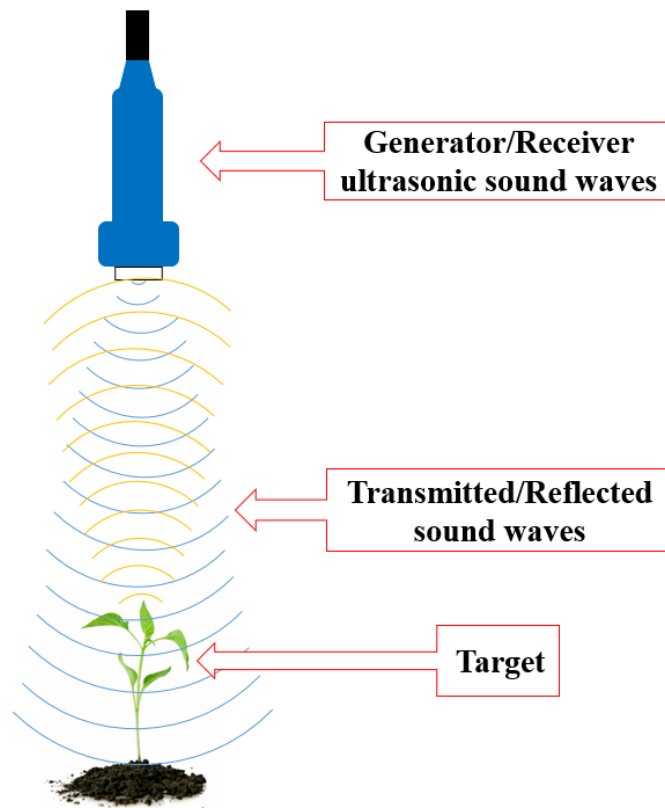


*Figure 2- 3: The schematic of ultrasonic sensor for distance measurement*



Table 2- 1: Comparison between laser and ultrasonic sensors

Criteria	Laser Sensor	Ultrasonic Sensor
FOV	Very low	Large
Signal	Light	Sound
Accuracy	High	Low(for large amount of measurement)
Response speed	Fast	Slow
Dust/water	Affected	Unaffected
Measuring range	Small	Large
Sensitive to	Sunlight	Temperature variations, humidity and ultrasonic noise

### 2.2.1. Height measurement method for 2018 data collections

As discussed, ultrasonic sensor measures distance by sending an ultrasound wave and receiving the reflected wave. The traveling time prepares an information about distance between the sensor and object, as:

$$Y_{US} = \frac{1}{2} (S * t_{US}) \quad (2-1)$$

where  $S$  is the traveling speed of sound ( $\sim 343\text{m/s}$  in dry air  $20^\circ\text{C}$ ),  $t_{US}$  is traveling time and  $y_{US}$  is distance between the object and sensor. The output of sensor ( $X_{US}$ ) is a raw data (current) and relationship between the output of sensor and the distance of the object is linear. Therefore, an equation between the sensor's output and the distance of objects can be modeled by linear regression as:

$$Y_{US} = (A * X_{US}) + B \quad (2-2)$$

Where  $X_{US}$  is current,  $A$  and  $B$  are coefficients that they can be found by measuring at least three different distances and relating them to the corresponding values. Table 2-2 shows an example for calibration. From this table, calibration graph (Figure 2-4) and Eq. 2-3 can be extracted.

$$Y_{US} = (-8.18 * X_{US}) + 187.33 \quad (2-3)$$

Table 2- 2: Collected data for calibration of ultrasonic sensor for measuring distance

R	Current value (mA )	Distance between sensor and object (cm)
1	4.90	147
2	7.82	124
3	8.58	117
4	10.03	105

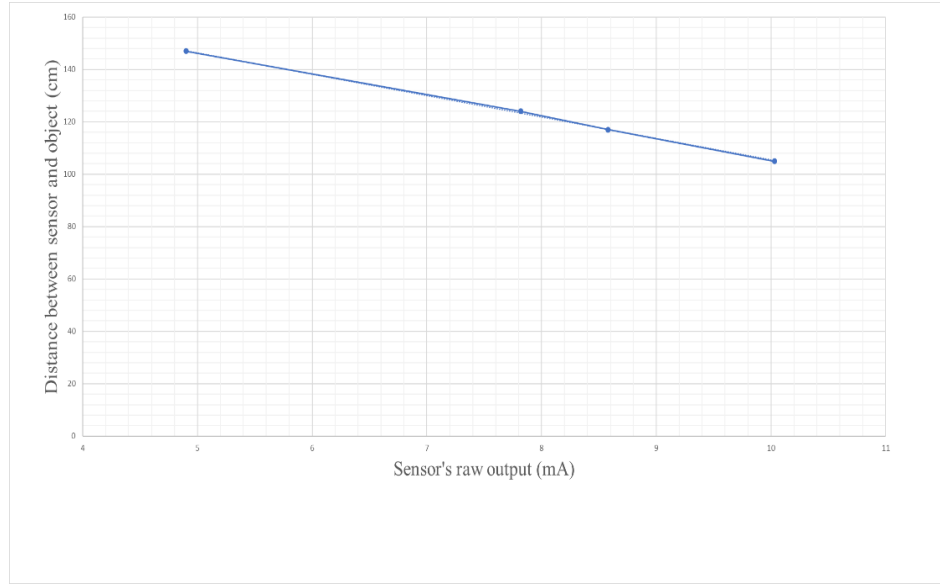


Figure 2- 4: Ultrasonic sensor's calibration graph

There is a fact that if the position of the sensor is fix on the structure, it can be calibrated in the way to measure the height of objects (Table 2-3). In other words, by subtracting the distance between the ground and the tip of the sensor from the distance between top of the crop or object and the tip of sensor, height value ( $h$ ) can be measured. An equation can be extracted from Table 2-3 as:

$$h = (8.18 * X_{US}) - 40.33 \quad (2-4)$$

Table 2- 3: Collected data for calibration of ultrasonic sensor for measuring height

R	Current value (mA )	Height of object (cm)
1	4.90	0
2	7.82	23
3	8.58	30
4	10.03	42

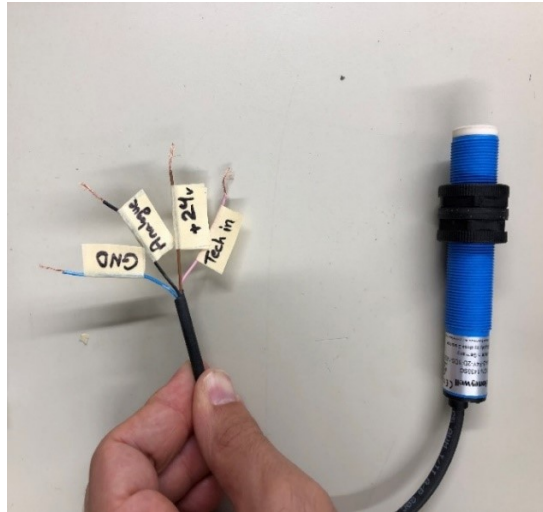


*Figure 2- 5: Honeywell ultrasonic sensor (model: 943-F4Y-2D-1D0-180E) and its wiring*

This approach is useable since the distance between the ground and the tip of the sensor is fixed. In this study, two model of ultrasonic sensor from different manufactures were selected. First, *Honeywell* ultrasonic distance sensor (943-F4Y-2D-1D0-180E) was selected for canopy's height measurement. The full data sheet of this sensor with the process of analogue output adjustment provided in Appendix A [26]. Figure 2-5 illustrates Honeywell ultrasonic sensor and its wiring. Effectivity and reliability of this sensor's performance was tested in the laboratory condition for many objects with different shapes and surfaces at the University of Saskatchewan [25].

*Sick* ultrasonic sensor (UM30-214113) is another sensor that was selected for the developed HTPP. Not only this sensor has its own display for showing distances (Figure 2-6), it has better performance in comparison with Honeywell sensor. The main advantage is that this sensor is faster. The full datasheet of this sensor can be found in Appendix A [27]. Table 2-4 compares two sensors. Ultrasonic frequency for this sensor is 200 kHz and its response time is 180 ms. Also the power supply for this sensor should be 9-30 DC volt. Therefore, this sensor can operate with one 12 DC volt battery. This sensor was tested in laboratory condition for different objects with different heights and surfaces and it has found that this sensor is operating reliably and effectively.



*Figure 2- 6: Sick ultrasonic sensor (model: UM30-214113) and its wiring*

Figure 2-7 illustrates the schematic of mechanical structure with ultrasonic sensors. Each side of mechanical boom was equipped with two ultrasonic sensors that they can measure height of a plant in its different points, simultaneously. Figure 2-8 shows developed HTPP with mechanical boom for canola field and four ultrasonic sensors. It should be mentioned that because the output of each sensor is current, an equation like Eq. 2-2 should be used for each sensor's output value to find the amount of height. This equation's coefficients will change, if the height of mechanical changes. Therefore, the disadvantage of this approach for measuring height of canopies is that sensors should be calibrated each time by changing the height of boom, which is time consuming.

*Table 2- 4: Comparison between Honeywell and Sick ultrasonic sensor*

Technical Data	Honeywell ultrasonic sensor	Sick ultrasonic sensor
Detection range	0.2 to 2 meter	0-5 meter
Response time	250 ms	180 ms
Carrier frequency	180 kHz	120kHz
Reparability	$\pm 0.2\%$	$\pm 0.15\%$
Temperature Range	-15 to 70 °C	-25 to 70 °C
Supply voltage	15 to 30 DC volt	9 to 30 DC volt
Analogue output	0 to 10 volt/4 to 20 mA	0 to 10 volt/4 to 20 mA

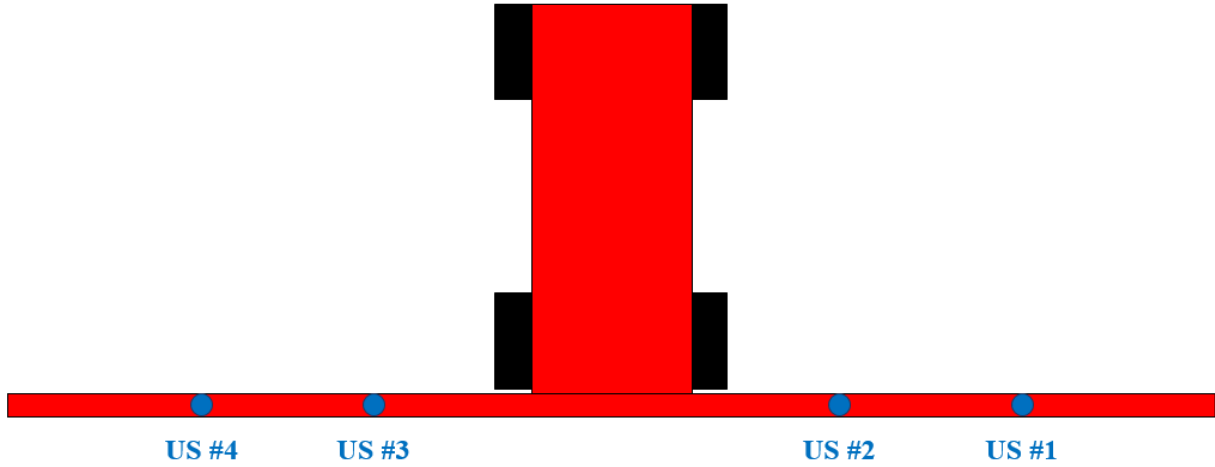


*Figure 2- 7: The schematic of mechanical boom with four ultrasonic sensors (US) for 2018 data collections*

### 2.2.2. Height measurement method for 2019 data collections

There is another approach for the height measurement of crops with ultrasonic sensors without any sensitivity to the variations of mechanical boom's height. In this method, distance measurement is using instead of height measurement. By using, two sensors like Figure 2-9, distance value for each sensor should be measured.  $Y_{US1}$  is distance between the tip of the sensor and ground, and  $Y_{US2}$  is distance between the tip of the sensor and object. These values are measured by using Eq. 2-5 and 2-6.



*Figure 2- 8: Utilized ultrasonic sensors (US) on the developed HTPP for canola data collections during 2018*

$$Y_{US1} = (A_1 * X_{US1}) + B_1 \quad (2-5)$$

$$Y_{US2} = (A_2 * X_{US2}) + B_2 \quad (2-6)$$

where  $X_{US1}$  and  $X_{US2}$  are current values (outputs of sensors),  $A_1$ ,  $A_2$ ,  $B_1$  and  $B_2$  are coefficients that they should be found by measuring the distance values of at least three different objects and relating them to the corresponding values like Table 2-2. The height of object ( $h$ ) is measured by subtracting  $y_2$  from  $y_1$  as:

$$h = Y_{US1} - Y_{US2} = (A_1 * X_{US1}) - (A_2 * X_{US2}) + B_1 - B_2 \quad (2-7)$$

This approach was tested for both model of ultrasonic sensors and it worked properly. Therefore, by adding another ultrasonic sensor to the previous four sensors, and measuring distances, crop's height can be measured without any sensitivity to the boom's height. In other words, by changing the height of boom, height measurement can be performed properly. Figure 2-10 shows the schematic of mechanical structure with five sensors for this approach. Ultrasonic sensors measure the height of canopy by using the following equations:

$$h_1 = Y_{US5} - Y_{US1} \quad (2-8)$$

$$h_2 = Y_{US5} - Y_{US2} \quad (2-9)$$

$$h_3 = Y_{US5} - Y_{US3} \quad (2-10)$$

$$h_4 = Y_{US5} - Y_{US4} \quad (2-11)$$

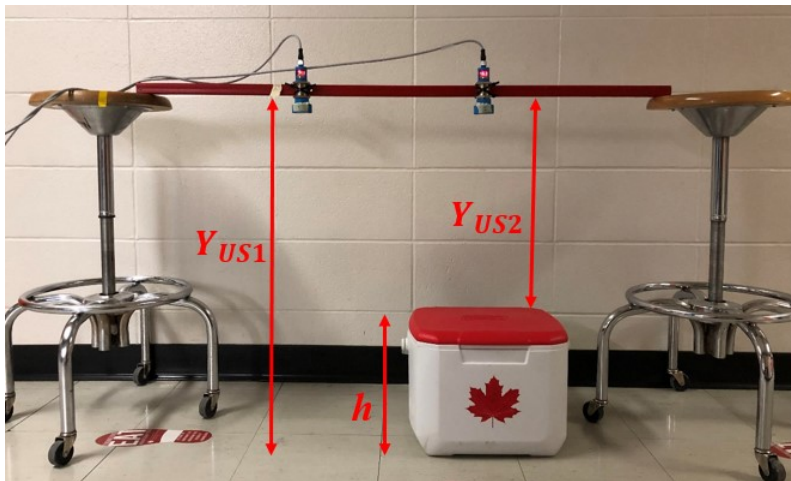
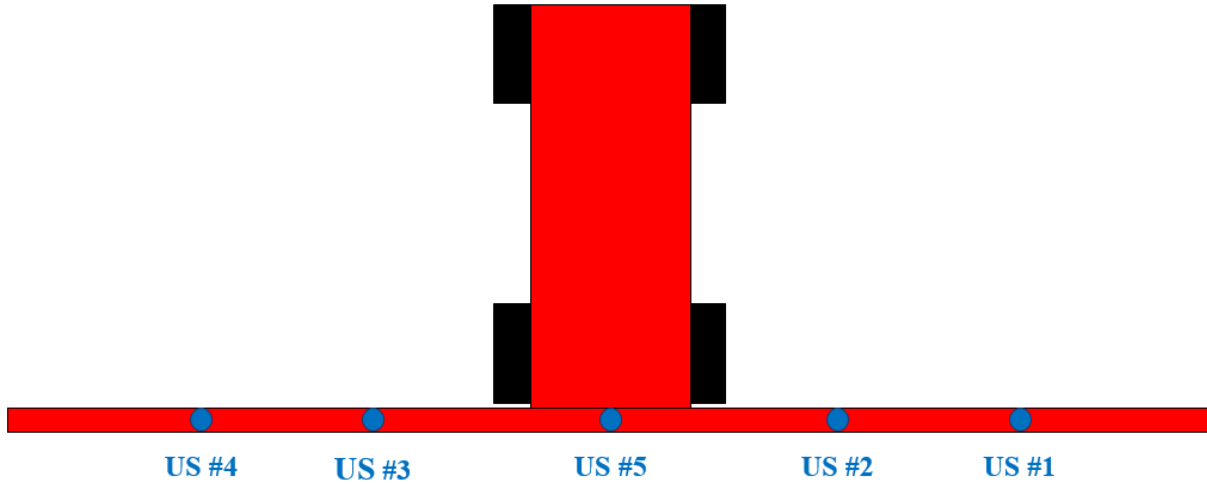


Figure 2- 9: height measurement based on measuring distance (2019 season)



where  $Y_{US1}$ ,  $Y_{US2}$ ,  $Y_{US3}$ ,  $Y_{US4}$  and  $Y_{US5}$  are distance measurements and  $h_1$ ,  $h_2$ ,  $h_3$  and  $h_4$  are measured height values. Figure 2-11 shows the developed HTPP for wheat field with mechanical boom and five sensors.



*Figure 2- 10: The schematic of mechanical boom with five Ultrasonic Sensors (US) for 2019 data collections*



*Figure 2- 11: Utilized ultrasonic sensors (US) on the developed HTPP for wheat data collections during 2019*

## 2.3. Canopy's temperature measurement methods

Plant's temperature is other important parameter in the area of agriculture and plant phenotyping. This trait can provide useful information like plant's water content. By analyzing crop's temperature during its growing season, information like the ability of vegetation to handle heat stress and its need for irrigation can be determined.

Temperature measurement methods can be classified into two main methods as contact and non-contact techniques. In contact method, a temperature sensor should touch plant like Figure 2-12. These kinds of sensors use a probe to display or record their measurements. Although these sensors are usually cheaper, they are not fast enough. Moreover, they should touch part of each plant, which can damage canopy gradually. Therefore, they cannot be proper temperature sensor for field-based mobile HTPPs.

Non-contact method is another main technique for the temperature measurement. This method applies usually for hazardous areas, unreachable objects and dynamic setups. IRT (Infra-Red Thermometer) and TIC (Thermal Imaging Camera) are most common non-contact devices. TIC is a type of thermographic camera that can record thermal image of plants as shown in Figure 2-13. A thermal image prepares information about temperature of different points and operator should extract data from it as illustrated in Figure 2-14. It is mentionable that for the autonomous image acquisition of thermal camera, specific program should be developed.



*Figure 2- 12: The schematic of contact temperature measurement sensor*



IRTs work properly and easily in the outdoor configurations and they are cheaper, more lightweight and reliable. Therefore, in this study for measuring temperature of plants, IRT was selected as the temperature sensor. They can measure and record wheat, canola or other kinds of crops' temperature by using infrared signals (Figure 2-15).



*Figure 2- 13: A portable thermal camera for taking thermal images from plants*

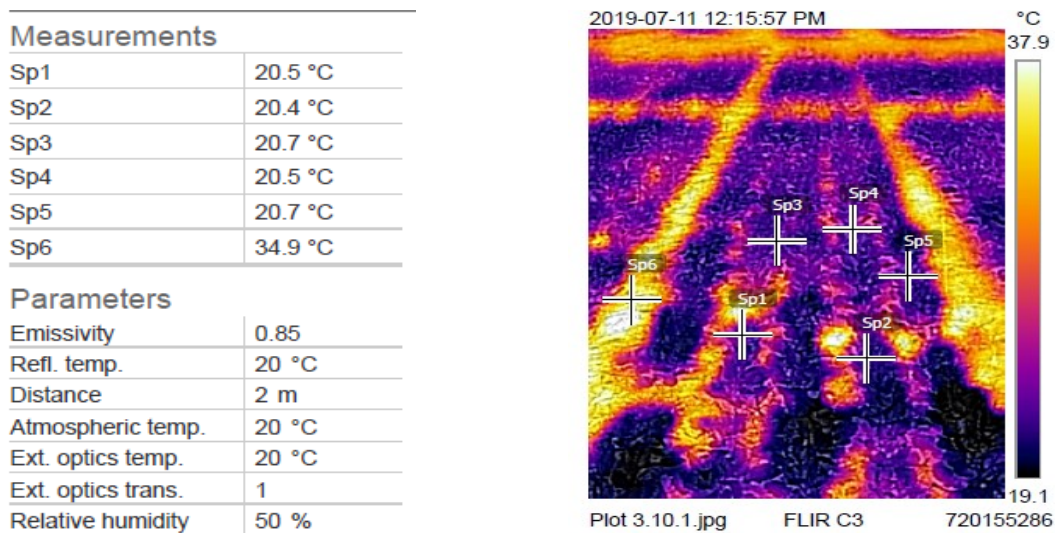


*Figure 2- 14: A sample thermal image from a plant and different random point's temperature*

### 2.3.1. Plant's temperature measurement system used

As discussed IRT sensor can measure temperature of plants without damaging them in the outdoor applications. This sensor does not need any field calibration before start of data collections. The manufacture usually prepares a product-specific parameter calibration for calculating the temperature.

It is considerable fact that in this approach, the temperature of the plants should be measured efficiently. For example, plant's surface temperature should be recorded without any environmental effect like ambient or soil temperature. Therefore, choosing a sensor with a narrower FOV is one of the solutions for this case. For this study, *Apogee (SI-131)* IRT is selected as a sensor for temperature measurement (Figure 2-16). This sensor is not sensitive to water vapor and carbon dioxide (CO<sub>2</sub>). Moreover, this sensor has a proper FOV, which is 14° half angle (Figure 2-15), and provides 20μv per each degree centigrade. The datasheet of this sensor can be found in Appendix A [28].

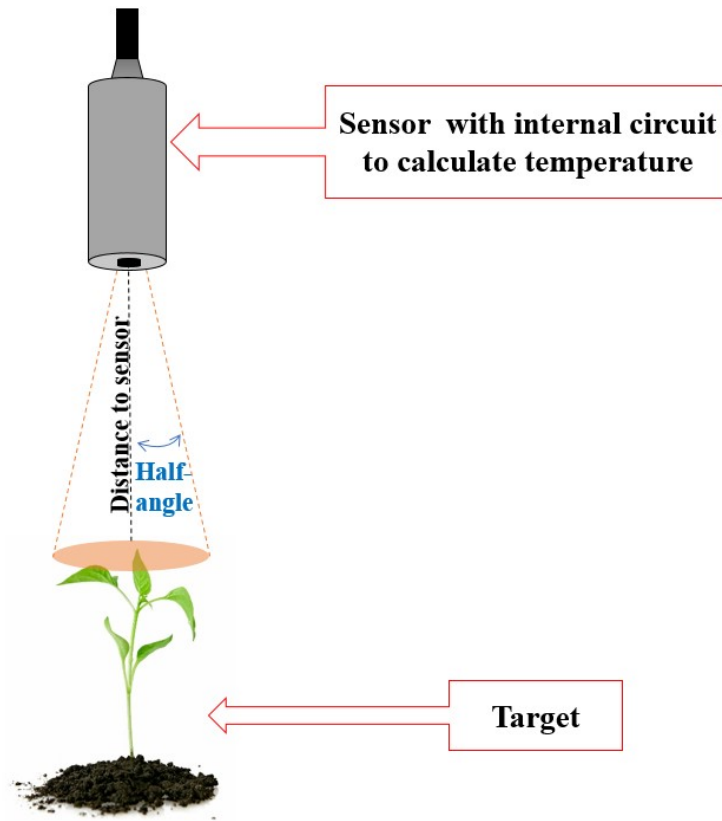


Figure 2- 15: The schematic of non-contact IRT sensor for temperature measurement



*Figure 2- 16: Apogee IRT sensor (model: SI-131)*

An internal circuit in this sensor works as thermistor for measuring temperature as Figure 2-17. An excitation voltage inputs across thermistor. This excitation voltage should be selected in the range to minimize current drain and self-heating. Therefore, 2.5 DC volt is suggested as excitation voltage. Resistance of the thermistor changes with temperature. This resistance value of thermistor is measured through half-bridge measurement as:

$$R_T = 24900 \left( \frac{V_{EX}}{V_{OUT}} - 1 \right) \quad (2-12)$$

Where  $V_{EX}$  is excitation voltage,  $V_{OUT}$  is output voltage and the resistance of the bridge resistor is 24900  $\Omega$ . Temperature should be calculated by using the Steinhart-Hart equation as:

$$T_k = \frac{1}{A + B \ln(R_T) + C (\ln(R_T))^3} \quad (2-13)$$

Where Steinhart-Hart coefficients are  $A=1.129241 \times 10^{-3}$ ,  $B=2.341077 \times 10^{-4}$  and  $C=8.775468 \times 10^{-8}$ . The temperature is measured in Kelvin. To convert it to Celsius following equation should be used.

$$T_c = T_k - 273.15 \quad (2-14)$$

Target temperature can be measured from Stefan-Boltzmann law as:

$$T_T^4 - T_D^4 = m \cdot S_D + b \quad (2-15)$$

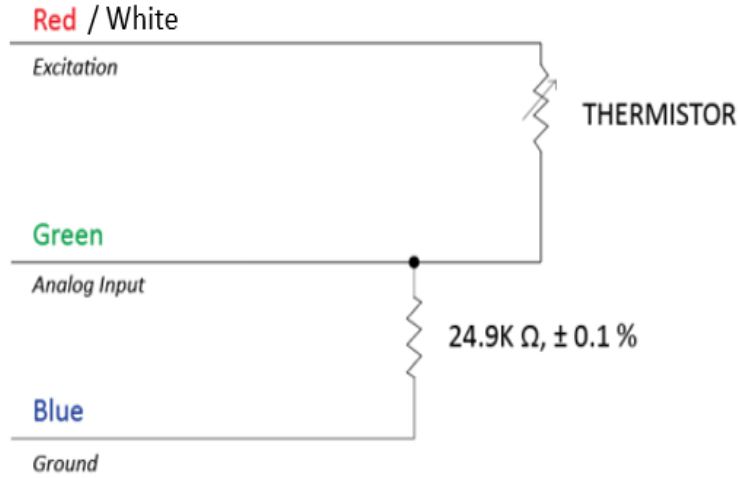


Figure 2- 17: Internal circuit diagram of IRT

Where  $T_T$  is target temperature in Kelvin,  $S_D$  is millivolt signal of the detector and  $T_D$  is detector temperature in Kelvin. For this equation  $m$  is slop and  $b$  is intercept and they can be calculated from following equations:

$$m = C_2 \cdot T_D^2 + C_1 \cdot T_D + C_0. \quad (2-16)$$

$$b = C_2 \cdot T_D^2 + C_1 \cdot T_D + C_0. \quad (2-17)$$

Where  $C_0$ ,  $C_1$  and  $C_2$  are the custom calibration coefficients that are different for each model of IRTs. By using Eq. 2-14 and 2-15, target temperature can be found in degree centigrade as:

$$T_T = (T_D^4 + m \cdot S_D + b)^{\frac{1}{4}} - 273.15 \quad (2-18)$$

Therefore, by using Eq. 2-16 to 2-18 the temperature of plants are measured. Utilized IRT sensor has tested in several ways in the laboratory conditions at University of Saskatchewan and it worked reliably accurate.

After verifying operation of IRT sensors, the mechanical boom was equipped with them. Figure 2-18 illustrates the schematic of mechanical boom with sensors. Each side of the mechanical boom has one IRT sensor to measure the temperature of a canopy in its different points, simultaneously. Figure 2-19 shows developed HTPP with mechanical boom for canola field and two IRT sensors. As it can be seen, these sensors are attached to the mechanical boom with adjustable-angle brackets.

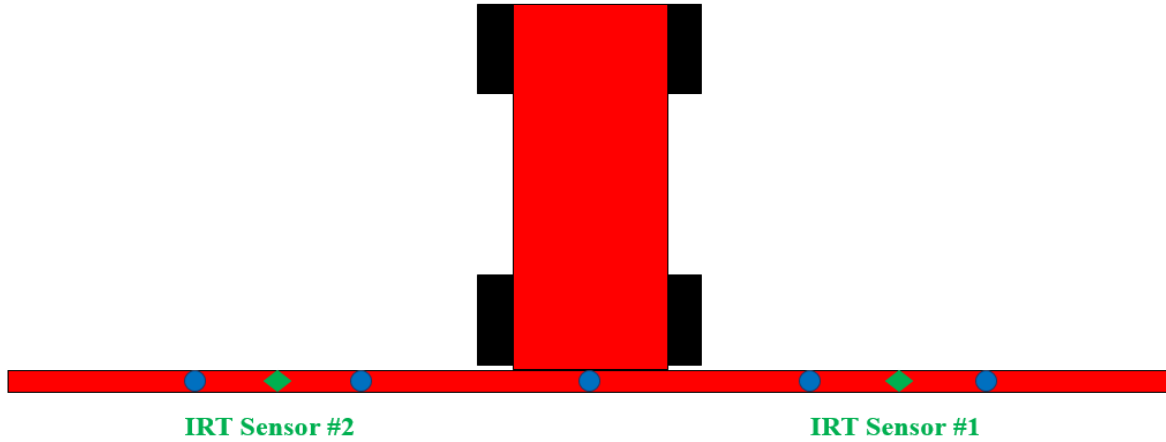


*Figure 2- 18: The schematic of mechanical boom with two Inferred Thermometer sensors (IRT) for 2018-2019 data collections*



*Figure 2- 19: Utilized Inferred Thermometer sensors (IRT) on the developed HTPP for canola data collections during 2018-2019*

## 2.4. Ambient temperature and humidity measurements

As discussed in the previous section, the temperature of a plant is an important feature and represents parameters like water status and usage of a plant. However, this character can be affected by the weather condition. Therefore, it is better to have information about ambient temperature. Analyzing the temperature of plants with different genotypes and considering



ambient temperature and humidity in these analyses, provides valuable information for crop scientists, including breeders.

### 2.4.1. The ambient and humidity measurement methods used

Different types of sensors exist for measuring and/or calculating temperature and humidity. The *HMP60*, which is manufactured by *Visala*, is a probe to measure temperature in the range of  $-40^{\circ}$  to  $+60^{\circ}\text{C}$ , and relative humidity (RH) for the range of 0 to 100% RH. This sensor is cost effective, suitable for long-term, unattended monitoring, and is compatible with our Data Logger (will be discussed in section 2.8). Figure 2-20 illustrates this probe and 6 plate solar radiation shield for it and its wiring. The datasheet of this sensor can be found in Appendix A [29]. Supply voltage range for this sensor is between 5 to 28 volt DC. Therefore, it can operate with 12 DC volt. This sensor measures the relative humidity using Eq. 2-19.

$$RH = \frac{e}{e_s} \times 100 \quad (2-19)$$

Where  $e$  is the vapor pressure in kPa, which is an absolute amount of water vapor in the air and is related to the dew point temperature. Also,  $e_s$  is the saturation vapor pressure in kPa, which is the maximum value of water vapor that air can hold at a given air temperature.

This sensor has an accuracy of ( $\pm 0.6^{\circ}\text{C}$ ) and was tested in the laboratory condition. Figure 2-21 shows the schematic of this mechanical structure and HTPP's weather station. Figure 2-22 shows developed HTPP for wheat field and ambient temperature/humidity sensor. As it can be seen, the sensor was attached to the platform with its shield.



Wire Color	Wire Function
Black	Temperature signal
White	Relative humidity signal
Blue	Power ground and signal reference
Brown	Power (12V)
Clear	EMF Shield

Figure 2- 20: Temperature and relative humidity probe with 6 plate solar radiation shield and its wire function

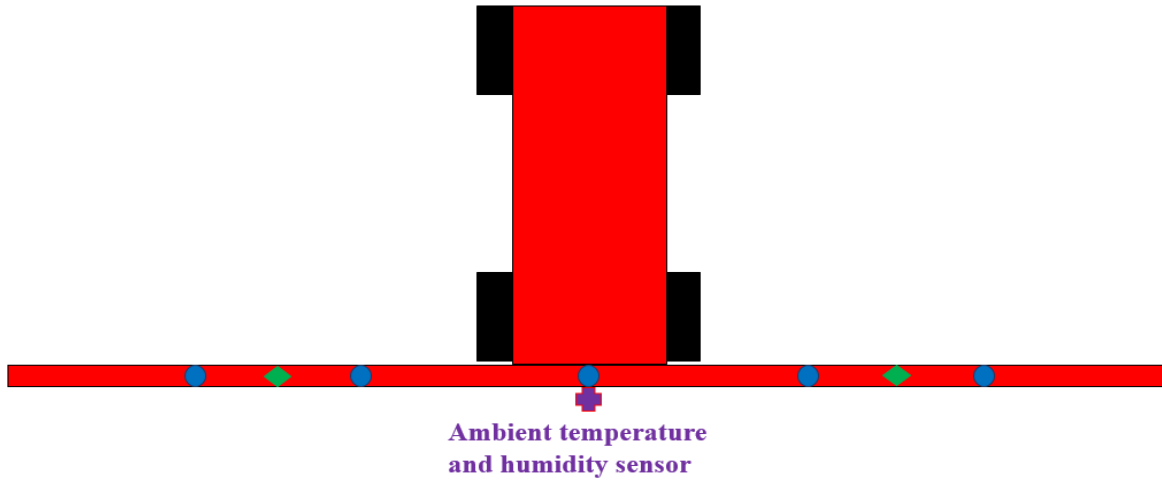


*Figure 2- 21: The schematic of mechanical boom with an ambient temperature/humidity sensor for 2018-2019 data collections*



*Figure 2- 22: Utilized ambient temperature/humidity sensor on the developed HTPP for wheat data collections during 2018-2019*

## 2.5. The NDVI measurement methods

The NDVI (Normalized Difference Vegetation Index) is another crucial feature of the plants which provides useful information for breeders. Different objects absorb and reflect different levels of solar radiation in the various spectral regions. By, uttering spectral signals on an object and analyzing the reflected signal, reflectance data can be obtained. The NDVI is a ratio derived from the reflectance data and is an indicator that quantifies live green vegetation status. In other

words, this indicator demonstrates green vegetation index of an area. NDVI management has several advantages like providing accurate growth trending, frost damage detection, biomass production, canopy coverage and density detection.

NDVI can be ranged from -1 to +1. For this range, if NDVI value is close to -1, it means there is no green vegetation in the observed area. On the other hand, if NDVI value is close to +1, highly likely dense green leaves exist on the area. NDVI values can be calculated from the following equation.

$$NDVI = \frac{NIR - Red}{NIR + Red} \quad (2-20)$$

Where *Red* and *NIR* (Near Infrared) are two basic spectral reflectance information of red and near-infrared wavelengths, respectively.

Moreover, NDVI ratio can be ranged from 0 to +1. By selecting this range, computational savings of 15-30% are possible that is significant for processing of vast amounts of data [30]. Therefore, in this study we are interested in calculating NDVI in the range of 0 to +1. For this range, NDVI index can be calculated from following equation:

$$NDVI = \frac{NIR}{NIR + Red} \quad (2-21)$$

This Equation measures percentage of *NIR* radiance in relation to the combined radiance in both *RED* and *NIR* bands. Eq. 2-22 shows the linear relationship between Eq. 2-20 and 2-21, and Figure 2-23 graphically shows this relationship [30].

$$\frac{NIR}{NIR + Red} = \frac{1}{2} \left( \frac{NIR - Red}{NIR + Red} + 1 \right) \quad (2-22)$$

Several sensors exist for measuring NDVI index of crops. These measurement devices are categorized into two: active and passive. Passive sensors are sensitive to ambient light conditions. However, active devices are not limited by environmental conditions. Therefore, in this study, we focused on active sensors for measuring NDVI value for our outdoor settings.



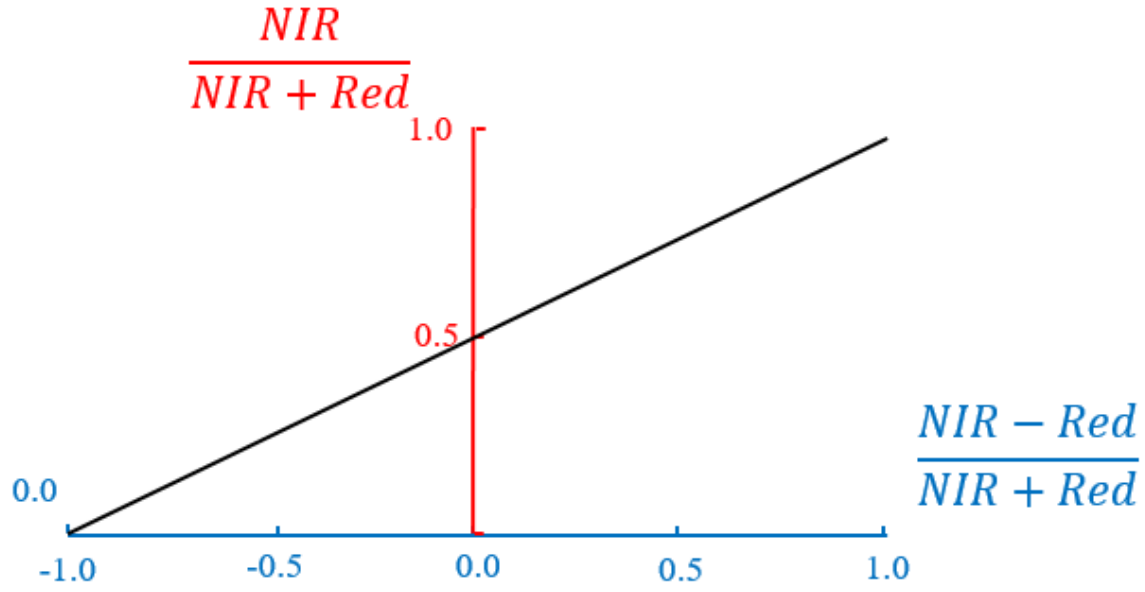


Figure 2- 23: Linear relationship between the NDVI equations (-1 to 1 and 0 to 1 ranges)

### 2.5.1. The NDVI measurement method used

The active crop canopy sensor, Holland Scientific **Crop Circle ACS-430** was selected to measure NDVI values of studied crops in this study. This sensor is lightweight and useable in the outdoor configurations. It needs 12 DC volt as power supply. The datasheet of Holland Scientific Crop Circle ACS-430 can be found in Appendix A [31]. This device measures ten samples per second in the auto-record mode. Figure 2-24 illustrates this sensor from different views and its wiring. This sensor provides NDVI value and delivers essential reflectance data from a plant. Moreover, it is applicable to use in the outdoor settings regardless of the time of the day due to its spectacular light source technology.

This sensor uses three optical measurement bands (670nm, 730nm and 780 nm). Three-channel silicon photodiode array with a spectral range of 320 nm to 1100 nm are used in this sensor to measure reflected signals (Figure 2-24). The spectral reflectance bands are scaled as percentages and will not vary with sensor's height above a target. The output of this sensor is digital signal. Therefore, it does not need any calibration. After testing and verifying the performance of this sensor for different objects in the laboratory conditions, it was installed on the mechanical boom for field test.

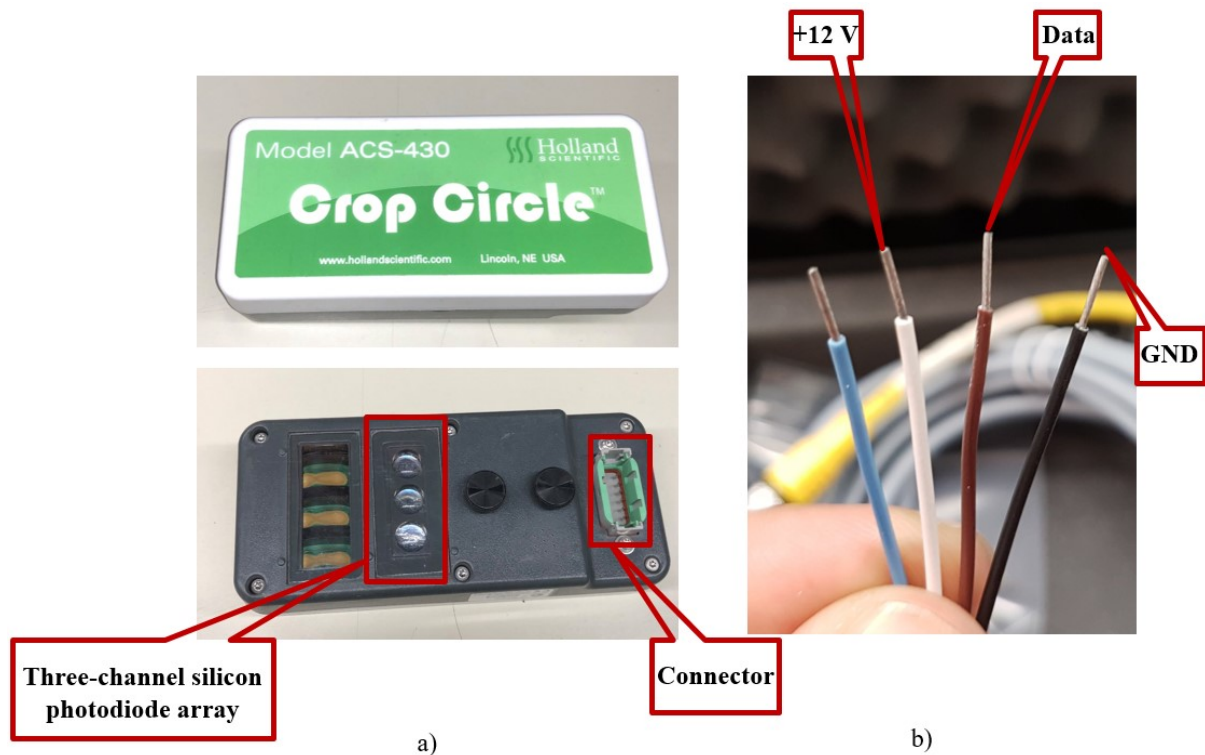


Figure 2- 24: Utilized Crop Circle sensor (a) and its wirings (b)



Figure 2- 25: Utilized multispectral camera

**Multispectral imaging** is the technique of acquiring a 2D image. A multispectral image is the one that captures image data within specific wavelength ranges across the electromagnetic spectrum and every pixel in the image contains a continuous spectrum. Usually multispectral imaging measures light in 3 to 15 spectral bands.

A multispectral image is one that captures projection data within specific wavelength ranges. By separating these wavelengths data and doing image processing and analysis valuable

information can be extracted about the vegetation index of crops. The *msCAM CMV4000* is a spectral device that was used in this study as multispectral camera to provide multispectral image for finding NDVI information (Figure 2-25). This camera connects through USB 3.0, a male to Micro B male cable to the computer. This device detects natural radiation that is reflecting by the crops.

This multispectral camera measures light in 4 bands as 580, 660, 735 and 820 nm (Figure 2-26) and uses a MFA, (Multispectral Filter Array) that incorporates proprietary pixelated band pass filters. The MFA works by breaking down the image (.PNG) into smaller parts. By using image-processing techniques and applying Eq.2-20 or 21 to the broken images, NDVI information can be extracted (more details will be discussed in the next chapter). The main advantage of using multispectral camera is giving detailed information and finding NDVI values for specific part of plants. For example, user can select area that has dense green leaves and eliminates soil parts to have more useful information.

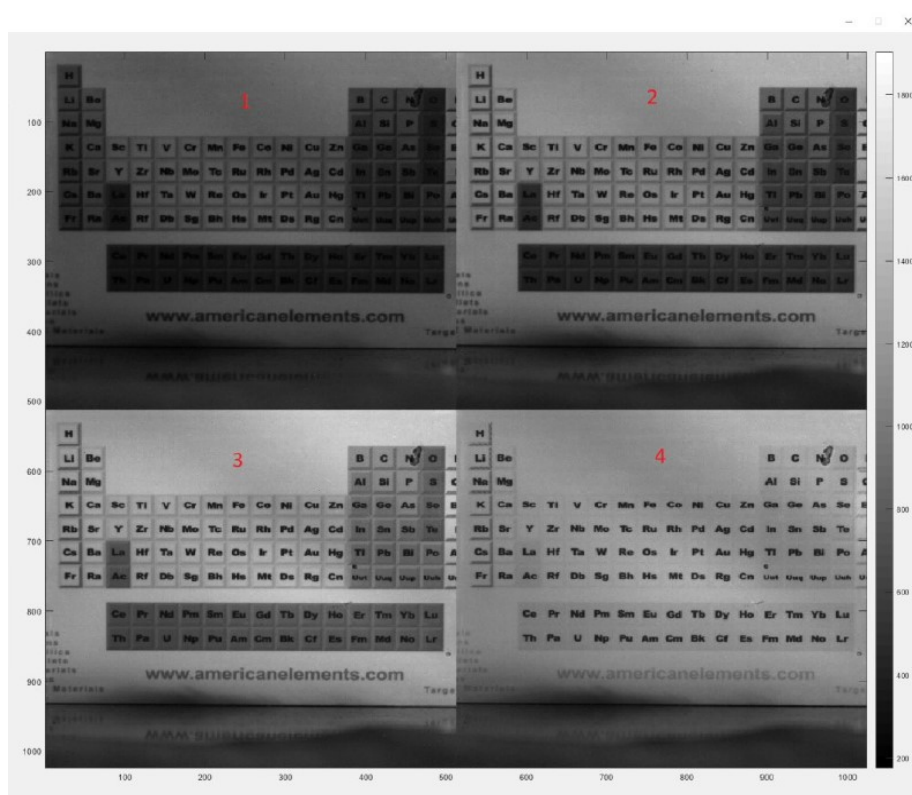


Figure 2- 26: An example of multispectral image with four bands as 1) 580, 2) 660, 3) 735, and 4) 820 nm

As discussed, during the development of the field-based HTPP, two model sensors were used to obtain NDVI index of crops– Crop Circle sensor, and multispectral camera. Table 2-5 compares both devices’ frequencies and projected areas. The projected area of devices vary by increasing or decreasing the height of mechanical boom and can be found from Eq. 2-23,as can be seen in Figure 2-27. In this equation,  $h$  is the distance between sensor and the plant, and  $\beta$  is an angular FOV of devices, which is different for each sensor.

$$\text{The projected area} = 2 \cdot d \cdot \tan\left(\frac{\beta}{2}\right) \quad (2-23)$$

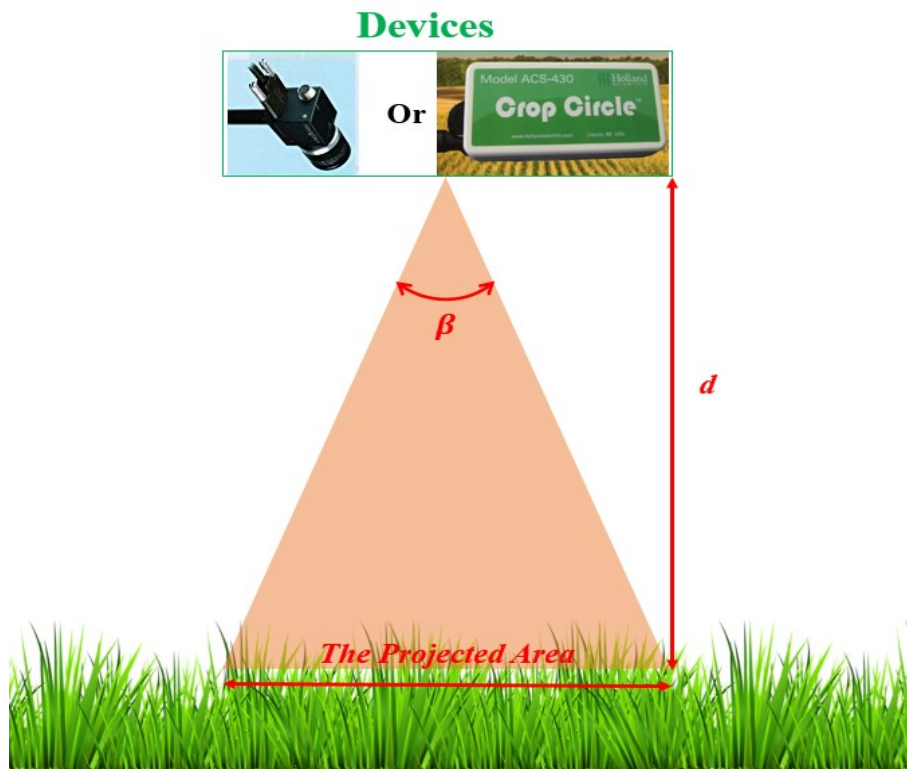


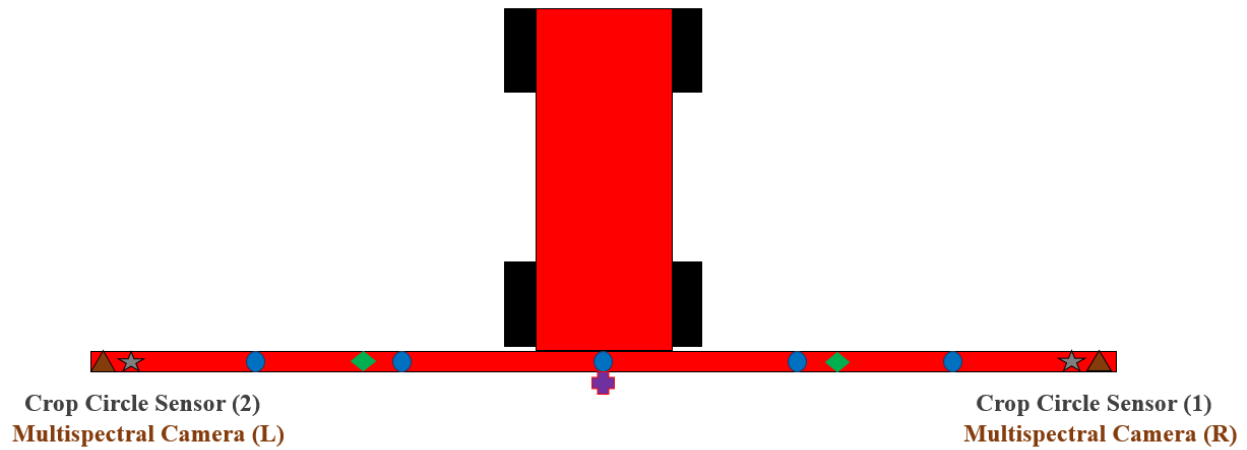
Figure 2- 27: Calculating projected area of multispectral camera and crop circle sensor

Table 2- 5: Comparison of Crop Circle and multispectral camera specifications

Sensors	The projected area (in)		Frequency (Hz)
	Sensor to canopy range 10 (in)	Sensor to canopy range 72 (in)	
Crop Circle ACS-430	$5.359 \times 2.4557$	$38.58 \times 7.68$	1 - 20
msCAM CMV4000 multispectral camera	$10.67 \times 8$	$76.8 \times 57.6$	1 - 100



Figure 2-28 shows the schematic of mechanical boom and utilized Crop Circle and multispectral sensors, and Figure 2-29 illustrates the developed HTPP for canola field and NDVI measuring devices.



*Figure 2- 28: The schematic of mechanical boom with two multispectral cameras and two Crop Circle sensors for 2018-2019 data collections*



*Figure 2- 29: Utilized devices on the developed HTPP for canola data collections to measure NDVI value of crops during 2018-2019*

## 2.6. RGB Image acquisition system

Suggested devices and sensors for developed HTPP calculate features of plants. At the same time, an RGB (Red-Green-Blue) image form crops is an informative source of information for breeders. For example, they can monitor crops to find possible effects of disease or they can check collected NDVI values with captured RGB images. In addition, other valuable information can be extracted from clear and high quality RGB images in the post-processing stage, such as height of crops or their biomass [3, 4].

Several cameras exists that they are able to take high quality RGB images. Since, the quality of images can be affected by the vibration of mechanical boom, proper camera should be selected. After having search over existing cameras a DSLR (Digital Single –Lense Reflex) camera and two model of webcams were selected for RGB image acquisition system of our HTPP. Figure 2-30 illustrates these cameras.



*Figure 2- 30: Selected cameras a) Logitech C920, b) Logitech BRIO, and c) Canon 70D*



*Figure 2- 31: The setup for testing camera's operation*

A good camera is the one that has a fast response time to capture and geo-tag images without any delay. After testing selected cameras, it was found that DSLR camera takes images and tag them with delay. Moreover, this camera needs external power supply for long duration data collection. Therefore, we focused on using of webcams.

By testing selected webcams in the laboratory condition, it was found that they are proper and fast enough to take and save images. In addition, they can communicate and be controlled with image acquisition toolbox of our software (MATLAB). To evaluate operation, first a test configuration was set up for webcams, as can be seen in Figure 2-31. Webcams were faced a screen that were showing the exact time, and webcams were taking images continuously for a long duration of time. Each taken image was tagged with time information. Therefore, by comparing time information that was in the picture and tag, it was found that selected webcams are proper and fast enough.

Further, webcams were tested to take images in the outdoor configuration. Images were captured by both model of webcams from objects with different environmental conditions like sunny and cloudy weather. Figure 2-32 shows a sample result. By comparing taken images, it was found that Logitech BRIO webcam takes image with better quality. Also, this 4k webcam can eliminate sunlight reflections.



*Figure 2- 32: Test images captured by two webcams a) Logitech C920 and b) Logitech BRIO*

An image histogram is a graph that represents the tonal distribution in a digital image. The horizontal and vertical axis of this graph are the tonal variations and the number of pixels in a particular tone, respectively. Figure 2-33 shows two histograms for the captured images with Logitech BRIO and C920 webcams. The *imhist* command of MATLAB, which gives histogram of image data, is used to extract these diagrams. It is clear from these histograms that for an image that was taken by Logitech BRIO webcam, the majority of pixels for all three red, green and blue channels are around 150. In addition, it has more uniform histogram in comparison with C920 webcam. It is mentionable that as long as all three channels of an image have uniform diagrams, image segmentation to extract meaningful information can be applied for further analysis[34].

Therefore, Logitech BRIO was selected as a proper camera for our field-based HTPP to take high resolution RGB images. An automated image acquisition program was developed to take control of the camera's shutter, which will be discussed in next chapter. By running this program in the control laptop and using GPS string, high quality geo-tagged images can be captured and saved. Logitech BRIO webcams were attached close to the multispectral cameras (Figure 2-28). Figure 2-34 illustrates the developed ground-based HTPP with the utilized webcams.

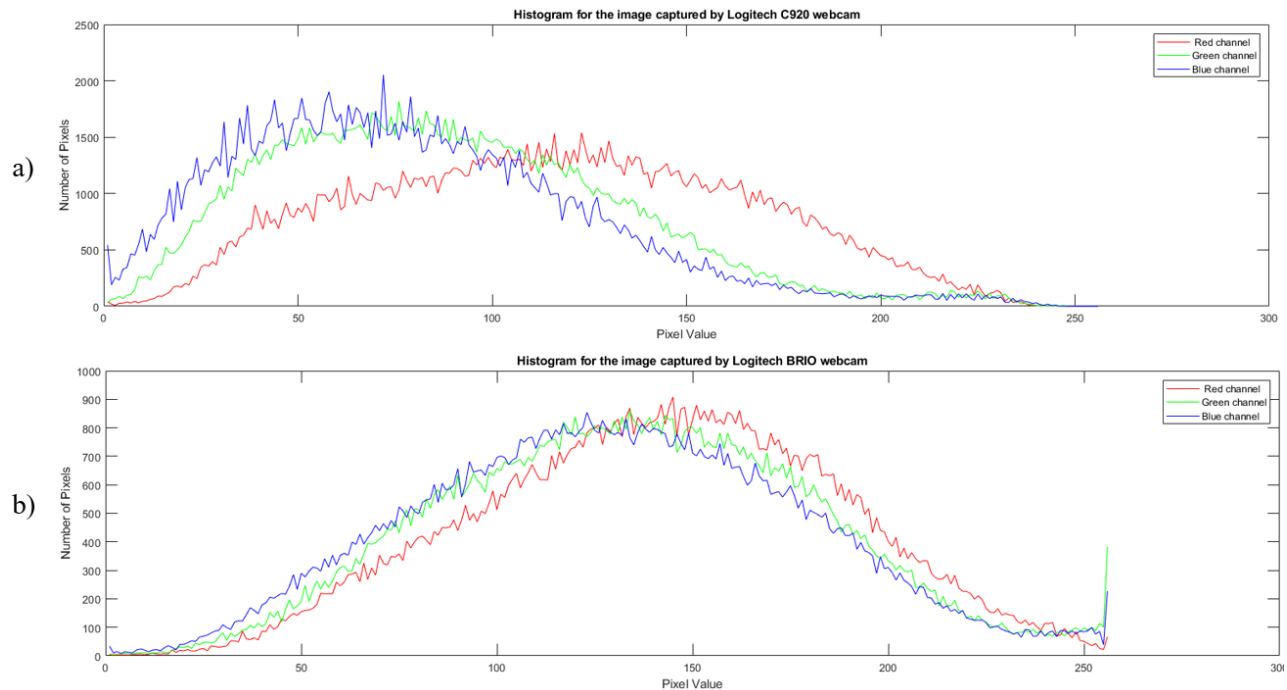


Figure 2- 33: Image histogram for the captured images by Logitech a) C920 and b) BRIO )





*Figure 2- 34: Utilized cameras on the developed HTPP for the wheat data collections to take RGB images from crops during 2018-2019*

## 2.7. GPS setup used

The GPS (Global Positioning System) is the most common navigation system. GPS provides location information anywhere in the Earth, 24 hours a day and in all weather conditions. Every point on the Earth can be addressed by its longitude and latitude values. There are two main methods for increasing accuracy of GPS system; RTK (Real-Time Kinematic) and RTX (Real-Time Extended). In the RTK technique the accuracy of GPS signals are increased by using a fixed base stations, like towers. These stations send out corrections to dynamic receivers. Therefore, by utilizing these corrections, the GPS system provides longitude and latitude values with 1-2 cm accuracy [35]. RTX is another lower cost GPS system that works without any need to a fixed base station and utilizes more than one satellite for data correction. It should be mentioned that RTX based GPS systems need long initialization time to connect the satellites to correct the precision of longitude and latitude values [36].



*Figure 2- 35: Existed GPS receiver on the developed HTPP for a) wheat and b) canola data collections during 2018- 2019*

There is a published work, which tested RTX and RTK GNSS (Global Navigation Satellite System) based on the autonomous agricultural vehicles under field conditions, and showed accuracy to be about 1.43 cm for GPS-RTK and 2.55 for GPS-RTX systems [37]. Both RTK and RTX GPS systems provide repeatable and reliable geospatial information by use of cell towers and satellites, respectively. Nowadays, farm vehicles like Tractors and Swathers are equipped with GPS systems for precision seeding, auto steering, and harvesting. In this study, as can be seen in Figure 2-35 a Swather and a Tractor which were equipped with RTK and RTX systems, respectively, are used as agricultural platform to carry sensors and devices.

By using GPS system, collected data and images can be geo-tagged to the plot level, which will be discussed in the next chapter. Therefore, GPS receiver's output should be connected to the Data Logger and laptop over a RS232 connector. This output can be showed as a NMEA (National Marine Electronics Association) RMC (Recommended Minimum Sentence C) data string like [38]:

*\$GPRMC,1,A,5211.13575747,N,10631.01441032,W,1.5,90.2,020818,15.2,E\*61.*

A standard RMC string is like  $[d_0, d_1, d_2, d_3, d_4, d_5, d_6, d_7, d_8, d_9, d_{10}, d_{11}, d_{12}]$ . This string can be broken down into separate parts, which are:

$d_0$ : \$GPRMC

$d_1$ : UTC (Coordinated Universal Time) of position (hour, min, sec)

$d_2$ : The status of GPS ( $A$ =active or  $V$ =void)

$d_3$  and  $d_4$ : Latitude information

$d_5$  and  $d_6$ : Longitude information

$d_7$ : Speed over the ground in knots

$d_8$ : Track angle in degrees

$d_9$ : Date

$d_{10}$ : Magnetic variation in degrees

$d_{11}$  and  $d_{12}$ : Checksum data.

To reduce the total cost of platform, just one GPS receiver was used for geotagging collected data and images. For geo-referencing and finding correlation of each device to the GPS receiver's location, distances and angles between them should be considered. Figure 2-36 illustrates a schematic from the top view of our platform and its devices. Latitude and longitude of a point (e.g.  $P_2$ ) can be related to another point (e.g.  $P_1$ ) on the Earth surface using the following relations [25]:

$$\text{lat}_2 = \sin^{-1}[\cos(\theta) \cos(\text{lat}_1) \sin(\delta) + \sin(\text{lat}_1) \cos(\delta)] \quad (2-24)$$

$$\text{lon}_2 = \text{lon}_1 + \tan^{-1}\left(\frac{\cos(\text{lat}_1) \sin(\theta) \sin(\delta)}{\cos(\delta) - \sin(\text{lat}_1) \sin(\text{lat}_2)}\right) \quad (2-25)$$

$$\delta = \frac{d}{R} \quad (2-26)$$

The  $\text{lat}_1$  is latitude at  $P_1$ ,  $\text{lon}_1$  is longitude at  $P_1$ ,  $\text{lat}_2$  is latitude at  $P_2$ ,  $\text{lon}_2$  is longitude at  $P_2$ ,  $\theta$  is vehicle's heading angle with respect to the Earth magnetic north pole,  $d$  is distance between  $P_1$  and  $P_2$  and  $R$  is the Earth's radius in meter (assuming earth is a complete sphere). This approach (using of Eq.2-24 to 26) gives exact locations of each sensor, which is then used to load data/images into the visualization module.

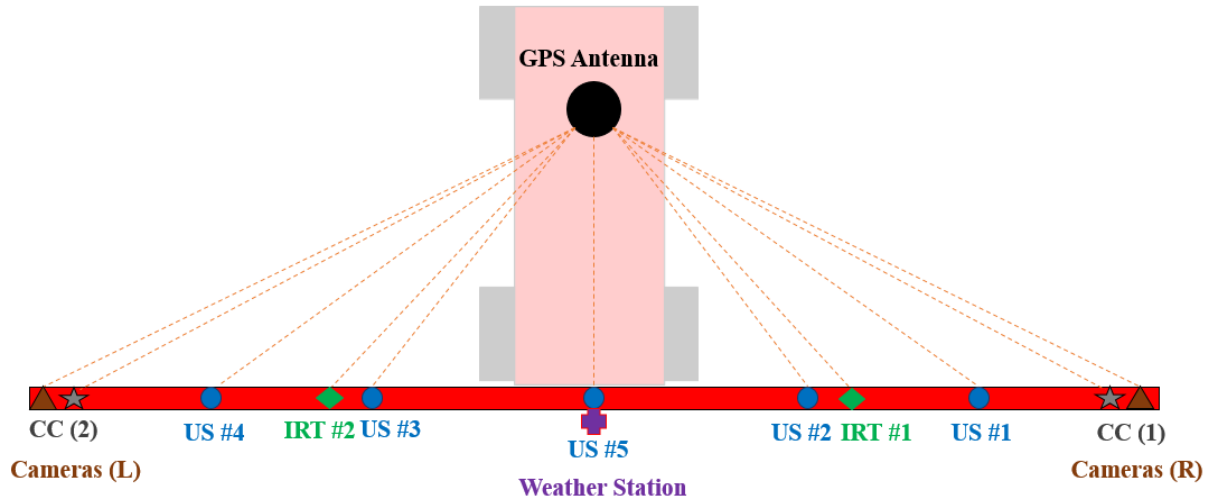


Figure 2- 36: Top view of the platform, which shows GPS antenna and sensors' location

## 2.8. Data storage system

Measured data and captured images should be saved into the storage system reliably and fast. Two data storage parts were dedicated for our HTPP, as Data Logger and laptop.

All recorded data and GPS string are saved into a Data Logger. Therefore, an ideal Data Logger should be selected for the HTPP. It should have enough channels to communicate with devices and enough memory to store their data. Since, the output of sensors are both analog and digital, selected Data Logger should be able to communicate with different protocols like voltage/current analog signals, RS232/485 and so on. After having several communications with different manufactures, *CR3000* Data Logger, which is manufactured by *Campbell Scientific* was selected. Its datasheet can be seen in the Appendix A [39].

Figure 2-37 illustrates the utilized Data Logger with its wirings and safety fuses as one of control parts of developed HTPP. These fuses protect this control panel from possible short circuits. This Data Logger needs 12 DC volt as its power supply and it should be programmed to work automatically and reliably during the data collection. In the next chapter, developed programs for the Data Logger will be discussed in detail.

For extracting collected data, from Data Logger, which is an Excel file, *LoggerNet* program is used. For this purpose, Data Logger was connected to a laptop computer over a RS232 link. As it can be seen from Figure 2-38 *LoggerNet* program has user-friendly graphical interface.



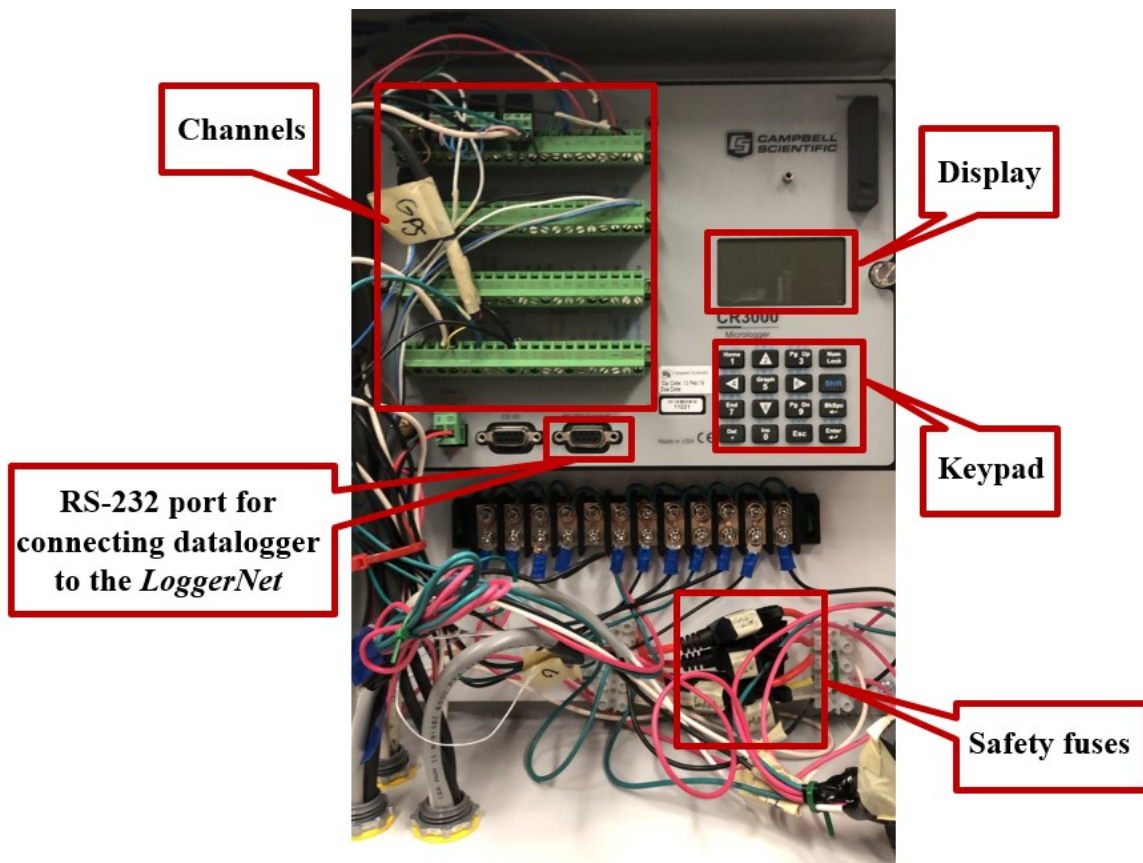


*Figure 2- 37: Utilized Data Logger and its wirings*

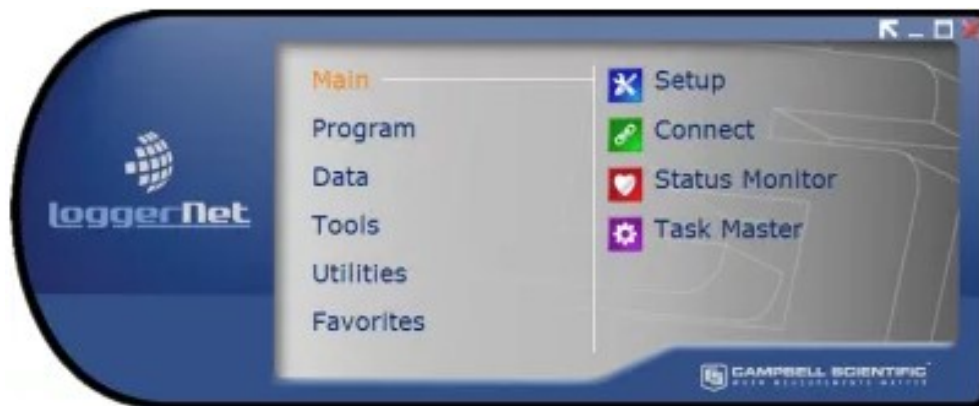


*Figure 2- 38: LoggerNet program to communicate with utilized Data Logger*

Another storage system for the developed HTPP is a laptop computer. All captured images (RGB and multispectral) are saved and tagged with geospatial information in this unit. In other words, laptop is other main control system of developed HTPP. Therefore, to have a reliable, autonomous and fast RGB or multispectral image collection, the utilized laptop is equipped with the developed programs which will be discussed in the next chapter.

## 2.9. The hardware system for HTPP

In this section, the system architecture for field-tests in 2018 and 2019 is discussed. After selecting, purchasing and testing selected devices to record and measure features of crops, hardware part of HTPP was assembled. Figure 2-39 and 2-40 illustrate an architecture of assembled system for 2018 and 2019 data collections. The main difference between these two systems' architectures is using multispectral camera and adding central ultrasonic sensor in the 2019 data collections. As discussed, by using central ultrasonic sensor, the height of mechanical boom can be recorded during the data collections and by using Eq. 2-5 to 2-11, accurate height measurement without any primary sensor calibration can be achieved.

All sensors' outputs and GPS strings are connected to the Data Logger which works as a central control system. Therefore, devices' captured data can be geo-tagged and recorded in the Data Logger. Moreover, RGB and multispectral cameras are connected to the laptop. Laptop works as other central control system and GPS receiver's output is connected to it. All captured images are saved and tagged with the geospatial information in the Laptop. Laptop and Data Logger are operating by the use of developed programs as software part of developed HTTP, will be discussed in detail in the next chapter.

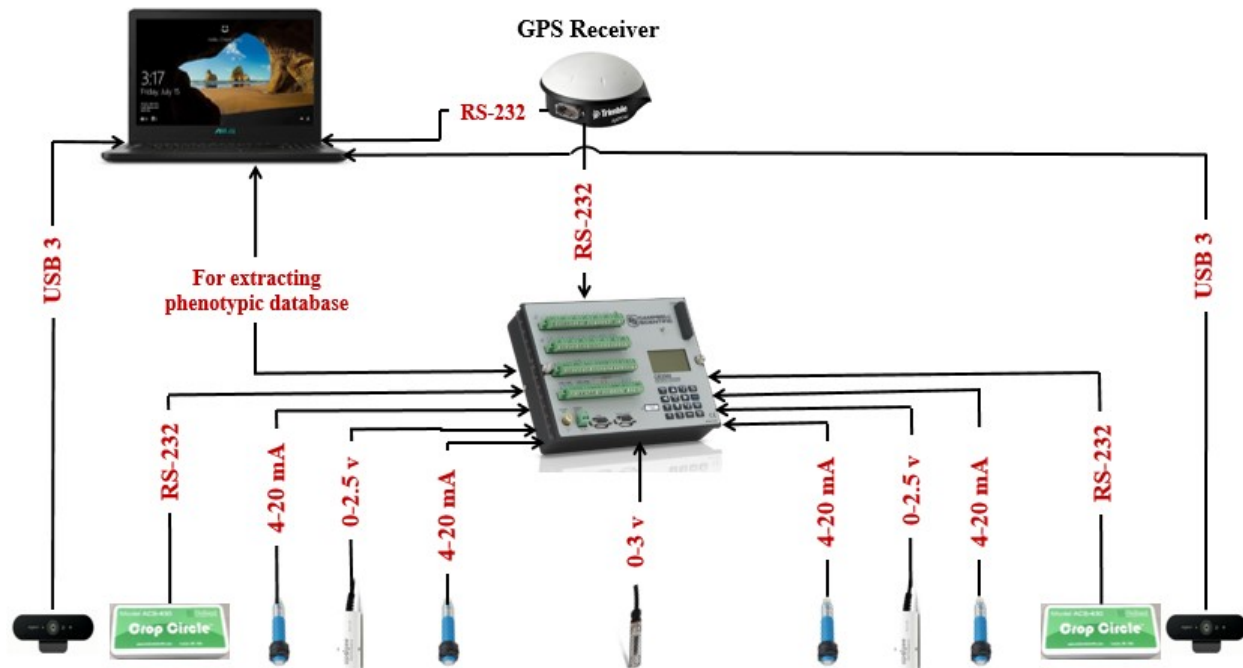


Figure 2- 39: System's hardware part for 2018 data collections with four ultrasonic sensors, two IRTs, ambient temperature and humidity sensor, two Crop Circle sensors and two BRIO webcams

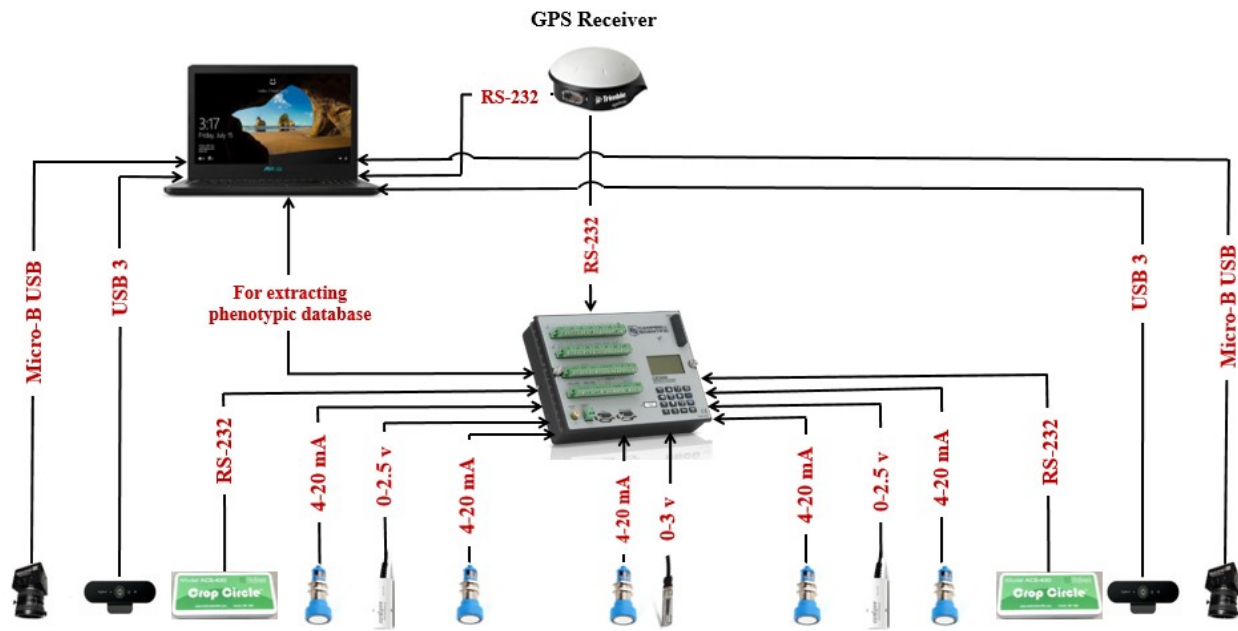


Figure 2- 40: System's hardware part for 2019 data collections with five ultrasonic sensors, two IRTs, ambient temperature and humidity sensor, two Crop Circle sensors, two BRIO webcams and two multispectral cameras

Mechanical design team of the Robotic Laboratory at the University of Saskatchewan, designed a mechanical boom for both Tractor and Swather. After wiring devices on these booms, they were used for data collection on wheat and canola fields in 2018 and 2019 (Figure 2-41 and 2-42). As can be seen, the developed mechanical boom can be folded for convenient transportation.



Figure 2- 41: Mounted boom on a Swather and wired with devices for canola data collections a) transportation and b) expanded mode



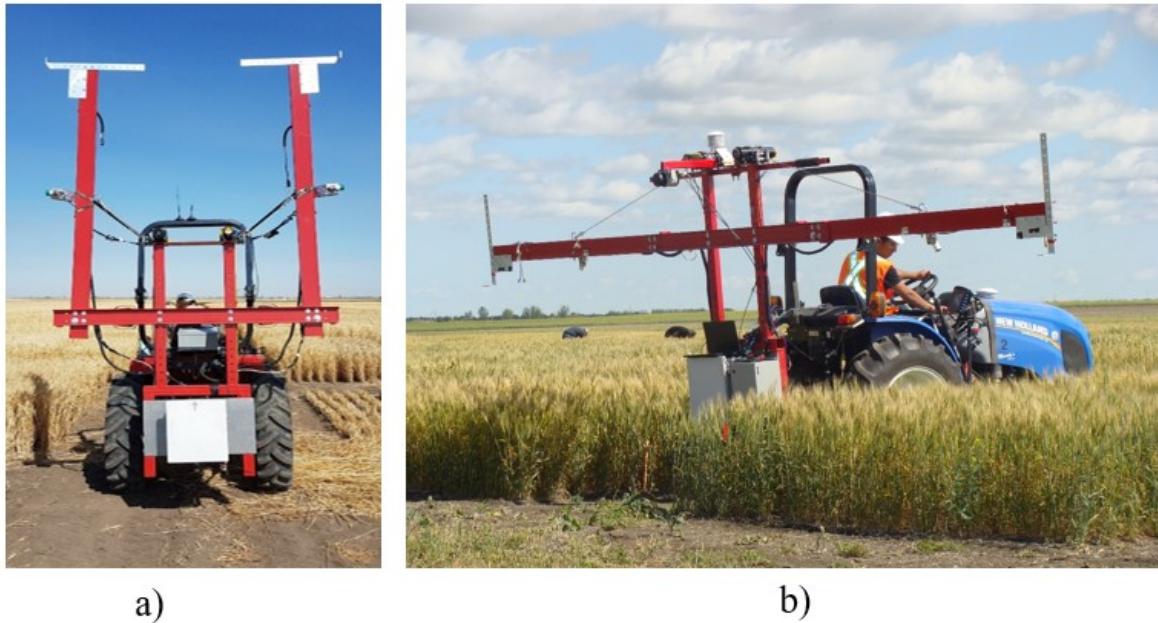


*Figure 2- 42: Mounted boom on a Tractor and wired with devices for wheat data collections a) transportation and b) expanded mode*

## 2.10. Summary

To summarize, the hardware part of the developed ground based HTPP was discussed in this chapter. After having several meetings and thorough literature review on the existing platforms, different features of canopies were targeted to be monitored. Measuring their height, temperature, NDVI value, ambient temperature and humidity, capturing RGB and multispectral images from them were selected as target traits.

For this purpose, after searching for existing sensors and contacting their manufactures, several devices were selected and procured. All these, devices were tested in the laboratory conditions and reliability and accuracy of them were verified before using in the field conditions.

Existing agricultural vehicles, were equipped with the mechanical boom. Sensors and cameras were wired on the mechanical boom. All captured data and images are tagging with the geospatial information (longitude and latitude) and saving into the Data Logger and laptop.



## CHAPTER 3- Software developed for the platform

### 3.1. Introduction

As discussed in the previous chapter, developed HTPP has a hardware part that consists of different sensors and devices. It is inevitable that these devices should be controlled by different programs. Moreover, several programs should be developed for different purposes such as visualization, sorting and post processing. It can be said that the most challenging achievement for this research is developing software part of proposed HTPP.

Indeed, several programs should be developed for different phases such as preparation, data collection and post-processing. The main essential programs that are critical for the operation of developed field-based HTPP can be categorized as:

- A mapping program for generating the map of field with the GPS information of each plot.
- A data acquisition program for collecting sensors' data and tagging them with the related geospatial information (longitude and latitude).
- An image acquisition program for capturing (RGB and multispectral) images of crops with their GPS information.
- A post-processing program for extracting NDVI information of plants from each of captured multispectral images.
- A data visualization program for post processing analysis (showing the map of field and loading all collected data and images).
- A sorting program for autonomously organizing collected data and images in the Excel sheets and related folders.

This chapter covers developed programs for the developed field-based HTPP. In this research MATLAB was used as the main programming language for developing the software. It was used for mapping, image acquisition, data visualization, post-processing and data/image sorting part. Furthermore, another programming language (*CRBasic*) was used for data acquisition program. This program is executed in the Data Logger to collect sensor's data and create phenotypic data base. The results of utilizing these programs in the developed HTPP will be discussed in chapter four.

## 3.2. Mapping programs

Creating the map of studied field was the first challenge for the development of proposed field-based HTPP. This map should be used for data visualization and sorting. In other words, the data are related to the plot level (geo-tagged) using this program.

As discussed in chapter 2, the developed HTPP has one GPS receiver. Using this receiver, longitude and latitude information of the vehicle can be determined. Also, this station prepares valuable information to create the map of targeted field. Consider the following sample GPS string:

*\$GPRMC,210952,A,5220.187369,N,10617.00265,W,1.5,90.2,020818,15.2,E\*61*

Longitude and latitude (*Lat /Lon*) are 5220.187369 and 10617.00265, respectively. These values are in degrees minute format (*Lat<sub>DM</sub> /Lon<sub>DM</sub>*). They need to be converted to decimal degrees (*Lat<sub>DD</sub> /Lon<sub>DD</sub>*) by using following equations (using floating point numbers) [44, 45]:

$$Lat_{DD} = \left( \frac{Lat_{DM} - 5200}{60} \right) + 52 \quad (3-1)$$

$$Lon_{DD} = \left( \left( \frac{Lon_{DM} - 10600}{60} \right) + 106 \right) \times (-1) \quad (3-2)$$

Therefore, by using these equations, the equivalent longitude and latitude values in decimal degrees format can be calculated as below:

$$Lat_{DD} = 52.3364561441667$$

$$Lon_{DD} = -106.283377549167$$

As discussed in section 2.7 longitude and latitude values of a point on the Earth surface can be found based on the another point's geospatial information by using the Eq. 2-23, 24 and 25. Therefore, as can be seen in Figure 3-1, using these equations and the output GPS string of receiver, the correlation of each plot's center can be calculated. A green rectangle represents the plot, black and white dots represent the center of plot and the GPS receiver, respectively.

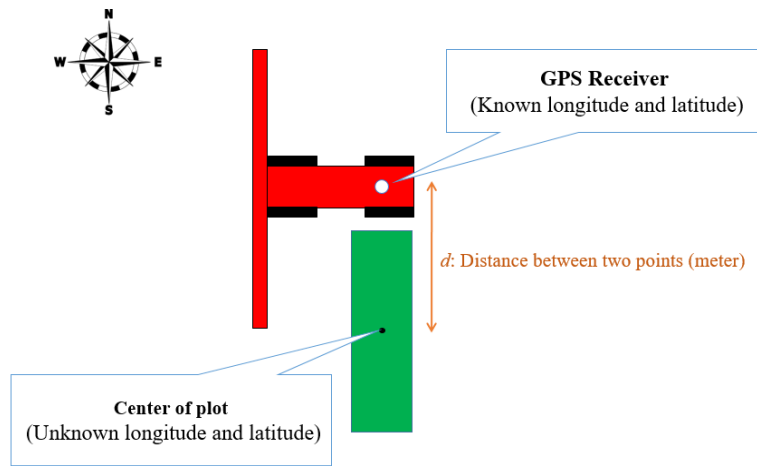


*Figure 3- 1: Using GPS receiver to find correlation of unknown point*

### 3.2.1. Mapping program- Version 2018

The studied fields' crops were bred in the way that they have rectangular shapes with the almost same dimensions and same distances between the plots. As can be seen in Figure 3-2, by having GPS correlation of the center of two known plots (first and last plots), which are in one row, longitude and latitude values of center of other plots, in the same row, can be found by interpolation. Therefore, for each row of the studied field, we can find first and last plots' geospatial information (longitude and latitude values of center of plots). Secondly, an Excel sheet should be prepared, which has the longitude and latitude values of plots' center for the entire of field as can be seen in Figure 3-3.

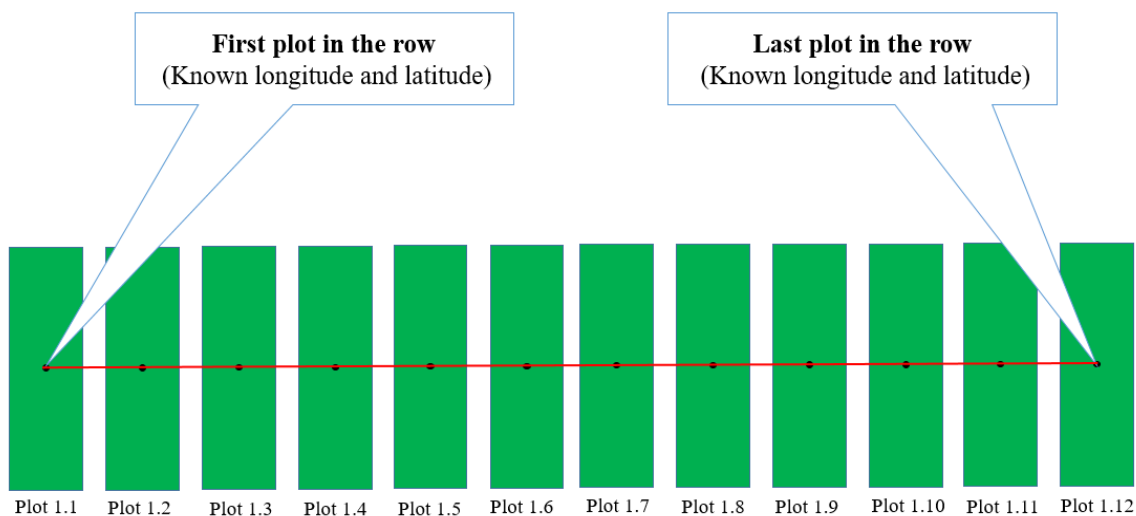


*Figure 3- 2: Using interpolation to find center of plots from information of the first plot*

	First Row		Second Row		Third Row	
	Latitude	Longitude	Latitude	Longitude	Latitude	Longitude
	A	B	C	D	E	F
1	52.1870685	-106.5161318	52.1869966	-106.5161309	52.1869246	-106.5161301
2	52.1870685	-106.5161580	52.1869966	-106.5161573	52.1869246	-106.5161565
3	52.1870685	-106.5161843	52.1869966	-106.5161836	52.1869246	-106.5161828
4	52.1870685	-106.5162106	52.1869966	-106.5162099	52.1869246	-106.5162092
5	52.1870685	-106.5162369	52.1869966	-106.5162362	52.1869246	-106.5162355
6	52.1870685	-106.5162632	52.1869966	-106.5162625	52.1869246	-106.5162619
7	52.1870685	-106.5162894	52.1869966	-106.5162888	52.1869246	-106.5162882
8	52.1870685	-106.5163157	52.1869966	-106.5163151	52.1869246	-106.5163146
9	52.1870685	-106.5163420	52.1869966	-106.5163415	52.1869246	-106.5163409
10	52.1870685	-106.5163683	52.1869966	-106.5163678	52.1869246	-106.5163673

Plot 3.9

Figure 3- 3: A screenshot of a part of the generated Excel sheet for the information of plots' center

By having information about the center of plots, coordinates of the four corners is calculated using the Eq. 2-23, 24 and 25 (Figure 3-4). As discussed in chapter 2,  $d$  is the distance between two points and  $\theta$  is angle with respect to the North Pole. A MATLAB function was developed (*Boom.m*) to use these equations, which can be found in the Appendix B. For example, to find longitude and latitude values of point A, firstly these equations should be used, where  $d$  and  $\theta$  are  $L/2$  meter and 0 degree, respectively. Next, these equations should be used with different values for  $d$  and  $\theta$ . This time,  $d$  and  $\theta$  are  $W/2$  meter and 270 degree, respectively. Therefore, latitude and longitude information of corner points (A, B, C and D) can be calculated and a rectangular schematic of each canopy plot can be drawn by using these values.

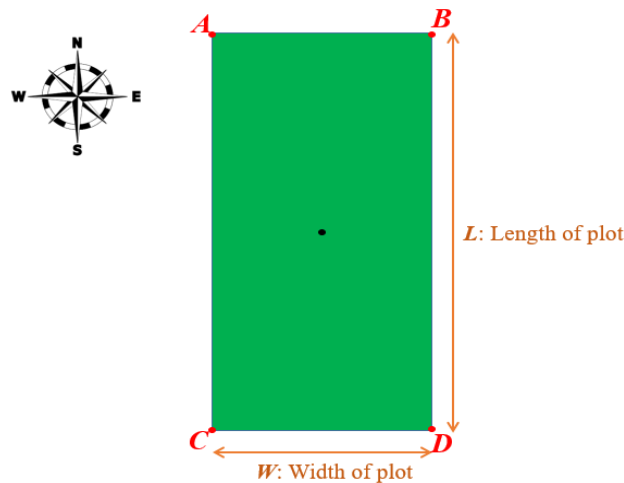
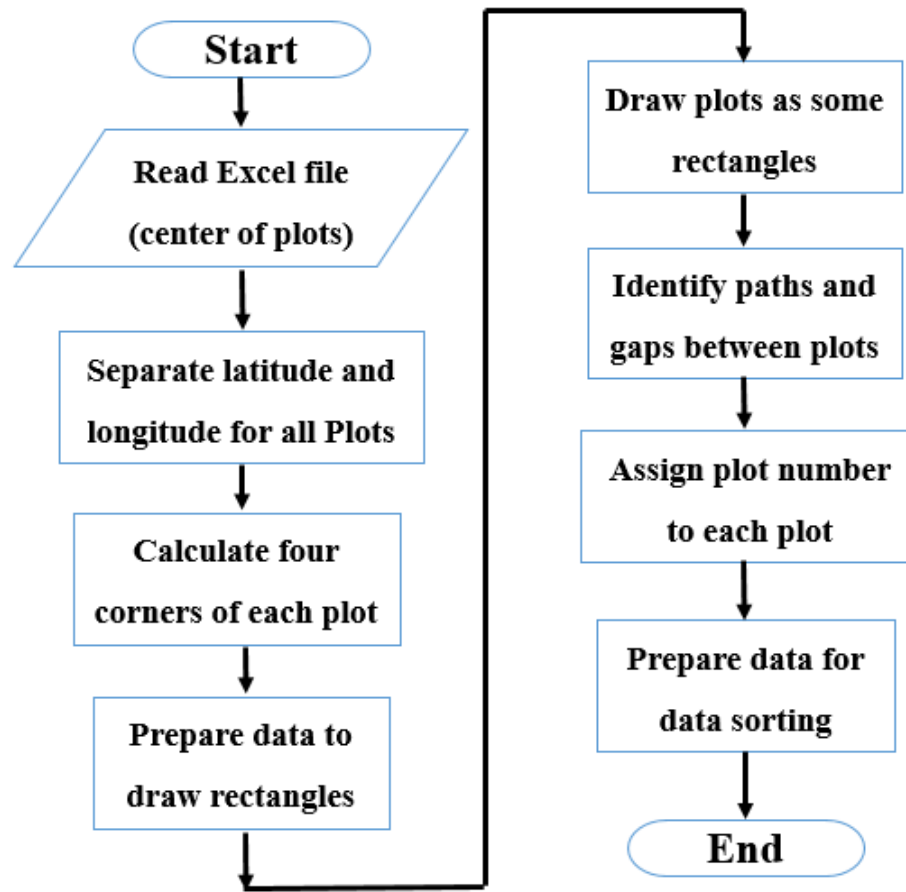


Figure 3- 4: A schematic of plot and its four corners



*Figure 3- 5: The flowchart of loading field's map (version 2018)*

An Excel sheet like Figure 3-3, which includes the center of plots' should be prepared for each studied field. This Excel sheet is necessary to use visualization program, which will be discussed in section 3.6, and it should be placed in the folder of the visualization program. Figure 3-5 illustrates the flowchart for importing and drawing the map of field.

### **3.2.2. Mapping program- Version 2019**

There were issues with mapping (version 2018) program. First, for the large-sized fields, finding and calculating the geospatial information of two plots in each row is challenging. A new version of mapping program, which is user friendly and automated, was developed for the mapping of fields on 2019. This programs was developed with the collaboration of Rahim Oraji (Robotics Laboratory's research assistant). By using this module, user can maps fields easier. For mapping

the field, as long as, the dimensions of plots and the gap between them are constant, the geospatial information (longitude and latitude) of a corner plot is enough to map the entire field. By using this GPS information, longitude and latitude values of the four corners of all plots can be calculated. The module supports multiple mapping with different angles respect to the north direction and also produces two main files (*.config* and *.csv* formats). After the map file creation, map file can be trimmed or in other words edge-effect consideration can be applied.

It is mentionable that for working with mapping module, firstly, the dimensions of drawn plots should be considered with the gap and the path between them as can be seen in Figure 3-6. The actual plot's dimensions will be applied in the next steps.  $W$ ,  $L$ ,  $G$ ,  $P$  are representing respectively, width, length of plots (considered with gap and path values), gap and path values of studied field. In other words,  $W$  and  $L$  are center to center dimensions.  $P_1$  is reference point, which is along plot's center. This reference point's longitude and latitude can be found by locating vehicle's GPS receiver in the mentioned point. Figure 3-7 illustrates developed GUI for the mapping module of Pheno-VISDM3. The manual for using this program can be found in the Appendix C.

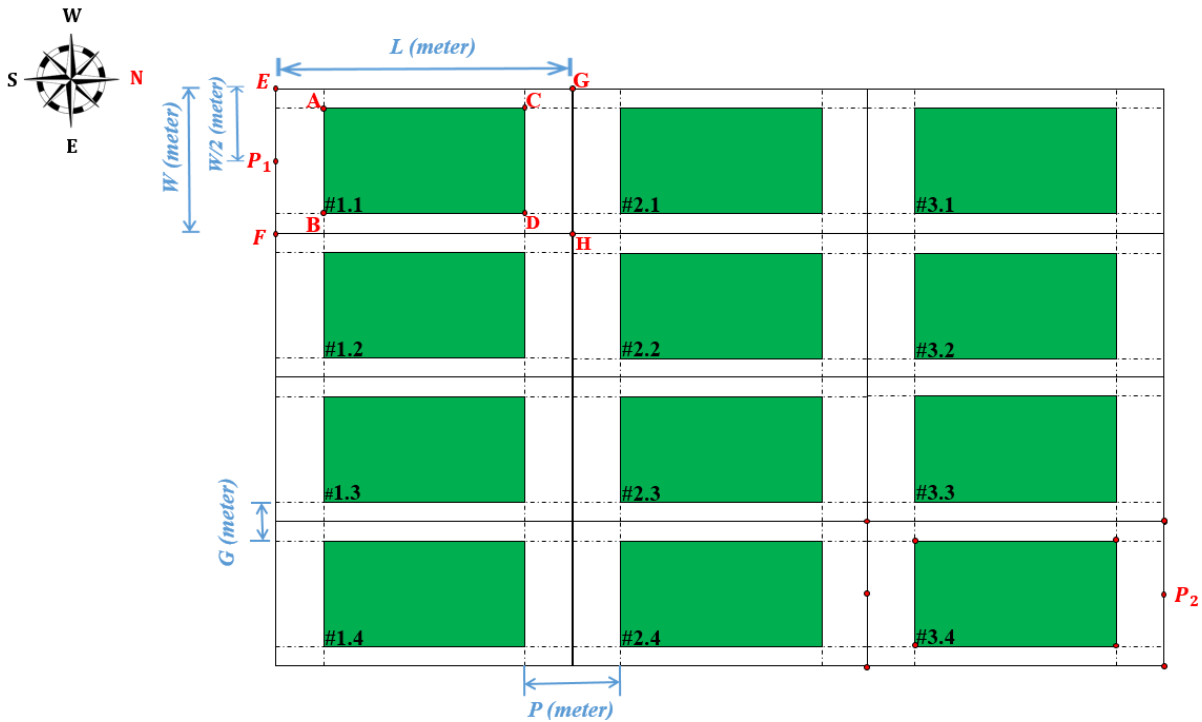


Figure 3- 6: Calculating the location of all plots using a starting point to create a map for the studied field

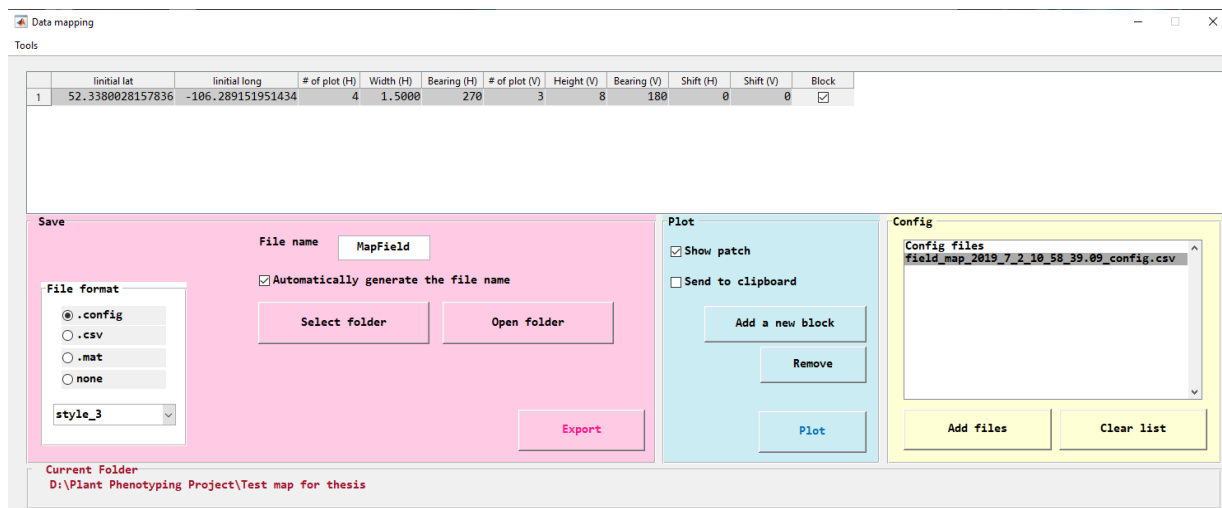


Figure 3- 7: Mapping module of PHENO-VISDM3 program

For mapping the studied fields several equations should be used in the steps 2-3 of manual. A calculator module is developed for the Pheno-VISDM3 to ease these calculations. To open calculator module, user should click on the *tools tab* in the Data handling window and then selects *mapping tools*, and after that selects *calculator*. A new window will be appeared. Figure 3-8 illustrates calculator module of Pheno-VISDM3 and its different modes.

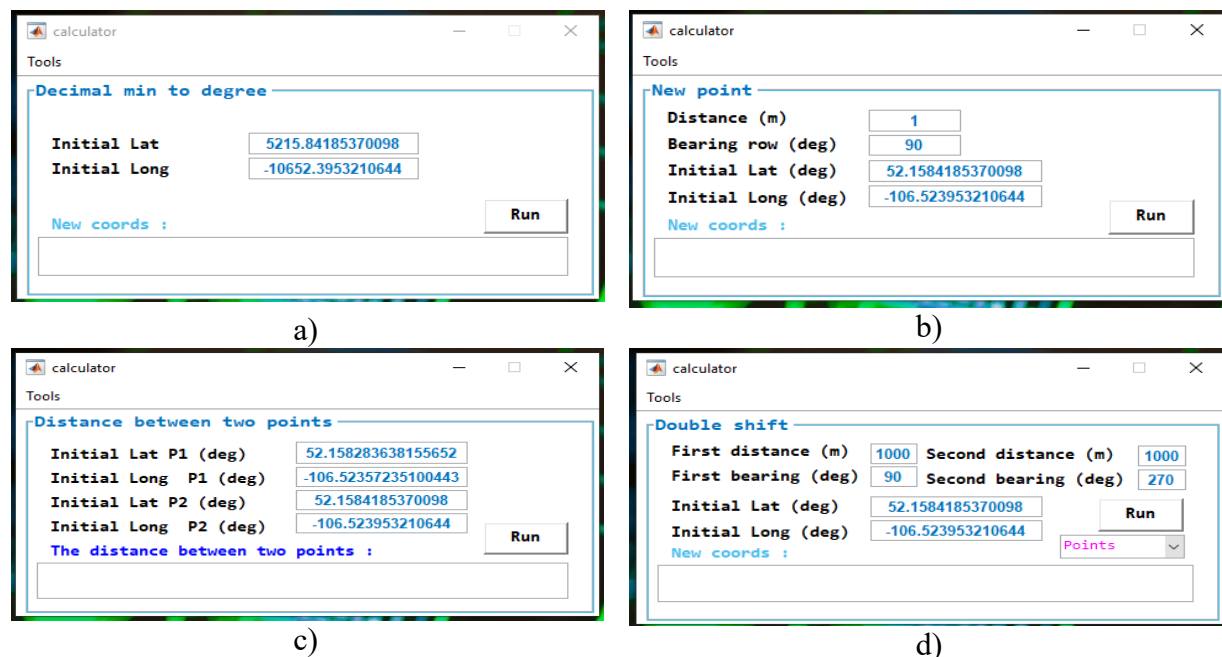


Figure 3- 8: Calculator module of Pheno-VISDM3 for a) converting decimal minutes to decimal degree b) calculation longitude and latitude values of a new point based on known point c) calculation distance of two points d) double shift of known point

### 3.3. Data acquisition program

Utilized sensors should measure and collect data and all these data should be saved into the control center. Data Logger is utilized as one of control centers in this study. Therefore, by using Data Logger and developing proper program for it, a phenotypic database, which includes collected data can be prepared. Figure 3-9 illustrates data acquisition system for the developed HTPP. For this system, a data acquisition program for collecting and saving data was developed. There were challenges for the development of this program, such as analog output of some sensors (their calibration), tagging collected data with the related time and geospatial information, and eliminating delay issue during the operation of program.

To develop data acquisition program, a programming environment called *LoggerNet* was utilized (Figure 3-10) and programming language is *CRBasic*. This environment is provided by the manufacture of the Data Logger.

In the developed codes, first required variables should be defined and they should be stored temporarily. Then, all phenotypic data should be transferred to an Excel file. The flowchart of developed data acquisition programs (versions 2018 and 2019) can be found in Figure 3-11.

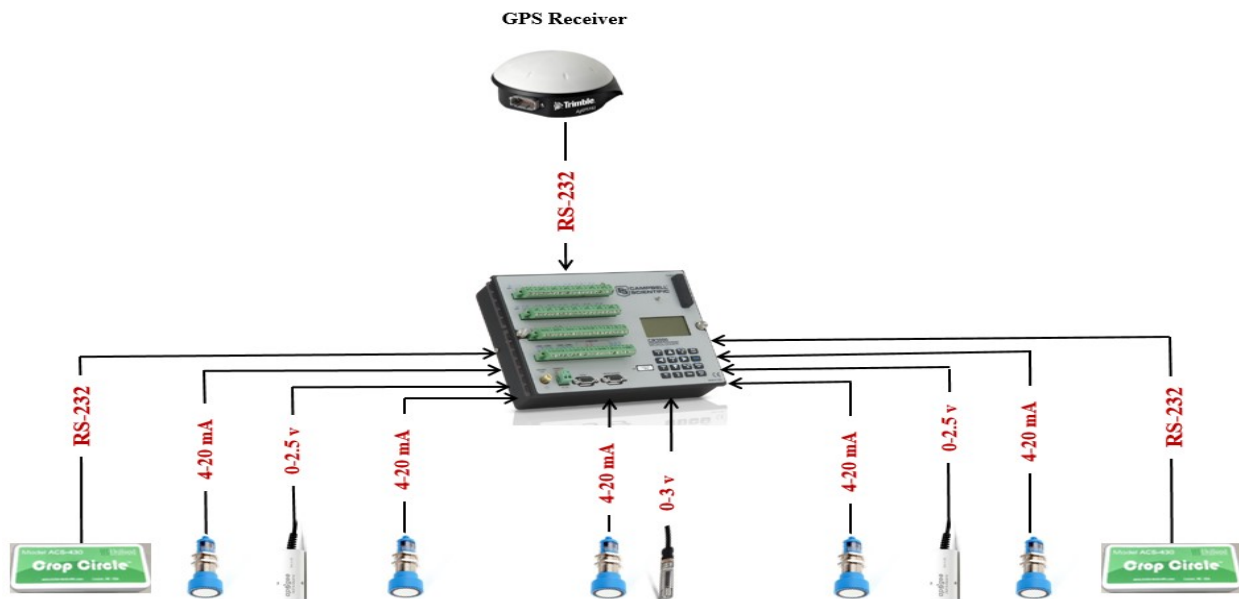


Figure 3- 9: Data acquisition system consists of Data Logger, GPS receiver for geo-tagging, five ultrasonic sensors for height measurement, two IRT for temperature measurement, two Crop Circle sensors for NDVI measurement, and a weather station sensor for measuring ambient temperature/humidity



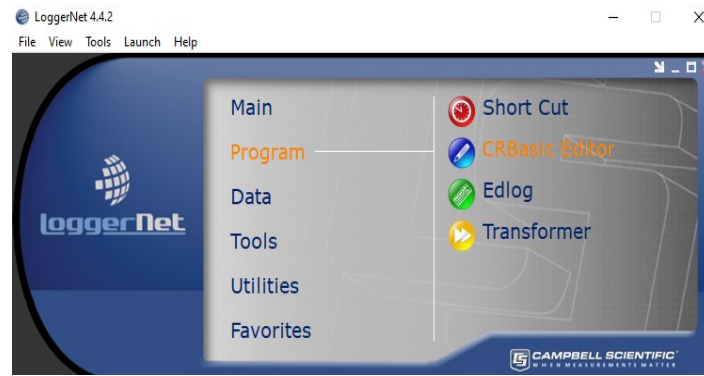


Figure 3- 10: Utilizing CRBasic Editor for programming Data Logger by using LoggerNet

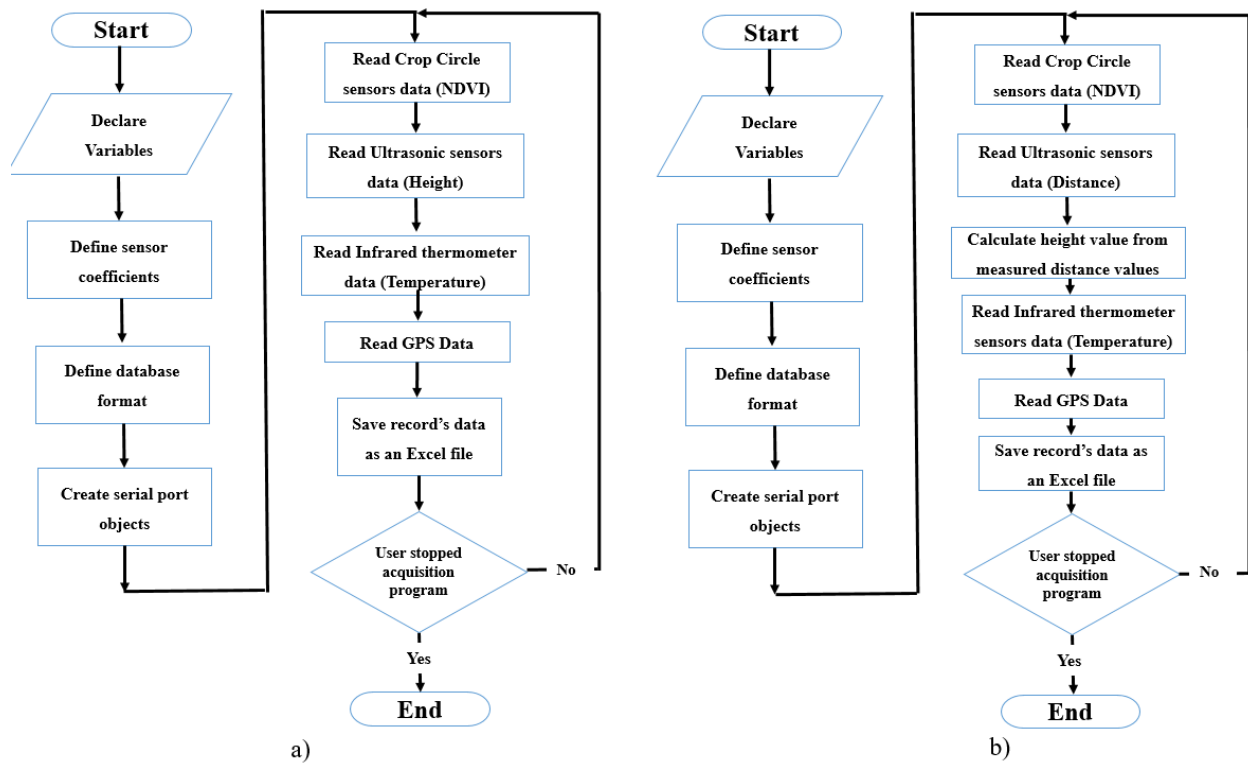


Figure 3- 11: The flowchart for the data acquisition program on a) 2018 b) 2019 data collections

The main difference between 2018 and 2019 versions is that, the utilized HTTP in 2018 data collections had four ultrasonic sensors that they were calibrated to measure the height of crops. Before, each field tests they were calibrated, which was time consuming issue especially in field conditions. Another ultrasonic sensor was added to the boom for 2019 data collections. All sensors were measuring distance values and by using these values, and subtracting them from the boom's height, then height of crops were calculated. Therefore, by using this approach ultrasonic sensors

do not need any calibration before start of data collections. More details were discussed in section 2.2

The baud rate to communicate with the utilized measurement devices is fixed to 38400bps (bits per second) to have reliable communication. The data acquisition cycle in the program is 250ms. In other words, four sample points can be captured per second. The number of collected data for each plot can be determined by selecting proper speed for the vehicle (Swather or Tractor). For the studied fields, it was achieved that by choosing traveling speed around 1.6mph, around eight data per plot was collected, which seems ideal. Prepared manual for executing Data Logger and extracting collected data can be found in the Appendix C.

Figure 3-12 illustrates two rows of generated Excel file to clarify structure of phenotypic table. Each row of this table (record) consists of time information of data collection, GPS string and sensors' values (ultrasonic, infrared thermometer, Crop Circle, weather station for ambient temperature and humidity). The number of records depends on the size of the studied field and the duration of data collection. IRT #1 (right) and IRT #2 (left) sensor columns encompass collected temperature of crops via infrared thermometers. NDVI sensor #1 (right) and 2 (left) columns represent the captured NDVI value by each sensor. Moreover, ultrasonic sensors #1-2 (right) and #3-4 columns show the height of canopies that are recorded by the utilized ultrasound sensors. Ultrasonic sensor #5 (center) column represents the height of the boom during the data collection.

GPS string column represents NMEA GPS string of each record. Collected data can be related to the plot level in the future retrieval. This string should be broken into meaningful pieces to extract latitude and longitude information.

Record	Date and Time	IRT Sensor #1	IRT Sensor #2	NDVI Sensor #1	NDVI Sensor #2	GPS String	Ultrasonic Sensor #1	Ultrasonic Sensor #2	Ultrasonic Sensor #3	Ultrasonic Sensor #4	Ultrasonic Sensor #5	Ambient Temperature	Ambient Humidity
1	August 18 2018, 12:45:40	24.3	26.1	0.52	0.78	GPS1	55.7	57.6	72.3	73.4	157.5	24.93	64.36
2	August 18 2018, 12:45:41	24.2	25.9	0.55	0.8	GPS2	56.3	52.3	72.6	74.3	157.5	24.93	64.36

GPS1: \$GPRMC,170004,V,5211.22654352,N,10630.96581787,W,0.0,360.0,180718,15.2,E\*4E

GPS2: \$GPRMC,170005,V,5211.22654352,N,10630.96581284,W,0.0,360.0,180718,15.2,E\*49

*Figure 3- 12: The structure of Excel database to store phenotypic data*

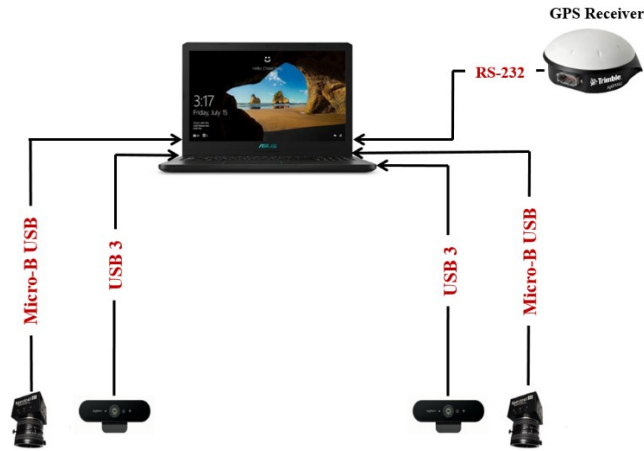


*Figure 3- 13: Image acquisition system consists of laptop, GPS receiver for geo-tagging, two webcam for capturing RGB images and two multispectral camera for capturing multispectral images*

### 3.4. Image acquisition programs

Not only a data acquisition program should be created for the developed HTPP but also another program should be developed for the image acquisition. Data Logger have limited amount of memory and they can just read and save signals, strings and numeric data. Another unit should exist to save taken images. In addition, the image acquisition programs should be executed on this unit. Therefore, a laptop computer was added to the hardware part of developed HTPP to execute image acquisition programs and save captured images (Figure 3-13).

Different image acquisition programs were developed to capture RGB and multispectral images. These programs were tested and used in the laboratory conditions and during field experiments in 2018 and 2019. It was found that the programs are working reliably and accurately. In the next sections, the developed programs will be discussed in detail.

#### 3.4.1. Image acquisition program for RGB camera

As discussed in section 2.6, to capture RGB images of crops, three model of cameras were tested, and Logitech BRIO webcam was selected as the proper camera for the image acquisition system. To develop RGB image acquisition program, image acquisition toolbox of MATLAB was employed. The main command that was used is *snapshot*. This command acquires single image frame from the connected cameras. By calling *snapshot* in a loop, a new frame will capture in each iteration. This command can use the camera's default resolution or another resolution that was

specified before. To have a reliable and fast geo-tagging process the taken images should be sorted in the temporary memory during data collection, and after finishing data collection they should be saved into the hard drive.

Two model of programs were developed in MATLAB GUI to communicate with the webcams. First model was developed previously by the robotic group of mechanical engineering department of University of Saskatchewan [25]. This program used and evaluated for 2017 and 2018 field experiments.

A newer version of image acquisition program was developed for 2019 field experiments. This program is user friendly and has more features. As can be seen in Figure 3-14, user can select format of saving (.jpg and .png) and resolution of cameras (640\*360, 960\*540, 1280\*720, and 1920\*1080). Table 3-1 shows measured required time for saving images with different resolutions and formats. Moreover, in 2019 version, user can pause the capture cycle of image acquisition and resume it, manually. However, the main advantage of new version image acquisition program is the existence of auto-pause feature. Because the output of GPS receiver is connected to the laptop, GPS string should be used for geo-tagging and the heading angle of vehicle can be extracted from this string as discussed in section 2.7. By using auto-pause option, program will be paused automatically in the places that vehicle is turning. User can determine two valid heading for the vehicle and tolerance value for them.

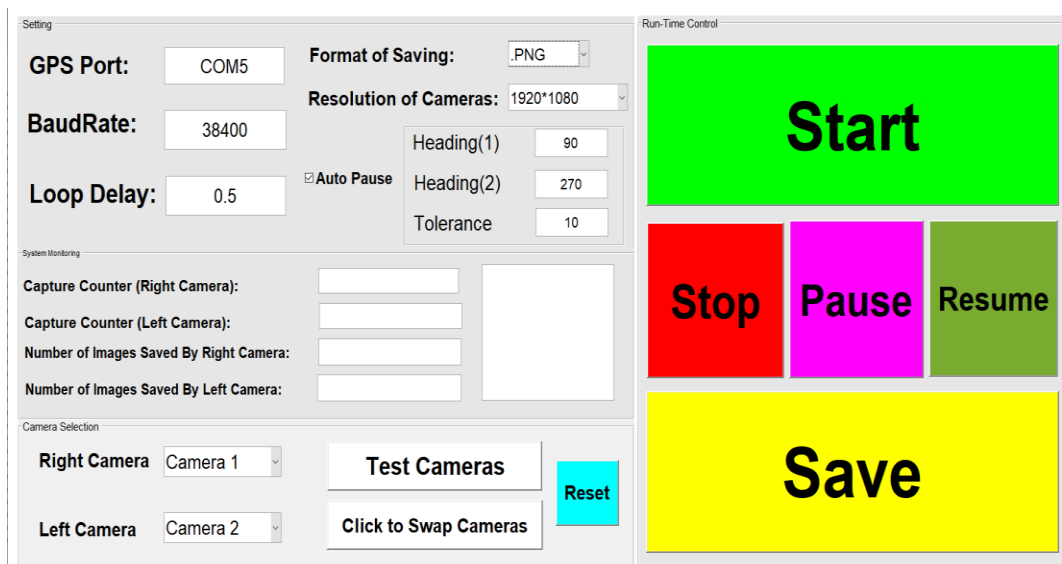


Figure 3- 14: The developed GUI for image acquisition program for RGB cameras

*Table 3- 1: Spent time for saving RGB images with different resolutions and formats*

No.	Resolution	Format	Size of each picture (average)	Number of captured images	Size of captured images	Required Time for saving images on the hard drive
Test 1	1920*1080	.png	4 MB	1658	6.55 GB	16:00
Test 2	1920*1080	.jpg	600 KB	1656	885 MB	1:30
Test 3	1280*720	.png	2.2 MB	1640	3.13 GB	6:00

For example, in Figure 3-15, by determining 90 degree for **Heading 1**, 270 degree for **Heading 2**, and 10 degree for **Tolerance**, image acquisition program will work for the headings that are between 80 to 100 degree and 260 and 280 degree. Thus, image acquisition program should be paused automatically, when vehicle is in position 3 or 4.

This program was tested and used in the laboratory condition and during field experiments. It was found that the program is working reliably and accurately. Table 3.2 compares number of captured images with the image acquisition program with and without auto-pause option for the studied wheat field in the 2019 data collections. From this table, it can be said that by using auto-pause feature, the image acquisition system captures just proper and valid images and as a result less time spent, which is more than 20% improvement in saving time. Figure 3-16 illustrates the flowchart of image acquisition program for RGB cameras.

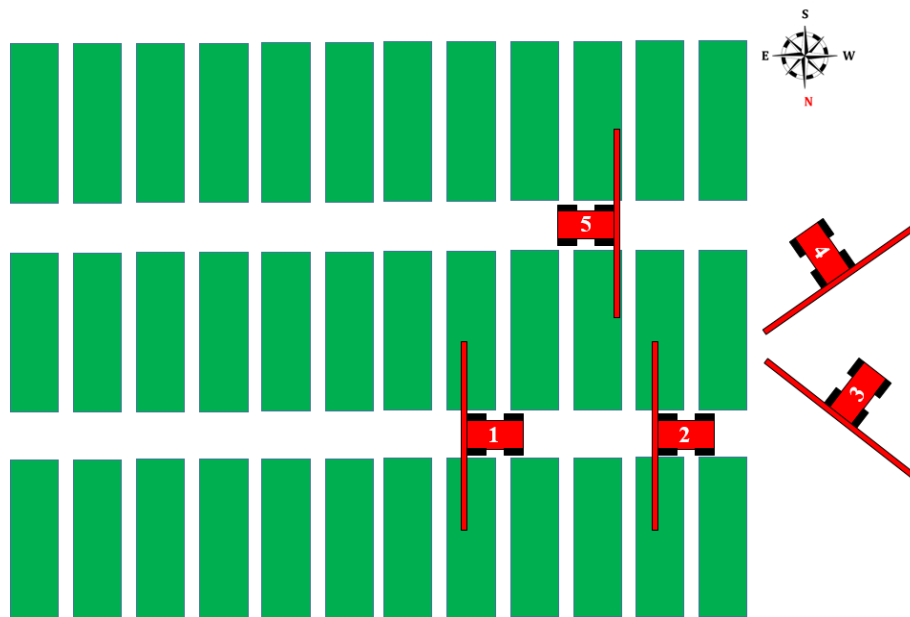


*Figure 3- 15: Automatic pause of image acquisition program during the data collection*

Table 3- 2: Comparison between the operation of developed image acquisition program for RGB images with and without auto-pause option for the entire studied wheat field

No.	Mode of image acquisition program	Format	Number of captured images
Test 1	With auto-pause feature	.png	~1900
Test 2	Without auto-pause feature	.png	~2400

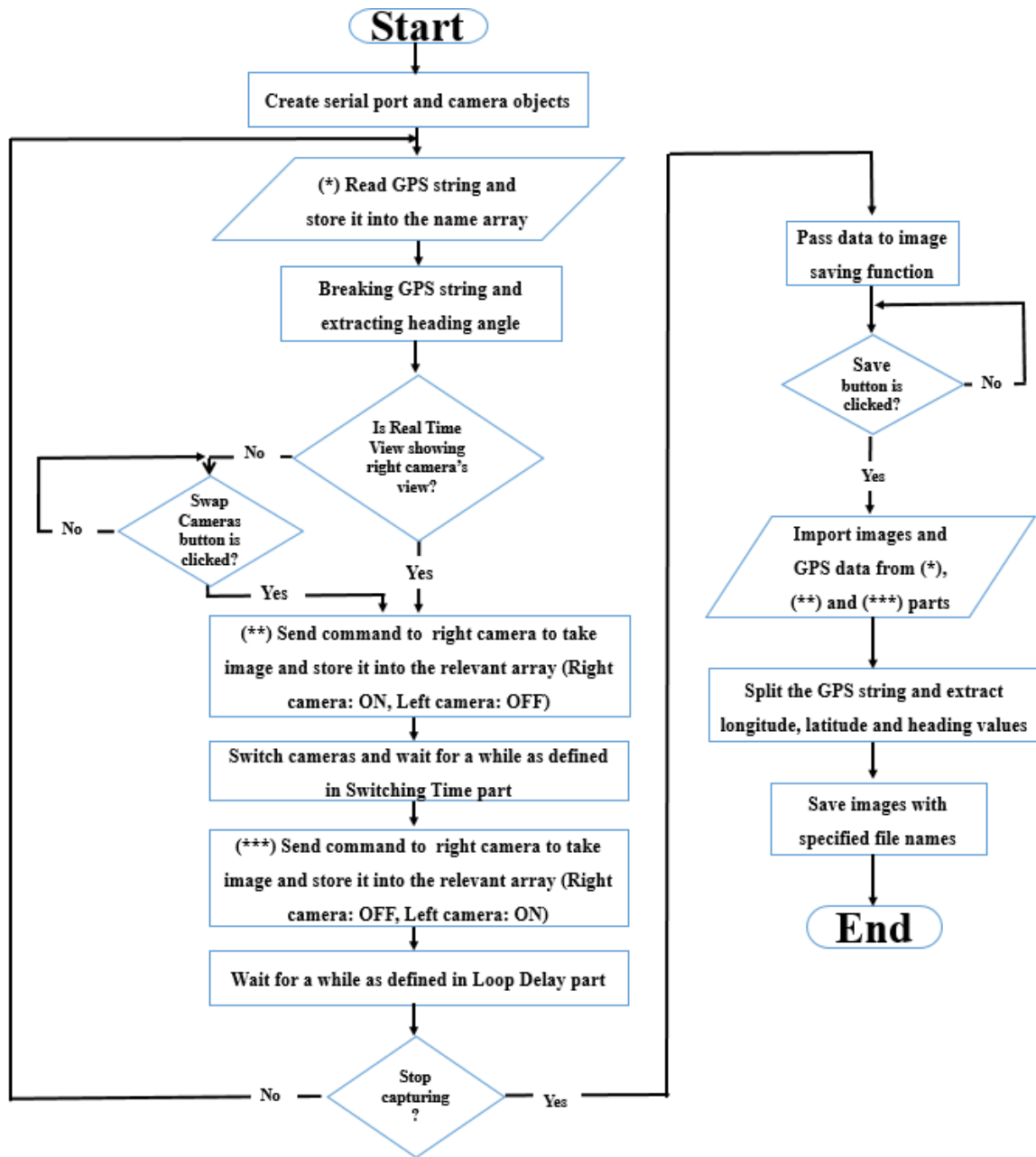


Figure 3- 16: The flowchart of developed image acquisition program for RGB cameras

### 3.4.2. Image acquisition program for multispectral camera

This sensor was added in late 2018 growing season, but wasn't fully incorporated into HTPP until 2019 growing season (May-Aug). Another program was developed for image acquisition of multispectral cameras. This program is written in the MATLAB and for its development, none of MATLAB toolboxes was used. However, *ActiveX* control unit was used for developing of this program. *ActiveX* is a software framework that adapts its earlier COM (Component Object Model) and is one of the main technologies used in component-based software engineering. In the developed image acquisition program for multispectral cameras, *ActiveX* prepares real-time view of connected multispectral camera to the selected COM port as can be seen in the Figure 3-17.

One of the issues with the selected model of multispectral camera is that the real time view of just one camera can be monitored in each moment as can be seen in Figure 3-17. Since, the HTPP needs one multispectral camera for each side of the mechanical boom, two cameras are needed, and they should be switched continuously with each other after taking images during the data collection period. User can import switching time between cameras. After several tests in the laboratory conditions, it was realized that the minimum switching time value for reliable operation of developed program is 0.08 second. Same as image acquisition program for RGB cameras, in this program all taken images are sorted in the temporary memory when tagging with geospatial information during the data collection. After image collection are concluded, sorted images are saved into the hard drive using *.png* format.



Figure 3- 17: The developed GUI for image acquisition program for multispectral cameras

This program is developed specifically for multispectral image acquisition. For extracting NDVI images and information, another program was used, which will be discussed in the next section. Figure 3-18 illustrates the flowchart of multispectral image acquisition program.

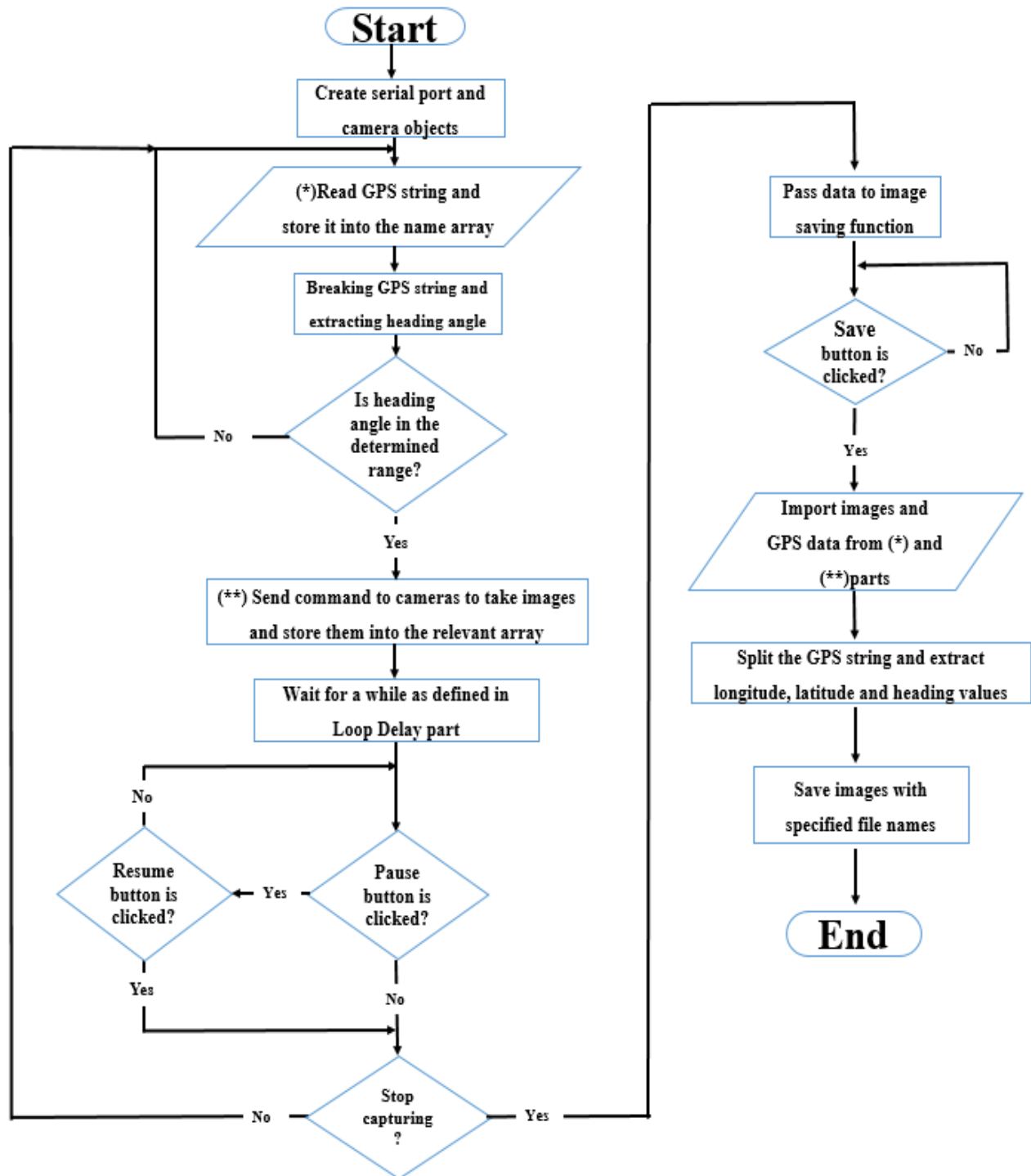


Figure 3- 18: The flowchart of developed image acquisition program for multispectral cameras



### 3.5. Multispectral images post processing program

As discussed in the previous section, using multispectral images, NDVI information of crops can be extracted. The NDVI value is an indicator that quantifies live green vegetation index.

The msCAM CMV4000 is the model of selected multispectral camera used in our HTPP. A captured image through this camera has four bands as 580, 660, 735 and 820 nm as can be seen in Figure 3-19. This camera uses a MFA, (Multispectral Filter Array) that incorporates proprietary pixelated band pass filters to break down the image (.PNG) into smaller parts. Therefore, each band's picture can be extracted from the captured multispectral image. As discussed in chapter two, NDVI information can be calculated and found in two different range by using following equations:

$$\text{For -1 to +1 Range: } NDVI = \frac{NIR - Red}{NIR + Red} \quad (3-3)$$

$$\text{For 0 to +1 Range: } NDVI = \frac{NIR}{NIR + Red} \quad (3-4)$$

Where *Red* and *NIR* (Near Infrared) are two basic spectral reflectance information of red and near-infrared wavelengths. The wavelengths of different spectral bands are [4-6]:

- **Blue**, 450–515..520 nm
- **Green**, 515..520–590..600 nm
- **Red**, 600..630–680..690 nm
- **Red Edge (RE)**, 690..700-750 nm
- **Near infrared (NIR)**, 750–900 nm

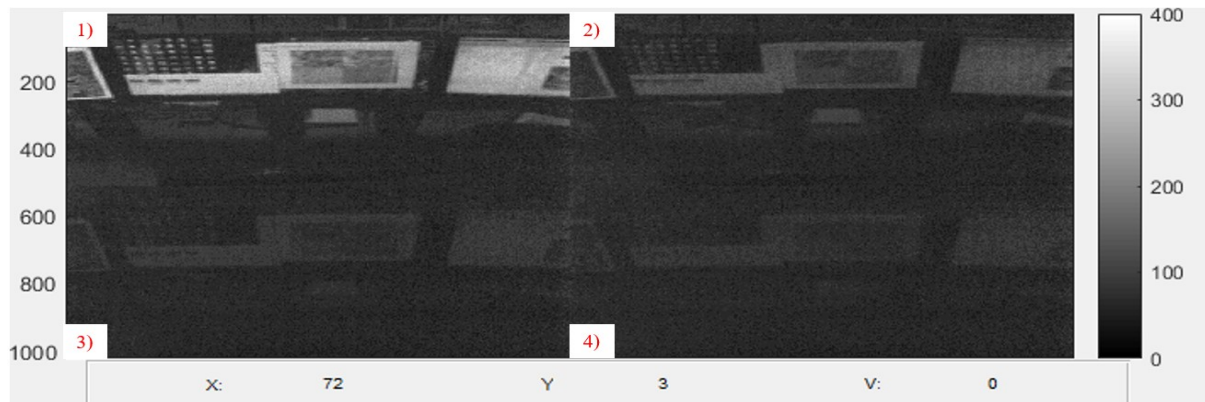


Figure 3- 19: A multispectral image with four bands as 1) 580, 2) 660, 3) 735, and 4) 820 nm

By considering these ranges, channels 1 to 4 of captured images can be considered respectively as Green, Red, RE and NIR spectral bands. Therefore, using pixel information of channels 2 and 4, and also using Eq. 3-3 and Eq. 3-4, NDVI information of imported image can be calculated. For this purpose, a user friendly program was developed in MATLAB. Figure 3-20 illustrates the GUI of multispectral image's post-processing program. By using this program minimum, maximum, range, standard derivation and mean values of imported multispectral image's pixels can be found in two different ranges, which are 0 to +1 and -1 to +1. Furthermore, the histogram of NDVI values in the imported image, NDVI image (gray and color) and its detail information can be extracted as can be seen in Figure3- 21. Figure 3-22 illustrates the flowchart of the multispectral image's post-processing program.

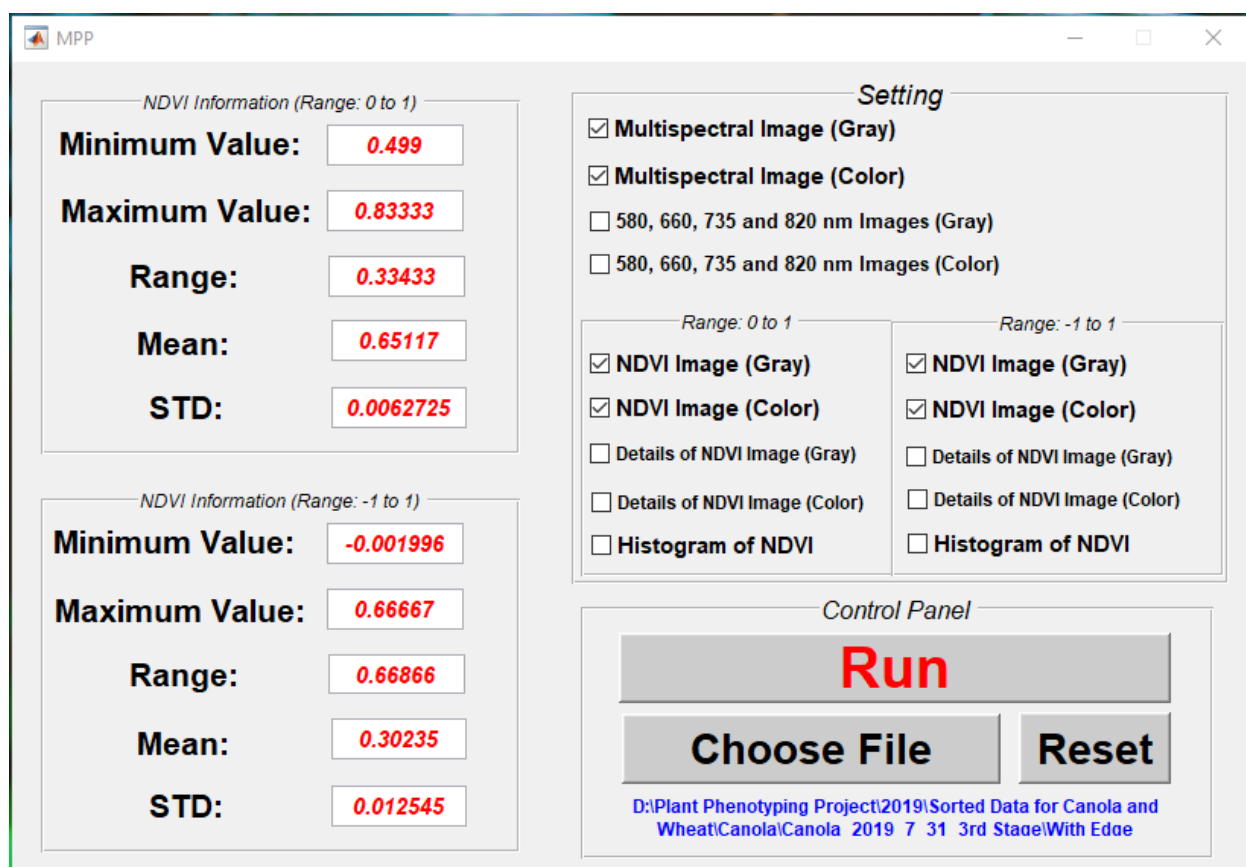


Figure 3- 20: The developed GUI for multispectral image's post-processing program

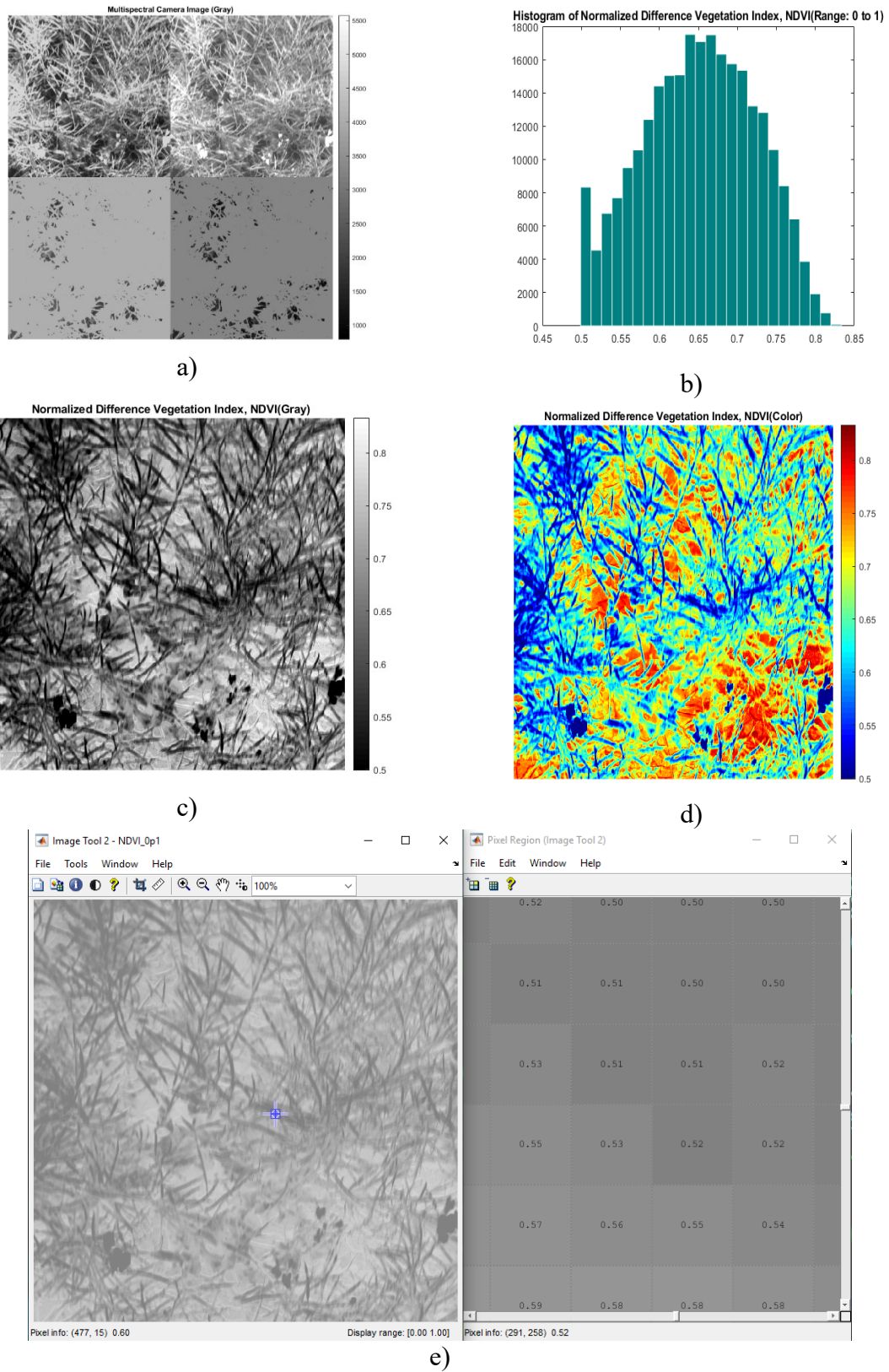
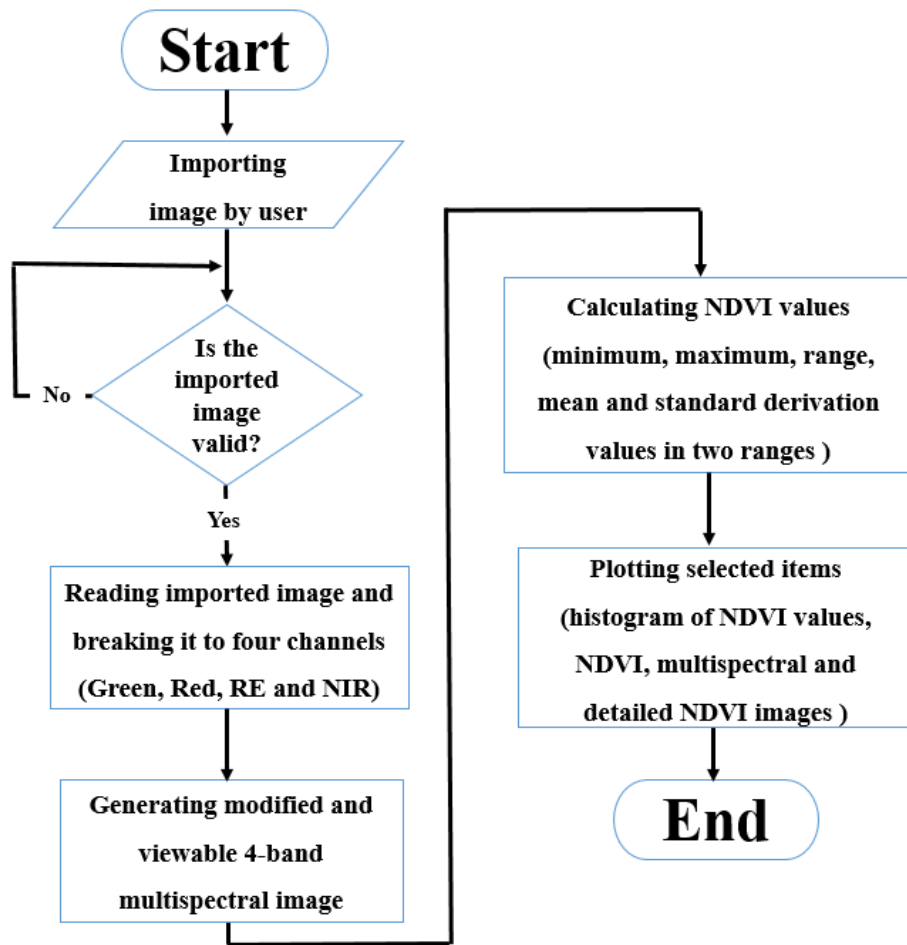


Figure 3- 21: Sample of extracted NDVI information via multispectral image's post processing program a) modified multispectral image of 4 bands b) histogram of NDVI pixels c) gray NDVI image d) color NDVI image e) detailed information of NDVI image



*Figure 3- 22: The flowchart of developed multispectral image's pre-processing program*

### 3.6. Data visualization programs

To analyze and monitor collected data and images a data visualization program was developed. By using this program breeder can load and monitor the field of map and collected data/images on a map. Moreover, by using this program geo-referencing of collected data/images were verified which will be discussed in chapter 4.

The collected phenotypic database consists of reordered data by different sensors such as infrared thermometer, ambient temperature/humidity, Crop Circle and ultrasonic sensors (Figure 3-23). The number of records (number of rows) depends on the excitation time of data acquisition program and the scale of the field monitored. All records of this database have geospatial information of that record. Column 7 of this database is representing GPS string and latitude,

longitude and heading angle of vehicle can be extracted from it. For example, consider the GPS string as

*\$GPRMC,210952,A,5220.187369,N,10617.00265,W,1.5,90.2,020818,15.2,E\*61*

The heading angle of vehicle is 90.2 degree with respect to the North Pole. Longitude and latitude are 5220.187369 and 10631.10617.00265, respectively, which are in degree minutes format.

Furthermore, all collected RGB and multispectral images are tagged with the GPS information during the operation of image acquisition programs like

*Latitude, Longitude, Heading, R/L*

For example, consider the tag of image as 5220.21174957, 10617.36839173, 270.2, L.png. Longitude and latitude are 5220.21174957 and 10617.36839173, respectively. The heading angle is 270.2 and this image was taken by Left side's camera.

All of these longitude and latitude values (for data and image) are in degrees minute format ( $Lat_{DM}/Lon_{DM}$ ) and they are converted to decimal degrees format ( $Lat_{DD}/Lon_{DD}$ ) using Eq.3-1 and 3-2. It is mentionable that all of these geospatial information (for data and image) are related to the location of GPS receiver. By using recorded GPS information and Eq. 2-24 to 2-26, longitude and latitude information of each device can be found for each record and this calculation is necessary for data and images loading. From Figure 3-24, it can be found that the distances between the devices are different and their angle with respect to the North Pole should be considered in using mentioned equations. IRT, US and CC are abbreviations of Inferred Thermometer, Ultrasonic Sensor and Crop Circle, respectively.

	A	B	C	D	E	F	G
1	20:35.5	0	36.36871	38.3862	.20,0.0692	.19,0.0875	8.2,150819,15.1,E*5C \$GPRMC,172032,A,5220.28090143,N,10617.35013314,W,0.0,268.2,15
2	20:35.7	1	36.39453	38.39807	0.24,0.26,(	0.23,0.27,(	8.2,150819,15.1,E*59 \$GPRMC,172033,A,5220.28090670,N,10617.35012813,W,0.0,268.2,15
3	#####	2	36.40829	38.42349	0.24,0.26,(	0.23,0.27,(	\$GPRMC,172033,A,5220.28090657,N,10617.35012848,W,0.0,268.2,150819,15.1,E*5D
4	20:36.2	3	36.45657	38.36581	0.24,0.26,(	0.23,0.27,(	\$GPRMC,172033,A,5220.28090654,N,10617.35012848,W,0.0,268.2,150819,15.1,E*5E
5	20:36.5	4	36.50485	38.35562	0.23,0.27,(	0.23,0.27,(	\$GPRMC,172033,A,5220.28090665,N,10617.35012725,W,0.0,268.2,150819,15.1,E*58
6	20:36.8	5	36.56683	38.33356	0.23,0.26,(	0.24,0.26,(	8.2,150819,15.1,E*58 \$GPRMC,172034,A,5220.28090143,N,10617.35012786,W,0.0,268.2,15
7	#####	6	36.58057	38.37091	0.23,0.26,(	0.23,0.27,(	\$GPRMC,172034,A,5220.28090155,N,10617.35012786,W,0.0,268.2,150819,15.1,E*52
8	20:37.2	7	36.61505	38.38446	0.23,0.27,(	0.23,0.27,(	\$GPRMC,172034,A,5220.28090169,N,10617.35012813,W,0.0,268.2,150819,15.1,E*5E
9	20:37.5	8	36.64081	38.44553	0.23,0.27,(	0.23,0.27,(	\$GPRMC,172034,A,5220.28090158,N,10617.35012725,W,0.0,268.2,150819,15.1,E*56
10	20:37.7	9	36.65457	38.45911	701,0.1448	0.24,0.26,(	8.2,150819,15.1,E*57 \$GPRMC,172035,A,5220.28090144,N,10617.35013314,W,0.0,268.2,15
11	#####	10	36.61841	38.50656	0.23,0.27,(	0.24,0.26,(	\$GPRMC,172035,A,5220.28090155,N,10617.35013228,W,0.0,268.2,150819,15.1,E*53
12	20:38.2	11	36.60635	38.50827	0.23,0.27,(	1503 0.24,	\$GPRMC,172035,A,5220.28090151,N,10617.35012786,W,0.0,268.2,150819,15.1,E*57
13	20:38.5	12	36.57187	38.55911	0.23,0.27,(	0.23,0.27,(	\$GPRMC,172035,A,5220.28090668,N,10617.35012849,W,0.0,268.2,150819,15.1,E*56
14	20:38.7	13	36.58563	38.56927	0.23,0.27,(	0.23,0.26,(	8.2,150819,15.1,E*54 \$GPRMC,172036,A,5220.28090160,N,10617.35013366,W,0.0,268.2,15
15	#####	14	36.62347	38.62009	0.23,0.27,(	0.23,0.27,(	\$GPRMC,172036,A,5220.28090195,N,10617.35012922,W,0.0,268.2,150819,15.1,E*5C

Figure 3- 23: A screenshot of a sample phenotypic database (details is explained in Figure 3-13)

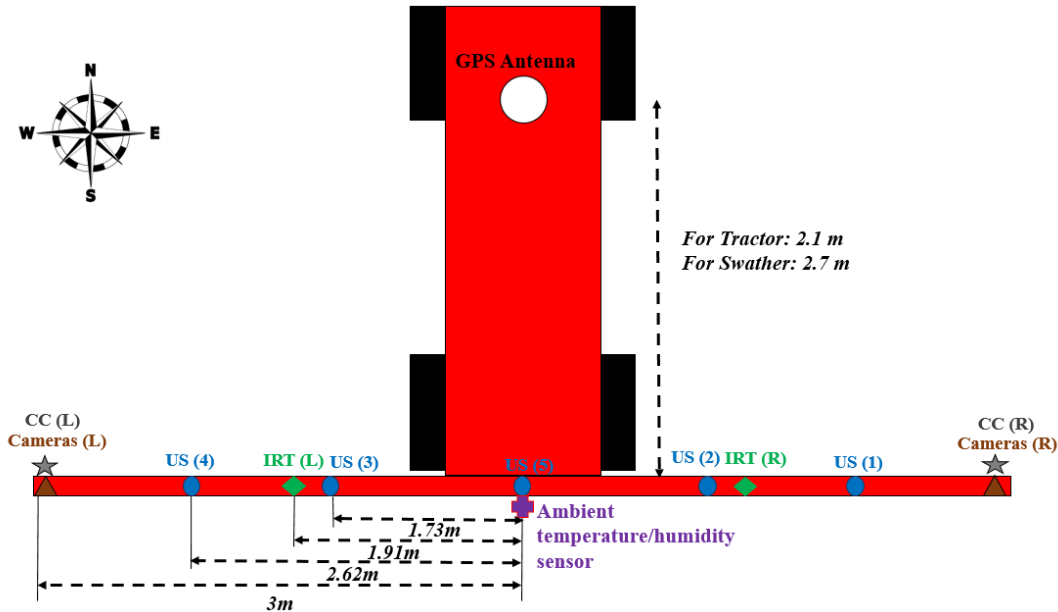


Figure 3- 24: Distances of devices in the developed HTPP

Two versions of visualization program was developed for further analysis of collected data. Both of them were written in MATLAB. It can be said that the crucial part to use these programs is using the map of field. The map should be prepared by using mapping module. In the next sections, two version of developed visualization programs is discussed in details.

### 3.6.1. Data visualization program- Version 2018

This program has several features such as importing the map of field, importing stored phenotypic database and collected images in their corresponding plot locations, zooming and panning into desired plot for closer investigations, and monitoring loaded data and images. Figure 3-25 illustrates a screenshot of the developed data visualization program.

All collected data and images, which are geo-tagged during the data collection phase, can be loaded through this program for post-processing. This program has several buttons, as shown in the right hand side of Figure 3-25 with blue colors. Also, data display area is located in the right bottom corner of developed GUI. The target-monitoring field should be mapped by mapping programs in a previous stage (more detailed information can be found in section 3.2.1). An Excel sheet that has longitude and latitude information of each plot's center is using to import and draw the map of studied field. For finding coordinates (longitude and latitude) of each sensor and camera based on the GPS antenna's location, distances and angles between devices and antenna was considered as shown in Figure 3-24.



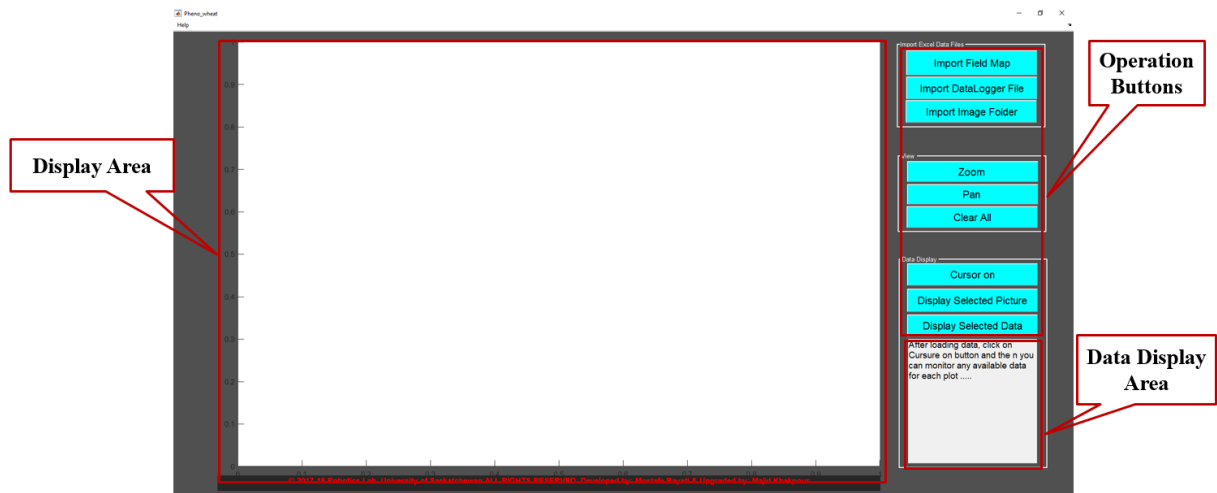


Figure 3- 25: The developed GUI for data visualization program- Version 2018

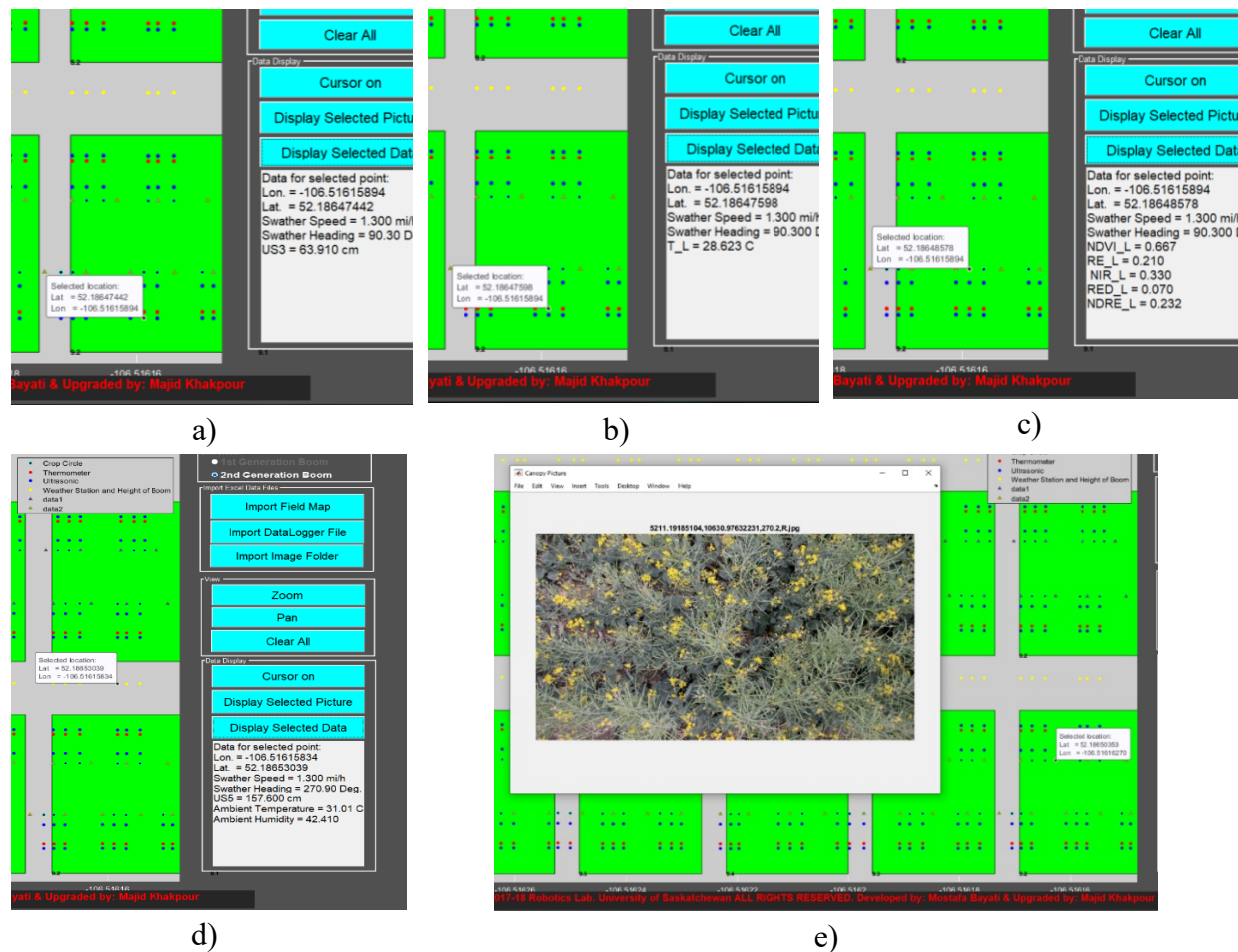


Figure 3- 26: Monitoring five sample data points via data visualization program-Version 2018 a) Height b) Temperature c) NDVI d) Boom's height and ambient temperature/humidity e) RGB image

Detail of this program can be found in Appendix C. Figure 3-26 illustrates examples of monitoring different data and image objects using developed visualization program. After loading data and images, green and red triangles, blue, black and red dots appear in the display area. They represent respectively the locations of left and right cameras, ultrasonic, Crop Circle, infrared thermometer sensors. By choosing any of these icons, the measured data and captured images appears. Also, yellow dots are used for height of the boom, ambient temperature and humidity. The flowchart of different operation of this visualization program can be found in Figure 3-27.

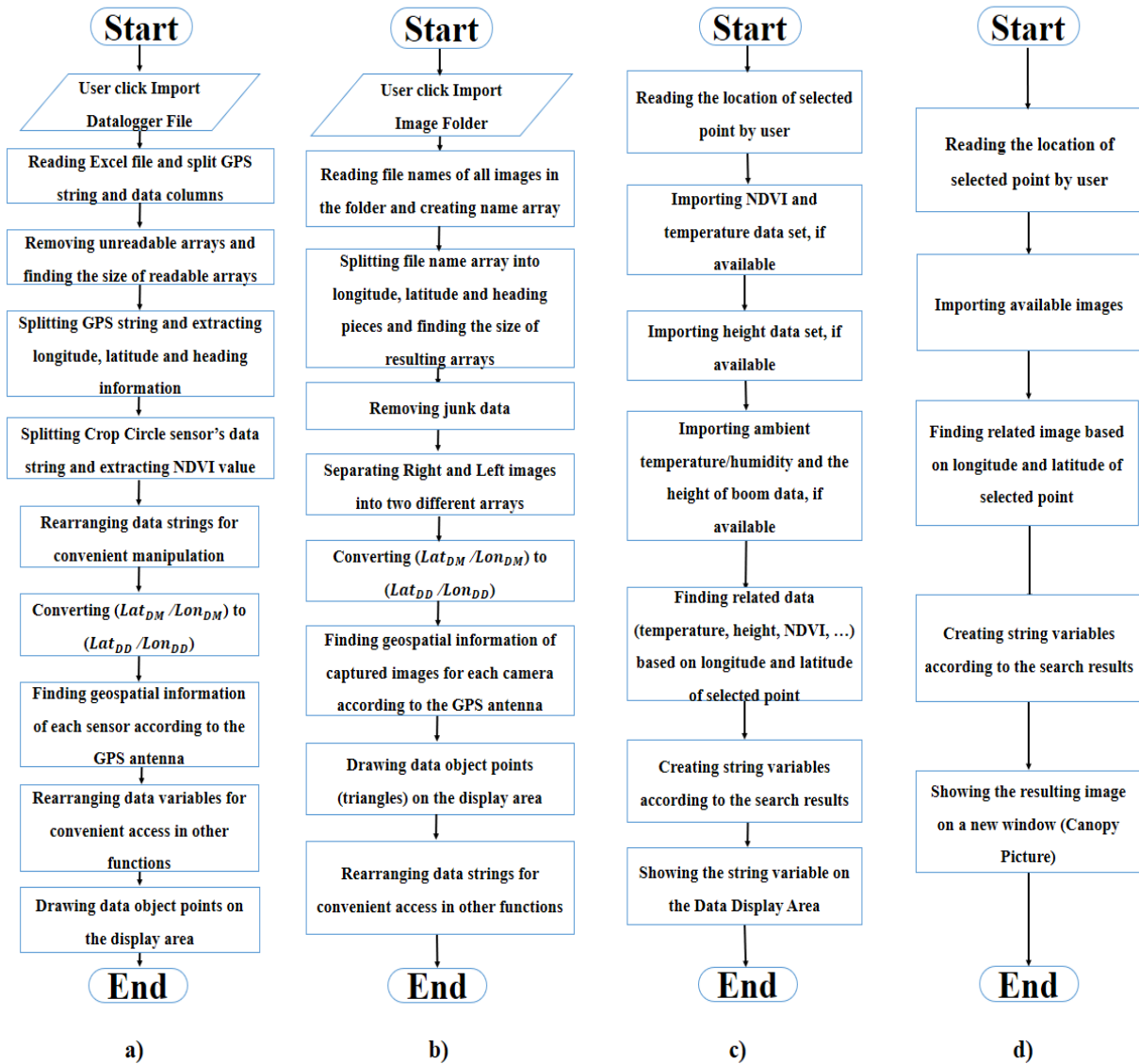


Figure 3- 27: Flowchart of different functions of developed data visualization program-Version 2018 a) Visualizing collected data b) Visualizing captured images c) Monitoring an available data point d) Monitoring an available image



### 3.6.2. Data visualization program- Version 2019

A new version of data visualization program which is user-friendly was developed for visualization of collected data and images on 2019 data collection. This program was written in MATLAB and is one of Pheno-VISDM3's modules. The functions, of this program are mostly like the previous version (2018 version), which was discussed in section 3.6.1. New version has several advantages such as:

- Flexibility in applying edge effect, path and gap values.
- Higher speed in the loading and sorting of collected data and images.
- Indicating that the loaded data is inside (with red color) or outside (with blue color) of plots.
- Showing more useful information in the data display area.

The main difference between 2018 and 2019 versions is that in the 2019 version, user is able to utilize it after sorting collected data and images. In other words, after using data/image sorting module of Pheno-VISDM3 essential files will be created, which are necessary for using data visualization module. Data and image sorting module of Pheno-VISDM3 will be discussed in the next section. User has access to this program through the main window of Pheno-VISDM3 as can be seen in Figure 3-28. To utilize this program, several steps should be completed. The manual of this program with its details can be found in Appendix C.

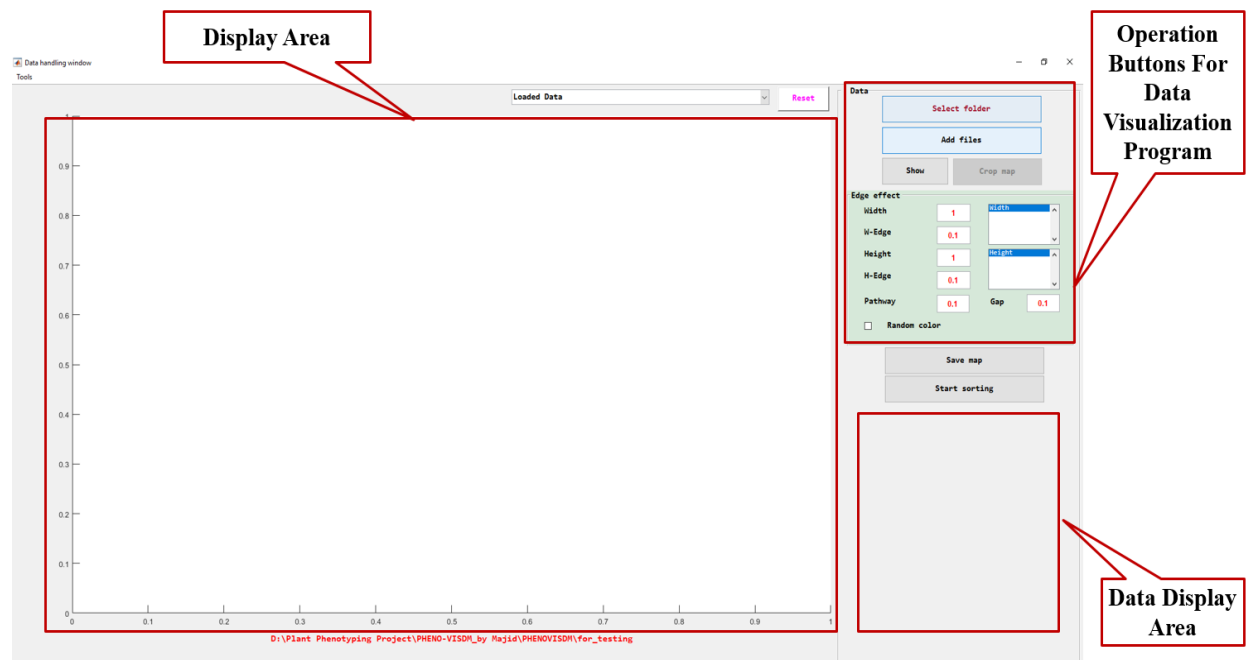


Figure 3- 28: The developed GUI for data visualization module of Pheno-VISDM3

Figure 3-29 illustrates examples of monitoring different data and image objects by using visualization module of Pheno-VISDM3. By selecting “**Cursor**” function and clicking on the all of the graphical objects, user can monitor related value or image to them. Red and blue colored objects are related to the records that are inside and outside of plots, respectively.

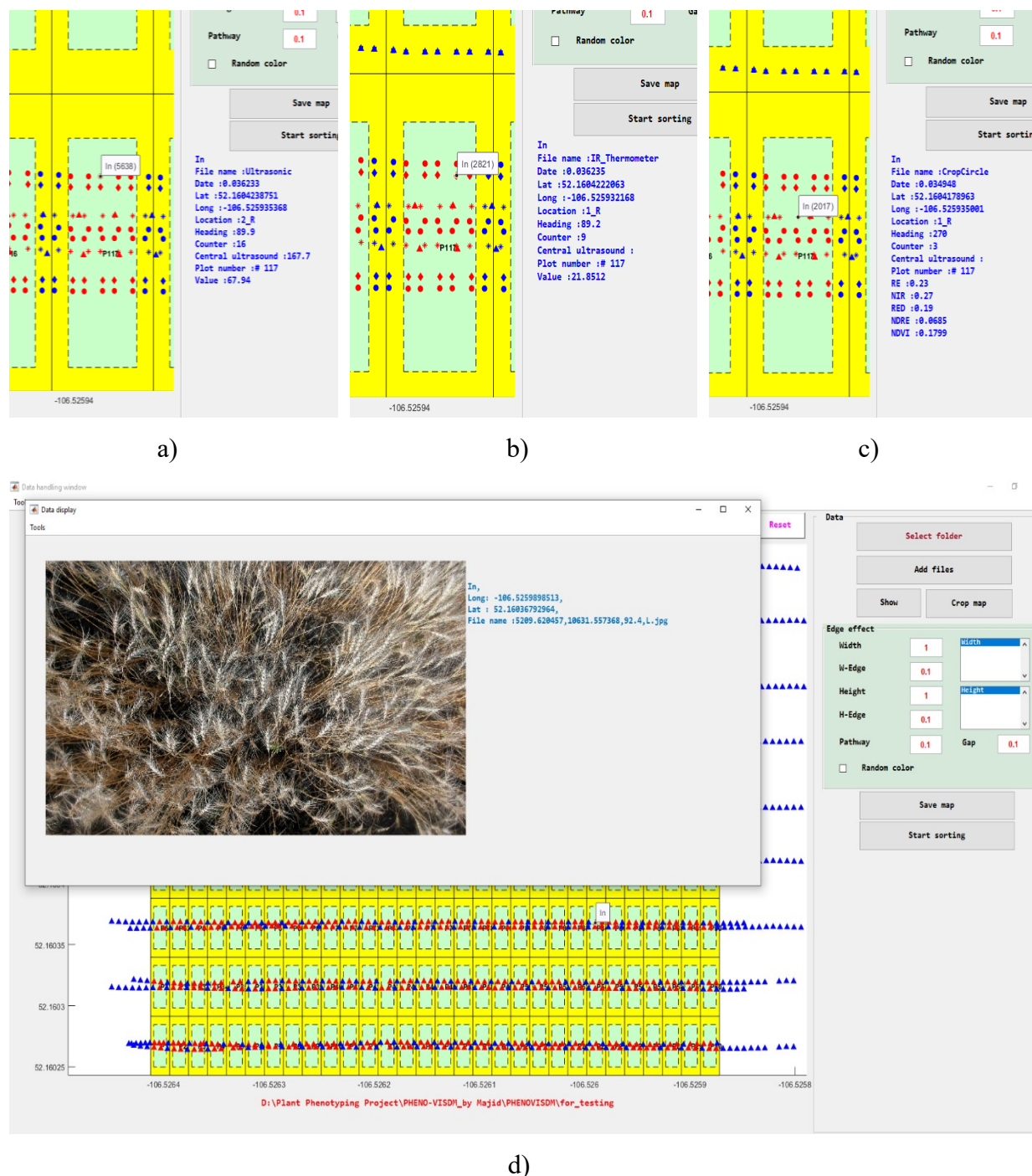


Figure 3- 29: Monitoring four sample data points via developed GUI for data visualization module of Pheno-VISDM3 a) Height b) Temperature c) NDVI d) RGB image

### 3.7. Sorting program for data and images

The developed data visualization programs are useful when a breeder wants to observe the collected information (sensors' records and taken images) in different regions of a particular plot.

Another program was developed for having statistically analysis over the collected data for the entire field. Using this program, all collected data (raw phenotypic database) and images (RGB and multispectral) can be sorted based on plot numbers.

This program generates two outputs. One of the outputs is an Excel sheet that summarizes all collected data with associating each data to the related plot as can be seen in Figure 3-30.

This Excel file has three sheets as

- **CropCircle Sheet:** This sheet indicates vegetation index or NDVI measurements of each particular plot.
- **Ultrasonic Sheet:** This sheet shows height records of each particular plot. Also, for each record, the height of boom is associated.
- **IR\_Thermometor Sheet:** This sheet shows particular plot's temperature records. For each record, the ambient temperature and humidity values are identified.

All three sheets of Excel file have “**Date**”, “**Plot Counter**” and “**Senor Location**” columns that represent the time of each record, counting number of associated data values for each plot, and the location of sensor that recorded the value, respectively. These Excel sheets ease statistical analysis of collected data according to the plot numbers.

Other output of sorting program is a folder of sorted images. Inside of generated main-file there are sub-folders that are tagged with plots' names and related taken RGB or multispectral images are copied to the inside of each related folder as can be seen in Figure 3-31. This feature of image sorting program is useful for using multispectral image's post-processing program. User can select the target plot and use multispectral images that are inside of the folder with related tag.

	A	B	C	D	E	F	G	H	I	J
1	Date	RE	NIR	RED	NDRE	NDVI	Plot number	Plot counter	Sensor location	
2	12:13:00 PM	0.21	0.31	0.09	0.1928	0.5426	# 2.1	1	2_L	
3	12:13:37 AM	0.21	0.32	0.08	0.2051	0.5846	# 2.1	2	2_L	
4	12:13:37 AM	0.21	0.32	0.1	0.2116	0.5416	# 2.1	3	2_L	
5	12:13:00 PM	0.21	0.33	0.05	0.2341	0.7177	# 2.1	4	2_L	
6	12:13:38 AM	0.21	0.32	0.06	0.2048	0.6771	# 2.1	5	2_L	
7	12:17:00 PM	0.21	0.33	0.05	0.2244	0.7198	# 2.1	6	2_L	
8	12:17:27 AM	0.21	0.33	0.05	0.2226	0.7434	# 2.1	7	2_L	
9	12:17:27 AM	0.21	0.32	0.06	0.2154	0.6863	# 2.1	8	2_L	
10	12:17:00 PM	0.21	0.32	0.07	0.2042	0.6362	# 2.1	9	2_L	
11	12:13:39 AM	0.21	0.31	0.12	0.1941	0.4583	# 2.2	1	2_L	
12	12:13:00 PM	0.21	0.32	0.08	0.1973	0.6151	# 2.2	2	2_L	
13	12:13:40 AM	0.21	0.32	0.08	0.2045	0.5548	# 2.2	2	2_L	

a)

	A	B	C	D	E	F	G	H	I	J	K
1	Date	Value	Plot number	Plot counter	Sensor location			AmbientTemperature			AmbientHumidity
2	12:13:00 PM	29.17783	# 2.1	1	2_L			22.11			66.08
3	12:13:37 AM	26.37866	# 2.1	2	2_L			22.11			66.05
4	12:13:37 AM	24.90762	# 2.1	3	2_L			22.11			66.03
5	12:13:00 PM	24.16074	# 2.1	4	2_L			22.11			66.02
6	12:13:38 AM	24.10492	# 2.1	5	2_L			22.11			66.02
7	12:17:00 PM	23.86624	# 2.1	6	2_L			23.33			66.21
8	12:17:27 AM	24.09073	# 2.1	7	2_L			23.33			66.18
9	12:17:27 AM	24.27277	# 2.1	8	2_L			23.33			66.16
10	12:17:00 PM	24.58005	# 2.1	9	2_L			23.33			66.1
11	12:13:39 AM	24.22049	# 2.2	1	2_L			22.11			66.93
12	12:13:00 PM	23.97299	# 2.2	2	2_L			22.11			67.54
13	12:13:40 AM	22.56962	# 2.2	2	2_L			22.11			67.71

b)

	A	B	C	D	E	F	G
1	Date	Value	Plot number	Plot counter	Sensor location	entral ultrasound	
2	12:13:00 PM	114.3	# 2.1	1	3_L	157.9	
3	12:13:00 PM	101.7	# 2.1	2	4_L	157.9	
4	12:13:37 AM	89.9	# 2.1	3	3_L	157.9	
5	12:13:37 AM	106.5	# 2.1	4	4_L	157.9	
6	12:13:37 AM	89.8	# 2.1	5	3_L	157.9	
7	12:13:37 AM	106.4	# 2.1	6	4_L	157.9	
8	12:13:00 PM	85.2	# 2.1	7	3_L	157.9	
9	12:13:00 PM	87.6	# 2.1	8	4_L	157.9	
10	12:13:38 AM	93	# 2.1	9	3_L	157.9	
11	12:13:38 AM	83.9	# 2.1	10	4_L	157.9	
12	12:17:00 PM	92	# 2.1	11	3_L	158	
13	12:13:40 AM	114.4	# 2.1	12	4_L	158	

c)

Figure 3- 30: A screen of generated Excel sheets for a) NDVI b) temperature c) height measurements via the developed data/image sorting module of Pheno-VISDM3

Data and image sorting module of Pheno-VISDM3 was written in MATLAB and user has access to this module through the main window of Pheno-VISDM3 (Figure 3-28) by clicking on the “**Start sorting**” button. Figure 3-32 illustrates developed GUI for data and image sorting module of Pheno-VISDM3. Details of this program can be found in Appendix C.

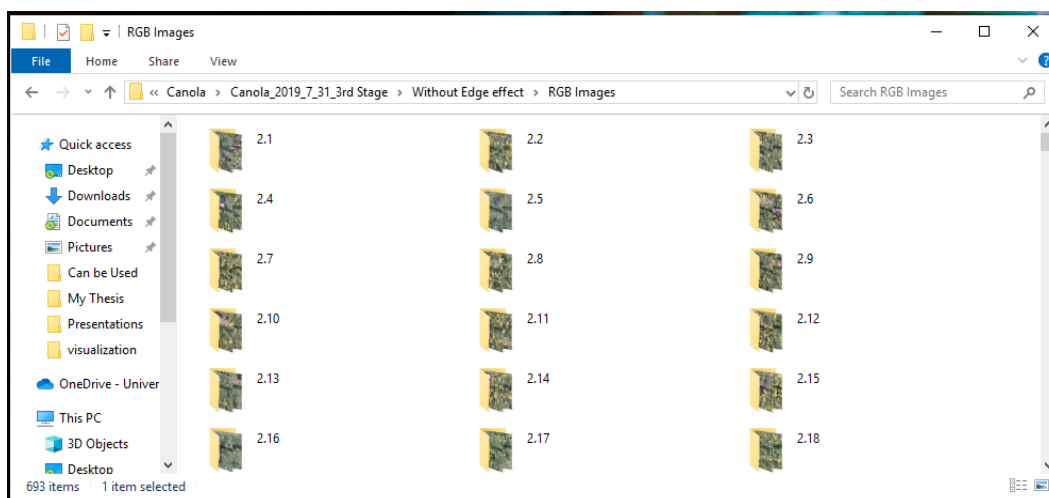


Figure 3- 31: A screen of generated images' folders via the developed data/image sorting module of Pheno-VISDM3



Figure 3- 32: The sorting data and images window of developed GUI for data and image sorting module of Pheno-VISDM3

### **3.8. Summary**

This chapter discussed software packages for the developed HTPP, which was one of the main objectives for this research. Having reliable and accurate programs is critical fact in this study. This chapter covered the developed programs for mapping the field, data acquisition, image acquisition (RGB and multispectral), multispectral image's post-processing, data visualization and data sorting. For most of topics two models were discussed, 2018 and 2019 versions. The 2019 version of programs are working more accurately and they are more user friendly and reliable. Each program was explained with detail in the related sections.

In next chapter, experimental results for the wheat and canola nurseries that were achieved using the hardware and software of developed HTPP are explained. I would like to acknowledge Dr. Rahim Oraji and Mostafa Bayati's contributions in developing of programs.

## **CHAPTER 4- Experimental results**

### **4.1. Introduction**

In this chapter, results that are achieved from experimental tests are discussed. To examine the performance of developed HTPP, several field tests were accomplished during the growing seasons of 2018 and 2019 that is May to August. The target fields were comprised from wheat (270 and 270 plots) and canola (3000 and 400 plots) canopies.

Several vibration experiments were performance on the mechanical boom to verify the reliability of its structure. The mechanical boom carried properly and reliably all devices during the data collections.

The assembled hardware of HTPP is tested in breeding field conditions. Furthermore, the developed programs are examined in in all phases of experiments (field mapping, data collection, visualization, sorting and post-processing).

Data collection were done in five stages for each of nurseries as seedling, start of flowering, end of flowering, start of maturity and end of maturity statues. The date of these stages were estimated by the breeders and agronomists. These dates were variable based on the weather conditions. Collected data are analyzed for different genotypes. The reliability and accuracy of measurements are discussed in this chapter.

### **4.2. Monitored Canola fields**

Several field experiments were performed in two canola fields, which were large-size (around 400 rectangular plots) and mega-size (around 3000 rectangular plots). These fields were arranged in several rows based on diverse genotypes, on growing seasons of 2018 and 2019. These nurseries were bred by Cargill, Incorporated, Canada. The location of studied nurseries, which are extracted from Google Maps are prepared in Appendix D.

The travelling path was 2 meter for both fields. The dimensions of canola plots were different for each year (Figure 4-1). It is mentionable that winter canola was cultivated between canola plots on 2018 filed, as shown in Figure 4-2. The purpose of cultivating winter canola was creating visible frontier between plots, which is useful for harvesting. Nevertheless, for 2019 field, winter canola was not seeded in the space between plots.

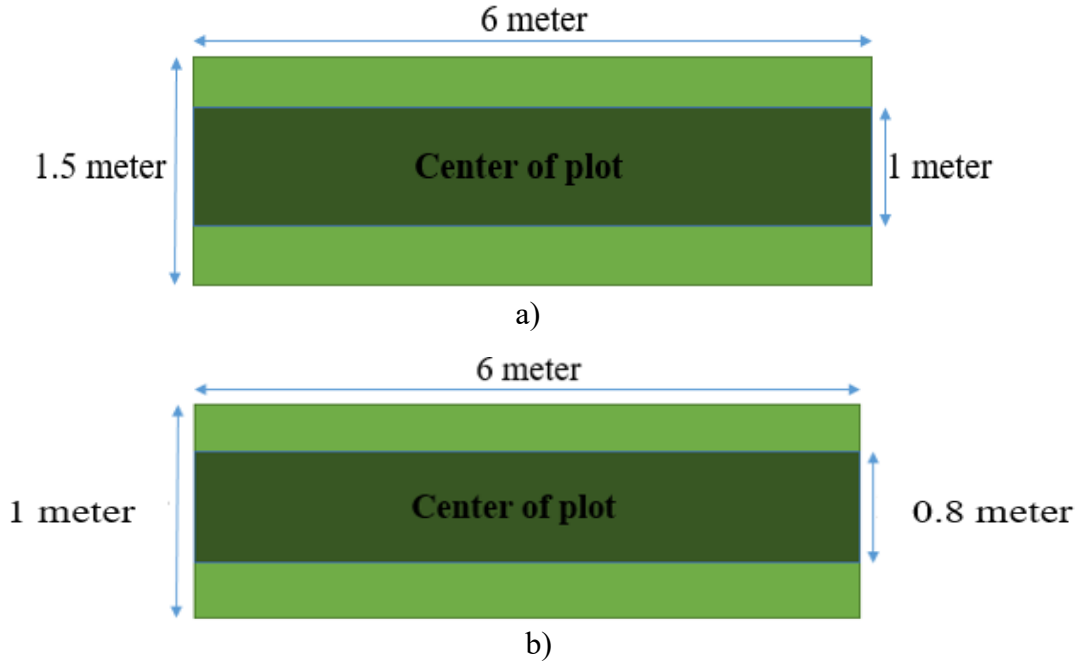


*Figure 4- 1: Dimensions of canola plots on a) 2018 b) 2019 fields*

It should be considered that in this research, there are two ways for sorting the collected data, which are with and without plots edges. When we are talking about edge-effect, we select part of plot as a valid part (Figure 4-1) and data, which is inside of the valid area (dark green) will be analyzed.

As discussed in chapter 2, Swather was selected as the vehicle to carry mechanical boom and utilized devices in Cargill fields. Swather is a semi-autonomous farm vehicle and has auto-steer navigation system, with help from an RTK-GPS with an accuracy of about 1 inch. Several vibration tests were done by mechanical team for different speeds of vehicle and it was concluded that when Swather's speed is 1.6 mph, the measurement devices could collect data reliably without any issue. Therefore, vehicle's speed was set to 1.6 mph (0.7 m/s) during most of data collection.

Moreover, for this speed, proper amount of data can be recorded with each of devices (GPS receiver, sensors and cameras). As discussed in chapter 3, the data acquisition cycle in the program is 250ms. In other words, four sample points can be captured per second. The time which takes for vehicle to pass through a single plot can be calculated from Eq. 4-1.



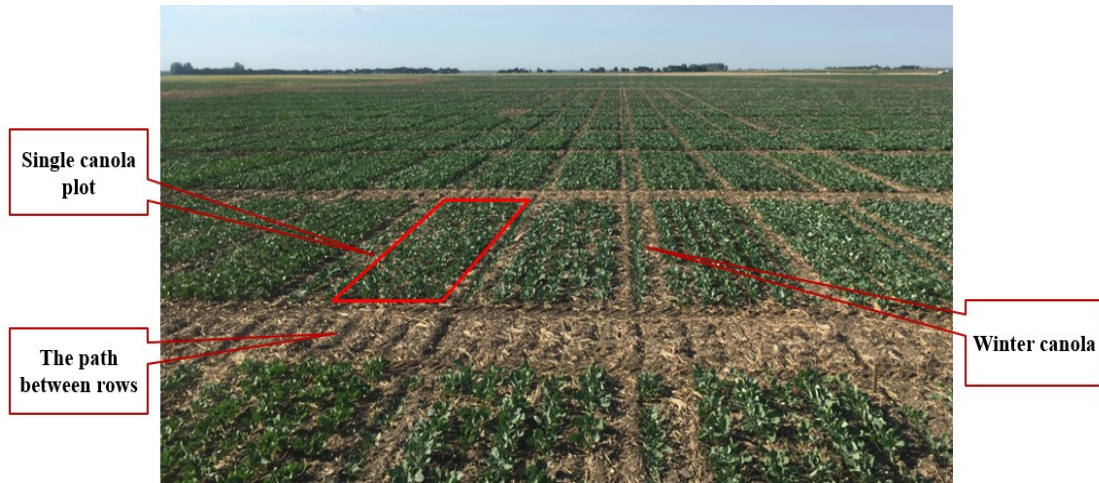


*Figure 4- 2: Studied canola field on 2018 with canola plots and winter canola between them*

$$t = \frac{x}{v} \quad (4-1)$$

Where  $x$  is the width of a single plot and  $v$  is the speed of vehicle (0.7 m/s). Therefore, for  $x= 1.5$  and  $1.8$  meter,  $t$  are 2.14 and 2.57 second, respectively. The number of data sampled per plot ( $X_s$ ) can be calculated from following equation:

$$\frac{X_s \text{ (samples)}}{1 \text{ (samples)}} = \frac{t \text{ (sec)}}{0.25 \text{ sec}} \quad (4-2)$$

Therefore, the number of collected data per plot for 2019 and 2018 canola nurseries in each run are 8-9 and 10-11, respectively. It is mentionable fact that these numbers can vary based on the availability of GPS signal. The field trials for 2018 and 2019 canola nurseries can be found in Appendix E. In the next sections, the collected data from two different canola nurseries is going to be analyzed and discussed.

#### **4.2.1. Analyzing growth of plots for canola field in 2018**

The developed HTPP was utilized to study a canola field with around 3000 plots during growing season on 2018 (June- August). The field had comprised from several genotypes. Each crop's traits such as canopy height, NDVI, temperature, and ambient temperature/humidity were targeted and recorded. Moreover, RGB images of canopies were captured, which prepare more details for breeders and statisticians for further analysis (Figure 4-3).

Five main stages of data collections was determined and completed during the growing season on 2018, as can be seen in Table 4-1. After sorting collected data and images via software package, valuable information were ready for analysis. Plot #30.77 was selected randomly to study its behavior during its growing season on 2018. More examples are prepared in Appendix F. Table 4-2 presents summary of captured data for this plot in 5 days during its growth. Columns (\*) and (\*\*) represent values that were extracted without and with considering edge-effect conditions, respectively.

From Figure 4-4, NDVI values for plot #30.77 was increased after first stage. For third stage this value was decreased and this decrease's reason is flowers of plots. Canopy's flowers made parts of plot yellow and decreased NDVI value (greenness) of crop. At the fourth stage of data collection, which was end of flowering status, NDVI value increased because of flower loosing. Finally, at the last stage, after maturity statues, crop's color was changed to brown and crop was ready for harvest. Moreover, ambient temperature is compared in Figure 4-4 with canopy's temperature, which gives information to breeder about irrigation of canopy. When ambient temperature is warmer than crop's temperature, canopy is under stress. This situation changes the amount of yields for different genotypes. Therefore, stronger genotypes to the temperature variations can be detected. As it was expected, the height of crops were increased gradually during their growth. The relation between height variations during different stages of growth and yield's amount can be extracted for each genotype.

Figure 4-3, shows available images for the targeted plot, which were captured from middle of the plot. These RGB images prepare more detailed information for breeders such as the growth rate of plot. For example, from Figure 4-3, it can be said that at the start of flowering status, NDVI values should decrease, which can be verified with NDVI variation diagram (Figure 4-4). Appendix F represents more examples for analyzes of canola crop's growth during 2018 season.

*Table 4- 1: Stages of data collection on canola 2018 field*

Stage	Description	Date
1 <sup>st</sup> Stage of data collection	Seeding Status	June 19, 2018
2 <sup>nd</sup> Stage of data collection	Flowering Status	June 29, 2018
3 <sup>rd</sup> Stage of data collection	End of Flowering	July 18, 2018
4 <sup>th</sup> Stage of data collection	Before Maturity	August 2, 2018
5 <sup>th</sup> Stage of data collection	Before Harvest	August 14, 2018

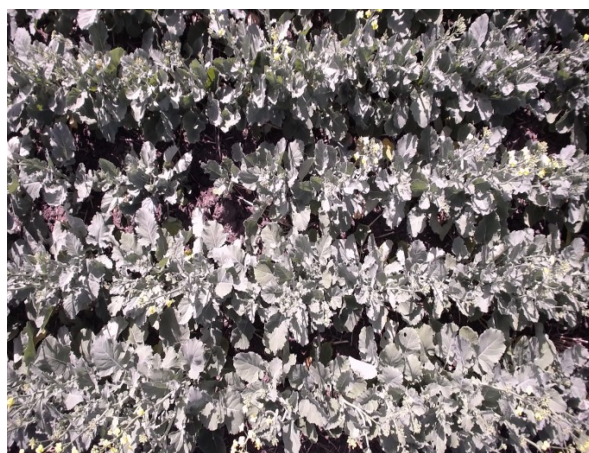


*Table 4- 2: Variation of NDVI, height, temperature, ambient temperature and humidity of plot #30.77 during summer 2018*

Stage	Date	NDVI		Height (cm)		Temp(C°)		Ambient Temp (C°) Ref: Platform's weather station		Ambient Humidity (%) Ref: Platform's weather station	
		*	**	*	**	*	**	*	**	*	**
1 <sup>st</sup>	June 19, 2018	0.49	0.50	-	-	34.09	34.33	-	-	-	-
2 <sup>nd</sup>	June 29, 2018	0.65	0.66	-	-	26.32	26.35	-	-	-	-
3 <sup>rd</sup>	July 18, 2018	0.63	0.65	57.99	57.99	26.77	26.82	29.20	29.67	56.13	54.36
4 <sup>th</sup>	August 2, 2018	0.65	0.69	61.07	62.92	28.42	28.20	29.10	29.08	40.09	39.94
5 <sup>th</sup>	August 14, 2018	0.53	0.52	69.26	70.40	27.93	27.75	28.60	28.60	23.01	23.01



a)



b)



c)



d)

*Figure 4- 3: Plot #30.77 on a) June 19, 2018 (Seedling Status) b) June 29, 2018 (Flowering Status) c) July 18, 2018 (End of Flowering Status) d) August 14, 2018 (Before Harvest Status)*

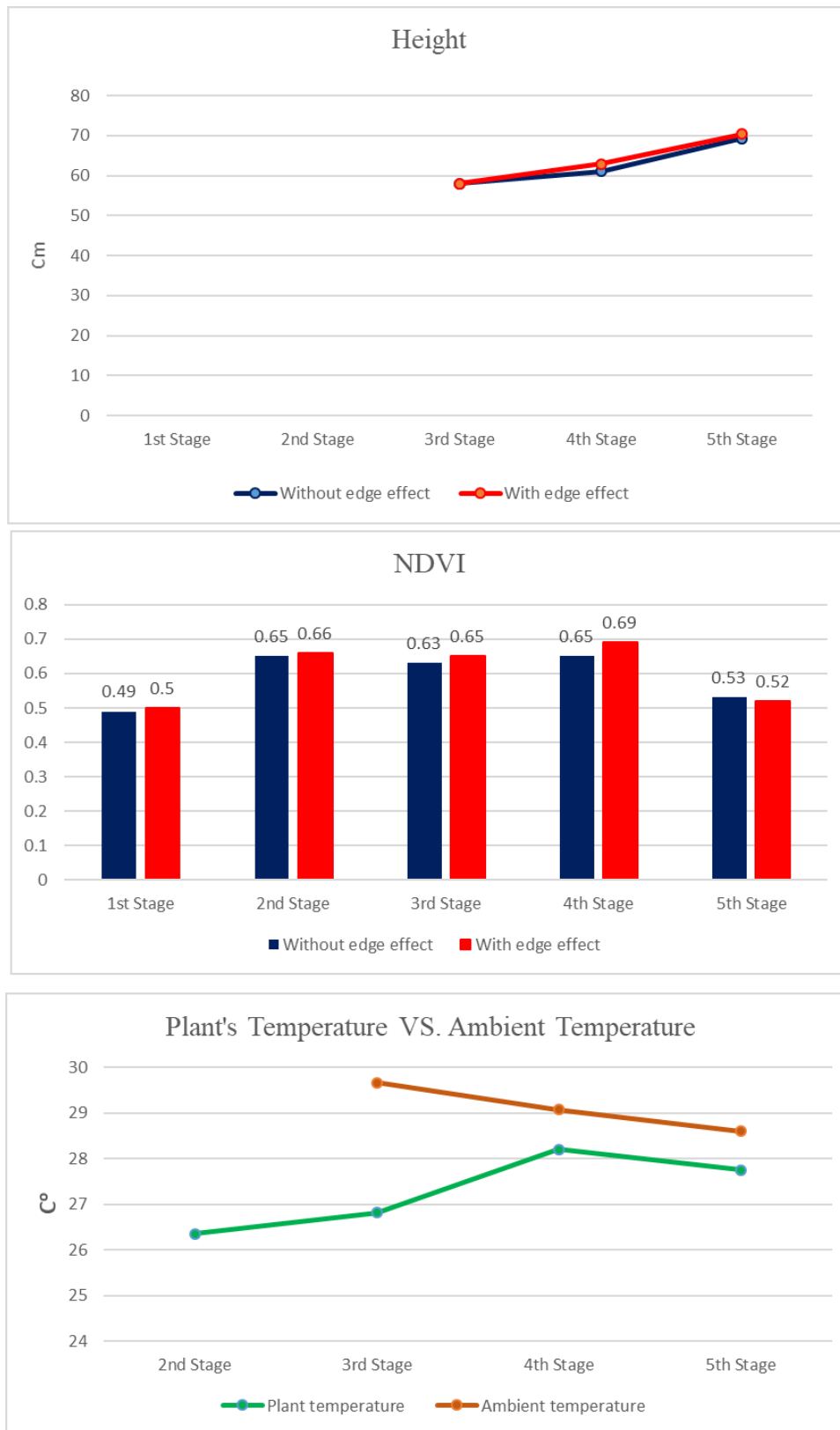


Figure 4- 4: Variation of NDVI, height, temperature, ambient temperature and humidity of plot #30.77 during summer 2018

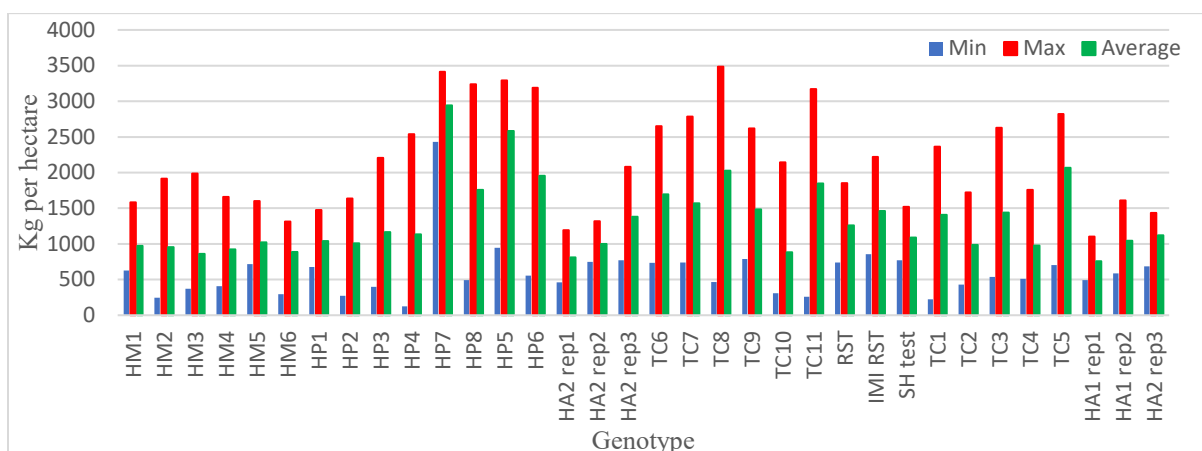


Figure 4- 5: Kilograms of harvest per hectare variation of different genotypes (Canola 2018 field)

After harvest, there is a criteria, kilograms of harvest per hectare (yield amount), for each plot that was prepared by Cargill Inc and is confidential. By analyzing of these numbers and related genotypes, it can be found that which plot and genotype is more productive (has high or less kilograms of harvest per hectare). Figure 4-5 represents kilograms of harvest per hectare different genotypes on the studied canola nursery (growing season 2018). Several plots existed for each genotype. Minimum, maximum and average amount of yield is showed for each genotypes in this Figure. It can be found that “HP7” and “HP5” are genotypes that they are yielding highest and “HA2 rep 1” and “HA2 rep 2” are genotypes with least kilograms of harvest per hectare. Therefore, features of crops with different genotypes can be compared with each other, as can be seen in Figure 4-6 to 4-9.

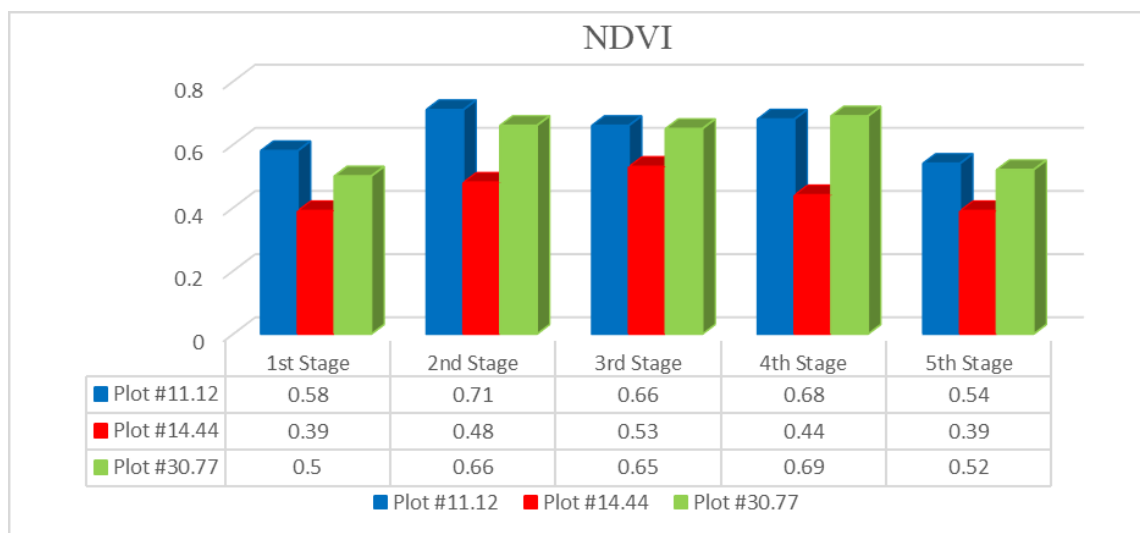
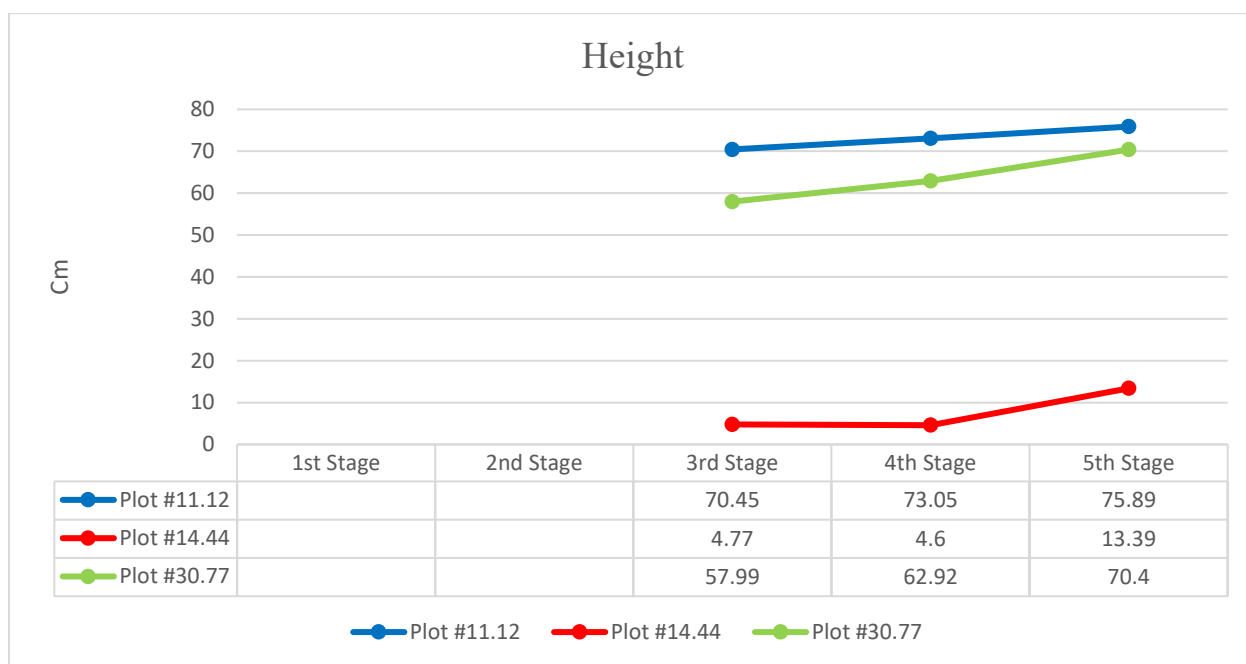
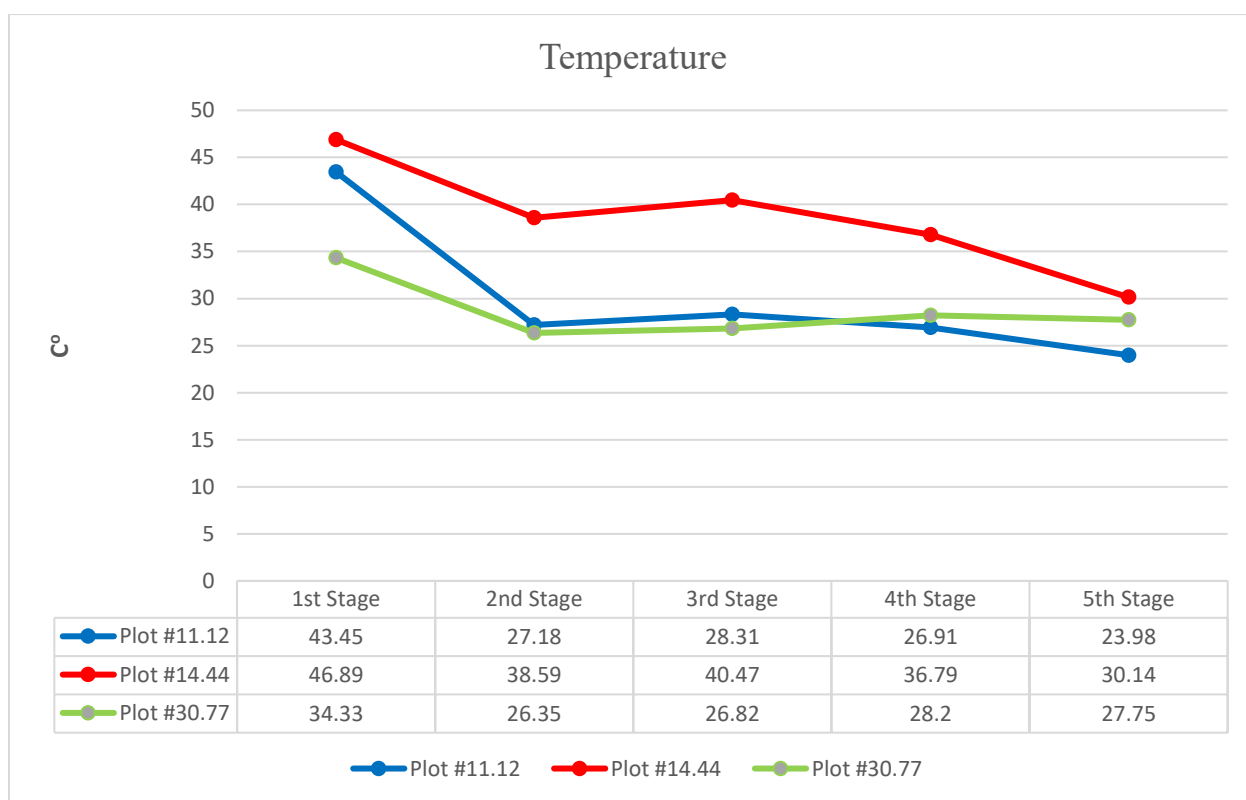


Figure 4- 6: Comparison different genotype's NDVI during different stages (Canola 2018 field)













*Figure 4- 7: Comparison different genotype's height during different stages (Canola 2018 field)*



*Figure 4- 8: Comparison different genotype's temperature during different stages (Canola 2018 field)*



Stages	Plot #11.12 (Genotype HP7)	Plot #14.44 (Genotype HA2 rep2)	Plot #30.77 (Genotype TC8)
1 <sup>st</sup> Stage			
2 <sup>nd</sup> Stage			
3 <sup>rd</sup> Stage			
4 <sup>th</sup> Stage			

*Figure 4- 9: Comparison different genotype's images during different stages<sup>1</sup> (Canola 2018 field)*

Another feature of sorted data is that user can study both the entire population of nursery and individual plots for more detailed investigations. Figure 4-11 shows the average NDVI values of the entire field for five different stages of data collection. Thus, it can be said that the majority of

---

<sup>1</sup> Large sized pictures can be found in Appendix F

canola crops were in their maximum greenness (maximum NDVI value) in July 18 trial. Figure 4-10 illustrates distribution of NDVI values with considering about edge-effect for around 3000 plots observed on a) June 19 b) June 29 c) July 18 d) August 2 e) August 14, 2018.

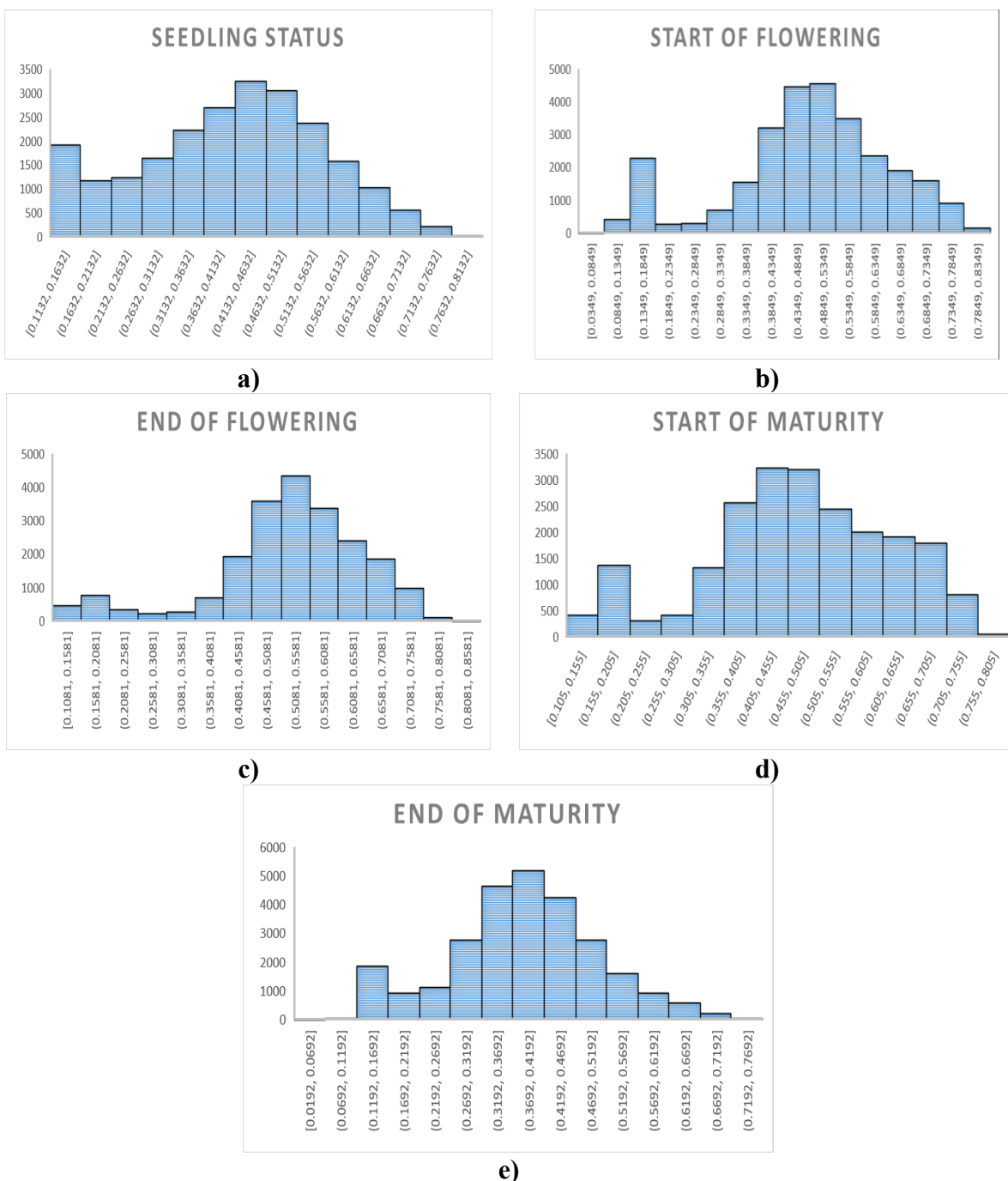
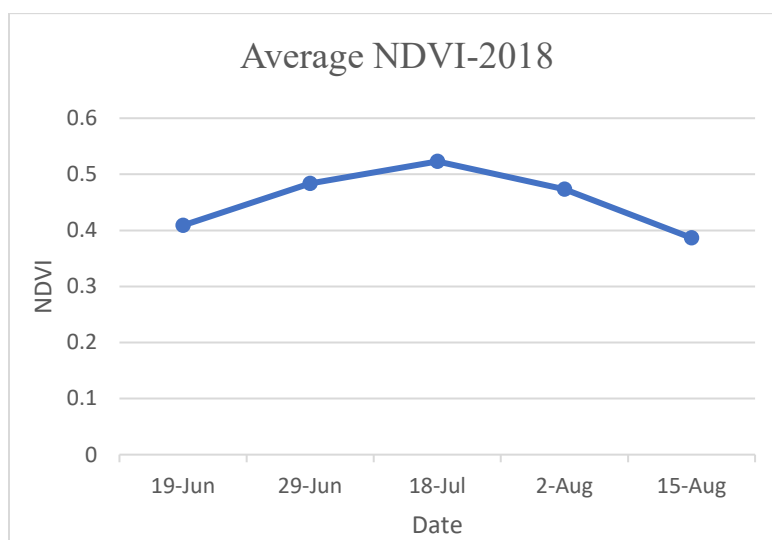


Figure 4- 10: Distribution of NDVI values with considering about edge-effect for around 3000 plots observed on a) June 19 b) June 29 c) July 18 d) August 2 e) August 14 (Canola 2018 field)





*Figure 4- 11: Average NDVI variation in the entire studied population with considering edge-effect (Canola 2018 field)*

#### 4.2.2. Analyzing growth of plots for canola field in 2019

The developed HTPP was improved and utilized to study a canola field with around 400 plots on 2019. The studied field in this year had comprised from several genotypes. The new version of data acquisition program was utilized for data collections, which does not need any sensor calibration in the field. Same as 2018, crop's traits such as its height, NDVI, temperature, and ambient temperature/humidity were targeted and recorded. Moreover, RGB images of canopies were captured by use of new version of image acquisition program. Auto-pause feature of this version was tested and verified during the data collection. Furthermore, multispectral images of crops were captured by use of multispectral image acquisition program. Utilized multispectral camera captures images in four bands, which are 580, 660, 735 and 820 nm.

*Table 4- 3: Stages of data collection on canola 2019 field*

Stage	Description	Date
1 <sup>st</sup> Stage of data collection	Seeding Status	June 26, 2019
2 <sup>nd</sup> Stage of data collection	Flowering Status	July 11, 2019
3 <sup>rd</sup> Stage of data collection	End of Flowering	July 31, 2019
4 <sup>th</sup> Stage of data collection	Before Maturity	August 15, 2019
5 <sup>th</sup> Stage of data collection	Before Harvest	August 28, 2019

Five main stages of data collections was determined and completed during the growing season on 2019, as can be seen in Table 4-3. By utilize of Pheno-VISDM3, collected data and images were sorted and valuable information were prepared for analysis. Appendix G represents examples for analyzes of canola crop's growth during 2019 season. From each genotype, a random plot was selected and behavior of selected plots were compared with each other, as can be seen in Figure 4-12 to 4-15. It is mentionable that all values are related to the considering edge-effect case. Figure 4-16 illustrates distribution of NDVI values with considering about edge-effect for around 400 plots observed on a) June 26 b) July 11 c) July 31 d) August 15 e) August 28, 2019.

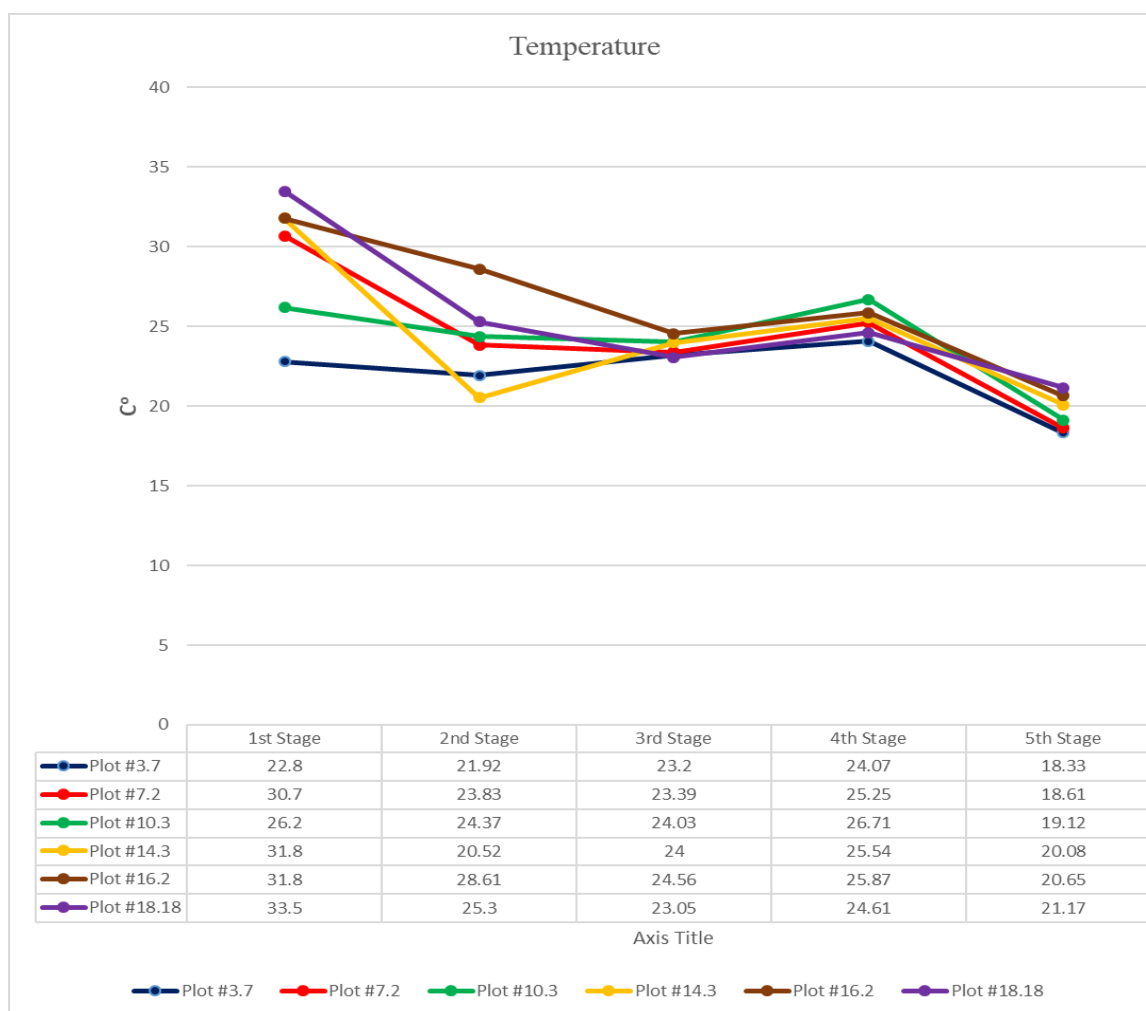


Figure 4- 12: Comparison different genotype's temperature during different stages (Canola 2019 field)

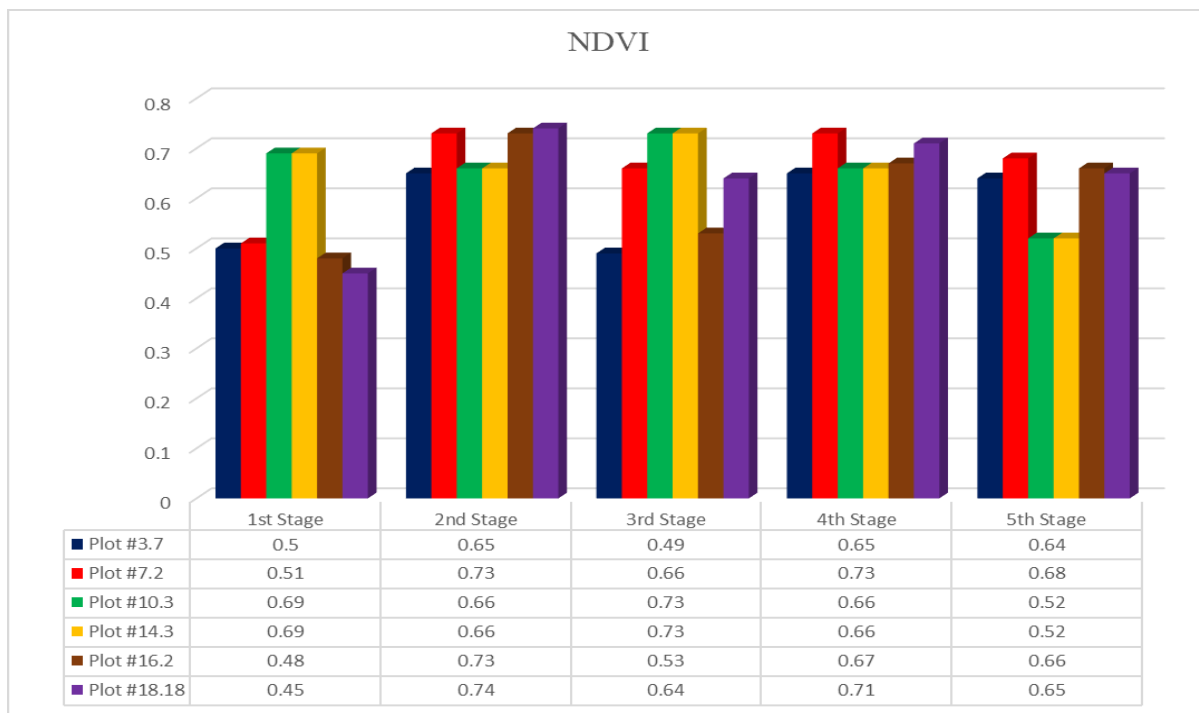


Figure 4- 13: Comparison different genotype's NDVI during different stages (Canola 2019 field)

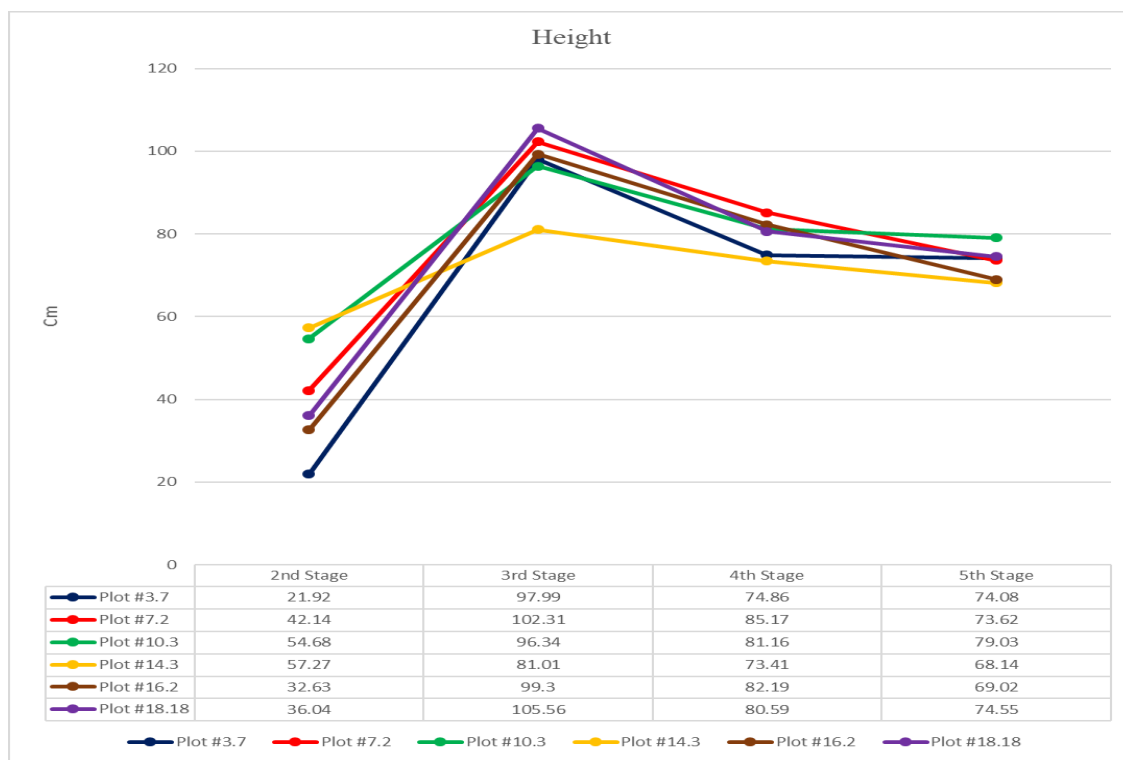


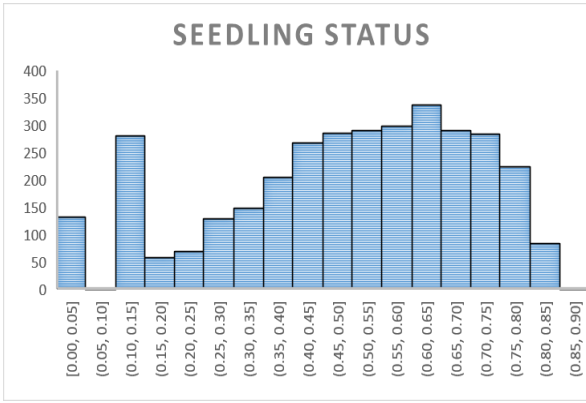
Figure 4- 14: Comparison different genotype's height during different stages (Canola 2019 field)



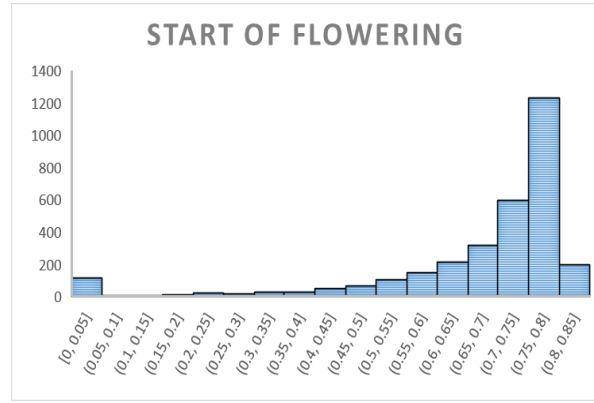


Figure 4- 15: Comparison different genotype's images during different stages<sup>1</sup> (Canola 2019 field)

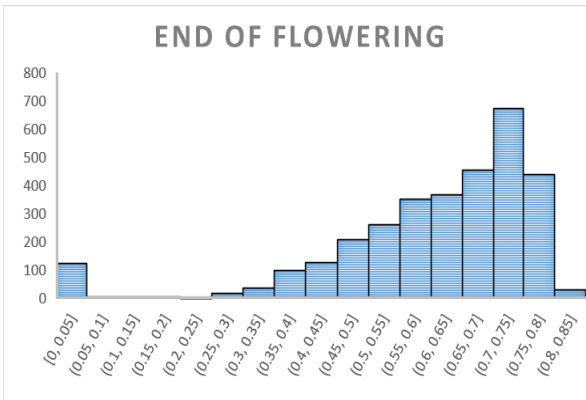
<sup>1</sup> Large sized pictures can be found in Appendix G



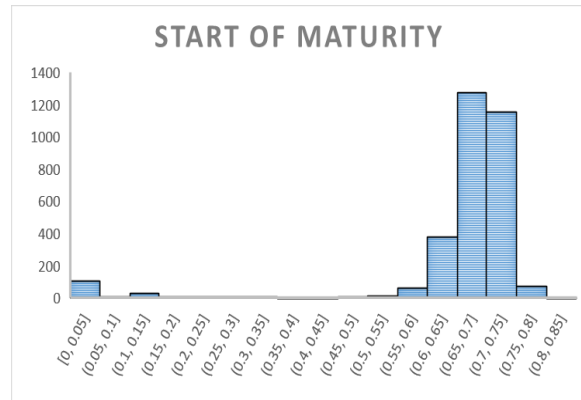
a)



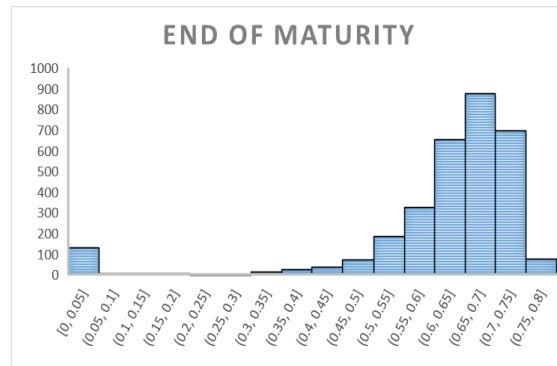
b)



c)



d)



e)


Figure 4- 16: Distribution of NDVI values with considering about edge-effect for around 400 plots observed on a) June 26 b) July 11 c) July 31 d) August 15 e) August 28 (Canola 2019 field)

### 4.3. Monitored Wheat fields

The performance of HTPP was evaluated on two wheat fields on growing seasons of 2018 and 2019, which were located on Kernan Farm, Saskatoon, Canada. These fields both have same number of plots, around 270 rectangular plots. However, the genotypes are different for each year.




Figure 4-17 and 4-18 illustrates the prepared map of nurseries, which is provided by crop science field laboratory. Each plot is identified by two numbers; top number shows genotype and the bottom one shows plot's number. Plot B is a border plot in each row. The location of studied wheat nurseries, which are extracted from Google Maps, are prepared in Appendix D.



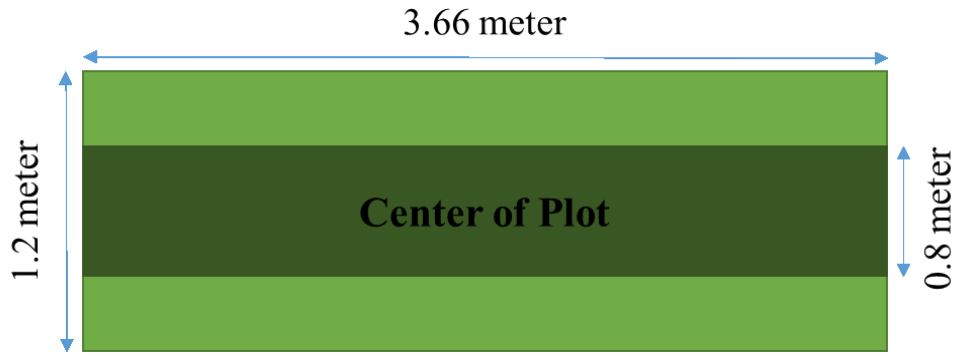
	49	18	62	37	51	4	50	39	47	80	72	19	68	70		6	73	42	21	33	10	69	55	16	35	13	43	34	
B	355	356	357	358	359	360	361	362	363	364	365	366	367	368	B.9.2	369	370	371	372	373	374	375	376	377	378	379	380	381	B.9.3
	76	59	7	45	26	32	9	28	46	60	77	78	64	57		40	79	71	27	36	1	11	5	63	25	74	56	38	
B.8.1	328	329	330	331	332	333	334	335	336	337	338	339	340	341	B.8.2	342	343	344	345	346	347	348	349	350	351	352	353	354	B.8.3
	30	17	58	2	61	41	81	31	23	53	48	65	67	29		52	12	3	8	14	22	54	20	15	75	44	66	24	
B.7.1	301	302	303	304	305	306	307	308	309	310	311	312	313	314	B.7.2	315	316	317	318	319	320	321	322	323	324	325	326	327	B.7.3
	34	46	12	1	66	31	71	42	51	3	23	35	54	80		79	47	32	74	36	21	67	22	78	76	16	2	37	
B.6.1	255	256	257	258	259	260	261	262	263	264	265	266	267	268	B.6.2	269	270	271	272	273	274	275	276	277	278	279	280	281	B.6.3
	72	62	15	25	40	55	28	65	17	48	68	11	50	81		75	64	33	9	69	53	26	56	4	57	73	58	20	
B.5.1	228	229	230	231	232	233	234	235	236	237	238	239	240	241	B.5.2	242	243	244	245	246	247	248	249	250	251	252	253	254	B.5.3
	70	8	43	18	59	60	14	38	41	7	29	27	63	24		19	49	10	61	44	5	30	39	45	77	6	13	52	
B.4.1	201	202	203	204	205	206	207	208	209	210	211	212	213	214	B.4.2	215	216	217	218	219	220	221	222	223	224	225	226	227	B.4.3
	67	9	14	47	71	30	55	63	73	3	49	34	44	70		64	28	58	36	59	54	50	25	12	57	61	21	13	
B.3.1	155	156	157	158	159	160	161	162	163	164	165	166	167	168	B.3.2	169	170	171	172	173	174	175	176	177	178	179	180	181	B.3.3
	23	51	43	11	22	65	77	26	19	29	41	37	6	33		40	74	20	46	53	32	5	75	17	10	78	18	42	
B.2.1	128	129	130	131	132	133	134	135	136	137	138	139	140	141	B.2.2	142	143	144	145	146	147	148	149	150	151	152	153	154	B.2.3
	52	76	4	66	35	38	81	72	27	7	31	8	39	68		79	15	16	56	62	45	80	60	2	69	24	1	48	
B.1.1	101	102	103	104	105	106	107	108	109	110	111	112	113	114	B.1.2	115	116	117	118	119	120	121	122	123	124	125	126	127	B.1.3

Figure 4- 17: The map of studied wheat field on 2018



	11	54	36	52	15	77	73	46	70	24	25	38	35	60		2	76	26	56	72	21	10	3	63	59	68	20	66	
B	355	356	357	358	359	360	361	362	363	364	365	366	367	368	B.9.2	369	370	371	372	373	374	375	376	377	378	379	380	381	B.9.3
	17	13	14	8	64	51	78	29	49	7	5	67	31	62		45	61	79	65	40	22	32	47	30	81	23	9	1	
B.8.1	328	329	330	331	332	333	334	335	336	337	338	339	340	341	B.8.2	342	343	344	345	346	347	348	349	350	351	352	353	354	B.8.3
	33	50	43	41	4	37	12	53	6	71	19	18	55	74		48	69	28	34	44	39	27	75	57	58	80	42	16	
B.7.1	301	302	303	304	305	306	307	308	309	310	311	312	313	314	B.7.2	315	316	317	318	319	320	321	322	323	324	325	326	327	B.7.3
	33	42	72	35	77	31	47	17	48	11	16	34	3	41		8	2	62	40	68	6	69	23	39	54	7	78	24	
B.6.1	255	256	257	258	259	260	261	262	263	264	265	266	267	268	B.6.2	269	270	271	272	273	274	275	276	277	278	279	280	281	B.6.3
	30	71	59	43	67	29	58	70	25	73	12	57	61	51		60	21	55	9	1	79	4	66	27	64	52	56	18	
B.5.1	228	229	230	231	232	233	234	235	236	237	238	239	240	241	B.5.2	242	243	244	245	246	247	248	249	250	251	252	253	254	B.5.3
	37	44	46	32	14	74	76	20	5	19	36	53	22	75		49	45	38	10	63	15	80	26	28	13	81	50	65	
B.4.1	201	202	203	204	205	206	207	208	209	210	211	212	213	214	B.4.2	215	216	217	218	219	220	221	222	223	224	225	226	227	B.4.3
	66	13	62	46	9	24	75	33	71	49	27	73	40	48		63	5	25	6	10	64	43	35	32	80	11	61	69	
B.3.1	155	156	157	158	159	160	161	162	163	164	165	166	167	168	B.3.2	169	170	171	172	173	174	175	176	177	178	179	180	181	B.3.3
	22	2	29	68	15	12	42	74	79	77	19	23	4	16		51	26	67	20	7	28	70	14	53	57	3	56	47	
B.2.1	128	129	130	131	132	133	134	135	136	137	138	139	140	141	B.2.2	142	143	144	145	146	147	148	149	150	151	152	153	154	B.2.3
	38	31	54	44	30	8	50	18	21	39	59	1	65	17		76	36	41	55	34	78	58	37	60	52	45	81	72	
B.1.1	101	102	103	104	105	106	107	108	109	110	111	112	113	114	B.1.2	115	116	117	118	119	120	121	122	123	124	125	126	127	B.1.3

Figure 4- 18: The map of studied wheat field on 2019



*Figure 4- 19: Dimensions of wheat plots on 2018 and 2019 fields*

The path of travelling was 1.5 meter for both fields. The dimensions of wheat plots were same in both 2018 and 2019 fields, as can be seen in Figure 4-19. The space between two-canopy plots was empty. As discussed, two approaches exist for data/image sorting, which are with and without considering about edge-effect. The valid part of plot after considering edge-effect is determined by dark green in Figure 4-19.

6-feet wide tractor was utilized as a vehicle to carry mechanical boom and attached devices. Utilized tractor was a semi-autonomous farm vehicle and has auto-steer navigation system, with help from an RTX-GPS with an accuracy of about 1 inch. After applying several vibration tests, it was concluded that when tractor travels with speed of 1.6 mph (0.7 m/s), devices can record data reliably without any issue.

The time which takes for vehicle to pass through a single plot can be calculated from Eq. 4-1 and 4-2. If 0.25 second takes for a record of sample data, then for each plot, HTPP can capture 6.8 records of data. These numbers can be varied based on the availability of GPS signal. The field trials for 2018 and 2019 wheat nurseries can be found in Appendix E. In the next sections, the collected data from studied wheat nurseries is analyzed and discussed.

#### **4.3.1. Analyzing growth of plots for wheat field in 2018**

The side that was studied in the summer of 2018 had comprised from two blocks and totally around 270 plots with different genotypes. Height, NDVI, temperature of crops, and ambient temperature/humidity were target traits for data collections. RGB images of wheat plots were captured, too.

Table 4- 4: Stages of data collection on wheat 2018 field

Stage	Description	Date
2 <sup>nd</sup> Stage of data collection	Flowering Status	July 13, 2018
3 <sup>rd</sup> Stage of data collection	End of Flowering	July 26, 2018
4 <sup>th</sup> Stage of data collection	Before Maturity	August 9, 2018
5 <sup>th</sup> Stage of data collection	Before Harvest	August 23, 2018

Table 4-4 represents 4 main stages of data collection that was completed during the growing season on 2018. Collected data and images were sorted by use of Pheno-VISDM2 and valuable information were prepared for analysis. Examples for analyzes of wheat crop's growth during 2018 season is prepared in Appendix H. Figure 4-20 to 4-22 compares the behavior of 6 random genotypes. It is mentionable that all values are related to the considering edge effect case.

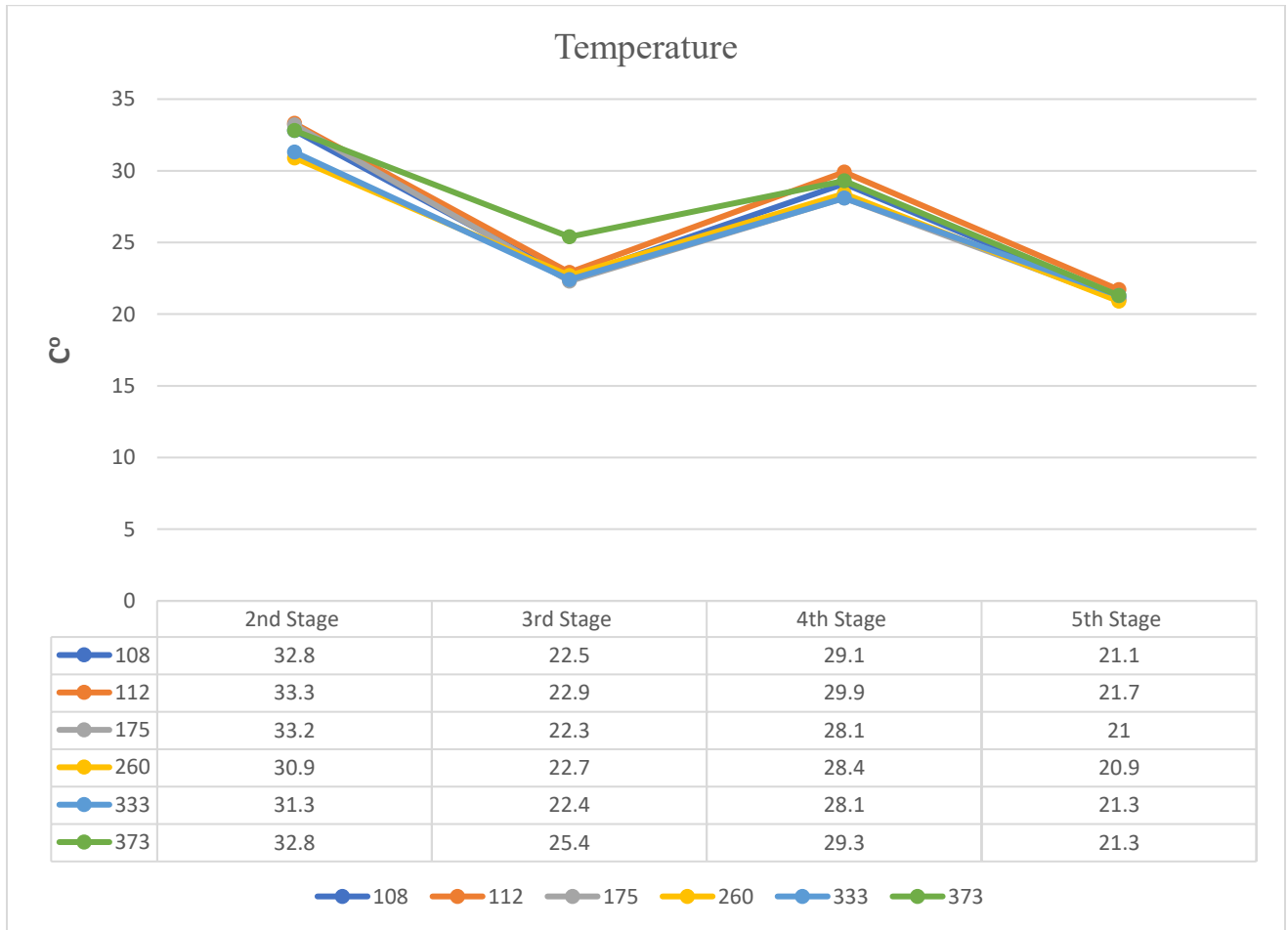


Figure 4- 20: Comparison different genotype's temperature during different stages (Wheat 2018 field)



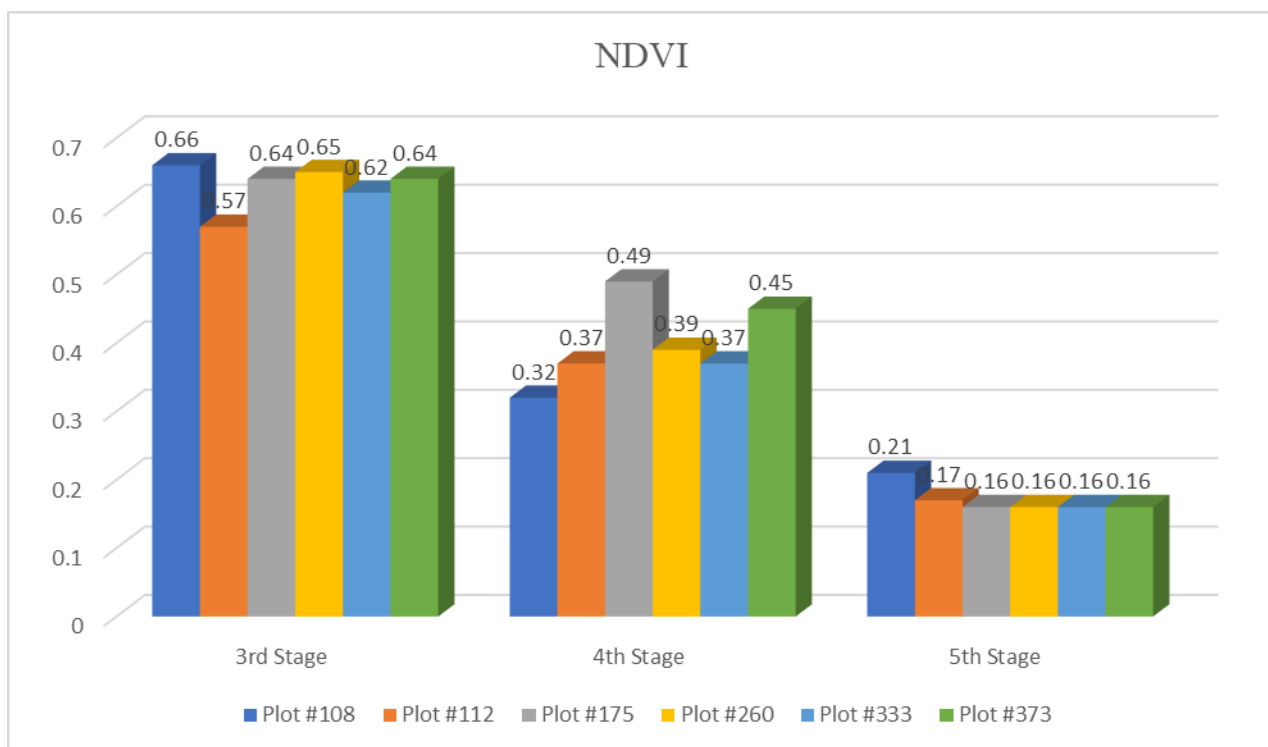


Figure 4- 21: Comparison different genotype's NDVI during different stages (Wheat 2018 field)

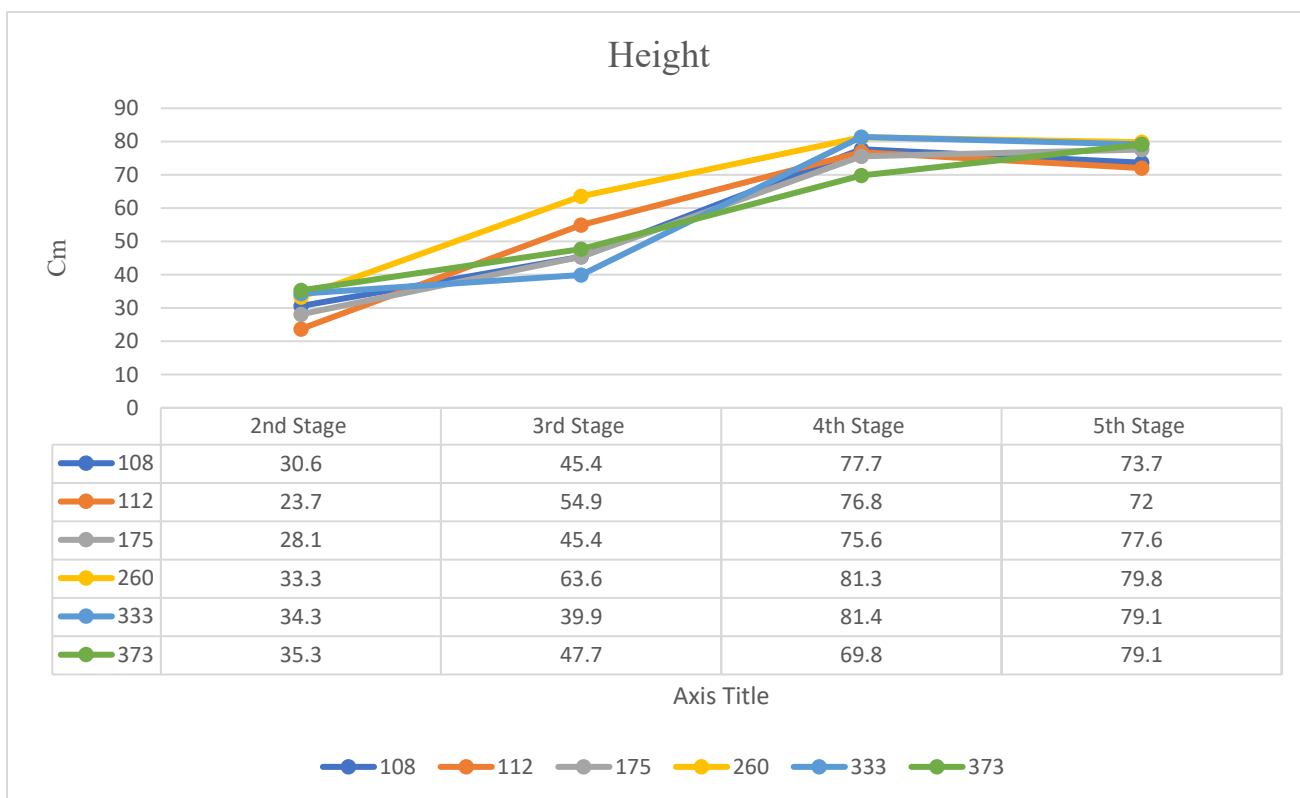


Figure 4- 22: Comparison different genotype's height during different stages (Wheat 2018 field)

Figure 4-23 illustrates distribution of NDVI values with considering about edge-effect for around 270 plots observed on a) July 26 b) August 9 c) August 23, 2018.

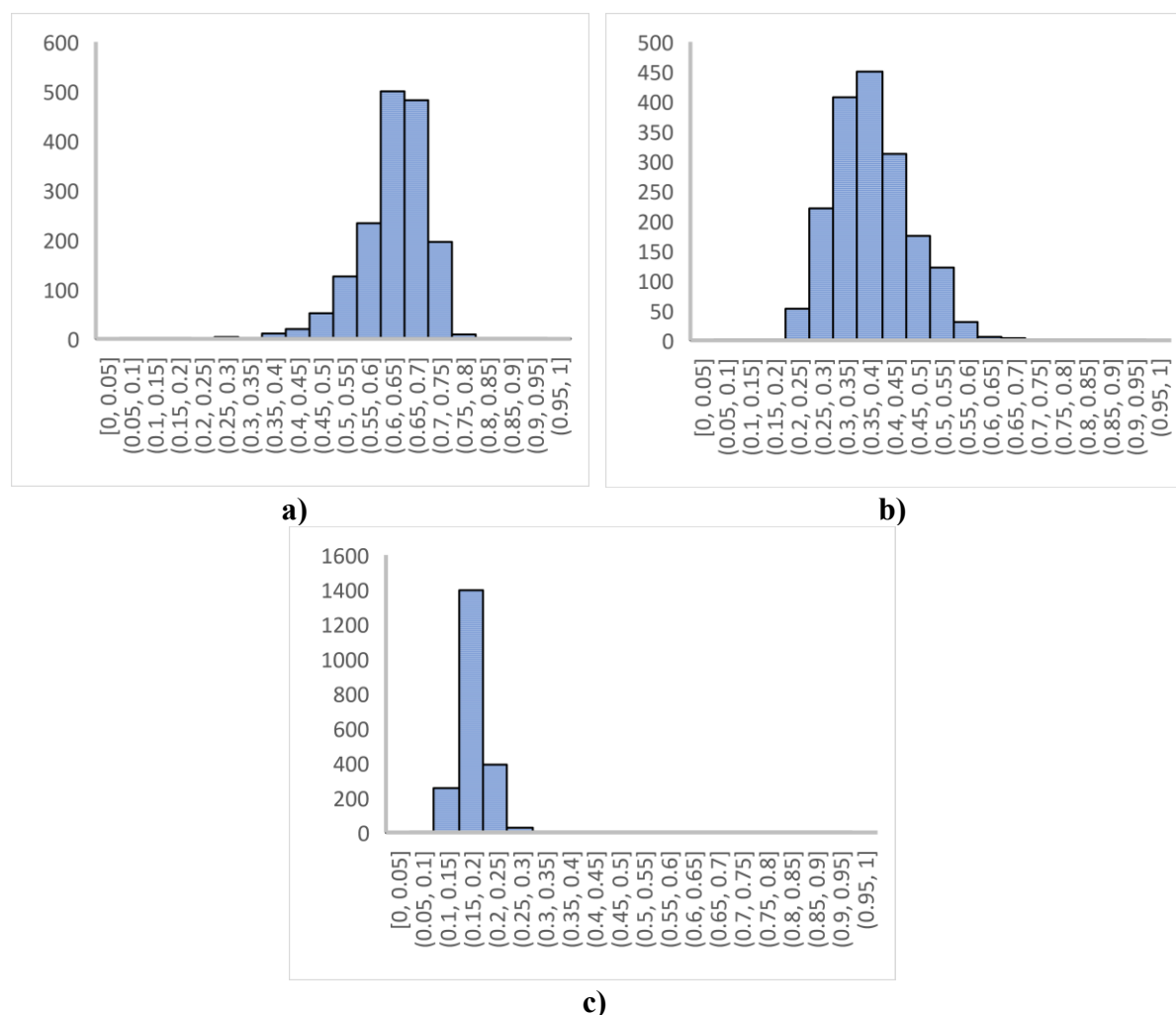


Figure 4- 23: Distribution of NDVI values with considering about edge-effect for around 270 plots observed on a) June 26 b) July 11 c) July 31 d) August 15 e) August 28 (Wheat 2018 field)

### 4.3.2. Analyzing growth of plots for wheat field in 2019

Studied wheat nursery in growing season of 2019 was close to the 2018's nursery. Same as 2018's wheat field, it had comprised from two blocks and totally around 270 plots with different genotypes. Height, NDVI, temperature of crops, and ambient temperature/humidity were target traits for data collections. Moreover, RGB images of wheat plots were captured. Furthermore, multispectral images of crops were captured by use of multispectral image acquisition program and their NDVI information was extracted, which will be discussed in section 4.9. Table 4-4 represents four different stages (dates) of data collections for the studied wheat field on 2019.

Table 4- 5: Stages of data collection on wheat 2019 field

Stage	Description	Date
2 <sup>nd</sup> Stage of data collection	Flowering Status	July 23, 2019
3 <sup>rd</sup> Stage of data collection	End of Flowering	August 1, 2019
4 <sup>th</sup> Stage of data collection	Before Maturity	August 20, 2019
5 <sup>th</sup> Stage of data collection	Before Harvest	September 17, 2019

Collected data and images were sorted by use of Pheno-VISDM3 and valuable information were prepared for breeders. Appendix I represents examples for analyzes of wheat crop's growth during 2019 season. Figure 4-24 to 4-27 compares the behavior of 6 random genotypes.

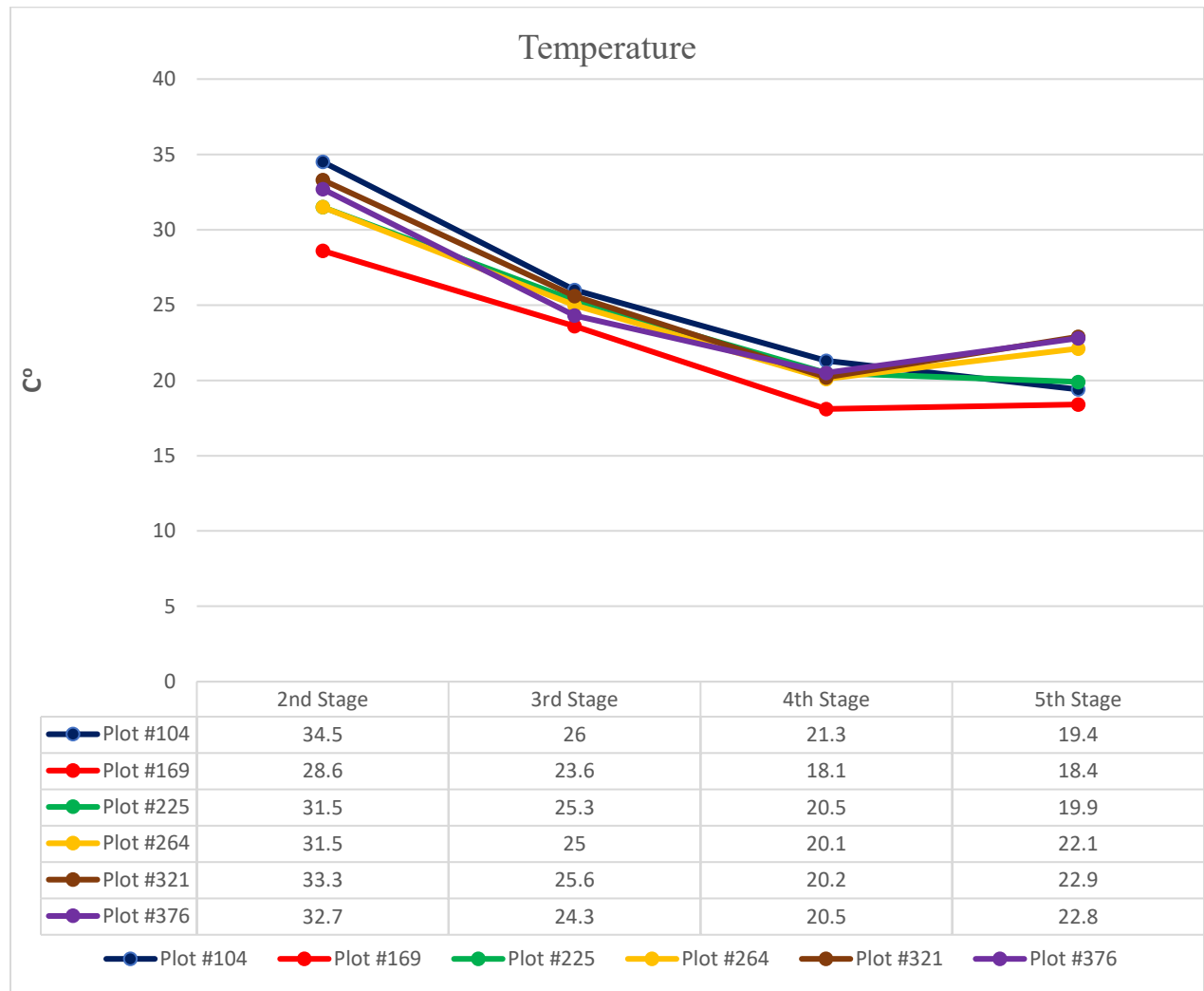


Figure 4- 24: Comparison different genotype's temperature during different stages (Wheat 2019 field)



Figure 4- 25: Comparison different genotype's height during different stages (Wheat 2019 field)

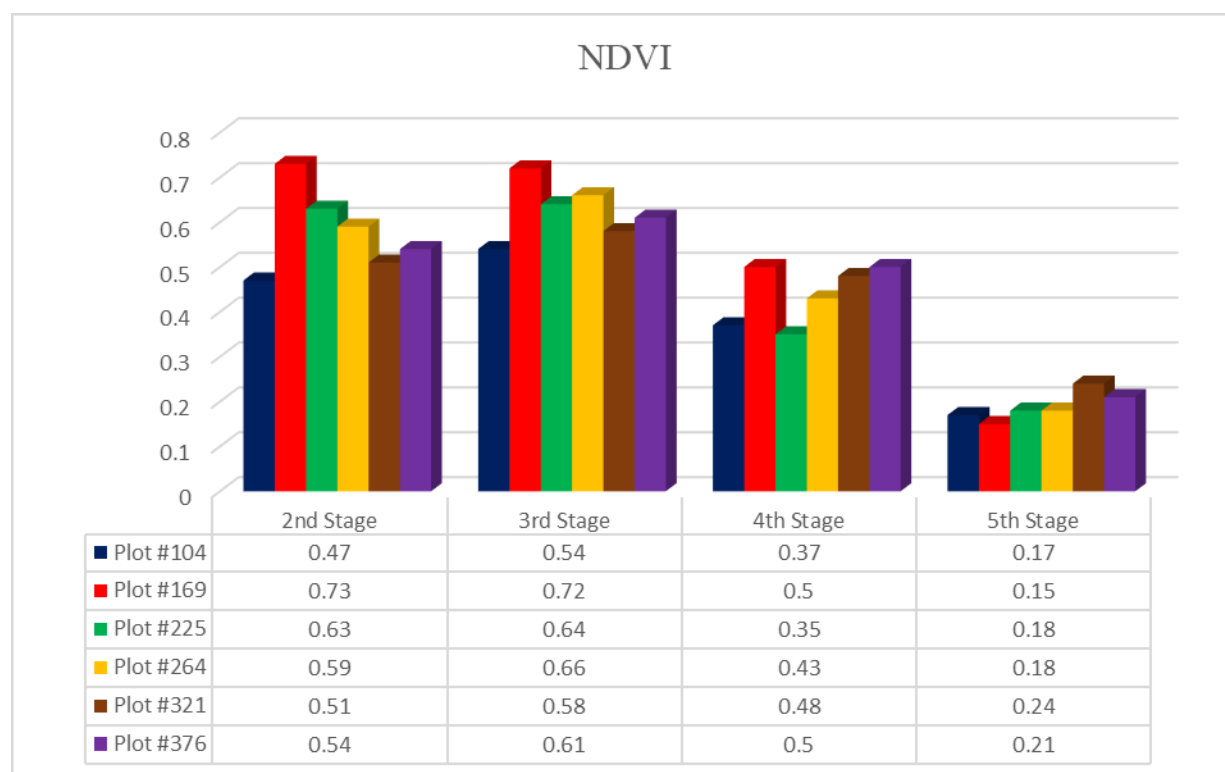


Figure 4- 26: Comparison different genotype's NDVI during different stages (Wheat 2019 field)



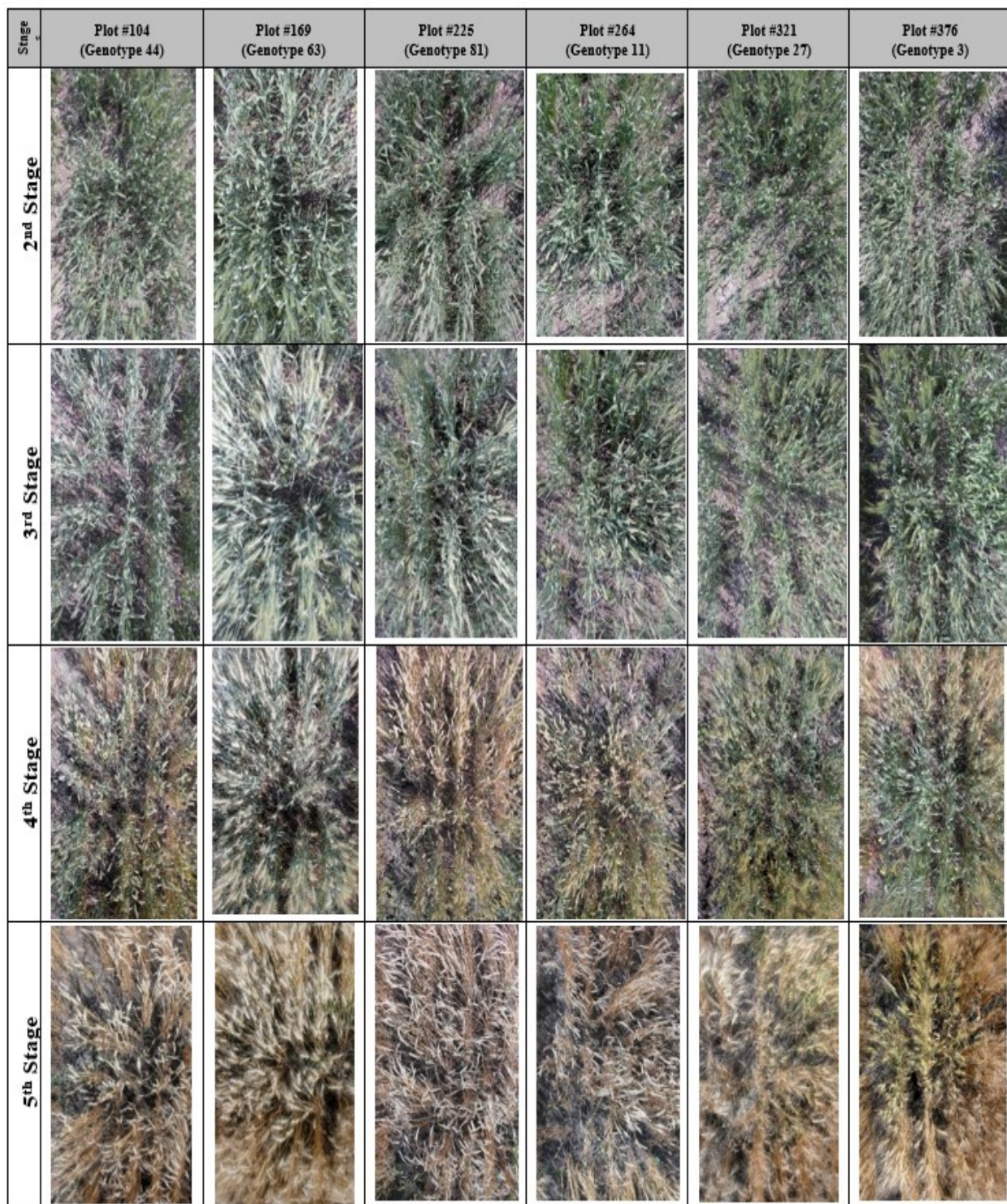


Figure 4- 27: Comparison different genotype's images during different stages<sup>1</sup> (Wheat 2019 field)

<sup>1</sup> Large sized pictures can be found in Appendix I

The distribution of NDVI values for around 270 plots observed on a) July 23 b) August 1 c) August 20 d) September 17, 2019 is illustrated in Figure 4- 28

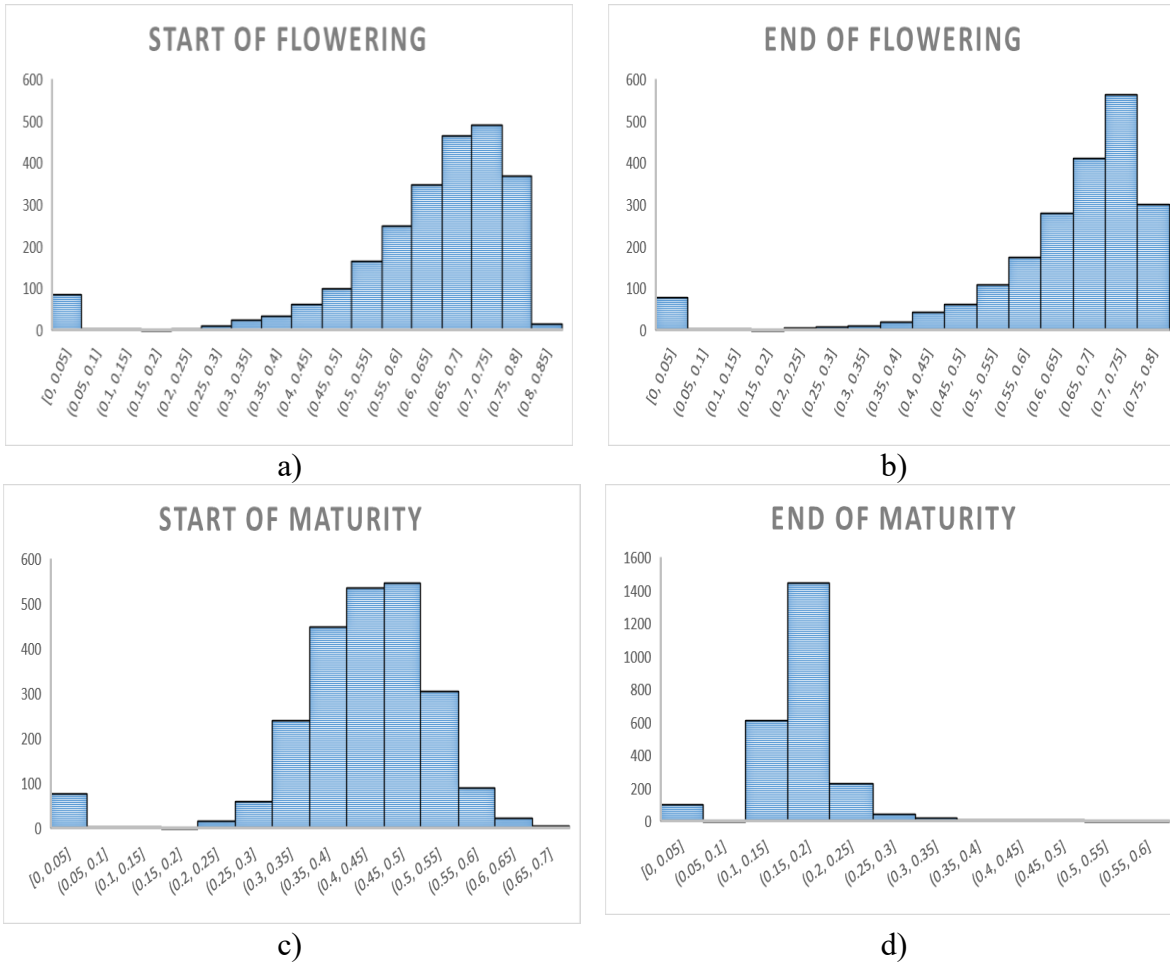


Figure 4- 28: Distribution of NDVI values for 243 plots observed on a) July 23 b) August 11 c) August 20 d) September 17 (Wheat 2019 field)

## 4.4. Mapping programs' performance

As discussed in chapter 3, the map of studied field is critical and essential for the use of other programs such as data visualization and sorting. Reliable map represents accurate geospatial information (longitude and latitude) of all plots. Two versions of mapping programs are developed and tested for both wheat and canola fields. In this section, their performance is evaluated.

### 4.4.1. Performance of mapping program-version 2018

In this program, interpolation is used for finding geospatial information of plots. For each row of the field, first and last plots were selected and their centers' coordinates were calculated



and recorded. Then, longitude and latitude values of the rest of the plots' center in the same row were found by using the interpolation, which was explained in section 3.2.1.

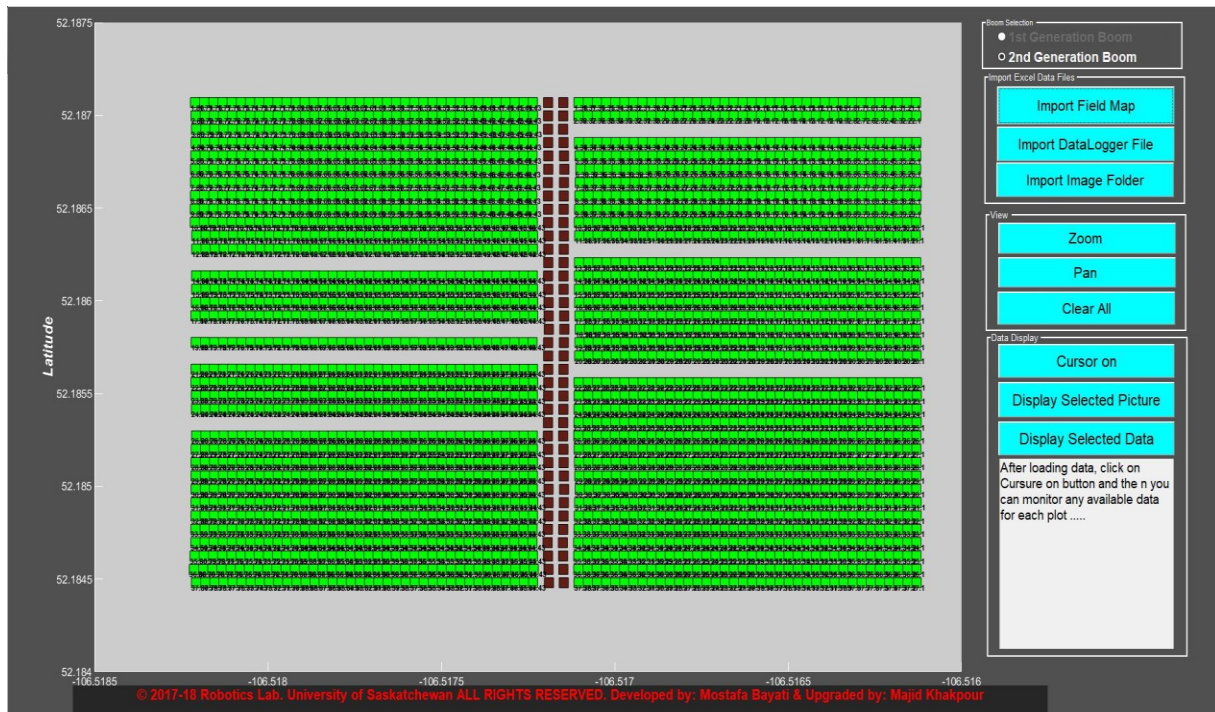


Figure 4- 29: Mapped and loaded map file of studied canola field on 2018 through mapping program- version 2018

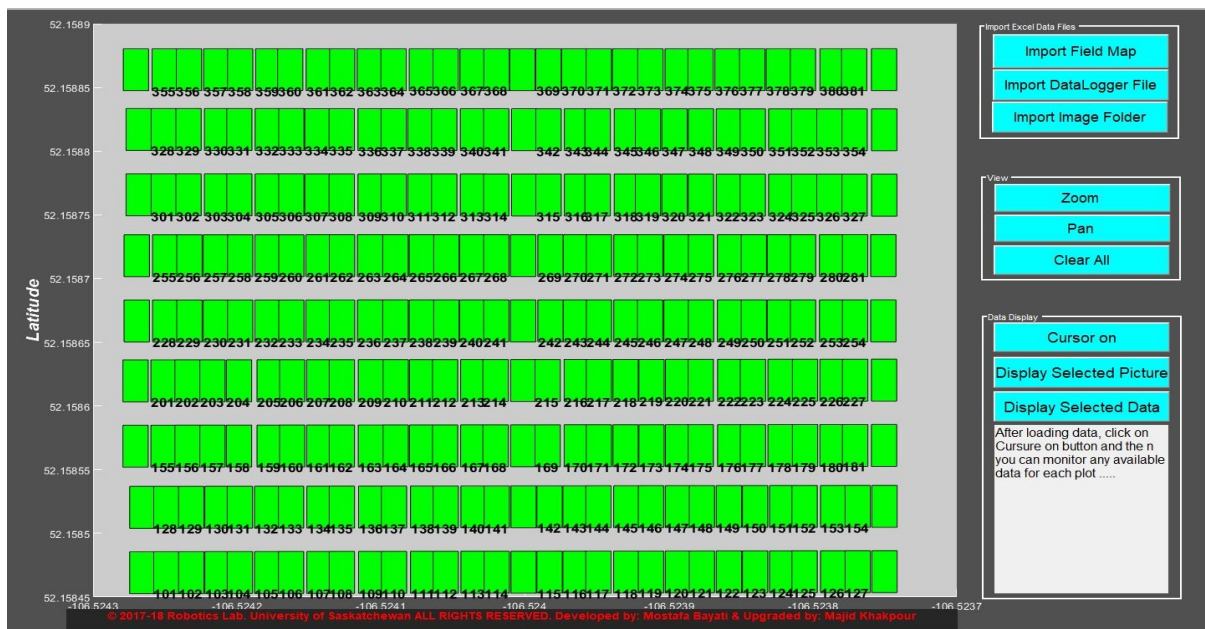


Figure 4- 30: Mapped and loaded map of studied wheat field on 2018 through mapping program- version 2018

As a result, an Excel file can be provided, which has the longitude and latitude information of plots' centers (entire of field). This Excel sheet is critical for the use of visualization program. Figure 4-29 and 4-30 illustrate the generated and loaded map of fields via mapping program-version 2018 for the studied canola and wheat nurseries on 2018 growing season. Green and brown rectangles are showing canopy plots and soil, respectively. X-axis and Y-axis represent the longitude and latitude.

It is mentionable that canola field on 2018 comprised from 67 rows of plots, which are in two blocks. Therefore, for generating the map of field the geospatial information of 134 plots' centers was calculated and recorded.

#### 4.4.2. Performance of mapping program-version 2019 (Pheno-VISDM3)

This program uses more efficient approach for determining longitude and latitude values of each plot in the studied field. It was developed based on the Eq. 2-24 to 2-6 to find geospatial information of entire field's plots.



Figure 4- 31: Mapped and loaded map of studied wheat field on 2019 through mapping program- version 2019 (Pheno-VISDM3)



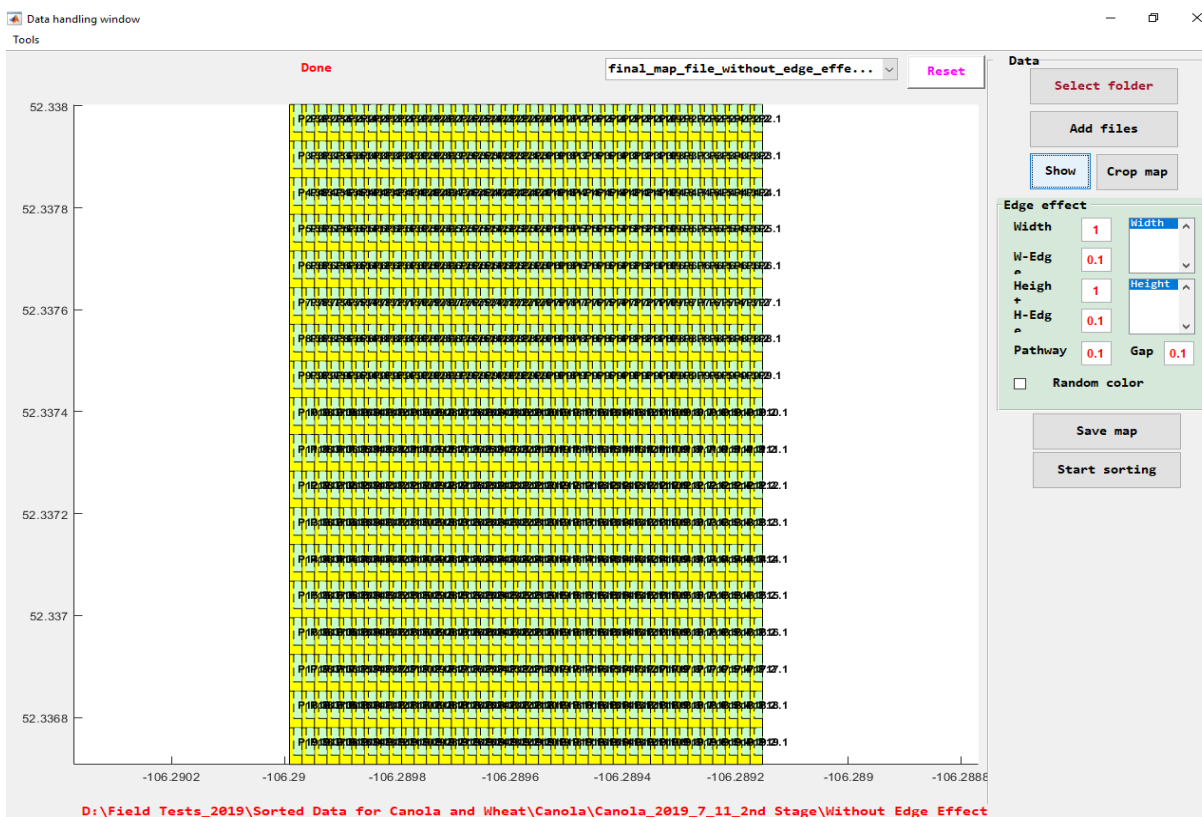


Figure 4- 32: Mapped and loaded map of studied canola field on 2019 through mapping program- version 2019 (Pheno-VISDM3)

For generating the map of field, the geospatial information (longitude and latitude) of just one plot (plots # 2.1 on canola and plot # B.1.1 on wheat fields) is enough. It should be considered that plots' dimension and their gap are fix. For using Pheno-VISDM3 to map studied fields, several steps should be completed by user, which is prepared in appendix C. Figure 4-31 and 4-32 show the generated and loaded map of fields by use of mapping program-version 2019 (Pheno-VISDM3) for the studied wheat and canola nurseries on 2019 growing season. X-axis and Y-axis represent the longitude and latitude. Green rectangles represent canopy plot and yellow parts are related to the gaps between plots (soil parts).

To verify the accuracy of generated map, another map can be generated based on the other corner plot of field (plots #37.38 on canola and plot # B.3.3 on wheat fields). This map can be created by adding a new block in the mapping module of Pheno-VISDM3. Figure 4-33 illustrates draft version of generated maps based on plot # 2.1 (yellow) and plot # 18.38 (pink) for the studied canola field on 2019. X-axis and Y-axis represent the longitude and latitude. These two maps can be loaded together and compared (Figure 4-33.c)

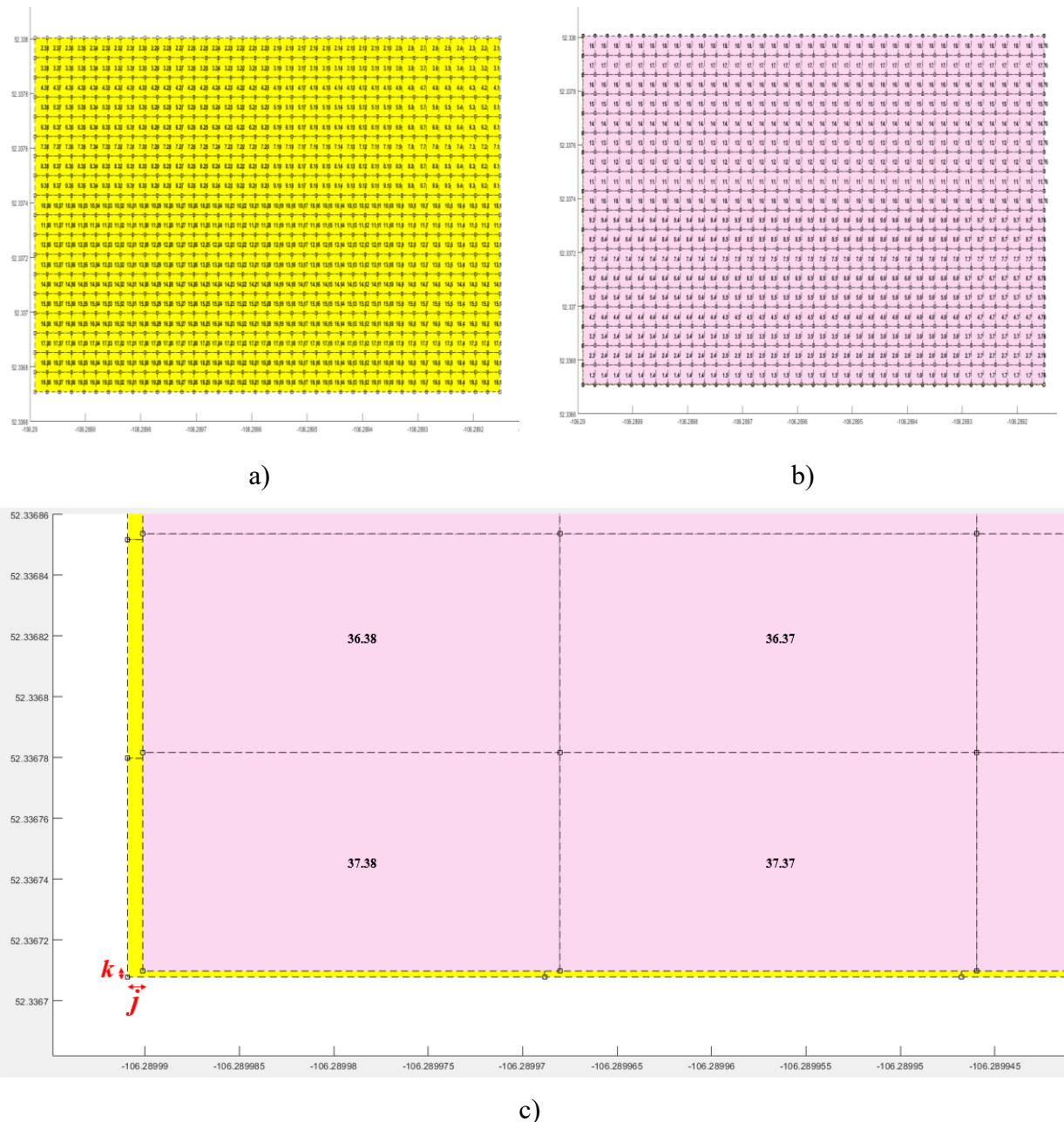


Figure 4- 33: A screen shot of generated draft map of studied canola field on 2019 through data mapping module of Pheno-VISDM3 a) based on plot 1.1 b) based on plot 37.38 c) comparing generated maps

The values of  $j$  and  $k$  are calculated by use of calculator module of Pheno-VISDM3 and they are 4.5 and 1.8 cm, respectively. Because the dimensions of field is 288\*68.4 m, it is clear that  $j$  and  $k$  are very less and the generated map is valid. Therefore, by use of just one plots' geospatial information, user can map the entire field reliably and accurately. There is another way to verify reliability and accuracy of generated maps, which is discussed in the next section.

## 4.5. Verifying geo-referencing reliability for canola and wheat fields

It is undeniable fact that the accuracy of collected data via developed HTPP (data/image acquisition, visualization, sorting programs and GPS string) should be confirmed. In other words, it should be verified that collected, tagged and sorted data/images are belonged to the related plot.

To verify the accuracy of programs and platform, several physical signs were placed next to different plots, randomly. Each sign had a tag that shows the corresponding plot number, as can be seen in Figure 4-34. The reliability of collected data and images can be verified if user monitors physical signs with related number by clicking on the corresponded data points on the visualization program.

Figure. 4-35 and 4-36 show the tags set to several plots, while the pictures are loaded into Pheno-VISDM2 and Pheno-VISDM3 programs, respectively. This was repeated for all plots with physical tags next to them. Programs brought up the right picture for all test days, 100% of time on both studied canola and wheat nurseries on 2018 and 2019. It was found that the programs are working very reliably, as this examination was continued for all other signs and each day of data collection. All physical signs matched with their corresponding location.



*Figure 4- 34: An example of utilized physical signs next to individual plots to verify the accuracy of geo-referencing*



Figure 4- 35: Verifying the accuracy of the geo-referencing using Pheno-VISDM2 (RGB image of wheat plot #274 on August 28, 2018)

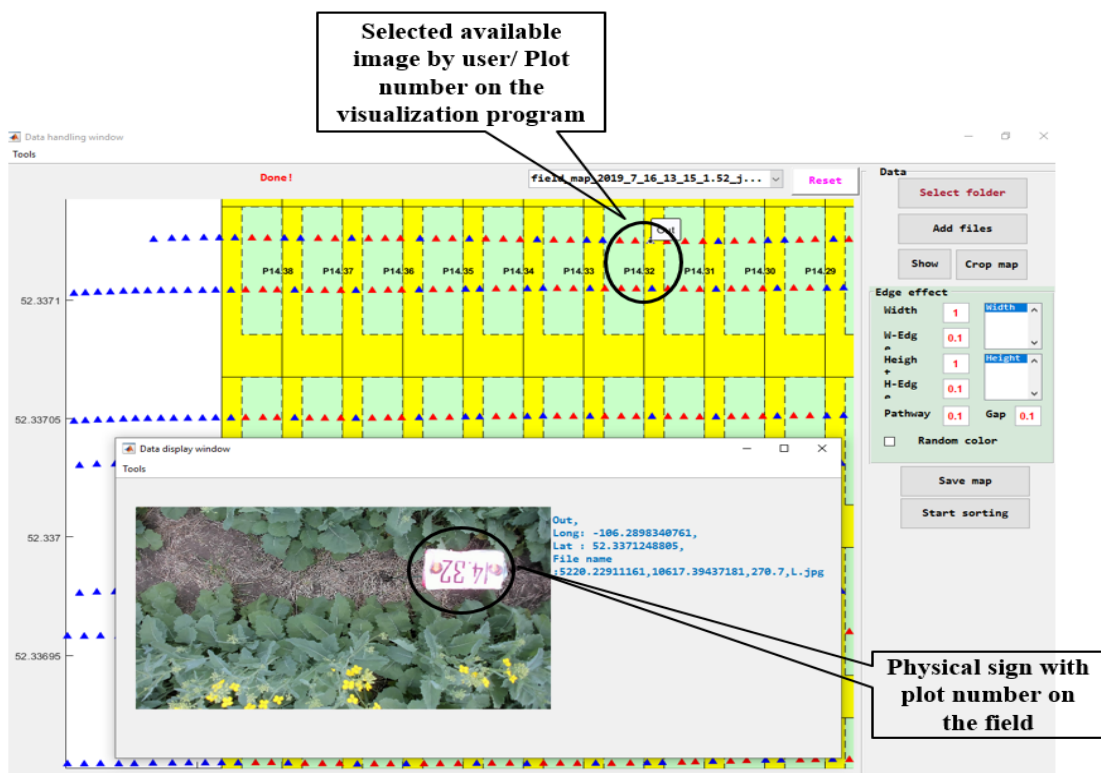


Figure 4- 36: Verifying the accuracy of the geo-referencing using Pheno-VISDM3 (RGB image of canola plot #14.23 on July 11, 2019)



## 4.6. Comparing manual and ultrasonic height measurements

In this section the validity of ultrasonic sensor's operation for measuring height of crops are discussed. The results of manual and ultrasonic sensor height measurements on certain days are provided.

A measure stick was used to measure heights of plots, manually (Figure 4-37). Two or three points' height was measured for the selected plots. On the other hand, data sorting program extracted height information for each plots (14-16 records).

Measurements are compared in both with and without edge effect considerations. Table 4-6, represents an example for comparison between manual and ultrasonic height measurements for canola field on July 31, 2019. In this table, which is for with considering edge-effect condition,  $h_m$ , represents manual height,  $h_u$  represents ultrasonic height and STD (Standard Deviation) is standard derivation of records. As can be seen from this table, average, maximum and minimum percent difference ( $\%Diff$ ), when maximum  $h_u$  is selected, are 4%, 0% and 21%, respectively. Also, average, maximum and minimum  $\%Diff$ , when average  $h_u$  is selected, are 14%, 3% and 35%, respectively. Figure 4-38 shows comparison results between manual and ultrasonic sensor's height measurements of different plots with considering edge-effect.



*Figure 4- 37: Manual height measurement*

Table 4- 6: Comparison between manual and ultrasonic sensor's height measurements of different canola plot (with considering edge-effects) on July 31, 2019

R	Plot	Average manual height(cm)	Ultrasonic Height				Diff= $h_m(\text{Average}) - h_u(\text{Max})$ (cm)	% Diff	Diff= $h_m(\text{Average}) - h_u(\text{Average})$ (cm)	% Diff
			STD	Min	Max	Average				
1	6.2	101.6	13.3	74.6	124.9	87.5	-23.3	-21	14.1	15
2	6.3	102.9	6.9	88.4	110.4	98.0	-7.5	-7	4.9	5
3	6.4	102.9	16.1	44.7	101.3	85.1	1.6	2	17.8	19
4	6.5	115.6	21.8	60.8	124.4	95.8	-8.8	-7	19.8	19
5	6.6	111.8	9.8	84.0	110.0	98.5	1.8	2	13.3	13
6	6.7	102.9	9.8	73.6	111.6	95.6	-8.7	-8	7.3	7
7	6.8	101.6	7.4	86.0	107.4	93.8	-5.8	-6	7.8	8
8	6.9	97.8	7.0	74.0	96.9	86.3	0.9	1	11.5	13
9	6.1	120.7	14.7	90.6	129.1	101.0	-8.4	-7	19.7	18
10	6.11	119.4	10.2	92.2	124.8	108.6	-5.4	-4	10.8	9
11	6.12	111.8	16.6	58.8	116.1	92.9	-4.3	-4	18.9	18
12	6.13	99.1	12.0	68.2	107.0	91.6	-7.9	-8	7.5	8
13	6.14	102.9	9.6	75.5	113.3	99.6	-10.4	-10	3.2	3
14	6.15	119.4	14.7	72.7	125.6	100.3	-6.2	-5	19.1	17
15	6.16	118.1	22.0	60.7	128.7	98.8	-10.6	-9	19.4	18
16	6.17	102.9	24.9	9.4	105.4	86.0	-2.5	-2	16.9	18
17	6.18	104.1	6.5	88.2	111.0	99.8	-6.9	-6	4.3	4
18	6.19	108.0	9.8	83.4	115.5	96.7	-7.6	-7	11.3	11
19	6.2	110.5	8.3	87.2	110.1	100.2	0.4	0	10.3	10
20	6.21	121.9	7.9	90.0	119.3	104.3	2.6	2	17.6	16
21	6.22	113.0	8.5	87.8	113.7	99.1	-0.7	-1	13.9	13
22	6.23	114.3	9.6	76.3	108.5	95.2	5.8	5	19.1	18
23	6.24	108.0	13.1	40.4	99.0	86.6	9.0	9	21.4	22
24	6.25	106.7	19.2	32.7	100.6	74.9	6.1	6	31.8	35
25	6.26	94.0	7.1	70.1	91.4	83.6	2.6	3	10.3	12
26	6.27	108.0	12.8	60.9	111.2	90.5	-3.3	-3	17.5	18
27	6.28	102.9	14.7	79.0	124.0	99.0	-21.1	-19	3.9	4
28	6.29	118.1	9.5	93.7	127.6	105.7	-9.5	-8	12.4	11
29	6.3	109.2	8.5	84.0	115.8	104.6	-6.6	-6	4.6	4
30	6.31	127.0	10.4	84.7	125.2	104.9	1.8	1	22.1	19
31	6.32	114.3	7.1	93.6	118.9	101.0	-4.6	-4	13.3	12
32	6.33	124.5	9.4	99.6	130.7	109.5	-6.2	-5	15.0	13
33	6.34	116.8	11.9	76.0	130.6	107.0	-13.8	-11	9.9	9
34	6.35	127.0	8.5	92.6	122.7	103.9	4.3	3	23.1	20
35	6.36	120.7	13.4	97.0	130.7	111.6	-10.1	-8	9.1	8
36	6.37	116.8	36.0	9.2	128.5	97.9	-11.7	-10	18.9	18

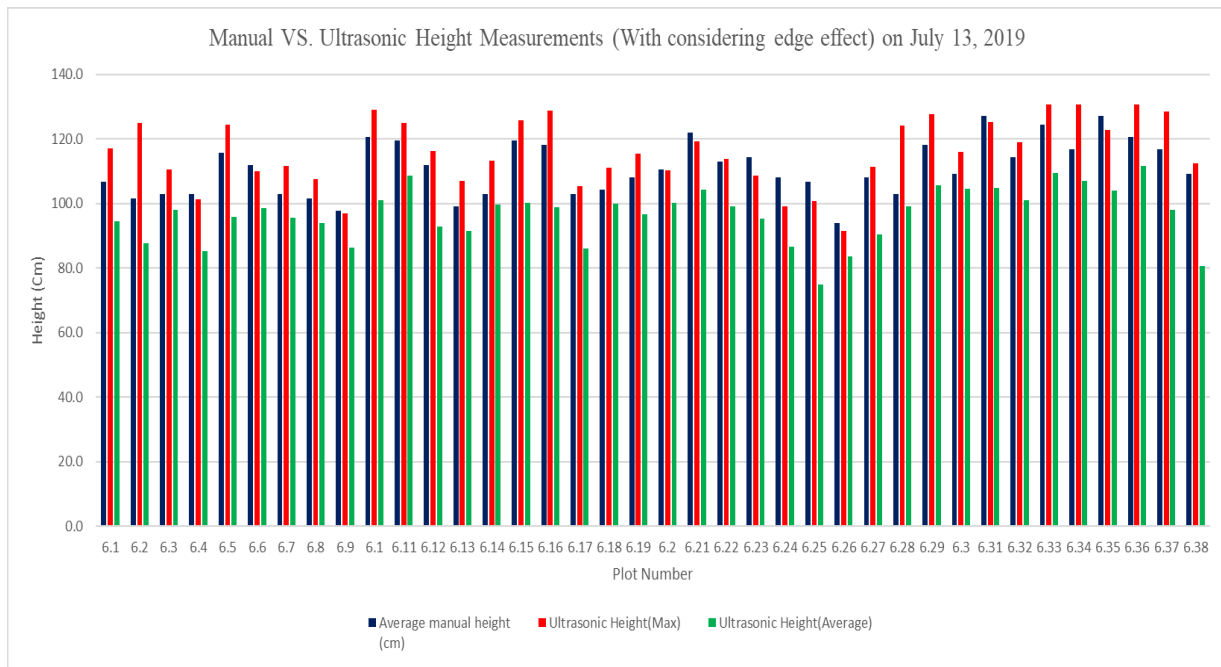


Figure 4- 38: Comparison between manual and ultrasonic sensor's height measurements of different canola plots (with considering edge-effects) on July 31, 2019

Correlation is statistical relationship between two quantitative variables. It has two types; positive and negative. If by increase of one variable, other one increases, the correlation value is positive number. When the values of one variable decrease, if the values of other variable increase, the correlation number is negative.

The correlation coefficient is a value between 0 to + 1 or -1 to 0. Figure 4-39 shows the spectrum of the correlation coefficient (-1 to +1) [44]. In this study, positive correlation approach is used for comparing manual measurements with sensor's data. The correlation coefficient of +1 is indicating perfect strong relation and 0 is indicating no relationship between two variables. The correlation value ( $r$ ) can be calculated from Pearson's correlation coefficient formula as Eq.4-3 [45].

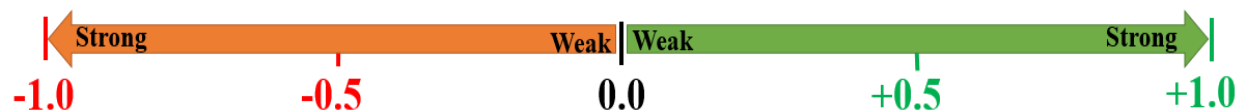


Figure 4- 39: The spectrum of the correlation coefficient (-1 to +1)

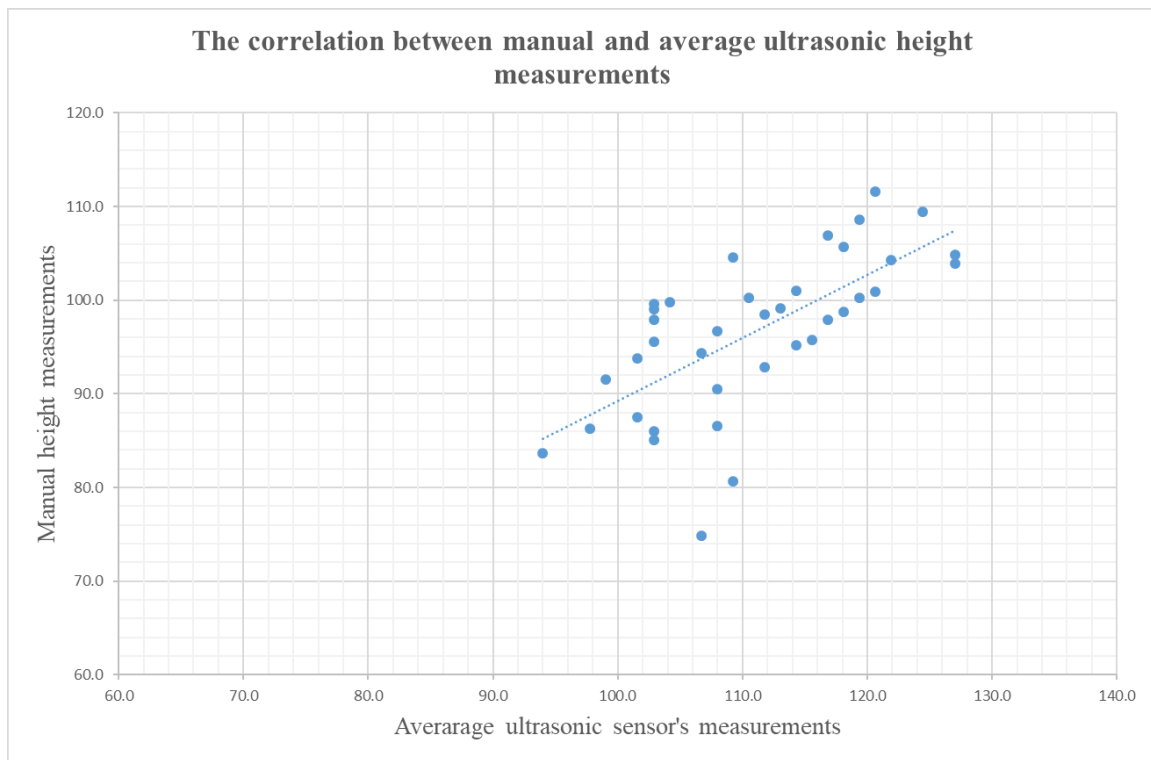
$$r = \frac{n(\sum_{i=1}^n p_i q_i) - (\sum_{i=1}^n p_i)(\sum_{i=1}^n q_i)}{\sqrt{n \sum_{i=1}^n p_i^2 - (\sum_{i=1}^n p_i)^2} \sqrt{n \sum_{i=1}^n q_i^2 - (\sum_{i=1}^n q_i)^2}} \quad (4-3)$$

Where  $p_i$  and  $q_i$  are values of variables indexed with  $i$ , and  $n$  is number of values for each variable. Therefore, the correlation between manual height measurement data and the ultrasonic measurement (Max) was found to be 0.75. Moreover, the correlation between manual height measurement data and the ultrasonic measurement (Average) was 0.68. Figure 4-40 show scatter diagrams (including regression line) for height measurement comparison of different canola plots on July 31, 2019. Table 4-7 represents summary of correlation values between manual and ultrasonic measurements for wheat and canola fields on 2018 and 2019 data collections.

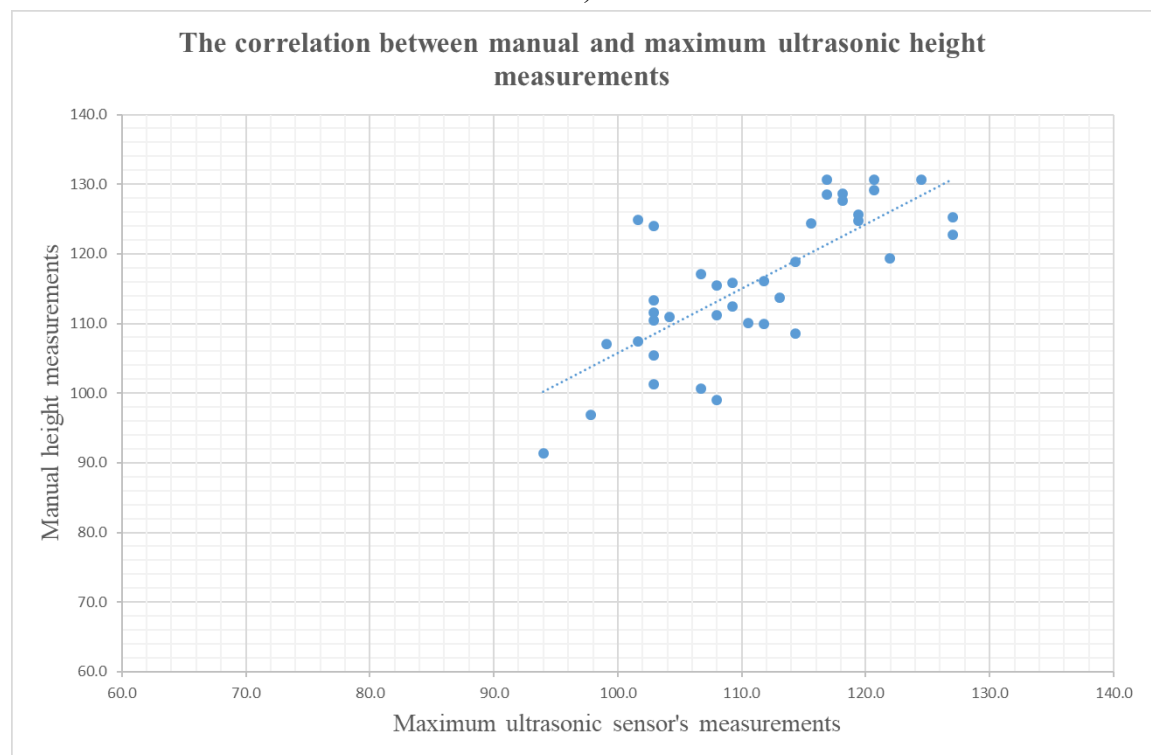
*Table 4- 7: Summary of correlation values between manual and ultrasonic measurements*

No.	Field	Date	Stage	Details	Correlation	
					manual and ultrasonic height measurement (Max)	manual and ultrasonic height measurement (Average)
1	Canola	July 28, 2018	3 <sup>rd</sup> Stage (End of flowering)	With edge-effect 22 Random plots	0.54	0.61
2	Canola	July 31, 2019	3 <sup>rd</sup> Stage (End of flowering)	Without edge-effect 1 row (6.1-6.38)	0.75	0.65
3	Canola	July 31, 2019	3 <sup>rd</sup> Stage (End of flowering)	With edge-effect 1 row (6.1-6.38)	0.75	0.68
4	Canola	August 15, 2019	4 <sup>th</sup> Stage (Start of maturity)	With edge-effect Entire field	0.75	0.74
5	Canola	August 28, 2019	5 <sup>th</sup> Stage (End of maturity)	With edge-effect 4 rows (2.1- 7.38)	0.63	0.73
6	Wheat	August 9, 2018	4 <sup>th</sup> Stage (Start of maturity)	With edge-effect 28 random plots	-0.11	0.34
7	Wheat	August 23, 2018	5 <sup>th</sup> Stage (End of maturity)	With edge-effect 28 random plots	0.23	-0.13
8	Wheat	July 23, 2019	2 <sup>nd</sup> Stage (Start of flowering)	Entire field	0.63	0.69
9	Wheat	August 20, 2019	4 <sup>th</sup> Stage (Start of maturity)	Entire field	0.63	0.77





a)



b)

*Figure 4- 40: Scatter diagrams (including regression line) between manual and a) average b) maximum ultrasonic height measurements of different canola plots on July 31, 2019.*

It is mentionable that the approach that was used for data acquisition program of ultrasonic sensors are different on 2018 and 2019 (discussed in chapter 3). In 2019, an extra ultrasonic sensor was added to the center of mechanical boom to measure boom's height continuously and it brings higher accuracy for height measurement.

Moreover, considering about edge-effect brings stronger correlation coefficient between manual and ultrasonic measurements. In other words, using edge-effect approach decreases absolute error between ultrasonic and manual height measurements (comparing No. 2 and 3 of Table 4-7).

From table 4-7, the correlation between ultrasonic and manual height measurements were very weak for wheat nurseries on 2018 data collections. For this reason, another model of ultrasonic sensor (Sick ultrasonic sensor-Model UM30-214113) was replaced in the data acquisition system for 2019 data collection. This sensor has less response time and is faster. Stronger correlation value was achieved between ultrasonic and manual height measurements (comparing No. 6-9 of Table 4-7).

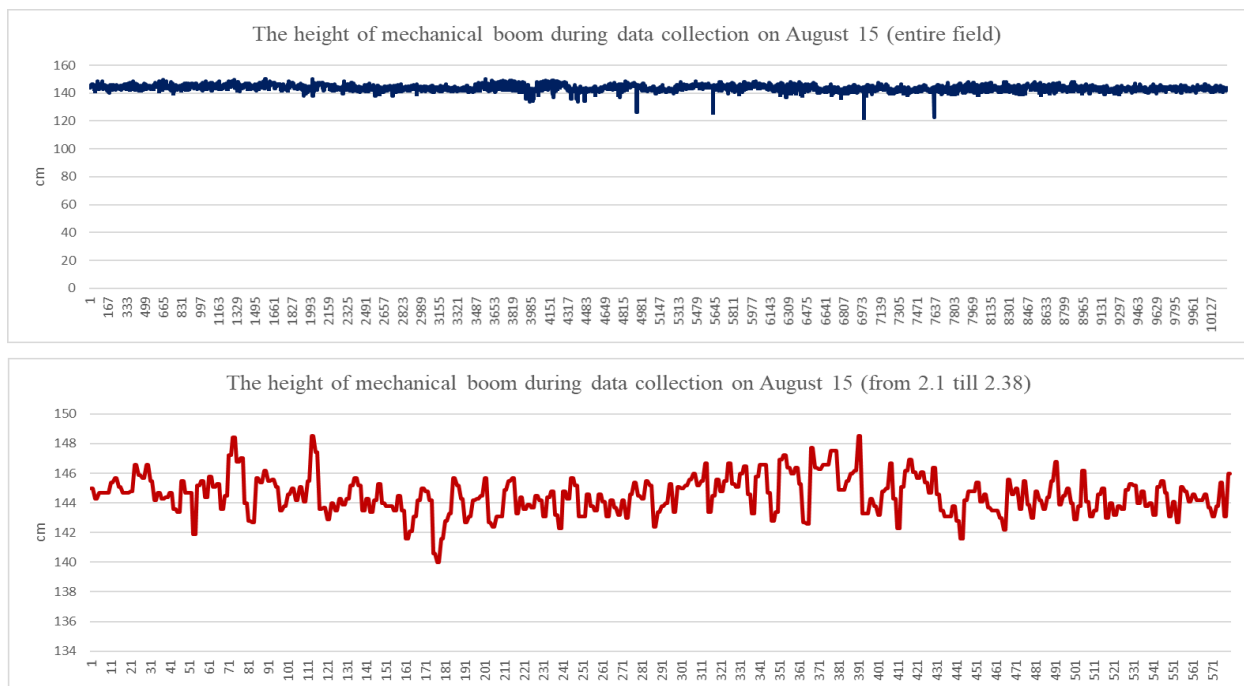


*Figure 4- 41: The height of boom during collecting data from entire and part of the field on August 15, 2019 (Measured by a separate ultrasonic sensor)*

For measuring height of plots, several issues exist that they affect the accuracy of measurements. In parts of plots, especially after the second stage (Start of flowering), tiny branches can be found. These branches affected ultrasonic sensors' operation. Although it has considered that the travelling path is flat. However, some ups and downs can be found on it, which affect ultrasonic sensors operation. Figure 4-41 illustrates the height of boom during the data collection from the studied field. These values were recorded by separate ultrasonic sensor (in the center of mechanical boom), continuously. Totally, as the developed HTPP is field-based and mobile, all these correlation and values are acceptable, and a few centimeters of difference is unescapable.

#### 4.7. Comparing manual and IRT measurements

To verify the validity of HTPP in measuring crop's temperature, their temperature were measured manually and compared. Two devices were used for manual temperature measurements, hand held thermometer and thermal camera (Figure 4-42).

By using hand held thermometer sensor (IRTC40), temperature of plots were measured manually for both canola and wheat fields on 2018 (Figure 4-42.a). Several plots with different genotypes were selected randomly and their temperature were measured with this device from 4-6 points.



*Figure 4- 42: Manual temperature measurement by portable a) hand held thermometer b) thermal camera*

Table 4- 8: Comparison between manual (hand held thermometer) and IRT sensor temperature measurements of different canola plot (with considering edge-effects) on August 2, 2018

R	Plot number	Manual Temperature Measurement						Average of Manual Temp.	IRT Temp.	Diff= (Ave of Manual Temp)-(IR Temp)	%Diff= $\frac{\text{Diff}}{(\text{Ave Temp}+\text{IR Temp})/2}$
		Temp. 1 (C°)	Temp. 2 (C°)	Temp. 3 (C°)	Temp. 4 (C°)	Temp. 5 (C°)	Temp. 6 (C°)				
1	21.5	27.5	29.8	32.8	29.1	30.0	N/A	29.8	35.9	-6.1	-19%
2	21.6	30.3	28.4	30.8	31.0	N/A	N/A	30.1	36.8	-6.7	-20%
3	22.6	27.4	29.3	28.6	27.9	28.2	N/A	28.2	36.1	-7.8	-24%
4	22.5	27.2	27.2	28.7	25.8	25.5	N/A	26.8	33.6	-6.7	-22%
5	23.2	28.9	30.0	28.4	27.5	N/A	N/A	28.7	35.5	-6.8	-21%
6	23.7	34.1	34.2	27.0	25.8	N/A	N/A	30.2	35.5	-5.2	-16%
7	24.7	27.0	28.4	28.7	27.5	29.8	28.1	28.2	39.2	-11.0	-32%
8	24.1	27.6	26.8	27.8	25.3	26.2	26.7	26.7	31.0	-4.3	-15%
9	25.2	27.2	26.7	28.2	27.4	26.5	N/A	27.2	35.4	-8.2	-26%
10	25.3	26.8	29.3	27.0	28.4	27.5	N/A	27.8	34.9	-7.1	-23%
11	26.7	26.5	26.0	27.5	27.5	28.6	N/A	27.2	35.3	-8.1	-26%
12	26.3	28.9	27.4	27.7	26.3	28.1	25.5	27.3	35.0	-7.7	-25%
13	27.2	29.1	29.1	31.1	29.8	N/A	N/A	29.7	34.9	-5.1	-16%
14	27.7	29.3	30.5	30.6	28.4	26.2	N/A	29.0	35.8	-6.8	-21%
15	28.5	27.2	28.1	26.8	26.3	28.4	27.5	27.3	34.4	-7.0	-23%
16	28.2	28.2	27.5	N/A	25.0	26.2	26.0	26.5	33.7	-7.2	-24%
17	29.2	26.8	25.8	28.7	28.4	27.2	27.7	27.4	33.1	-5.7	-19%
18	29.7	25.8	25.6	25.8	25.8	25.6	N/A	25.7	29.8	-4.0	-15%
19	30.7	25.5	23.9	25.8	26.3	26.2	N/A	25.5	30.2	-4.7	-17%
20	30.3	30.8	29.1	31.1	28.6	26.7	30.6	29.4	36.2	-6.7	-20%
21	31.2	28.1	30.0	29.1	29.1	30.8	28.9	29.3	35.5	-6.2	-19%
22	31.6	28.2	27.0	27.0	29.8	27.4	26.3	27.6	30.5	-2.8	-10%
23	32.6	26.2	26.7	N/A	25.8	26.2	N/A	26.2	30.1	-3.9	-14%
24	32.3	26.0	29.1	27.4	26.5	26.5	N/A	27.1	32.4	-5.3	-18%
25	33.1	27.0	27.4	28.4	27.5	26.7	29.0	27.6	30.2	-2.6	-9%
26	33.2	28.1	29.4	28	27.9	28.5	27.0	28.1	31.0	-2.8	-10%
27	33.5	26.7	27.7	26.7	29.1	30.0	27.5	27.9	31.2	-3.3	-11%
28	34.6	26.8	28.2	26.8	25.0	25.6	N/A	26.4	32.7	-6.2	-21%
29	34.2	26.3	25.6	N/A	26.5	27.9	27.5	26.7	30.3	-3.5	-13%
30	35.3	25.8	26.5	26.2	26.7	N/A	N/A	26.3	29.9	-3.6	-13%
31	35.7	28.1	28.9	28.6	29.3	N/A	N/A	28.7	33.5	-4.7	-15%
32	36.5	27.0	26.8	26.7	26.5	25.3	25.7	26.3	33.5	-7.1	-24%
33	36.2	28.1	26.7	27.0	25.8	26.5	N/A	26.8	31.5	-4.7	-16%
34	37.1	26.3	26.0	26.8	25.8	N/A	N/A	26.2	28.7	-2.5	-9%
35	37.6	27.4	27.5	29.6	31.0	N/A	N/A	28.8	33.2	-4.3	-14%

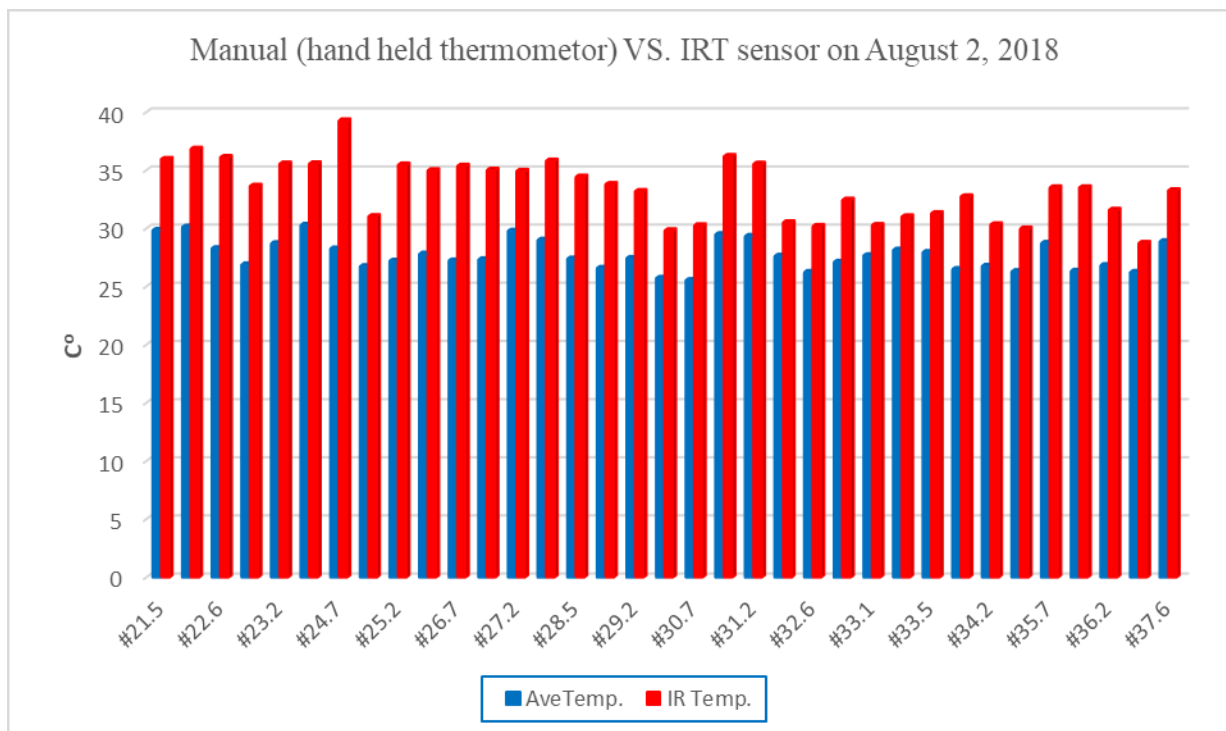


Figure 4- 43 Comparison between manual (hand held thermometer) and IR sensor temperature measurements of different canola plot (with considering edge-effects) on August 2, 2018:

Table 4-8 shows an example for comparison between manual (hand held thermometer) and IRT temperature measurements for canola field on August 2, 2018. Figure 4-43 shows the bar graph of comparison between manual (hand held thermometer) and IRT temperature measurements of different canola plots.

From table 4-8, it can be found that the maximum and minimum percent difference (% Diff) are -26% and -9%, respectively. The correlation between the manual temperature measurements (handheld thermometer) data and IR-thermometer sensor's measurements was 0.66. Figure 4-44 shows scatter diagram (including regression line) for temperature measurement comparison (hand held thermometer vs. IRT sensor) for different canola plots on August 2, 2018.

A TIC (Thermal Imaging Camera) is a device that is able to record thermal images of crops, shown in Figure 4-42.b. A thermal image captures information on the temperature of different points, and then an operator can extract data from taken images, as illustrated in Figure 4-45. The model of thermal camera, which was used in 2019 growing season was FLIR C3. Fifty-two (52) plots were selected, randomly, for taking thermal image. In this part, comparison of the IRT sensor, and the manual measurements (using thermal camera) is provided.



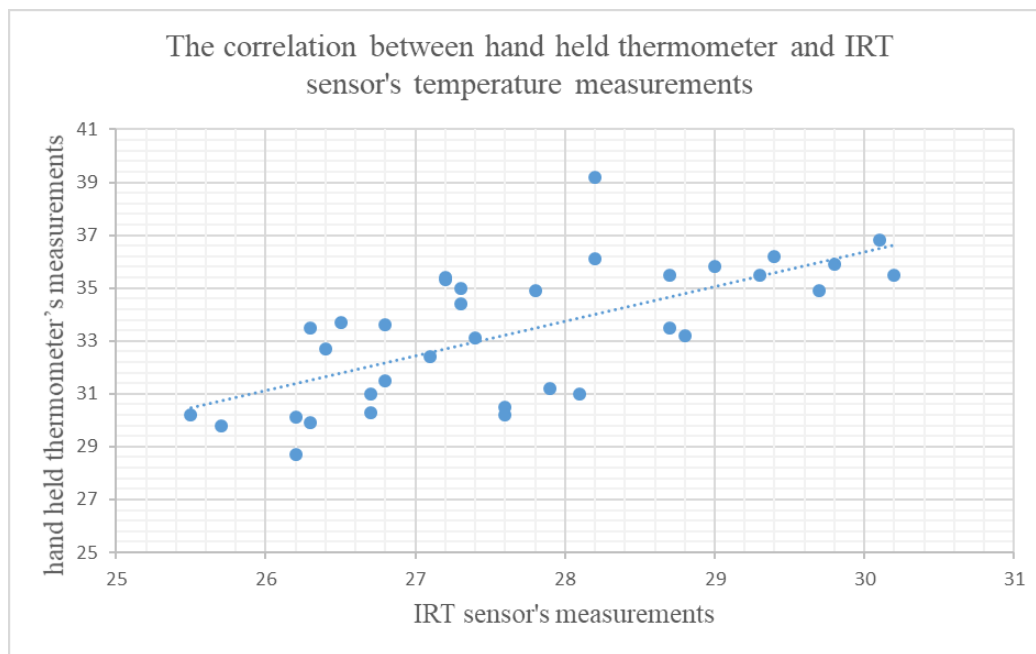


Figure 4- 44: Scatter diagram (including regression line) between hand held thermometer and IRT sensor's temperature measurements of different canola plots on August 2, 2018

For extracting temperature values from thermal images, 6 almost random points (S1-S6) were selected for each image. As can be seen in Figure 4-45, S1-S5 were selected from the area of plots' inside and S6 was selected from the soil, which is the gap between two plots. It was found that the temperature of soil always is higher than the crop's temperature.

Measurements	
Sp1	20.5 °C
Sp2	20.4 °C
Sp3	20.7 °C
Sp4	20.5 °C
Sp5	20.7 °C
Sp6	34.9 °C
Parameters	
Emissivity	0.85
Refl. temp.	20 °C
Distance	2 m
Atmospheric temp.	20 °C
Ext. optics temp.	20 °C
Ext. optics trans.	1
Relative humidity	50 %

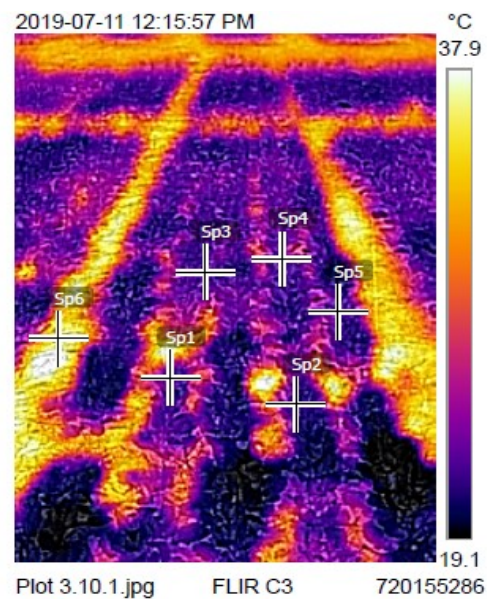


Figure 4- 45: A sample thermal image from a plant and selected different points for reading temperature from thermal camera

For this comparison, average recorded values of these two sensors per plot were used. For a sample plot, average values of 5 points (S1-S5) from thermal camera picture was compared with average value of about 8-10 data points from IRT measurements. Table 4-9 shows comparison between the thermal camera and IRT sensor temperature measurements of several plots on July 11, 2019. From this table, maximum and minimum percent difference (*% Diff*) are 20% and 0%, respectively. The correlation between the camera and the IRT sensor measurements was found to be 0.85. Figures 4-46 and 4-47 illustrate the bar graph of this comparison.

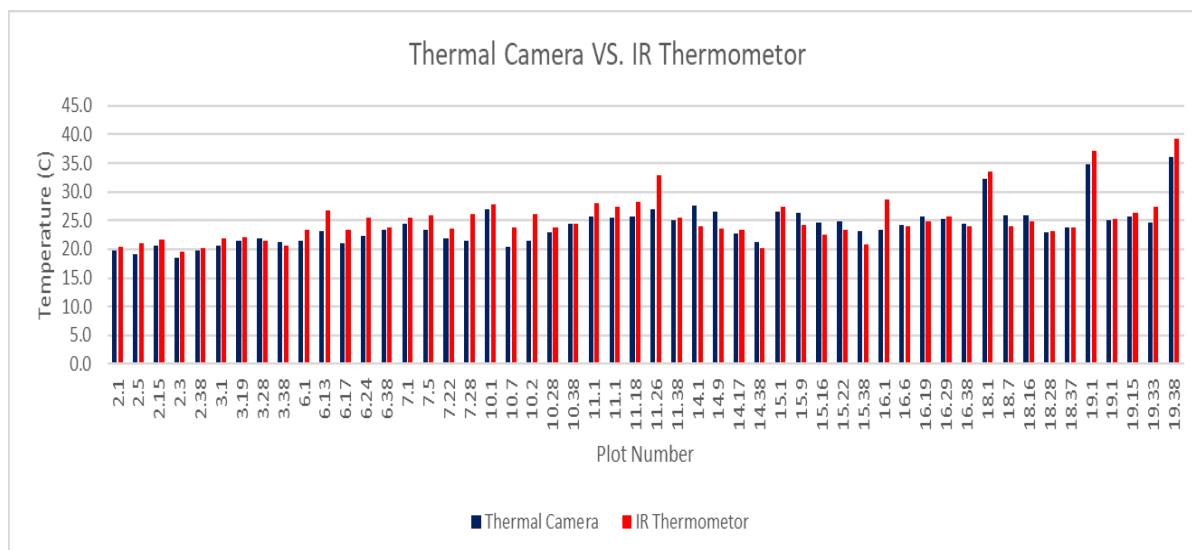


Figure 4- 46: Comparison between the thermal image and IRT sensor temperature measurements of different random canola plots on July 11, 2019

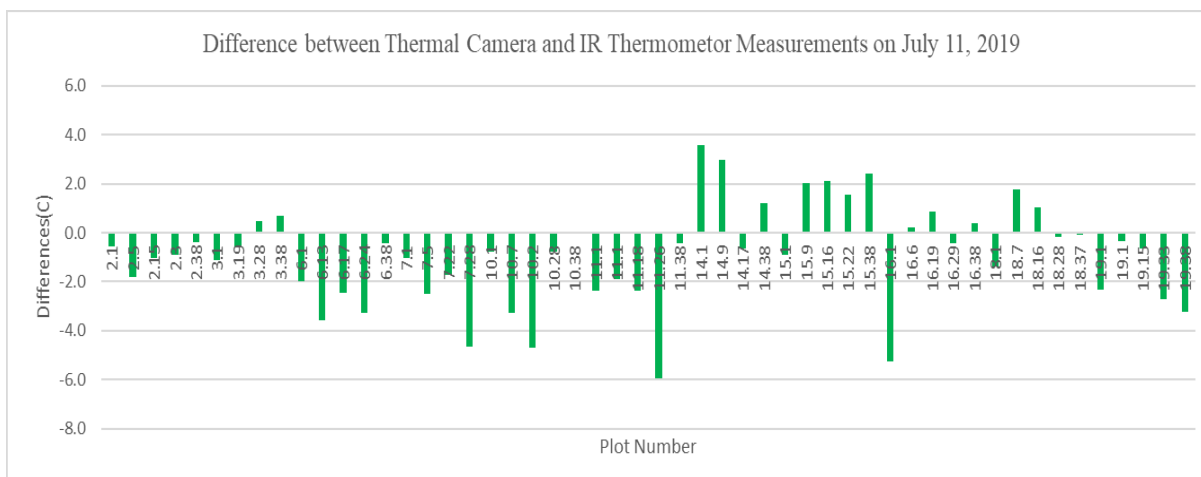


Figure 4- 47: Differences between the thermal image and IRT sensor temperature measurements of different random canola plots on July 11, 2019



*Table 4- 9: Comparison between the thermal image and IR sensor temperature measurements of different random plots on July 11, 2019*

R	Plot number	Manual Temperature Measurement				IRT Measurement				Diff= (Ave of Manual Temp)-(IR Temp)	%Diff
		STD	Min	Max	Average	STD	Min	Max	Average		
1	2.1	0.1	19.7	20.0	19.8	1.1	18.9	21.5	20.4	-0.6	-3
2	2.5	0.1	19.0	19.4	19.2	1.2	19.4	22.8	21.0	-1.8	-9
3	2.15	0.5	19.9	21.1	20.6	0.6	21.0	22.6	21.6	-1.0	-5
4	2.3	0.1	18.4	18.7	18.6	0.9	18.5	20.8	19.5	-0.9	-5
5	2.38	0.3	19.5	20.1	19.9	0.4	19.6	21.1	20.2	-0.4	-2
6	3.1	0.5	20.3	22.3	20.7	1.8	19.5	25.3	21.8	-1.1	-5
7	3.19	1.2	20.1	23.1	21.4	1.7	20.4	25.3	22.0	-0.6	-3
8	3.28	1.2	20.5	23.4	22.0	1.4	19.6	23.2	21.5	0.5	2
9	3.38	1.3	19.9	23.0	21.3	0.9	19.7	22.2	20.6	0.7	3
10	6.1	0.3	21.0	21.8	21.4	2.7	21.4	30.1	23.4	-2.0	-9
11	6.13	0.3	22.8	23.3	23.1	3.3	23.6	32.1	26.7	-3.6	-14
12	6.17	0.5	20.5	21.5	20.9	0.4	22.9	23.9	23.4	-2.5	-11
13	6.24	0.4	21.8	22.6	22.3	2.1	22.8	28.5	25.5	-3.3	-14
14	6.38	0.7	22.8	24.4	23.3	1.6	22.1	26.7	23.8	-0.4	-2
15	7.1	0.8	23.5	25.5	24.4	2.1	23.8	30.3	25.4	-1.0	-4
16	7.5	1.2	21.7	24.9	23.3	0.7	25.0	27.1	25.8	-2.5	-10
17	7.22	1.9	19.9	24.1	21.8	2.5	21.2	28.0	23.6	-1.7	-8
18	7.28	0.8	20.5	22.7	21.5	4.5	21.7	33.7	26.2	-4.6	-19
19	10.1	0.9	25.8	27.8	27.1	2.6	25.6	33.5	27.8	-0.8	-3
20	10.7	1.0	19.3	21.6	20.4	0.6	23.1	25.0	23.7	-3.3	-15
21	10.2	0.5	20.7	22.0	21.4	1.8	24.0	29.8	26.1	-4.7	-20
22	10.28	0.5	22.2	23.3	22.9	1.8	22.1	27.5	23.7	-0.8	-3
23	10.38	0.3	24.1	24.8	24.4	1.0	23.5	26.3	24.5	-0.1	0
24	11.1	1.5	24.0	28.2	25.7	4.2	25.3	37.2	28.1	-2.4	-9
25	11.1	0.9	24.2	27.1	25.5	1.8	25.7	30.1	27.4	-1.9	-7
26	11.18	0.8	24.4	26.9	25.8	3.1	26.0	34.7	28.1	-2.4	-9
27	11.26	3.2	23.7	33.4	27.0	1.8	29.9	35.1	33.0	-6.0	-20
28	11.38	1.7	23.1	28.0	25.0	2.3	24.0	28.9	25.4	-0.4	-2
29	14.1	1.1	26.8	29.2	27.6	1.0	22.7	26.2	24.0	3.6	14
30	14.9	0.3	26.2	26.9	26.5	0.7	22.5	24.3	23.6	3.0	12
31	14.17	0.4	22.2	23.1	22.6	1.9	21.3	27.1	23.3	-0.7	-3
32	14.38	0.6	20.7	22.1	21.3	1.4	18.8	22.6	20.1	1.2	6
33	15.1	1.7	24.7	27.9	26.4	4.8	23.5	37.0	27.4	-0.9	-3
34	15.9	1.0	25.5	27.7	26.3	2.6	21.5	28.5	24.3	2.0	8
35	15.16	0.5	24.3	25.3	24.6	1.0	21.5	24.7	22.5	2.1	9

36	15.22	0.4	24.3	25.3	24.9	1.2	21.8	25.1	23.3	1.6	6
37	15.38	0.2	22.9	23.4	23.2	1.6	19.4	22.6	20.8	2.4	11
38	16.1	1.6	21.6	25.9	23.3	7.9	22.0	40.8	28.6	-5.3	-20
39	16.6	2.8	21.5	27.1	24.3	1.9	22.1	26.4	24.1	0.2	1
40	16.19	1.8	23.6	28.1	25.7	1.1	23.5	27.1	24.8	0.9	3
41	16.29	1.6	23.0	27.1	25.2	2.0	24.5	30.1	25.7	-0.4	-2
42	16.38	1.3	22.9	25.8	24.3	0.4	23.5	24.4	24.0	0.4	2
43	18.1	6.1	26.3	39.6	32.2	1.4	32.1	36.4	33.5	-1.4	-4
44	18.7	0.7	24.9	26.5	25.8	0.5	23.4	24.7	24.1	1.8	7
45	18.16	1.0	25.0	27.3	25.9	1.6	22.9	27.0	24.8	1.0	4
46	18.28	0.3	22.8	23.4	23.0	1.0	22.2	24.7	23.2	-0.2	-1
47	18.37	0.5	23.2	24.3	23.8	0.5	23.3	24.6	23.9	-0.1	0
48	19.1	4.6	26.9	40.3	34.8	2.5	33.2	40.1	37.1	-2.3	-6
49	19.1	0.7	24.1	26.0	25.0	0.7	24.6	26.6	25.4	-0.3	-1
50	19.15	0.8	24.6	26.8	25.6	1.2	25.4	28.7	26.3	-0.7	-3
51	19.33	1.1	23.5	26.7	24.6	3.4	23.9	31.1	27.3	-2.7	-10
52	19.38	3.1	31.9	40.4	36.0	1.4	37.9	41.4	39.2	-3.2	-9

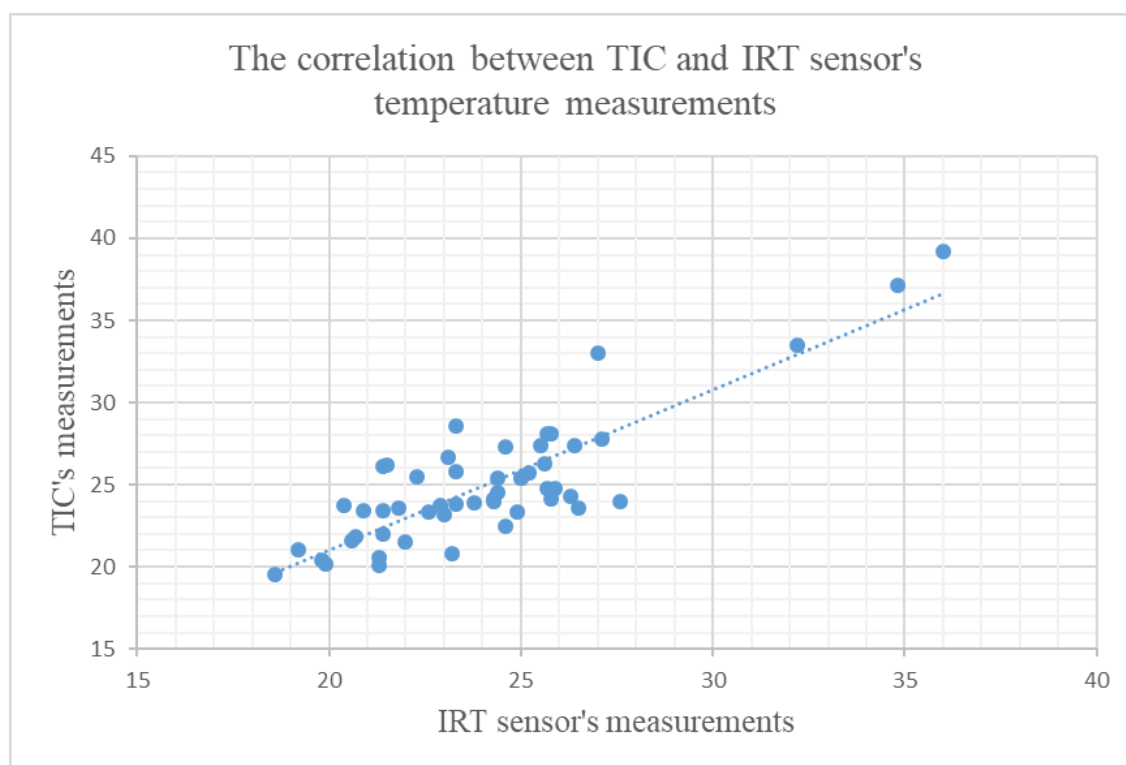


Figure 4- 48: Scatter diagram (including regression line) between TIC and IRT sensor's temperature measurements of different canola plots on July 11, 2019

*Table 4- 10: Summary of correlation values between manual (hand held thermometer and thermal camera) and IRT measurements*

No.	Field	Date	Stage	Details	Manual measurement device	Manual and IRT measurement
1	Canola	August 2, 2018	4 <sup>th</sup> Stage (Start of maturity)	With edge-effect 35 Random plots	Hand held thermometer	0.66
2	Canola	July 11, 2019	2 <sup>nd</sup> Stage (Start of flowering)	With edge-effect 52 Random plots	Thermal camera	0.85
3	Wheat	August 9, 2018	4 <sup>th</sup> Stage (Start of maturity)	Without edge-effect 40 random plots	Hand held thermometer	0.6
4	Wheat	August 1, 2019	3 <sup>rd</sup> Stage (End of flowering)	Without edge-effect 28 random plots	Thermal camera	0.52

Figure 4-48 shows scatter diagram (including regression line) for temperature measurement comparison (TIC vs. IRT sensor) of different canola plots on July 11, 2019. The correlation value for 2019 growing season (0.85) is stronger. As discussed, for 2018 data collection, the correlation coefficient between the manual temperature measurements (handheld thermometer) data and IR-thermometer sensor's measurements was about 0.66. Table 4-11 represents summary of correlation values between manual (hand held thermometer and thermal camera) and IRT measurements for wheat and canola fields on 2018 and 2019 data collections on different days. All these correlation values are acceptable and strong enough to conclude that the developed field-based and mobile HTPP is working reliably and accurately.

#### **4.8. Comparing weather stations (HTPP vs. Local)**

In this section the validity of weather station probe's operation for measuring ambient temperature and humidity are discussed. For this reason, the results of comparing operation of HTPP's weather station (HMP60) (Figure 4-49) with local weather station (Figure 4-50), which was in the side of data collection, are provided. Table 4-11, represents comparison between local and HTPP's weather station measurements for canola field on July 18, 2018.  $T_c$  and  $H_c$  are representing related values to the local weather station's temperature and humidity records.  $T_p$  and  $H_p$  are representing related values to the HTPP weather station's temperature and humidity measurements. Figures 4-51 and 4-52 compares local and HTPP's weather station's operations (temperature and humidity measurements).



Figure 4- 49: HTPP's weather station for canola data collections



Figure 4- 50: local weather station in the side on 2018 data collections

It can be found that the maximum and minimum percent difference (%Diff) for temperature measurements are -21% and 0%, respectively. In addition, maximum and minimum %Diff for humidity measurements are 54% and 2%, respectively.

Table 4- 11: Comparison between local and HTPP's weather station measurements during different times on July 18, 2018

R	Time	Local weather station		HTPPs' weather station		$Diff_T = T_c - T_p$	$Diff_H = H_c - H_p$	$\%Diff_T = \frac{Diff_T}{(T_c + T_p)/2}$	$\%Diff_H = \frac{Diff_H}{(H_c + H_p)/2}$
		Temperature ( $T_c$ )	Humidity ( $H_c$ )	Temperature ( $T_p$ )	Humidity ( $H_p$ )				
1	7/18/2018 11:00	27.0	61.4	24.9	64.2	2.0	-2.8	8%	-5%
2	7/18/2018 12:32	26.6	64.2	32.9	36.5	-6.3	27.6	-21%	54%
3	7/18/2018 13:00	26.3	61.7	31.7	40.2	-5.4	21.4	-19%	42%
4	7/18/2018 15:30	26.6	64.8	30.2	46.7	-3.6	18.0	-13%	32%
5	7/18/2018 16:30	25.2	64.2	28.9	54.8	-3.7	9.3	-14%	16%
6	8/02/2018 11:30	25.3	54.8	26.5	47.7	-1.2	7.0	-5%	14%
7	8/02/2018 12:00	26.3	53.0	28.1	48.4	-1.8	4.5	-7%	9%
8	8/02/2018 12:30	27.1	52.3	29.4	45.1	-2.3	7.1	-8%	15%
9	8/02/2018 15:30	29.1	42.5	29.3	39.8	-0.2	2.6	-1%	6%
10	8/02/2018 16:00	29.4	42.9	29.4	40.0	-0.0	2.8	0%	7%
11	8/14/2018 11:30	21.6	39.1	20.8	41.0	0.8	-1.9	4%	-5%
12	8/14/2018 12:30	23.5	35.6	23.4	34.7	0.0	0.8	0%	2%
13	8/14/2018 15:00	26.8	28.4	26.2	27.1	0.5	1.2	2%	4%
14	8/14/2018 16:30	27.8	26.5	27.0	25.2	0.7	1.2	3%	5%

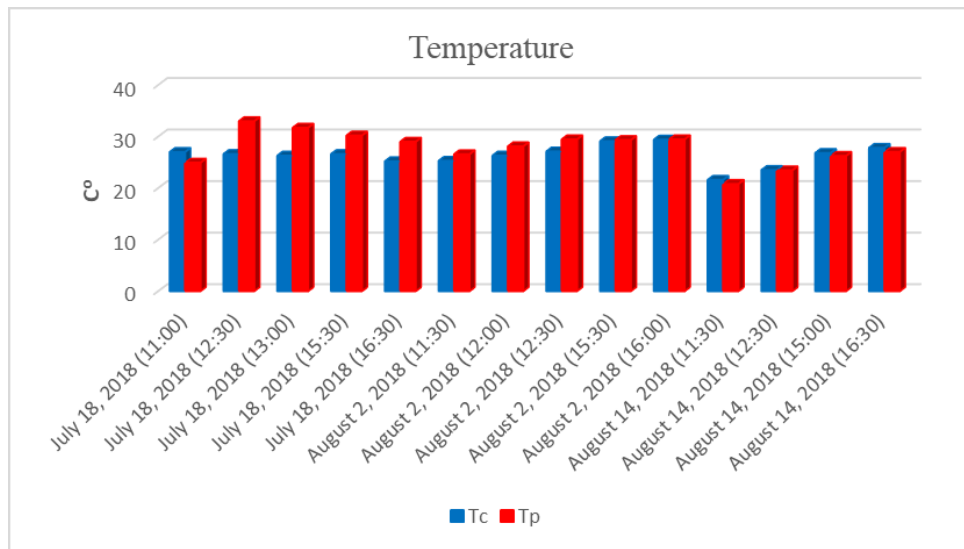


Figure 4- 51: Comparison between local and HTPP's weather station measurements for temperature during different times on July 18, 2018

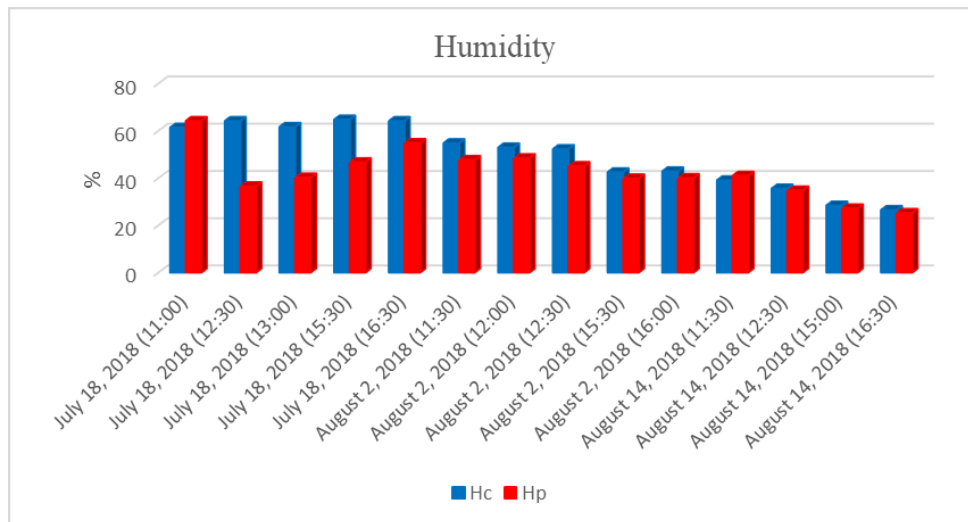


Figure 4- 52: Comparison between local and HTPP's weather station measurements for humidity during different times on July 18, 2018

The correlation coefficients for Table 4-11 was calculated from Eq. 4-3. The correlation between  $T_c$  and  $T_p$  values was found to be 0.63, and between  $H_c$  and  $H_p$  values was 0.73. Figure 4-53 and 4-54 show scatter diagram (including regression line) for ambient temperature and humidity comparison on July 18, 2018. These correlation values are strong enough to conclude that selected, wired and programmed ambient temperature and humidity probe is working reliably on the outdoor configurations.

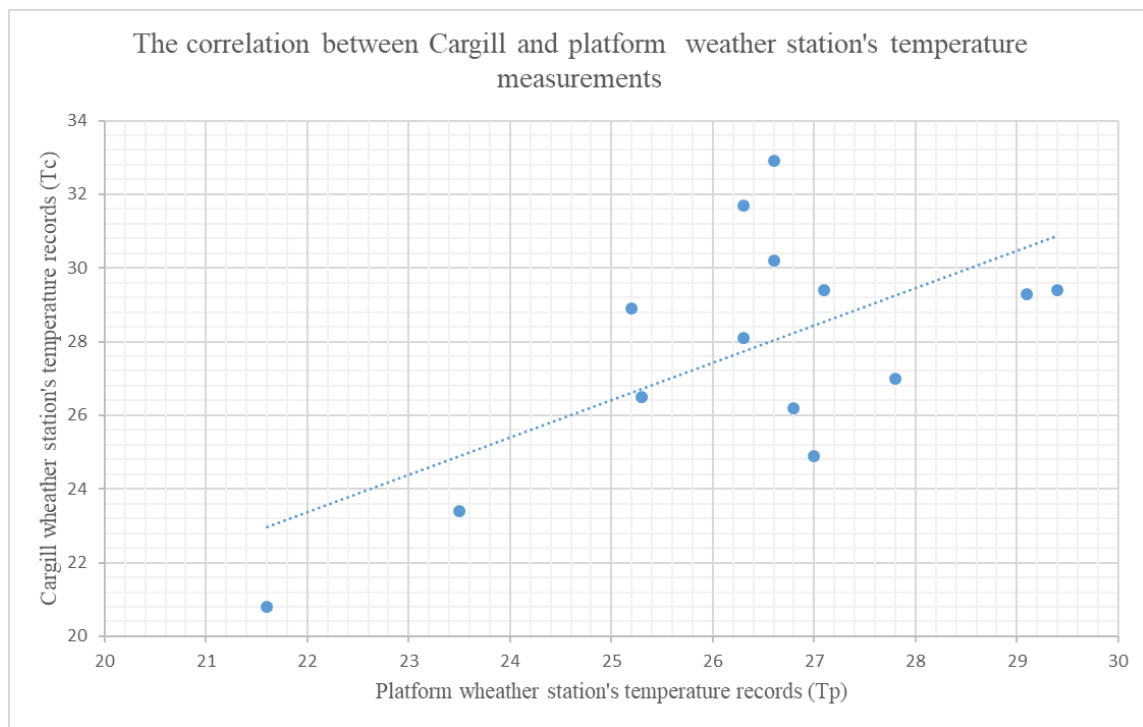


Figure 4- 53: Scatter diagram (including regression line) between temperature records of local and HTPP's weather station on July 18, 2018

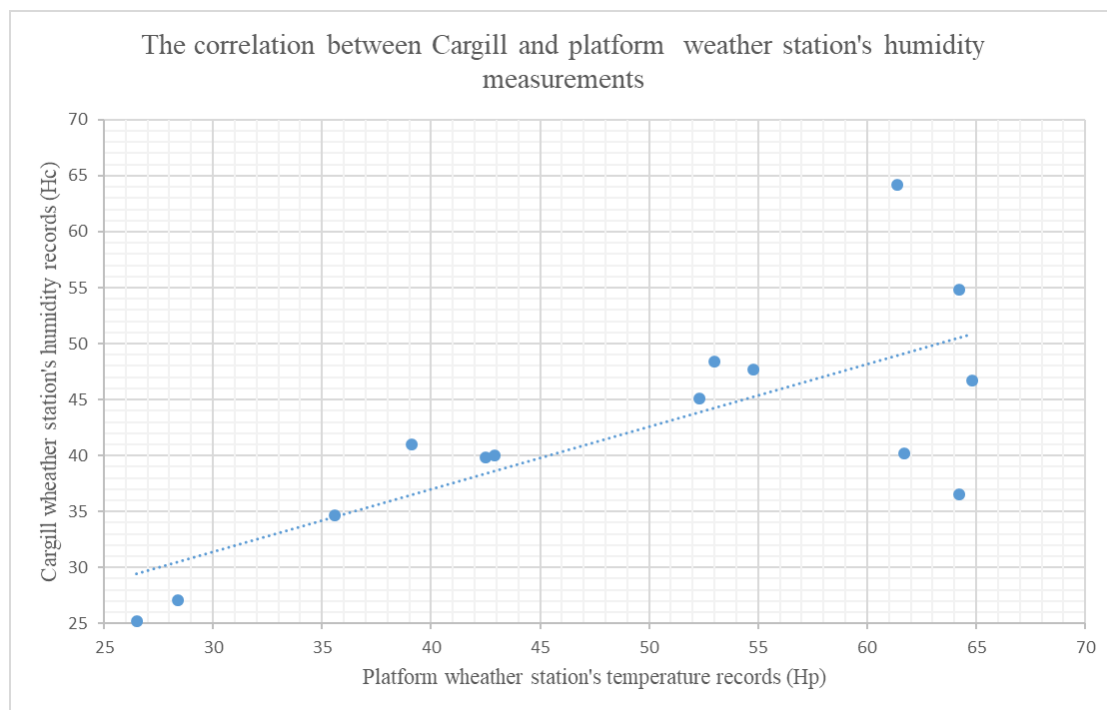


Figure 4- 54: Scatter diagram (including regression line) between humidity records of local and HTPP's weather station on July 18, 2018

## 4.9. Comparing Crop Circle and multispectral camera

In this section, the operation of NDVI measurement devices is compared. As mentioned in section 2.4, two different devices, Crop Circle (Holland Scientific ACS-430) and multispectral camera (msCAM CMV4000), were used for NDVI measurement.

Crop Circle measures and records NDVI values by using of a data acquisition program. The sensor's output is digital and shows vegetation index values as string.

Data acquisition program prepares phenotypic database and one of its item is NDVI value of plants in canopy. This program records four sample points per second. Since, vehicle's speed was set to 1.6 mph, NDVI values of about 8-10 data points were recorded for each plot. Table 4-12 provides NDVI values of a random canola plot (#14.30) on July 31, 2019.

*Table 4- 12: Sorted NDVI data for plot #14.30 on July 31, 2019 (End of flowering status)*

Record	NDVI value	
	Without Edge Effect	With Edge Effect (10 cm eliminated from each side)
1	0.789	N/A
2	0.802	0.802
3	0.781	0.781
4	0.797	0.797
5	0.774	0.774
6	0.804	0.804
7	0.784	0.784
8	0.799	0.799
9	0.796	0.796
10	0.784	N/A
Min	0.774	0.774
Max	0.804	0.804
Average	0.791	0.792
STD	0.010	0.011



To utilize multispectral camera, two different programs were developed, which are multispectral image acquisition for autonomous image capturing and post-processing for extracting NDVI information from captured images.

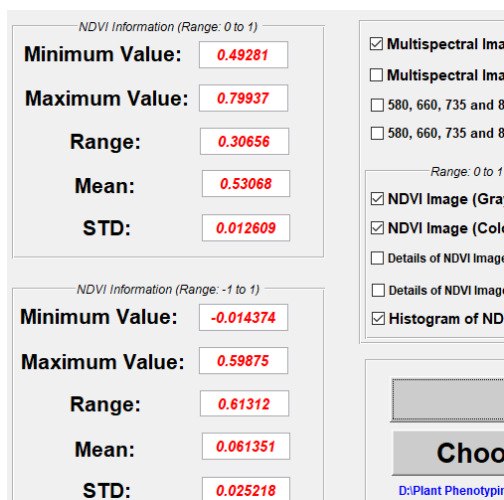
Multispectral image acquisition program captures pictures of a crop within specific wavelengths. This program records two sample points per second and as a result, about 2-4 multispectral images were captured for each plot. To extract NDVI information, post-processing program was utilized. Figure 4-55, illustrates extracted NDVI information for a canola plot (#14.30) on July 31, 2019.

For both measuring devices, the amount of standard derivation between records is very small and reasonable. Multispectral camera monitors wider area (as discussed in section 2.4) and NDVI information of crops was effected by soil's NDVI values in some parts of the image. Therefore, minimum and average pixel values of NDVI image is lower than Crop Circle records. By this reason, for comparing operation of two devices within 0 to 1 range, their maximum records are compared. Percent difference (*%Diff*) for plot #14.30, can be calculated as:

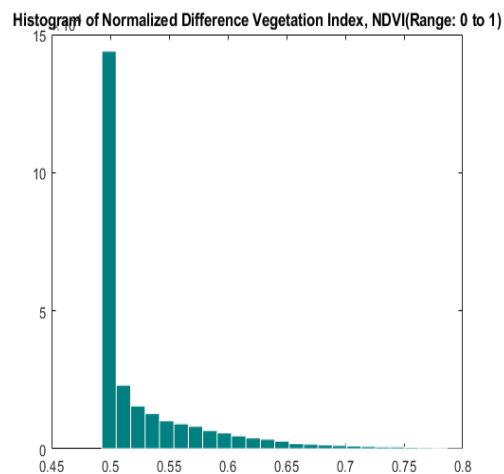
$$\% Diff = \frac{NDVI_{Crop\ Circle} - NDVI_{Multispectral}}{(NDVI_{Crop\ Circle} + NDVI_{Multispectral})/2} \times 100 = \frac{0.804 - 0.799}{(0.804 + 0.799)/2} \times 100 = 0.62\% \quad (4-4)$$

This *%Diff* value is very reasonable. Table 4-13 provides more example of monitored canola plots in the growing season of 2019. All *%Diff* values are acceptable and the correlation value between Crop Circle and multispectral camera is 0.94. This value is excellent and indicates the validity of HTPP in the NDVI measurement.

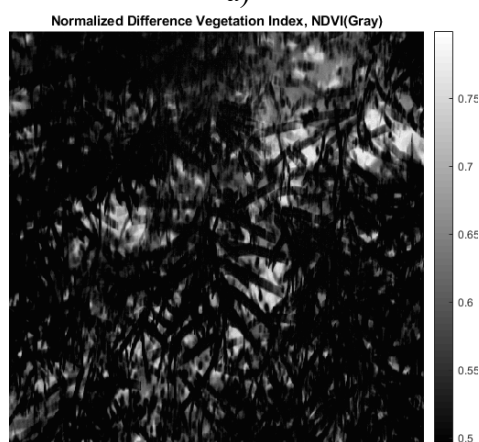
Defining the superiority of these two sensors depends on breeders and plant scientist' demands. Each method of NDVI measurement has pros and cons, which are listed in table 4-14. Totally, multispectral image gives more and detail information about NDVI of crops. However, many challenges such as multispectral camera's calibration and its sensitivity to ambient light exist. For example, during the data collection, clouds may cover sun and this will affect calibration of multispectral camera and quality of captured images.



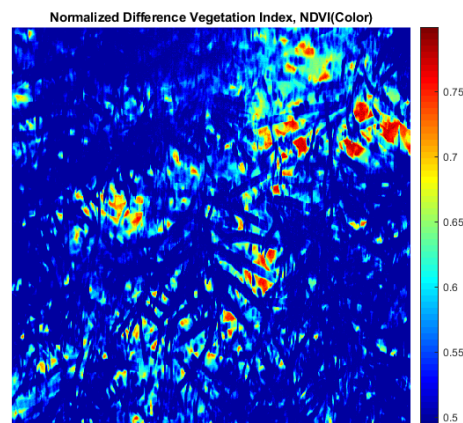
a)



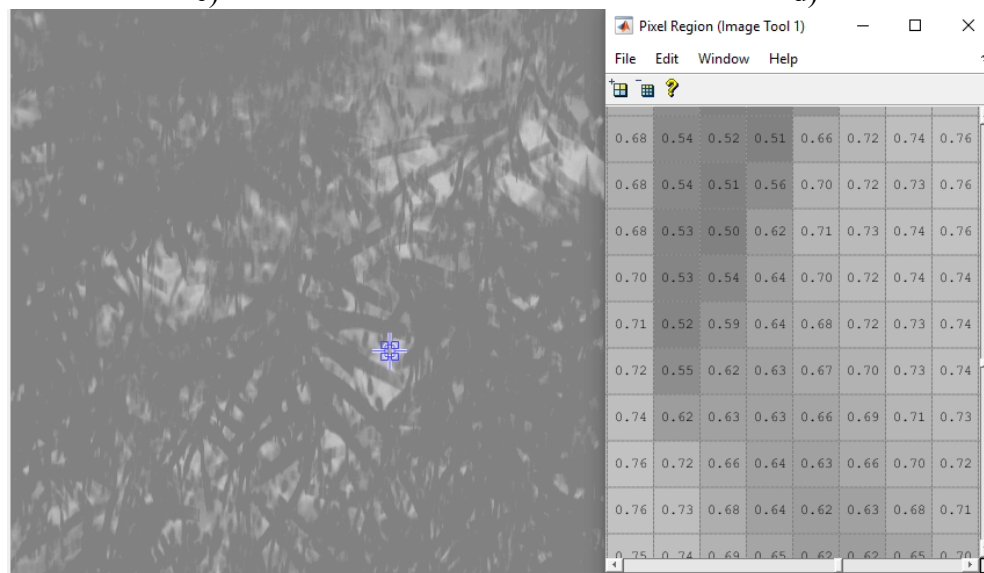
b)



c)



d)



e)

Figure 4- 55: Extracted NDVI information via multispectral image's post processing program for canola plot #14.30 on July 31, 2019 a) NDVI values within two ranges b) histogram of NDVI pixels c) gray NDVI image d) color NDVI image e) detailed information of NDVI image

*Table 4- 13: Comparison between Crop Circle and Multispectral camera's NDVI measurements of different canola plot on 2019*

R	Date	Plot Number	Measured NDVI		%Diff
			Crop Circle Sensor	Multispectral Camera	
1	2019.6.26	# 2.9	0.672	0.574	15.7
2	2019.6.26	# 11.15	0.581	0.577	0.7
3	2019.7.11	# 6.22	0.783	0.807	-3.0
4	2019.7.11	# 18.7	0.794	0.792	0.3
5	2019.7.31	# 14.30	0.792	0.799	-0.9
6	2019.7.31	# 3.6	0.770	0.764	0.8
7	2019.8.28	# 10.33	0.702	0.691	1.6
8	2019.8.28	# 15.10	0.708	0.718	-1.4

*Table 4- 14: Advantages and disadvantages of NDVI measurement devices*

Device	Advantages	Disadvantages
Crop Circle Sensor	<ul style="list-style-type: none"> <li>• Insensitive to ambient light.</li> <li>• No necessity for calibration before data collection.</li> <li>• Less response time and fast device.</li> </ul>	<ul style="list-style-type: none"> <li>• Preparing just NDVI value of each record. This value can be effected by the area that is not target such as soil part.</li> <li>• Calculating NDVI values within just 0 to 1 range.</li> </ul>
Multispectral Camera	<ul style="list-style-type: none"> <li>• Preparing more detailed and specific information about NDVI of plants in canopy such as histogram of pixels, NDVI image (gray and color).</li> <li>• Selecting target points of captured multispectral image and reading related NDVI values (Figure 4-55.e).</li> <li>• Calculating NDVI values within two ranges (0 to 1 and -1 to 1).</li> <li>• Ability to extract other vegetation index like NDYI (Normalized Difference Yellow Index), which prepares valuable information for flowering status of growth.</li> </ul>	<ul style="list-style-type: none"> <li>• Should be calibrated before each data collection.</li> <li>• Sensitive to ambient light.</li> <li>• Slower device.</li> </ul>

## **4.10. Summary**

This chapter provided the experimental results. In other words, collected data from nurseries were studied and analyzed. Several field tests were accomplished during the growing seasons of 2018 and 2019 from wheat and canola fields. The variation of canopy plots with different genotypes were analyzed and compared. Their variation in their height, temperature and NDVI was explored with other detailed information about them (high quality RGB image, ambient temperature and humidity). Developed software package and assembled hardware part (sensors, cameras, GPS receiver, mechanical boom, etc.) were evaluated. The accuracy and reliability of both hardware development and installation, and software operation were proven in different sections. The results of comparing manual measurements with sensor's operation were discussed in details. Moreover, extracted NDVI information of canopy plots using Crop Circle and multispectral camera, and developed programs were compared. Next chapter provides conclusion and potential future works of this research.

## **CHAPTER 5- Conclusions and future works**

### **5.1. Conclusions**

To find the correlation between genotypes and phenotypes, proper High-Throughput Phenotyping Platform plays a significant role to decrease data collection time and costs in phenotyping research. Informative data about crop's traits such as their height, temperature, ambient temperature and humidity, plant's vegetation index (such as NDVI), RGB and multispectral images of crops prepare valuable information for breeders and other crop scientists. Further analysis of these datasets prepares useful information such as relation between genotype and phenotype, enhancing yield, identifying stronger genes, and improving global food security.

After completing comprehensive literature review about plant phenotyping and existing platform, their strength and weakness were figured out. Potential possible improvements and new parts for existing HTPP was proposed.

New electrical devices were selected, purchased and retro fitted to the HTPP system. They utilized on the existing HTPP to measure and collect other features of canopies. All new parts were tested in the laboratory conditions at the Robotics Laboratory of University of Saskatchewan. Moreover, a 6-feet Tractor and Swather were equipped with mechanical booms and data collection equipment. All sensors and devices were wired and connected to their power supplies and their control center (Data Logger and laptop). Altogether, the utilized electrical devices for data collection can be listed as:

- Five ultrasonic sensors for height measurement.
- Two inferred thermometers for temperature measurements.
- Two Crop Circle sensors for measuring NDVI.
- A weather station probe for measuring ambient temperature and humidity.
- Two high quality cameras to take RGB images of crops.
- Two multispectral cameras to capture images of plants within specific wavelengths.
- A GPS system for geo-tagging collected data and images.
- A Data Logger as a control unit to save collected sensor's data.
- A laptop computer as a control unit to save captured images.

After wiring and assembling hardware part of HTPP, user-friendly and mostly automated programs were developed for different purposes. Software package is customized and developed programs can be listed as:

- A mapping program for generating the map of field with the GPS information of each plot.
- A data acquisition program for collecting sensors' data and tagging them with the related geospatial information (longitude and latitude).
- An image acquisition program for capturing (RGB and multispectral) images of crops and tagging them with their GPS information.
- A post-processing program for extracting NDVI information of plants from multispectral image.
- A data visualization program for loading the map of field and loading all collected data and images
- A sorting program for arranging collected data and images in the Excel sheets and related folders.

To validate the effectiveness and reliability of the developed HTPP with new parts and programs, different types of nurseries such as canola and wheat, with different numbers of plots (mega, large and medium size) were studied during their growth seasons in 2018 and 2019. Using our platform, a valuable phenotypic database that consists of different genotypes and phenotypes was created that can be analyzed by breeders.

Several verification tests were conducted to verify accuracy and reliability of our HTPP in the field condition. The variation of crop's traits can be studied during the growing season and plant's characteristics can be compared with each other to find strong genotype and increase yield amount.

## **5.2. Future works**

More research should be conducted to improve existing HTPP. Following are some suggestion as potential future works:

1. Changing the structure of utilized mechanical boom or utilizing new model and collecting data in the next growing season (2020). Recently, mechanical team of Robotics Laboratory of University of Saskatchewan are working on developing a lightweight long-reach 5-DOF

(Degree of Freedom) robot arm, as can be seen in Figure 5-1 [46]. This manipulator is going to replace existing mechanical boom and data collection equipment will be attached to it. The utilization of this manipulator has several advantages such as its long reach features(about 3 meter), its ability to collect data (especially taking pictures) from different angles, it can be adapted for the various plot dimensions quickly, and active vibration control of it for higher data collection accuracy.

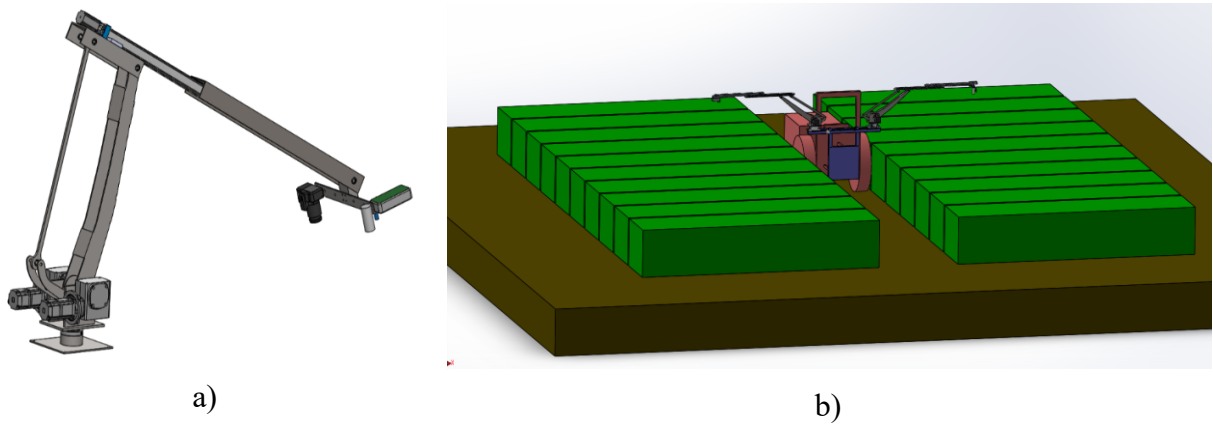


*Figure 5- 1: Schematic of a) 5-DOF robot arm b) mounted manipulator to the vehicle*

2. Further analysis of collected data and images. For example, MATLAB toolboxes such as image processing, deep learning, statistics and machine learning toolboxes and so on can be used to prepare more valuable information. For example, image processing toolbox can be utilized to detect and eliminate shade of mechanical boom from some pictures (Figure 5-2). Also, by use of this toolbox, flowers of canopy can be detected and counted in flowering stage of growth.



*Figure 5- 2: Examples of captured RGB images that were affected with mechanical boom's shade*



3. Analyzing ambient conditions (light, temperature, etc.) effects on sensor's operation and the quality of images (RGB and multispectral). In this way, proper time of data collection can be found and sensors which are very sensitive can be replaced. For example, solar simulator can be used to generate artificial sunlight that has characteristics of sunlight. Therefore, ambient light variations and its effects can be controlled.
4. Adding more sensors and devices to the existing HTPP to measure other features of crops. Moreover, existing sensors can be replaced with new models. For example, LiDAR sensor can be utilized for height measurement to find which sensor is giving more accurate information. Recently, Robotics Laboratory of University of Saskatchewan has developed a program (written in the MATLAB) for data collection purpose for a LIDAR (LMS111) sensor. The results of height measurement devices can be compared to find reliable measurement device.
5. Using other programming languages like Python to increase the speed of data collection and processing time. Furthermore, Raspberry Pi can be added to the HTPP as an extra control unit to execute developed image acquisition programs. Devices like RGB and multispectral cameras have different image acquisition programs and only one program can be executed during each run of data collection and this issue increases data collection time. To solve this problem, a new sparse network is proposed, where a central computer manipulates multiple Raspberry Pis. Ideally, each Raspberry Pi executes specific program and controls one or multiple devices.
6. Utilizing the developed HTPP in other types of nurseries such as lentil and bean. It is better to analyze and verify the operation of developed HTPP on other fields that has different types of canopies, where dimensions of plots are different.

## References

- [1] “State of food security and nutrition in the world 2019, Safeguarding against economic slowdowns and downturns.” [Online]. Available: <https://www.unicef.org/media/55921/file/SOFI-2019-full-report.pdf>.
- [2] R. T. Furbank and M. Tester, “Phenomics – technologies to relieve the phenotyping bottleneck,” *Trends Plant Sci.*, vol. 16, no. 12, pp. 635–644, 2011.
- [3] J. Cobb, G. DeClerck, A. Greenberg, R. Clark, and S. McCouch, “Next-generation phenotyping: requirements and strategies for enhancing our understanding of genotype–phenotype relationships and its relevance to crop improvement,” *Theor. Appl. Genet.*, vol. 126, no. 4, pp. 867–887, 2013.
- [4] M. Tester and P. Langridge, “Breeding technologies to increase crop production in a changing world.,” *Science*, vol. 327, no. 5967, pp. 818–822, 2010.
- [5] J. W. White *et al.*, “Field-based phenomics for plant genetics research,” *F. Crop. Res.*, vol. 133, no. C, pp. 101–112, 2012.
- [6] M. E. Ghanem, H. Marrou, and T. R. Sinclair, “Physiological phenotyping of plants for crop improvement,” *Trends Plant Sci.*, vol. 20, no. 3, pp. 139–144, 2015.
- [7] D. Rundquist, A. Gitelson, B. Leavitt, A. Zygielbaum, R. Perk, and G. Keydan, “Elements of an Integrated Phenotyping System for Monitoring Crop Status at Canopy Level,” *Agronomy*, vol. 4, no. 1, pp. 108–123, 2014.
- [8] M. Bayati and R. Fotouhi, “A Mobile Robotic Platform for Crop Monitoring,” *Adv. Robot. Autom.*, vol. 07, no. 01, 2018.
- [9] M. G. Salas Fernandez, Y. Bao, L. Tang, and P. S. Schnable, “A High-Throughput, Field-Based Phenotyping Technology for Tall Biomass Crops,” *Plant Physiol.*, vol. 174, no. 4, pp. 2008–2022, 2017.
- [10] C. Zhang and J. Kovacs, “The application of small unmanned aerial systems for precision agriculture: a review,” *Precis. Agric.*, vol. 13, no. 6, pp. 693–712, 2012.
- [11] S. Kipp, B. Mistele, P. Baresel, and U. Schmidhalter, “High-throughput phenotyping early plant vigour of winter wheat,” *Eur. J. Agron.*, vol. 52, pp. 271–278, 2014.
- [12] A. B. Potgieter *et al.*, “Multi-Spectral Imaging from an Unmanned Aerial Vehicle Enables the Assessment of Seasonal Leaf Area Dynamics of Sorghum Breeding Lines,” *Front. Plant Sci.*, vol. 8, 2017.
- [13] S. Tisné *et al.*, “Phenoscope: an automated large-scale phenotyping platform offering high spatial homogeneity,” *Plant J.*, vol. 74, no. 3, pp. 534–544, 2013.

- [14] R. T. Furbank and M. Tester, “Phenomics - technologies to relieve the phenotyping bottleneck,” *Trends in Plant Science*. 2011.
- [15] J. M. Montes, A. E. Melchinger, and J. C. Reif, “Novel throughput phenotyping platforms in plant genetic studies,” *Trends in Plant Science*. 2007.
- [16] H. Wang, Y. Lin, Z. Wang, Y. Yao, Y. Zhang, and L. Wu, “Validation of a low-cost 2D laser scanner in development of a more-affordable mobile terrestrial proximal sensing system for 3D plant structure phenotyping in indoor environment,” *Comput. Electron. Agric.*, 2017.
- [17] Y. Ge, G. Bai, V. Stoerger, and J. C. Schnable, “Temporal dynamics of maize plant growth, water use, and leaf water content using automated high throughput RGB and hyperspectral imaging,” *Comput. Electron. Agric.*, vol. 127, pp. 625–632, 2016.
- [18] J. L. Crain *et al.*, “Development and deployment of a portable field phenotyping platform,” *Crop Sci.*, 2016.
- [19] T. Bak and H. Jakobsen, “Agricultural Robotic Platform with Four Wheel Steering for Weed Detection,” *Biosyst. Eng.*, 2004.
- [20] J. Svensgaard, T. Roitsch, and S. Christensen, “Development of a Mobile Multispectral Imaging Platform for Precise Field Phenotyping,” *Agronomy*, 2014.
- [21] J. M. Montes, F. Technow, B. S. Dhillon, F. Mauch, and A. E. Melchinger, “High-throughput non-destructive biomass determination during early plant development in maize under field conditions,” *F. Crop. Res.*, vol. 121, no. 2, pp. 268–273, 2011.
- [22] P. Rischbeck, S. Elsayed, B. Mistele, G. Barmeier, K. Heil, and U. Schmidhalter, “Data fusion of spectral, thermal and canopy height parameters for improved yield prediction of drought stressed spring barley,” *Eur. J. Agron.*, vol. 78, pp. 44–59, 2016.
- [23] J. Barker *et al.*, “Development of a field-based high-throughput mobile phenotyping platform,” *Comput. Electron. Agric.*, vol. 122, no. C, pp. 74–85, 2016.
- [24] G. Bai, Y. Ge, W. Hussain, P. S. Baenziger, and G. Graef, “A multi-sensor system for high throughput field phenotyping in soybean and wheat breeding,” *Comput. Electron. Agric.*, vol. 128, pp. 181–192, 2016.
- [25] M. Bayati, “Development of a field-based platform for plant phenotyping,” University of Saskatchewan, 2017.
- [26] “Datasheet of Honeywell Ultrasonic Distance Sensor (943-F4Y-2D-1D0-180E).” [Online]. Available: <https://www.datasheet.directory/index.php?title=Special:PdfViewer&url=https%3A%2F%2Fdatasheet.iic.cc%2Fdatasheets-0%2Fhoneywell%2F943-F4Y-2D-1C0-180E.pdf>. [Accessed: 16-Sep-2019].

- [27] “Datasheet of Sick Ultrasonic Sensor (UM30-21\_113).” [Online]. Available: [https://cdn.sick.com/media/docs/4/64/464/Product\\_information\\_Ultrasonic\\_Sensors\\_UM30\\_UM18\\_UM12\\_UC30\\_UC12\\_UC4\\_en\\_IM0052464.PDF](https://cdn.sick.com/media/docs/4/64/464/Product_information_Ultrasonic_Sensors_UM30_UM18_UM12_UC30_UC12_UC4_en_IM0052464.PDF). [Accessed: 16-Sep-2019].
- [28] “Datasheet of Apogee SI-131 IR Thermometer.” [Online]. Available: <https://www.apogeeinstruments.com/content/SI-100-manual.pdf>. [Accessed: 16-Sep-2019].
- [29] “Datasheet of Vaisala HMP60 Temperature and Relative Humidity Probe.” [Online]. Available: <https://www.vaisala.com/sites/default/files/documents/HMP60-Datasheet-B210851EN-F.pdf>. [Accessed: 16-Sep-2019].
- [30] R. E. Crippen, “Calculating the vegetation index faster,” *Remote Sens. Environ.*, 1990.
- [31] “Datasheet of Crop Circle Sensor ACS-430.” [Online]. Available: [https://hollandscientific.com/wp-content/uploads/2017/02/ACS-430\\_DataSheet\\_v6.pdf](https://hollandscientific.com/wp-content/uploads/2017/02/ACS-430_DataSheet_v6.pdf). [Accessed: 16-Sep-2019].
- [32] T. Sritarapipat, P. Rakwatin, and T. Kasetkasem, “Automatic rice crop height measurement using a field server and digital image processing,” *Sensors (Switzerland)*, 2014.
- [33] J. Bendig, A. Bolten, S. Bennertz, J. Broscheit, S. Eichfuss, and G. Bareth, “Estimating biomass of barley using crop surface models (CSMs) derived from UAV-based RGB imaging,” *Remote Sens.*, 2014.
- [34] V. Rajinikanth and M. S. Couceiro, “RGB histogram based color image segmentation using firefly algorithm,” in *Procedia Computer Science*, 2015.
- [35] Y. Feng and J. Wang, “GPS RTK Performance Characteristics and Analysis,” *J. Glob. Position. Syst.*, 2008.
- [36] R. Leandro *et al.*, “RTX positioning: The next generation of cm-accurate real-time GNSS positioning,” in *24th International Technical Meeting of the Satellite Division of the Institute of Navigation 2011, ION GNSS 2011*, 2011.
- [37] J. Carballido, M. Perez-Ruiz, L. Emmi, and J. Agüera, “Comparison of positional accuracy between rtk and rtx gnss based on the autonomous agricultural vehicles under field conditions,” *Appl. Eng. Agric.*, 2014.
- [38] [Online]. Available: <https://www.gpsinformation.org/dale/nmea.htm>. [Accessed: 04-Feb-2020].
- [39] “Datasheet of Campbell Scientific CR3000 Datalogger.” [Online]. Available: <https://s.campbellsci.com/documents/us/manuals/cr3000.pdf>. [Accessed: 16-Sep-2019].
- [40] [Online]. Available: <http://notinthemanual.blogspot.com/2008/07/convert-nmea-latitude-longitude-to.html>. [Accessed: 08-Oct-2019].
- [41] [Online]. Available: <https://www.calculatorsoup.com/calculators/conversions/convert->

decimal-degrees-to-degrees-minutes-seconds.php.

- [42] [Online]. Available: [https://en.wikipedia.org/wiki/Multispectral\\_image](https://en.wikipedia.org/wiki/Multispectral_image). [Accessed: 30-Oct-2019].
- [43] S. Seager, E. L. Turner, J. Schafer, and E. B. Ford, "Vegetation's red edge: A possible spectroscopic biosignature of extraterrestrial plants," *Astrobiology*, 2005.
- [44] N. J. Gogtay and U. M. Thatte, "Principles of correlation analysis," *J. Assoc. Physicians India*, 2017.
- [45] F. Smarandache, "Alternatives to Pearson's and Spearman's Correlation Coefficients," *SSRN Electron. J.*, 2017.
- [46] Zhang, "Lightweight Long-reach 5-DOF Robot Arm For Farm Application," *IDETC2019*, 2019.

## APENDIX A- Datasheets of utilized equipment

Refer to chapter two different devices were selected as hardware part of developed field-based HTPP. This section provides the datasheet and technical information of utilized devices, which are Honeywell and Sick ultrasonic distance sensor, Apogee IR Thermometer, Visala temperature and humidity probe, Crop Circle sensor and Campbell Scientific Data Logger.

### A1- Honeywell Ultrasonic Distance Sensor (943-F4Y-2D-1D0-180E) [26]

This sensor has 250ms response time and uses 180 kHz carrier frequency. Moreover, it operates properly in the outdoor configuration for measuring height of crops. This sensor's detection range is between 0.2 to 20 meter and its temperature range is between -15 to 70 °C. Its supply voltage is 15 to 30 DC volt and its output is current where the range is 4-20 mA. Two 12 volt battery are used for powering up of this sensor. These two batteries together can generate 24 DC volt.

Specifications (at 25° typically)

Technical Data	Technische Daten	Données techniques	943...130E	943...180E	943...300E	943...330E
Detection range	Erfassungsbereich	Portée	300...3500 mm	200...2000 mm	100...800 mm	60...500 mm
Response time	Ansprechzeit	Temps de réponse	400 ms	250 ms	100 ms	100 ms
Carrier frequency	Trägerfrequenz	Fréquence porteuse	130 kHz	180 kHz	300 kHz	330 kHz
Beam angle (°)	Schallkegelöffnung (°)	Angle du faisceau (°)	8			
Linearity error	Lineartätsfehler	Erreur de linéarité	< 0.3 %			
Repeatability	Wiederholgenauigkeit	Répétabilité	±0.2 %, ±2 mm		±0.2 %, ±1 mm	
Temperature range	Temperaturbereich	Température de service	-15 °C to 70 °C			
Temperature compensation	Temperaturkompensation	Compensation en température	Yes/Ja/Oui			
Supply voltage	Versorgungsspannung	Tension d'alimentation	15 Vdc to 30 Vdc			
Possible minimum supply	Mögliche min. Versorgung	Min. alimentation possible	12 Vdc			
Current consumption	Stromaufnahme	Courant consommé	< 40 mA			
Analogue output	Analogausgänge	Sortie analogique	0...10 V (1C0) / 4...20 mA (1D0)			
Output adjustment	Einstellung des Ausgangs	Réglage de la sortie analogique	Teach In			
Teach In P1/P2 determines 0 V and 10 V position	Teach In Der Bereich wird durch P1 and P2 festgelegt	Apprentissage La gamme est défini par les positions P1 et P2	Pin 5/Pink cable			
Plastic housing	Kunststoffgehäuse	Boîtier plastique	M30x1.5	M18x1	M18x1	M18x1
Sealing <sup>[1]</sup>	Schutzart <sup>[1]</sup>	Étanchéité <sup>[1]</sup>	IP67			
Connector	Steckeranschluss	Connecteur	M12x1 (943-F/T4V) Mating connector not included			
Cable connection	Kabelanschluss	Connection câble	2 m (943-F/T4V)			

<sup>[1]</sup> Do not expose head to hot water > 50 °C or water steam.

Den Sensorkopf nicht heißem Wasser > 50 °C oder Wasserdampf aussetzen.

Ne pas mettre en contact continu la tête du capteur avec de l'eau avec une température supérieur à 50 °C ou avec de la vapeur d'eau.

Figure A- 1: Technical information of Honeywell Ultrasonic Distance Sensor (943-F4Y-2D-1D0-180E)

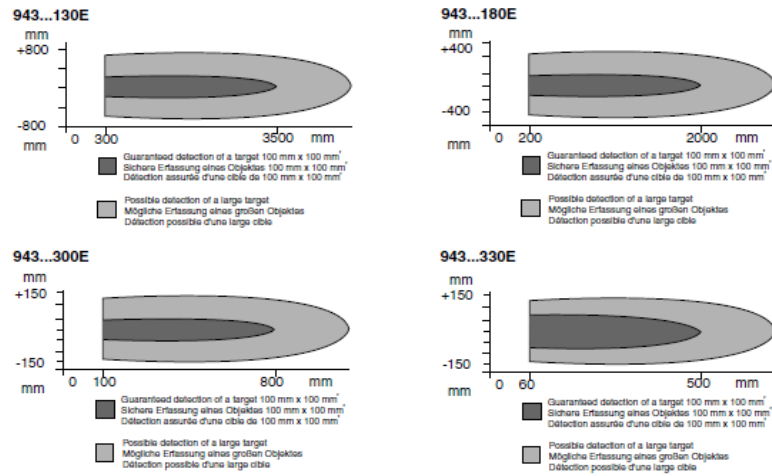


Figure A- 2: Detection range of Honeywell Ultrasonic Distance Sensor (943-F4Y-2D-1D0-180E)

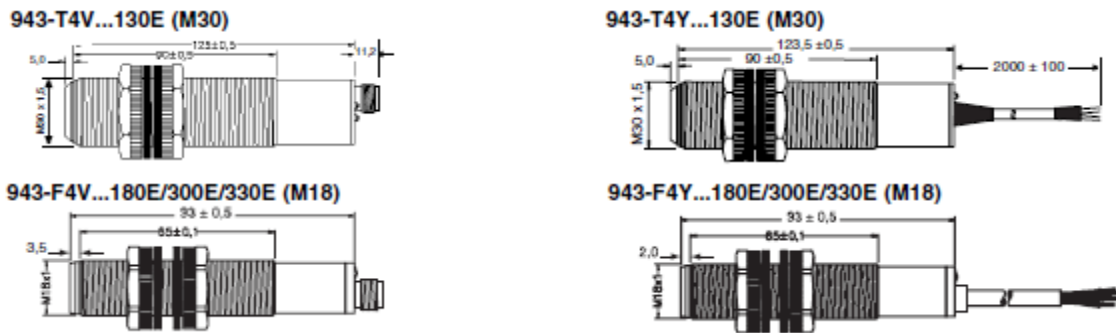


Figure A- 3: Dimensions of Honeywell Ultrasonic Distance Sensor (943-F4Y-2D-1D0-180E)

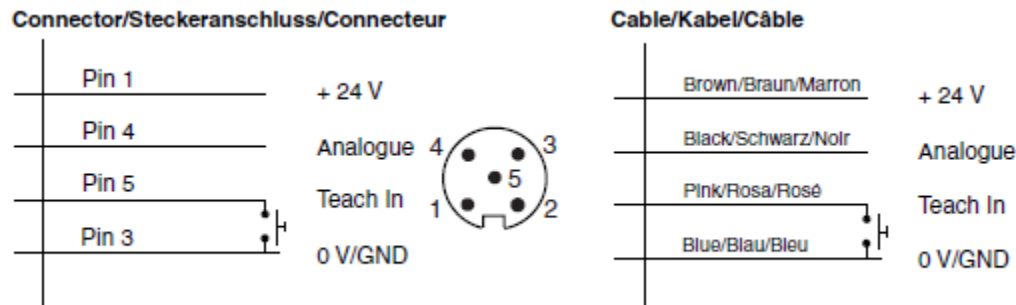
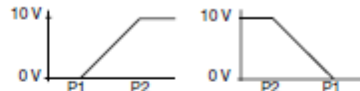
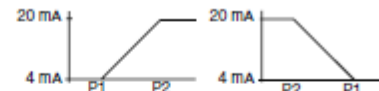


Figure A- 4: Wiring of Honeywell Ultrasonic Distance Sensor (943-F4Y-2D-1D0-180E)



**943-F/T4V****943-F/T4Y****0 V to 10 V (943...1C0...)****4 mA to 20 mA 943...1D0...**

### Analogue output adjustment 0 V...10 V/4 mA...20 mA

P1 and P2 define the analogue output slope. P1 determines the 0 V/4 mA position and P2 the 10 V/20 mA position.  
Positive slope: P1 < P2  
Negative slope: P2 < P1

#### Normal function

The Echo LED is ON when the echo is received (this is the alignment LED confirming that the target is properly aligned). The LED P1 is ON, when the target is between the sensor face and P1. The LED P2 is ON when Target is farther than P2.

#### Teach In of P1 position (0V/4 mA output)

Connect the Teach In line (pink/5) with GND for 8 seconds until the LEDs P1 and Echo LED are blinking simultaneously (blinking rate will be 2 Hz). Then release the contact: the sensor is now in Teach In mode for P1 (0 V/4 mA):

- LED P1 change the blinking to 1 Hz and the Echo LED returns to normal function to show if the target is properly aligned.
- There is a time window of 1 minute to teach P1 position.
- Place target at the right distance P1.
- Contact and release Teach In line (pink/5) with the GND, and P1 is now programmed.

The sensor returns into **normal function** with the new value for P1.

#### Teach In of P2 position (10V/20 mA output)

Connect the Teach In line (pink/5) with GND for 13 seconds until LEDs P2 and Echo LED start blinking simultaneously (blinking rate will be 2 Hz). It is important to note that before reaching the P2 teach in mode, P1 LED will be blinking for few seconds before reaching P2. After 8 seconds the LEDs P1 and Echo will be blinking, however after an additional 5 seconds P2 LED and Echo LED will be blinking with a 2 Hz rate. Release contact Teach in (pink/5) contact and now the sensor is in Teach In mode for P2:

- The P2 LED will be blinking now at 1 Hz rate and the Echo LED will return to its normal function (alignment LED).
- There is a time window of 1 minute to do the programming of P2.
- Place the target to the position P2.
- Contact and release Teach In line (pink/5) with GND.

P2 is programmed and the sensor returns into **normal function** with the new value for P2 in memory.

### Analoge Kennlinie 0 V...10 V/4 mA...20 mA

Mit P1 und P2 wird der Arbeitsbereich der analogen Kennlinie festgelegt: P1 bestimmt die Position an der die Kennlinie den Wert 0 V/4 mA annimmt, P2 bestimmt die Position 10 V/20 mA.

Positive Kennlinie: P1 < P2  
Negative Kennlinie: P2 < P1

#### Normale Funktion

Echo LED an, wenn Echo empfangen wird (Ausrichthilfe). LED P1 ist an, wenn Objekt sich vor P1 befindet. LED P2 ist an, wenn sich Objekt hinter P2 befindet.

#### Teach In Modus P1 (Position 0V/4 mA)

Verbinde Teach In Ausgang mit GND ca. 8 sec. bis LEDs P1 und Echo anfangen mit ~2 Hz zu blinken.

Verbindung lösen: jetzt ist Sensor im Teach In Modus für P1:

- LED P1 blinkt mit ~1 Hz; Echo LED normale Funktion (Ausrichthilfe).
- Innerhalb von 1 min. muss P1 eingelesen werden!
- Objekt an neue Position P1 bringen Teach In Ausgang kurz mit GND verbinden und lösen: P1 ist eingelesen.

Sensor arbeitet jetzt in **normaler Funktion** mit neuem eingestellten Wert für P1.

#### Teach In Modus P2 (Position 10V/20 mA)

Verbinde Teach In Ausgang mit GND ca. 13 sec. bis LED P2 und Echo LED anfangen mit ~2 Hz zu blinken.

Nach 8 sec. fangen LED P1 und Echo LED an zu blinken, nach weiteren 5 sec. blinkt dann LED P2 und Echo LED mit ~2 Hz. Verbindung lösen: jetzt ist Sensor im Teach In Modus für P2:

- LED P2 blinkt mit ~1 Hz; Echo LED normale Funktion (Ausrichthilfe).
- Innerhalb von 1 min muß jetzt P2 eingelesen werden!
- Objekt an neue Position P2 bringen.
- Teach In Ausgang kurz mit GND verbinden und lösen: P2 ist eingelesen.

Sensor arbeitet jetzt in **normaler Funktion** mit neuem eingestellten Wert für P2.

### Sortie analogique 0 V...10 V/4 mA...20 mA

P1 et P2 définissent les deux limites de la sortie analogique du capteur. P1 correspond à la limite 0 V/4 mA, et le point correspond à la limite 10 V/20 mA.

Pour obtenir une pente positive, il faut donc que P1 < P2

Pour obtenir une pente négative il faut donc que P1 > P2

#### Fonction en situation normale

Le LED correspondant à l'Echo reste allumé si un écho est reçu par le capteur. Cela permet de vérifier que le capteur est correctement aligné avec la cible. Le LED P1 est allumé si la cible est placée avant la position P1. Le LED P2 est allumé si la cible est placée après la position P2.

#### Apprentissage de la position P1 (sortie 0 V/4 mA)

Connecter la sortie Teach In (apprentissage, câble rosé/5) avec GND (masse) pendant 8 secondes jusqu'à ce que les LEDs P1 et Echo clignotent à une cadence de 2 Hz. A ce moment, déconnecter la sortie GND (masse) pour permettre au capteur de rentrer en mode programmation pour la limite P1:

- Le LED P1 change de clignotement et passe à une cadence de 1 Hz; le LED Echo retrouve sa fonction normale d'alignement.
- A ce moment, une séquence d'un minute commence pour effectuer la programmation de la position P1.
- Placer la cible à la position souhaitée.
- Connecter puis déconnecter la sortie Teach In (apprentissage, câble rosé/5) avec GND (masse).

La position P1 est maintenant mémorisée. Le capteur travaille en **fonction normale** avec la nouvelle valeur pour P1.

#### Apprentissage de la position P2 (Sortie 10 V/20 mA)

Connecter la sortie apprentissage (Teach In, rosé/5) à la masse (GND) pendant environ 13 secondes et cela jusqu'à ce que les LEDs P2 et Echo clignotent à une cadence de 2 Hz. Après 8 secondes, les LEDs P1 et Echo commenceront à clignoter mais il faudra attendre 5 secondes supplémentaires pour que les LEDs P2 et Echo clignotent et atteignent l'apprentissage de la position P2. A ce moment, il faut déconnecter la masse (GND) et le capteur est maintenant en mode programmation P2:

- Le LED P2 clignote maintenant à une cadence de 1 Hz et le LED Echo retourne à sa fonction normale de témoin d'alignement de la cible.
- A ce moment, une séquence d'un minute commence pour effectuer la programmation de la position P1.
- Situation la cible à la position P2 désirée.
- Connecter et déconnecter la sortie apprentissage avec la sortie masse (GND). P2 est maintenant programmée.

Le capteur est maintenant en **fonction normale** avec la nouvelle valeur pour la position P2.

Figure A- 5: Tech in procedure of Honeywell Ultrasonic Distance Sensor (943-F4Y-2D-1D0-180E)

## A2- Sick Ultrasonic Sensor (UM30-21\_113)[27]

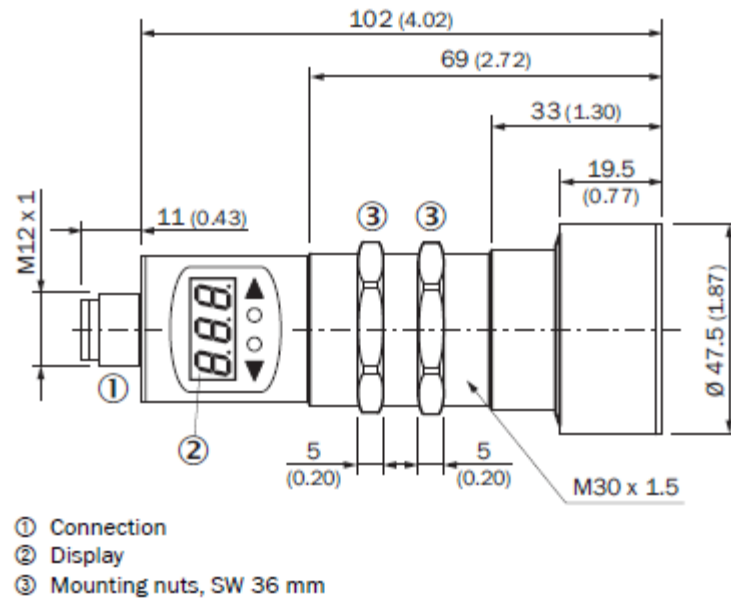


Figure A- 6: Dimensions of Sick Ultrasonic Sensor (UM30-21\_113)

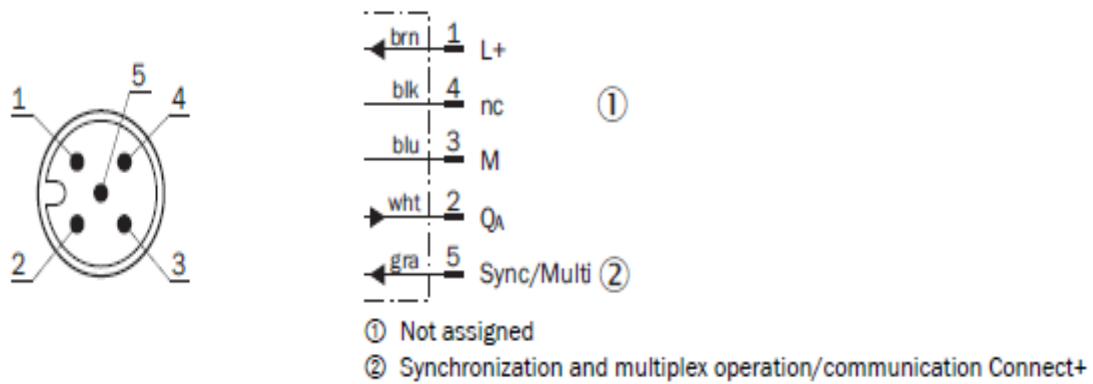


Figure A- 7: Connection type and diagram of Sick Ultrasonic Sensor (UM30-21\_113)

## Performance

<b>Operating range, limiting range</b>	350 mm ... 3,400 mm, 5,000 mm
<b>Target</b>	Natural objects
<b>Resolution</b>	$\geq 0.18$ mm
<b>Repeatability</b>	$\pm 0.15$ % <sup>1)</sup>
<b>Accuracy</b>	$\pm 1$ % <sup>1) 2)</sup>
<b>Temperature compensation</b>	✓
<b>Response time</b>	180 ms
<b>Output time</b>	43 ms
<b>Ultrasonic frequency (typical)</b>	120 kHz
<b>Detection area (typical)</b>	See diagrams
<b>Additional function</b>	Teach-in of analog output, scaling of analog outputs, Invertable analog output, automatic selection of analog current or voltage output, temperature compensation, synchronization of up to 10 sensors, multiplexing: no cross talk of up to 50 sensors, set measurement filters: value filter, filter strength, adjustable sensitivity, foreground suppression and detection area, switch-off display, reset to factory default

<sup>1)</sup> Referring to current measurement value.

<sup>2)</sup> Temperature compensation can be switched off, without temperature compensation: 0.17 % / K.

## Mechanics/electronics

<b>Supply voltage <math>V_s</math></b>	DC 9 V ... 30 V <sup>1) 2)</sup>
<b>Power consumption</b>	$\leq 2.4$ W <sup>3)</sup>
<b>Initialization time</b>	< 300 ms
<b>Design</b>	Cylindrical
<b>Housing material</b>	Nickel-plated brass, PBT Display: TPU Ultrasonic transducer: polyurethane foam, glass epoxy resin
<b>Connection type</b>	Male connector, M12, 5-pin
<b>Indication</b>	LED display, 2 x LED
<b>Weight</b>	210 g
<b>Sending axis</b>	Straight
<b>Enclosure rating</b>	IP67
<b>Protection class</b>	III

<sup>1)</sup> Limit values, reverse-polarity protected Operation in short-circuit protected network: max. 8 A, class 2.

<sup>2)</sup> 15 V ... 30 V when using the analog voltage output.

<sup>3)</sup> Without load.

## Interfaces

<b>Analog output</b>	1 x 0 V ... 10 V ( $\geq 100$ k $\Omega$ ) 1 x 4 mA ... 20 mA ( $\leq 500$ $\Omega$ ) <sup>1) 1) 2) 3)</sup>
<b>Resolution analog output</b>	12 bit
<b>Multifunctional input (MF)</b>	1 x MF

<sup>1)</sup> Automatic selection of analog current or voltage output dependent on load.

<sup>2)</sup> For 4 mA ... 20 mA and  $V_s \leq 20$  V max. load  $\leq 100$   $\Omega$ .

<sup>3)</sup> Subsequent smoothing of the analog output, depending on the application, may increase the response time by up to 200 %.

*Figure A- 8: Detailed technical information for Sick Ultrasonic Sensor (UM30-21\_113)*

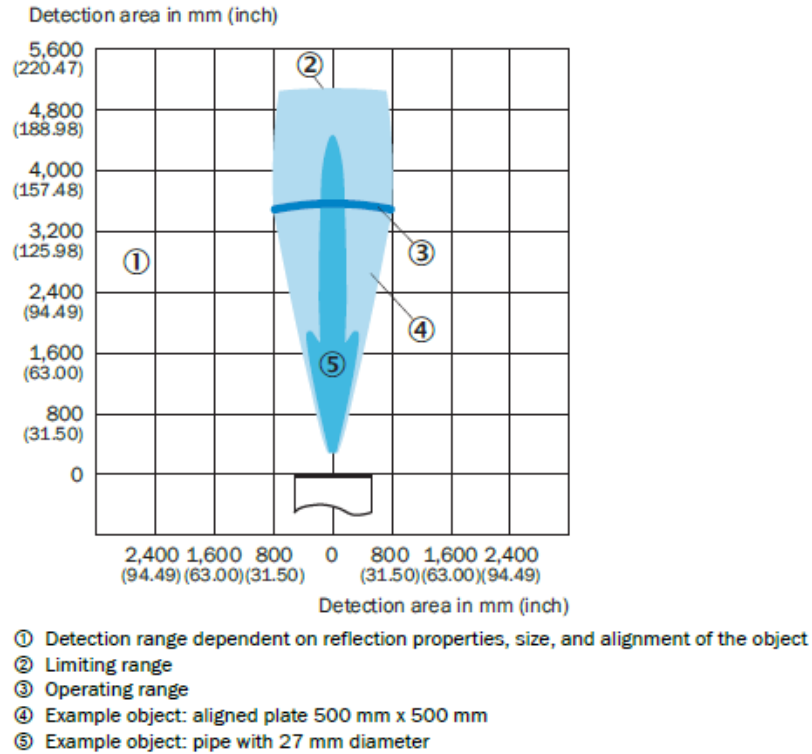


Figure A- 9: Detection area of Sick Ultrasonic Sensor (UM30-21\_113)

### A3- Apogee SI-131 IR Thermometer[28]

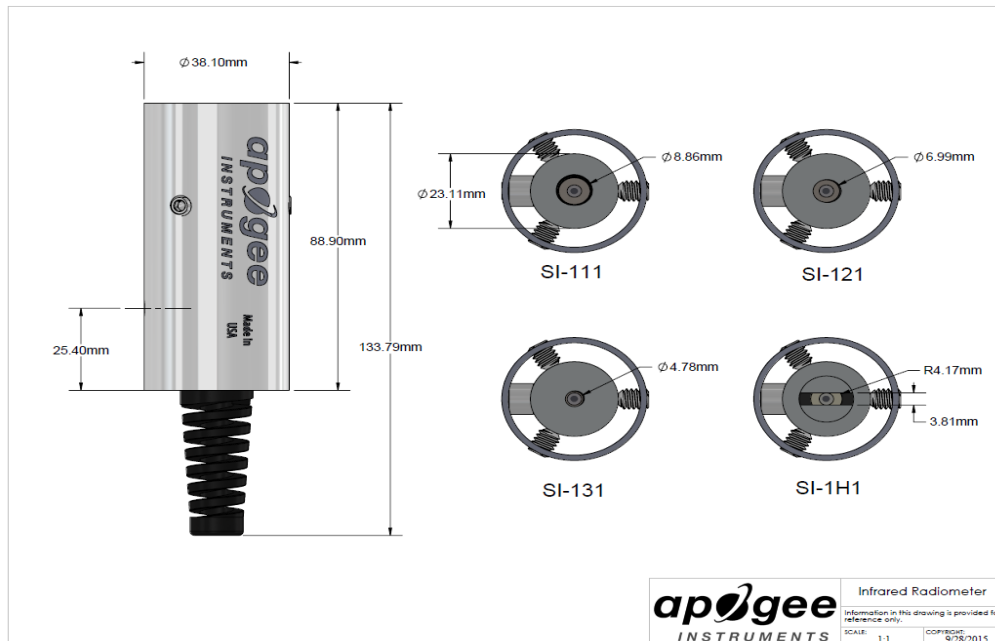


Figure A- 10: Dimensions of Apogee SI-131 IR Thermometer

**Wiring for SI-100 Series with Serial Numbers 7283 and above or has a cable connector**



- Red: Excitation channel (excitation for thermistor)
- Black: Low side of differential channel (negative thermopile lead)
- Clear: Shield/Ground
- Green: Single-ended channel (positive thermistor lead)
- Blue: Analog ground (negative thermistor lead)
- White: High side of differential channel (positive thermopile lead)

**Wiring for SI-100 Series with Serial Numbers range 0-7282**



- Red: High side of differential channel (positive thermopile lead)
- Black: Low side of differential channel (negative thermopile lead)
- Clear: Analog ground (thermopile ground)
- Green: Single-ended channel (positive thermistor lead)
- Blue: Analog ground (negative thermistor lead)
- White: Excitation channel (excitation for thermistor)

*Figure A- 11: Apogee IRT sensor (model: SI-131) wiring diagram*

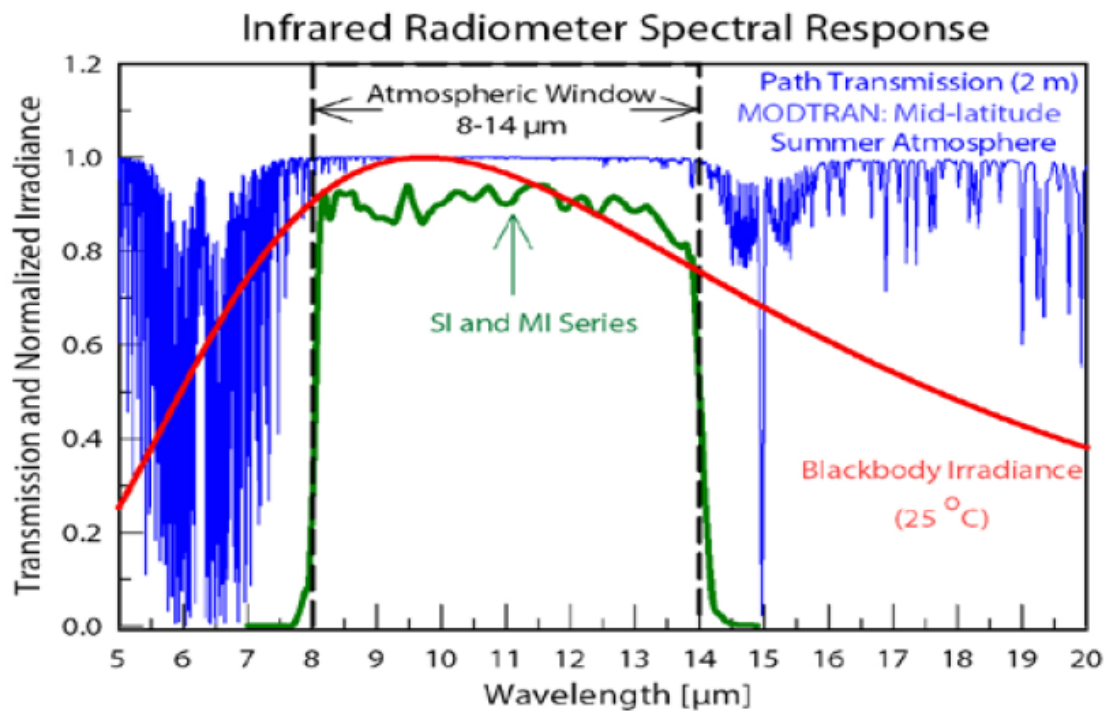


*Figure A- 12: Spectral response of Apogee SI-131 IR Thermometer*

All Models -SS	SI-111	SI-121	SI-131	SI-1H1	SIF-111	SIF-121	SIF-1H1	SI-411	SI-421	SI-431	SI-4H1
Analog Model Output (Difference between Target and Detector)	≈ 60 μV per C	≈ 40 μV per C	≈ 20 μV per C	≈ 40 μV per C	≈ 15 μV per C	≈ 10 μV per C			Digital Models (SDI-12)		
Input Voltage Requirement	2500 mV thermistor excitation (typical, other voltages can be used)								5.5 to 24 V DC with current draw of 1.4 mA (quiescent), 1.8 mA (active)		
Analog Output from Thermistor	0 to 2500 mV (typical, depends on input voltage)								—		
Calibration Uncertainty (-20 to 65 C), when target and detector ΔT are < 20 C	0.2 C		0.3 C		0.2 C				0.3 C		0.2 C
Calibration Uncertainty (-40 to 80 C), when target and detector ΔT are > 20 C	0.5 C		0.6 C		0.5 C				0.6 C		0.5 C
Measurement Repeatability	Less than 0.05 C										
Long-term Drift	Less than 2 % change in slope per year when germanium filter is maintained in clean condition										
Response Time	0.6 s, time for detector signal to reach 95 % following a step change				0.2 s, time for detector signal to reach 95 % following a step change			0.6 s, time for detector signal to reach 95 % following a step change			
Field of View (half-angle)	22°	18°	14°	32° horizontal; 13° vertical	22°	18°	32° horizontal; 13° vertical	22°	18°	14°	32° horizontal; 13° vertical
Spectral Range	8 to 14 μm; atmospheric window										
Operating Environment	-55 to 80 C; 0 to 100 % relative humidity (non-condensing)										
Dimensions	23 mm diameter, 60 mm length										
Cable	5 m of four conductor, shielded, twisted-pair wire; TPR jacket (high water resistance, high UV stability, flexibility in cold conditions); pigtail lead wires; stainless steel (316), M8 connector located 25 cm from sensor head										
Mass	190 g (with 5 m of lead wire)										
Warranty	4 years against defects in materials and workmanship										

Figure A- 13: Detailed technical information for Apogee SI-131 IR Thermometer

## A4- Visala HMP60 Temperature and Relative Humidity Probe[29]

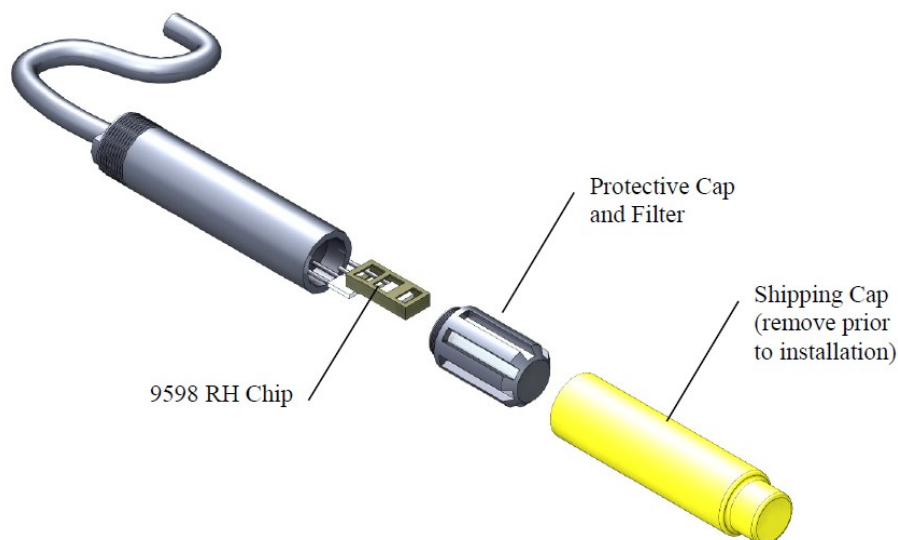


Figure A- 14: Exploded view of HMP60 Temperature and Relative Humidity Probe



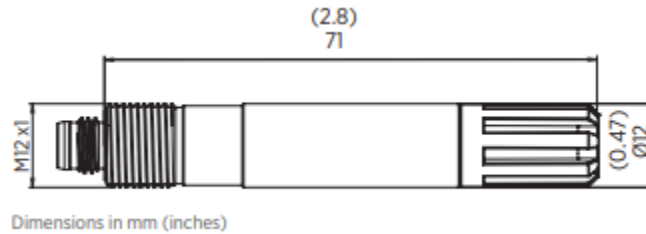


Figure A- 15: Dimensions of HMP60 Temperature and Relative Humidity Probe

## Measurement Performance

Relative Humidity	
Measurement range	0 ... 100 %RH
Typical Accuracy:	
Temperature range	0 ... +40 °C
0 ... 90 %RH	±3 %RH
90 ... 100 %RH	±5 %RH
Temperature range	-40 ... 0 °C, +40 ... +60 °C
0 ... 90 %RH	±5 %RH
90 ... 100 %RH	±7 %RH
Humidity sensor	Vaisala INTERCAP®
Temperature	
Measurement range	-40 ... +60 °C
Accuracy over Temperature Range:	
+10 ... +30 °C	±0.5 °C
-40 ... +10, +30 ... +60 °C	±0.6 °C
Dew Point	
Measurement range	-40 ... +60 °C
Typical Accuracy:	
Temperature range	0 ... +40 °C
When dew point depression <sup>1</sup> < 15 °C	±2 °C
Temperature range	-40 ... 0 °C, +40 ... +60 °C
When dew point depression < 10 °C <sup>1)</sup>	±3 °C
Analog Outputs	
Accuracy at 20 °C	±0.2 % of FS
Temperature dependence	±0.01 % of FS/°C

<sup>1)</sup> Dew point depression = ambient temperature - dew point

## Operating Environment

Operating temperature	-40 ... +60 °C
EMC compliance	EN 61326-1, industrial environment

## Mechanical Specifications

IP rating	IP65
Body thread	M12x1 / 10 mm
Cable connector	4-pin M8 (IEC 60947-5-2)
Materials	
Body	Stainless steel (AISI 316)
Grid filter	Chrome coated ABS plastic
Cable	Polyurethane or FEP
Weight	
Probe	17 g
Probe with 0.3 m cable	28 g

## Inputs and Outputs

Power consumption	1 mA average, max. peak 5 mA
Operating Voltage <sup>1)</sup>	
With 1 V / 2.5 V output	5 ... 28 VDC
With 5 V output	8 ... 28 VDC
With loop power converter	8 ... 28 VDC
With digital output	5 ... 20 VDC
Start-Up Time	
Probes with analog output	4 s at operating voltage 13.5 ... 16.5 VDC 2 s at other valid operating voltages
Probes with digital output	1 s
Outputs	
2 channels	0 ... 1 VDC / 0 ... 2.5 VDC / 0 ... 5 VDC / 1 ... 5 VDC
1-channel loop-power converter (separate module, compatible with humidity accuracy only)	4 ... 20 mA
Digital output (optional)	RS-485 2-wire half duplex, supports Modbus RTU
External Loads	
0 ... 1 V	R <sub>L</sub> min. 10 kΩ
0 ... 2.5 V / 0 ... 5 V	R <sub>L</sub> min. 50 kΩ

<sup>1)</sup> (Use Lowest Available Operating Voltage to Minimize Heating)

## Spare Parts and Accessories

Vaisala INTERCAP® Sensor, 1 piece	15778HM
Vaisala INTERCAP® Sensor, 10 pcs	INTERCAPSET-10PCS
4 ... 20mA loop power converter	UI-CONVERTER-ICB
Mounting bracket for converter	225979
Plastic M12 installation nuts, pair	18350SP
USB cable for PC connection	219690
Probe mounting clamp set, 10 pcs	226067
Probe mounting flange	226061
Sensor Protection	
Plastic grid	DRW010522
Membrane filter	DRW010525
Stainless steel sintered filter	HM46670SP
PTFE sintered filter	DRW244938SP
Connection Cables	
0.3 m PU	HMP50Z032SP
3 m PU	HMP50Z300SP
180 °C 3 m FEP	226902SP

Figure A- 16: Detailed technical information of HMP60 Temperature and Relative Humidity Probe



TABLE 7-1. Wire Color, Function, and Datalogger Connection		
Wire Color	Wire Function	Datalogger Connection Terminal
Black	Temperature signal	U configured for single-ended analog input <sup>1</sup> , SE (single-ended, analog-voltage input)
White	Relative humidity signal	U configured for single-ended analog input, SE
Blue	Power ground and signal reference	G
Brown	Power	12V
Clear	EMF Shield	⊥ (analog ground)
<sup>1</sup> U channels are automatically configured by the measurement instruction.		

Figure A- 17: Wiring of HMP60 Temperature and Relative Humidity Probe

## A5- Crop Circle Sensor ACS-430 [31]

<p><b>SPECIFICATIONS</b></p> <p><b>Sensor-to-Canopy Range:</b> Typically 10 in (25 cm) to &gt;72 in (183 cm)</p> <p><b>Field-of-View:</b> ~30 degrees by ~14 degrees</p> <p><b>Active Light Source:</b> Modulated polychromatic LED array</p> <p><b>Photodetection:</b> Three channel silicon photodiode array with spectral range of 320 nm to 1100 nm</p> <p><b>Optical Measurement Bands:</b> 670 nm, 730nm and 775nm</p> <p><b>ELECTRICAL SPECIFICATIONS</b></p> <p><b>Sample Output Rate:</b> Programmable for 1 sample per second to 20 samples per second; Factory default 10 samples per second</p> <p><b>Operating Range:</b> 0 to 50 °C</p> <p><b>Communication Interface:</b> RS-485 multidrop (bidirectional communication); RS-232 (autosend, output only)</p> <p><b>RS-232 Serial Communication:</b> 76800, no parity, 8 data bits, 1 stop bit</p> <p><b>Power:</b> 9 to 17V DC @ ~350 mA</p> <p><b>EMC Certifications:</b> C-Tick, CE</p>	<p><b>MECHANICAL SPECIFICATIONS</b></p> <p><b>Enclosure:</b> Injection molded polycarbonate</p> <p><b>Environmental:</b> IP68 for dust and water resistance</p> <p><b>Weight:</b> 0.94 lb. (430 gm)</p> <p><b>Sensor Mount:</b> (2) ¼ - 20 threaded holes in base of sensor spaced 1.25 in (3.18 cm)</p> <p><b>Dimensions:</b> Width 3.5 in (8.9 cm), Length 7.9 in (20.1 cm), Height 1.9 in (4.8 cm)</p> <p><b>Serial/Power Connector:</b> Four pin male Eurofast type, O-ring sealed</p> <p><b>ACCESSORIES AND SYSTEM PACKAGES</b></p> <p><b>Crop Circle ACS-430 Handheld.</b> System includes: Crop Circle ACS-430, GeoSCOUT 400, FieldPAK PS-12 power supply, extension pole apparatus, cables, storage case, charger and user's guide</p> <p><b>Crop Circle ACS-430 Mapping System. System includes:</b> Crop Circle ACS-430, GeoSCOUT 400, cables, storage case, mounting plate and user's guide</p>
--	--

Figure A- 18: Technical information for Crop Circle Sensor ACS-430

## A6- Campbell Scientific CR3000 Data Logger [39]

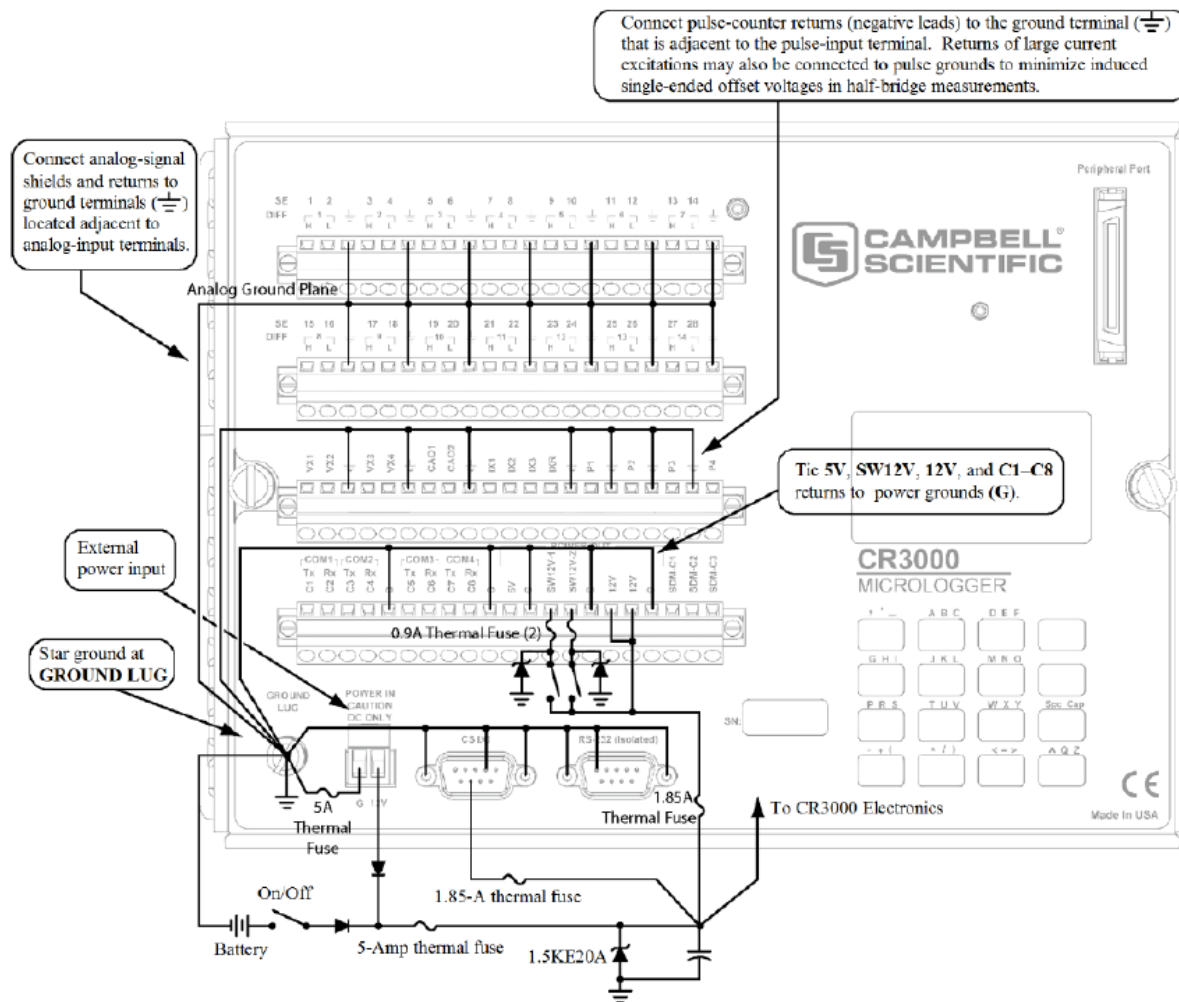


Figure A- 19: Schematic of grounds for Campbell Scientific CR3000 Data Logger

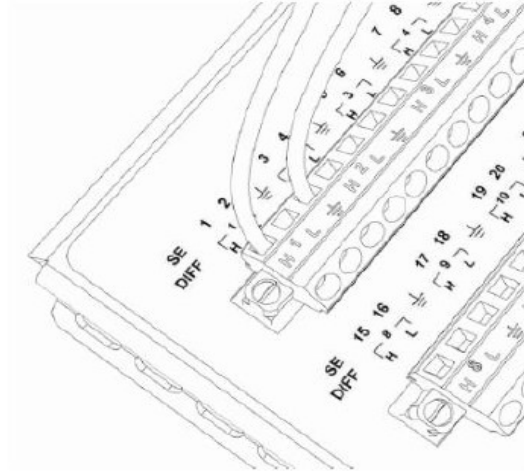


Figure A- 20: Analog sensor wired to single-ended channel

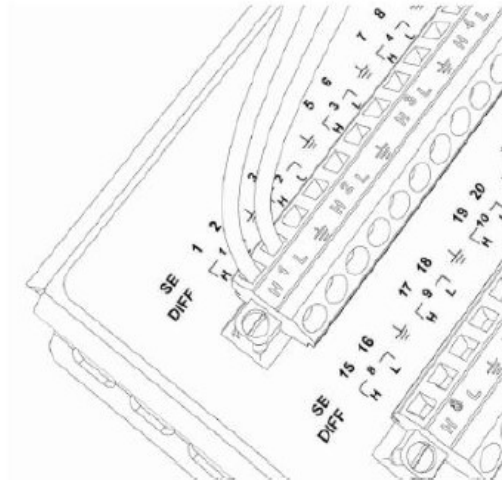


Figure A- 21: Analog sensor wired to differential channel

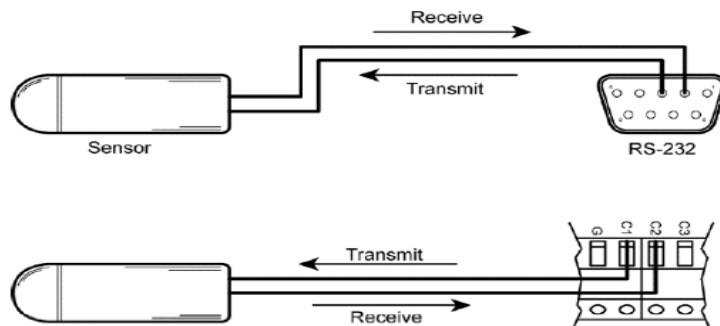


Figure A- 22: Use of digital I/O and RS-232 when reading RS-232 devices

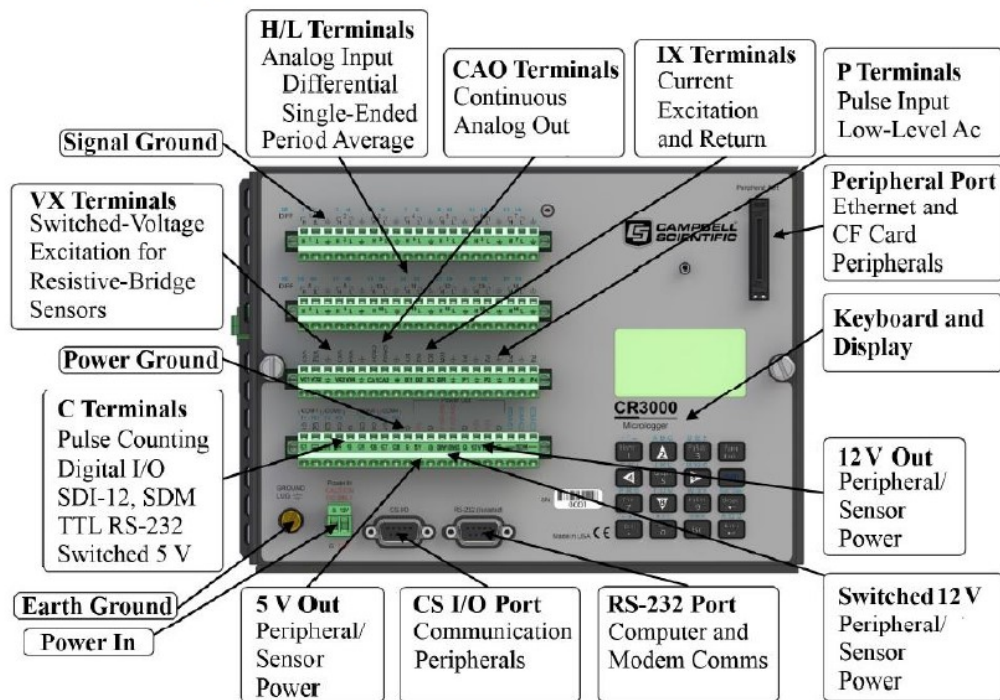


Figure A- 23: Pinouts diagram for Campbell Scientific CR3000 Data Logger

## APPENDIX B- The source code to find correlation of a point 2 according to the latitude and longitude of point 1

This code is provided to calculate geospatial information of point 2 based on the point 1's information (Figure B-1).

**Note:** *lat1d* is the latitude at point 1, *long1d* is the longitude at point 1, *d* is the distance (meter) between two points 1 and 2 and *thd* is the angle (degrees) in respect to the North Pole.

```
function [lat2,long2]=Boom(lat1d,long1d,d,thd)
format longG

R=6371000;

thr=deg2rad(thd);
lat1r=deg2rad(lat1d);
long1r=deg2rad(long1d);

lat22=asin(sin(lat1r)*cos(d/R)+cos(lat1r)*sin(d/R)*cos(thr));
long22=long1r+atan2(sin(thr)*sin(d/R)*cos(lat1r),cos(d/R)-sin(lat1r)*sin(lat22));

lat2=rad2deg(lat22);
long2=rad2deg(long22);

end
```

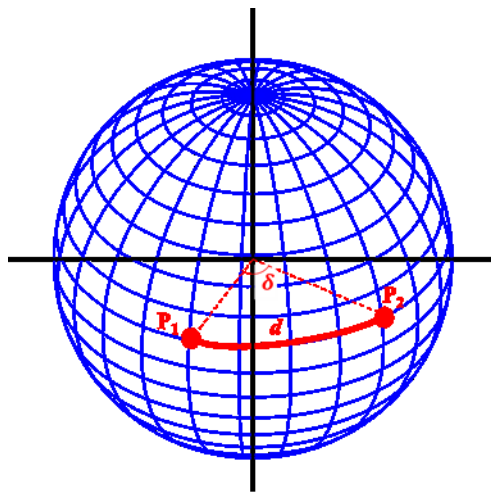


Figure B- 1: Distances between two points on spherical coordinates

## **APPENDIX C- Manuals for the developed programs**

In this section the manual of developed programs are provided. Since there are proprietorship information on this section, details of manual are available by contacting my supervisor (Professor. Fotouhi).

**C1- Manual for the using mapping module of Pheno-VISDM3**

**C2- Manual for the using Data Logger**

**C3- Manual for the using data visualization program-Version 2018**

**C4- Manual for the using data visualization program-Version 2019**

**C5- Manual for the using data and image sorting of Pheno-VISDM3**



## APPENDIX D- The location of studied nurseries

In this section the location of studied nurseries, which are extracted from Google Maps are prepared.



*Figure D- 1: Location of studied canola field on 2018 data collections (Photo extracted from Google Map)*



*Figure D- 2: Location of studied canola field on 2019 data collections (Photo extracted from Google Map)*





*Figure D- 3: Location of studied wheat fields on 2018 and 2019 data collections (Photo extracted from Google Map)*

## APPENDIX E- Summary of conducted field trials

The field trials for 2018 and 2019 canola and wheat nurseries is summarized in this section.

### E1- Preparation and test dates for the studied canola field on 2018

*Table E- 1: List of conducted field trials during 2018 growing season on canola field*

Date	Tasks
May 11, 2018	<ul style="list-style-type: none"> <li>- The second generation of the mechanical boom was assembled.</li> <li>- Electrical system including sensors and Data Logger were wired.</li> </ul>
May 14, 2018	<ul style="list-style-type: none"> <li>- Required GPS data for mapping test field (252 plots) was collected.</li> <li>- All sensors and webcams has tested to see if they are working properly.</li> </ul>
June 5, 2018	<ul style="list-style-type: none"> <li>- A test data collection was conducted to the test field.</li> </ul>
June 8, 2018	<ul style="list-style-type: none"> <li>- Required GPS data for field mapping (around 3000 plots) was collected.</li> </ul>
June19, 2018	<ul style="list-style-type: none"> <li>- <b>1<sup>st</sup> data collection (Seeding Status)</b> was conducted.</li> <li>- Canopy NDVI and temperature were target traits.</li> <li>- RGB images (PNG format and 1280*720 resolution) were captured from <u>whole of field</u>.</li> </ul>
June27, 2018	<ul style="list-style-type: none"> <li>- The mechanical team conducted vibration tests to find natural frequency &amp; vibration response of the 2<sup>nd</sup> generation boom.</li> </ul>
June29, 2018	<ul style="list-style-type: none"> <li>- <b>2<sup>nd</sup> data collection (Flowering Status)</b> was conducted.</li> <li>- Canopy NDVI and temperature were target traits.</li> <li>- RGB images (PNG format and 1280*720 resolution) were captured from <u>whole of field</u>.</li> <li>- Visible signs were used to validate the geo-referencing.</li> </ul>
July 16, 2018	<ul style="list-style-type: none"> <li>- The weather station and new ultrasonic sensor were wired and Data Logger was programmed.</li> <li>- Logitech BRIO webcams were tested with different formats and resolutions.</li> </ul>
July 18, 2018	<ul style="list-style-type: none"> <li>- Ultrasonic sensors were calibrated.</li> <li>- <b>3<sup>rd</sup> data collection (End of Flowering)</b> was conducted.</li> <li>- Canopy height, NDVI and temperature were target traits.</li> <li>- Ambient temperature and humidity were collected during data collection. In addition, height of boom was recorded during data collection by using ultrasonic sensor.</li> <li>- RGB images (JPG format and 1920*1080 resolution) were captured from <u>whole of field</u> by Logitech BRIO webcam. Visible signs were used to validate the geo-referencing.</li> </ul>
August 2, 2018	<ul style="list-style-type: none"> <li>- Ultrasonic sensors were calibrated.</li> <li>- <b>4<sup>th</sup> data collection (Before Maturity)</b> was conducted.</li> <li>- Canopy height, NDVI and temperature were target traits. .</li> <li>- Ambient temperature and humidity were collected during data collection. In addition, height of boom was recorded during data collection by using ultrasonic sensor.</li> </ul>
August 14, 2018	<ul style="list-style-type: none"> <li>- Ultrasonic sensors were calibrated.</li> <li>- <b>5<sup>th</sup> data collection (Before Harvest)</b> was conducted.</li> <li>- Canopy height, NDVI and temperature were target traits.</li> <li>- Ambient temperature and humidity were collected during data collection. In addition, height of boom was recorded during data collection by using ultrasonic sensor.</li> <li>- RGB images (JPG and PNG format and 1920*1080 resolution) were captured from <u>part of field</u> by Logitech BRIO webcam. Visible signs were used to validate the geo-referencing.</li> </ul>
September 25, 2018	<ul style="list-style-type: none"> <li>- Changing broken turnbuckles of 2<sup>nd</sup> generation boom.</li> <li>- Testing LiDar (Light Detection and Ranging) on one of Cargill's fields in the Aberdeen.</li> </ul>

## E2- Preparation and test dates for the studied canola field on 2019

*Table E- 2: List of conducted field trials during 2019 growing season on canola field*

Date	Tasks
June 19, 2019	<ul style="list-style-type: none"> <li>- The second-generation boom was assembled.</li> <li>- Electrical system, including sensors and Data Logger, were wired. All sensors, cameras were tested to see if they are working correctly.</li> <li>- Required GPS data for mapping this year's field was collected.</li> </ul>
June 27, 2019	<ul style="list-style-type: none"> <li>- <b>1<sup>st</sup> data collection (Seeding Status)</b> was conducted with the speed of 1.6 mph.</li> <li>- Canopy NDVI and temperature were target traits.</li> <li>- Ambient temperature and humidity were collected during data collection.</li> <li>- RGB images (JPG format and 1920*1080 resolution) were captured from the whole of the field by webcam.</li> <li>- Multispectral images and LiDAR data were collected for the entire field.</li> </ul>
July 11, 2019	<ul style="list-style-type: none"> <li>- <b>2<sup>nd</sup> data collection (Flowering Status)</b> was conducted with the speed of 1.6 mph.</li> <li>- Canopy height, NDVI and temperature were target traits.</li> <li>- Ambient temperature and humidity were collected during data collection. In addition, the height of the boom was recorded during data collection by using the ultrasonic sensor.</li> <li>- RGB images (JPG format and 1920*1080 resolution) were captured from the whole of the field by webcam.</li> <li>- Multispectral images and LiDAR data were collected for the entire field.</li> </ul>
July 31, 2019	<ul style="list-style-type: none"> <li>- Data Logger was programmed with the new program, which doesn't need any calibration for ultrasonic sensors.</li> <li>- Thermal picture of crops were taken. Also, for the one row, the height of crops were measured manually.</li> <li>- <b>3<sup>rd</sup> data collection (End of Flowering)</b> was conducted with the speed of 1.6 mph.</li> <li>- Canopy height, NDVI, and temperature were target traits.</li> <li>- Ambient temperature and humidity were collected during data collection. In addition, the height of the boom was recorded during data collection by using the ultrasonic sensor.</li> <li>- RGB images (JPG format and 1920*1080 resolution) were captured from the whole of the field by webcam.</li> <li>- Multispectral images and LiDAR data were collected for the entire field.</li> </ul>
August 15, 2019	<ul style="list-style-type: none"> <li>- Thermal picture of crops were taken. Also, for the entire field, the height of crops were measured manually.</li> <li>- <b>4<sup>th</sup> data collection (Before Maturity)</b> was conducted with two speeds: 1.6 and 3.2 mph.</li> <li>- Canopy height, NDVI, and temperature were target traits.</li> <li>- Ambient temperature and humidity were collected during data collection. In addition, the height of the boom was recorded during data collection by using the ultrasonic sensor.</li> <li>- RGB images (JPG format and 1920*1080 resolution) were captured from the whole of the field by webcam.</li> <li>- Multispectral images and LiDAR data were collected for the entire field.</li> </ul>
August 28, 2019	<ul style="list-style-type: none"> <li>- Thermal images of crops were taken and their height (for 4 row) were recorded manually.</li> <li>- <b>5<sup>th</sup> data collection (Before Maturity)</b> was conducted with different speeds: 1.6, 1.8, 2.4, 2.8 and 3.2 mph.</li> <li>- Canopy height, NDVI, and temperature were target traits.</li> <li>- Ambient temperature and humidity were collected during data collection. In addition, the height of the boom was recorded during data collection by using the ultrasonic sensor.</li> <li>- RGB images (JPG format and 1920*1080 resolution) were captured.</li> <li>- Multispectral images and LiDAR data were collected for the entire field.</li> <li>- The second-generation boom and electrical system were deassembled.</li> </ul>

## E3- Preparation and test dates for the studied wheat field on 2018

*Table E- 3: List of conducted field trials during 2018 growing season on wheat field*

Date	Tasks
June 21, 2018	- The second generation of the mechanical boom was assembled and attached to the wheat phenotyping platform.
June 27-28, 2018	- Electrical system including sensors and Data Logger were wired.
July 4, 2018	- Electrical system was wired and the boom was stabilized in order for secure transport.
July 9, 2018	- A path through the field on the GPS display in order for auto-steering to work was generated.
July 6, 2018	- Required GPS data for field mapping was collected. - All sensors and webcams has tested via programs to see if they are working properly.
July 13, 2018	- Ultrasonic sensors were calibrated. - <b>2<sup>nd</sup> data collection (Flowering Status)</b> was conducted. - Canopy's height and temperature were target traits. - Ambient temperature and humidity were collected during data collection. In addition, height of boom was recorded during data collection by using ultrasonic sensor. - RGB images (PNG and JPG format with 1280*720 resolution) were captured from <u>whole of field</u> by webcams (High and low quality). Visible signs were used to validate the geo-referencing.
July 26, 2018	- Ultrasonic sensors were calibrated. - <b>3<sup>rd</sup> data collection (End of Flowering)</b> was conducted. - Canopy height, NDVI and temperature were target traits. - Ambient temperature and humidity were collected during data collection. In addition, height of boom was recorded during data collection by using ultrasonic sensor. - RGB images (JPG format and 1920*1080 resolution) were captured from <u>whole of field</u> by high quality webcam in two modes: normal and maximum height of the boom. Also, Visible signs were used to validate the geo-referencing.
August 9, 2018	- Ultrasonic sensors were calibrated. - <b>4<sup>th</sup> data collection (Before Maturity)</b> was conducted. - Canopy height, NDVI and temperature were target traits. - Ambient temperature and humidity were collected during data collection. In addition, height of boom was recorded during data collection by using ultrasonic sensor. - RGB images (JPG format and 1920*1080 resolution) were captured from <u>whole of field</u> by high quality webcam in two modes: normal height of the boom and mounting bracket. Also, Visible signs were used to validate the geo-referencing. - Some Canopy's temperature have measured by hand held thermometer. - Random crops' height has measured by tape measurement.
August 23, 2018	- Ultrasonic sensors were calibrated. - <b>5<sup>th</sup> data collection (Before Harvest)</b> was conducted. - Canopy height, NDVI and temperature were target traits. - Ambient temperature and humidity were collected during data collection. In addition, height of boom was recorded during data collection by using ultrasonic sensor. - RGB images (JPG format and 1920*1080 resolution) were captured from <u>whole of field</u> by high quality webcam. Also, Visible signs were used to validate the geo-referencing. - Canon camera was tested for part of field. Multispectral camera was tested just for one row.
September 21, 2018	- Canon camera was tested for whole of field. LiDar Sensor was tested for one row.
September 29, 2018	- LiDar Sensor was tested for whole of field. Multispectral camera was tested for whole of field.

## E4- Preparation and test dates for the studied wheat field on 2019

*Table E- 4: List of conducted field trials during 2019 growing season on wheat field*

Date	Tasks
<b>June 30, 2019</b>	<ul style="list-style-type: none"> <li>- Electrical system including sensors and Data Logger were wired.</li> <li>- All sensors and devices were tested to see if they are working properly.</li> </ul>
<b>July 4, 2019</b>	<ul style="list-style-type: none"> <li>- Required GPS data for mapping this year's field was collected.</li> <li>- Visible signs were used to validate the geo-referencing.</li> <li>- Ultrasonic sensors were calibrated.</li> <li>- <b>1<sup>st</sup> data collection (Seeding Status)</b> was conducted with the speed of 1.6 mph.</li> <li>- Canopy height, NDVI and temperature were target traits. Ambient temperature/humidity and the height of the boom were recorded during data collection.</li> <li>- RGB images (JPG format and 1920*1080 resolution) were captured from <u>whole of field</u> by webcams in two modes: normal height of the boom and mounting bracket.</li> <li>- Multispectral images and LiDAR data were collected for the entire field.</li> </ul>
<b>July 10, 2019</b>	<ul style="list-style-type: none"> <li>- New ultrasonic sensors (Sick ultrasonic sensor) were wired.</li> <li>- Required GPS data for mapping this year's field was collected.</li> </ul>
<b>July 13, 2019</b>	<ul style="list-style-type: none"> <li>- Data Logger was programmed with new data acquisition program.</li> <li>- GPS system was calibrated.</li> </ul>
<b>July 23, 2019</b>	<ul style="list-style-type: none"> <li>- Required GPS data for mapping this year's field was collected.</li> <li>- <b>2<sup>nd</sup> data collection (Flowering Status)</b> was conducted with the speed of 1.6 mph.</li> <li>- Canopy height, NDVI and temperature were target traits. Ambient temperature/humidity and the height of the boom were recorded during data collection.</li> <li>- RGB images (JPG format and 1920*1080 resolution) were captured from <u>whole of field</u> by webcams in two modes: normal height of the boom and mounting bracket.</li> <li>- Multispectral images and LiDAR data were collected for the entire field.</li> <li>- Canopy's height has measured by measure stick.</li> </ul>
<b>August 1, 2019</b>	<ul style="list-style-type: none"> <li>- <b>3<sup>rd</sup> data collection (End of Flowering)</b> was conducted with the speed of 1.6 mph.</li> <li>- Canopy height, NDVI and temperature were target traits. Ambient temperature/humidity and the height of the boom were recorded during data collection.</li> <li>- RGB images (JPG format and 1920*1080 resolution) were captured from <u>whole of field</u> by webcams in two modes: normal height of the boom and mounting bracket.</li> <li>- Multispectral images and LiDAR data were collected.</li> <li>- Canopy's height has measured by measure stick. Thermal picture of random crops were taken.</li> </ul>
<b>August 20, 2019</b>	<ul style="list-style-type: none"> <li>- <b>4<sup>th</sup> data collection (Before Maturity)</b> was conducted with two speeds: 1.6 and 3.2 mph.</li> <li>- Canopy height, NDVI and temperature were target traits. Ambient temperature/humidity and the height of the boom were recorded during data collection.</li> <li>- RGB images (JPG format and 1920*1080 resolution) were captured from <u>whole of field</u> by webcams in two modes: normal height of the boom and mounting bracket.</li> <li>- Multispectral images and LiDAR data were collected for the entire field.</li> <li>- Some Canopy's temperature have measured by hand held thermometer.</li> <li>- Canopy's height has measured by measure stick.</li> </ul>
<b>September 17, 2019</b>	<ul style="list-style-type: none"> <li>- <b>5<sup>th</sup> data collection (Before Harvest)</b> was conducted with the speed of 1.6 mph.</li> <li>- Canopy height, NDVI and temperature were target traits. Ambient temperature/humidity and the height of the boom were recorded during data collection.</li> <li>- RGB images (JPG format and 1920*1080 resolution) were captured from <u>whole of field</u> by webcams in two modes: normal height of the boom and mounting bracket.</li> <li>- Multispectral images and LiDAR data were collected for the entire field.</li> <li>- Canopy's height has measured by measure stick.</li> </ul>
<b>October 3, 2019</b>	<ul style="list-style-type: none"> <li>- The mechanical team conducted vibration tests to find natural frequency &amp; vibration response of the 2<sup>nd</sup> generation boom and extension brackets.</li> </ul>



## APPENDIX F- Analyzing growth of canola plots over summer 2018

This section provides obtained results from the collected data over summer 2018 and use of Pheno-VISDM2 for 5 different plots with diverse genotype.

### F1. Analyzing growth of the plot #11.12 (Selected randomly from HP7 genotype)



*Figure F- 1: Plot #11.12 on June 19, 2018 (Seedling Status)*



*Figure F- 2: Plot #11.12 on June 29, 2018 (Flowering Status)*





*Figure F- 3: Plot #11.12 on July 18, 2018 (End of Flowering Status)*

## F1.1. Summary of captured data for plot # 11.12 during summer 2018

*Table F- 1: Variation of NDVI, height, temperature, ambient temperature and humidity of plot #11.12 during summer 2018*

Stage	Date	NDVI		Height (cm)		Temp(C°)		Ambient Temp (C°) Ref: Platform's weather station		Ambient Humidity (%) Ref: Platform's weather station	
		*	**	*	**	*	**	*	**	*	**
1 <sup>st</sup>	June 19, 2018	0.56	0.58	-	-	43.45	41.6	-	-	-	-
2 <sup>nd</sup>	June 29, 2018	0.68	0.71	-	-	27.18	26.01	-	-	-	-
3 <sup>rd</sup>	July 18, 2018	0.65	0.66	70.45	68.82	28.31	28.31	31.52	31.58	40.67	40.56
4 <sup>th</sup>	August 2, 2018	0.69	0.68	73.05	74.47	26.91	27.11	27.95	28.03	45.68	45.98
5 <sup>th</sup>	August 14, 2018	0.53	0.54	75.89	76.70	23.98	24.13	22.70	22.70	36.46	36.45

\*: Without edge-effect

\*\*: With edge-effect



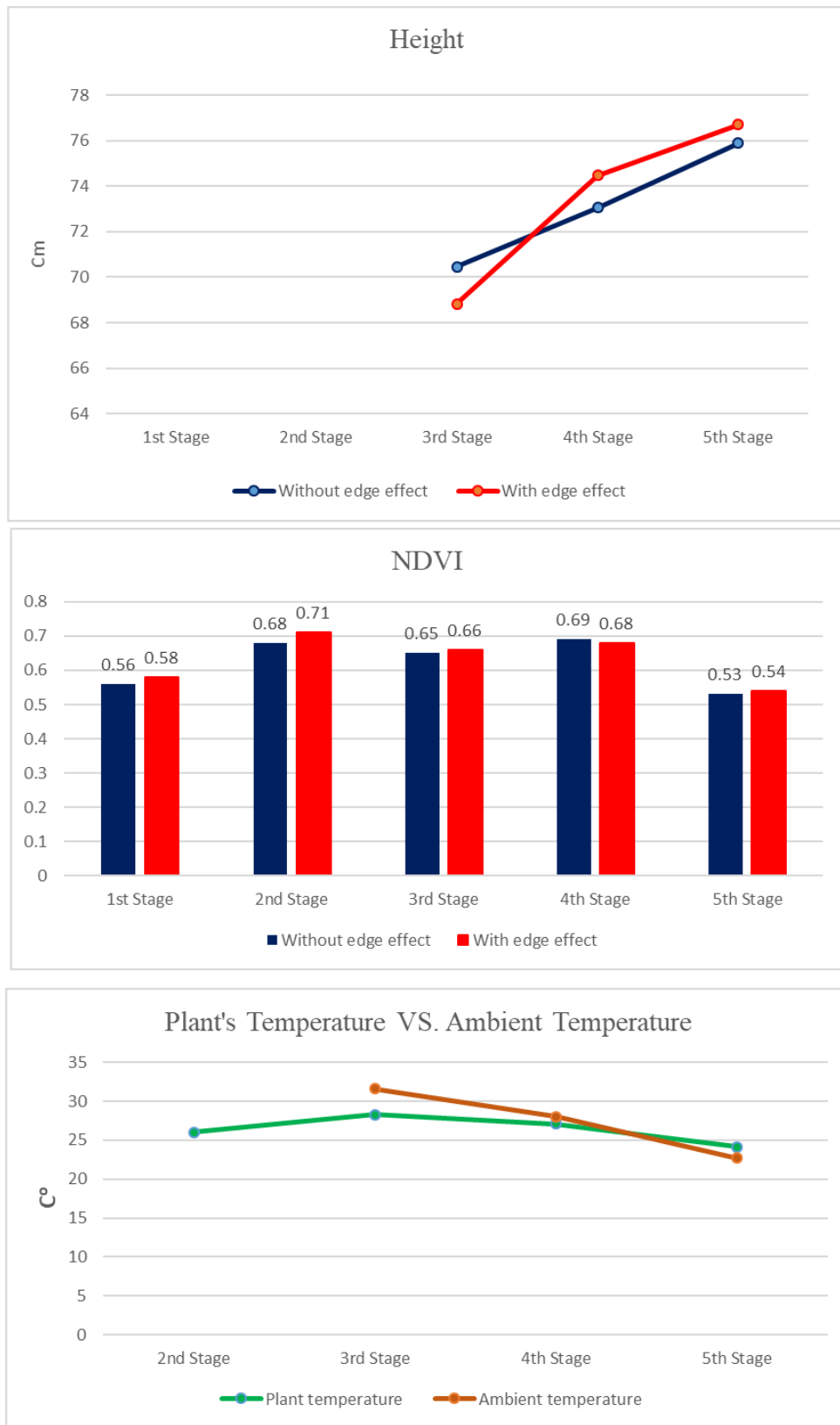


Figure F- 4: Variation of NDVI, height, temperature, ambient temperature and humidity of plot #11.12 during summer 2018

**F2. Analyzing growth of the plot #9.18 (Selected randomly from HP5 genotype)**



*Figure F- 5: Plot #9.18 on June 19, 2018 (Seedling Status)*



*Figure F- 6: Plot #9.18 on June 29, 2018 (Flowering Status)*





*Figure F- 7: Plot #9.18 on July 18 (End of Flowering Status)*

## F2.1. Summary of captured data for plot # 9.18 during summer 2018

*Table F- 2: Variation of NDVI, height, temperature, ambient temperature and humidity of plot #9.18 during summer 2018*

Stage	Date	NDVI		Height (cm)		Temp(C°)		Ambient Temp (C°) Ref: Platform's weather station		Ambient Humidity (%) Ref: Platform's weather station	
		*	**	*	**	*	**	*	**	*	**
1 <sup>st</sup>	June 19, 2018	0.53	0.56	-	-	44.04	42.98	-	-	-	-
2 <sup>nd</sup>	June 29, 2018	0.73	0.73	-	-	24.75	24.24	-	-	-	-
3 <sup>rd</sup>	July 18, 2018	0.61	0.64	74.17	72.26	27.41	26.88	31.16	31.12	42.4	42.35
4 <sup>th</sup>	August 2, 2018	0.70	0.71	69.57	69.99	26.97	26.96	27.79	27.85	47.89	47.81
5 <sup>th</sup>	August 14, 2018	0.59	0.59	70.78	71.71	23.28	23.33	22.32	22.35	38.43	38.49

\*: Without edge-effect

\*\*: With edge-effect

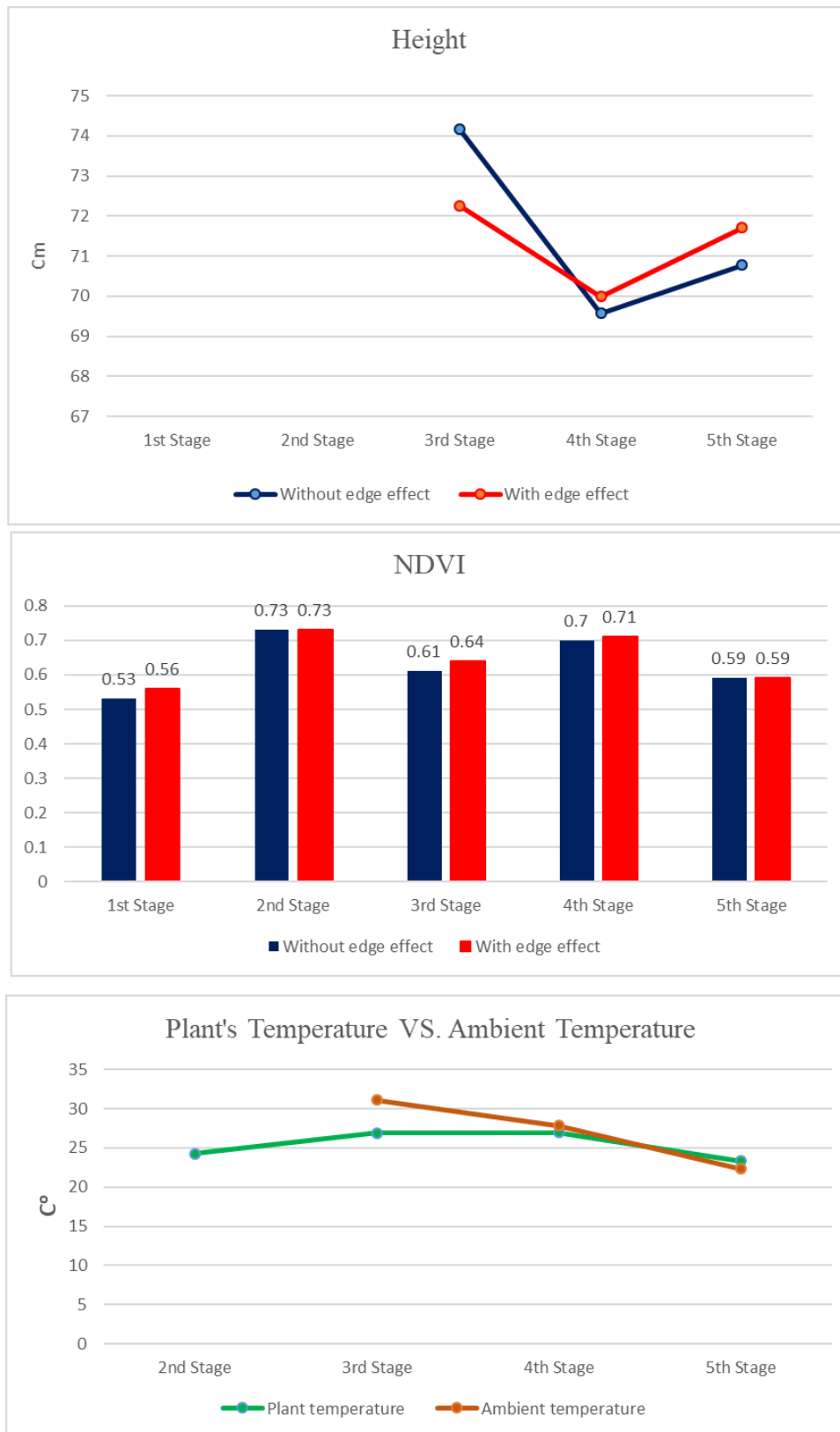


Figure F- 8: Variation of NDVI, height, temperature, ambient temperature and humidity of plot #9.18 during summer 2018



**F3. Analyzing growth of the plot #17.46(Selected randomly from HA2 rep1 genotype)**



*Figure F- 9: Plot #17.46 on June 19, 2018 (Seedling Status)*



*Figure F- 10: Plot #17.46 on June 29, 2018 (Flowering Status)*





*Figure F- 11: Plot #17.46 on July 18, 2018 (End of Flowering Status)*

### **F3.1. Summary of captured data for plot # 17.46 during summer 2018**

*Table F- 3: Variation of NDVI, height, temperature, ambient temperature and humidity of plot #17.46 during summer 2018*

Stage	Date	NDVI		Height (cm)		Temp(C°)		Ambient Temp (C°) Ref: Platform's weather station		Ambient Humidity (%) Ref: Platform's weather station	
		*	**	*	**	*	**	*	**	*	**
1 <sup>st</sup>	June 19, 2018	0.36	0.37	-	-	37.7	37.82	-	-	-	-
2 <sup>nd</sup>	June 29, 2018	0.41	0.41	-	-	41.28	41.15	-	-	-	-
3 <sup>rd</sup>	July 18, 2018	0.46	0.45	4.98	4.70	36.58	36.36	31.70	31.57	39.79	40.27
4 <sup>th</sup>	August 2, 2018	0.37	0.37	2.08	0.25	36.29	36.74	30.85	30.82	40.50	40.59
5 <sup>th</sup>	August 14, 2018	0.35	0.35	5.74	1.99	29.88	30.12	24.25	24.28	33.17	33.07

\*: Without edge-effect

\*\*: With edge-effect

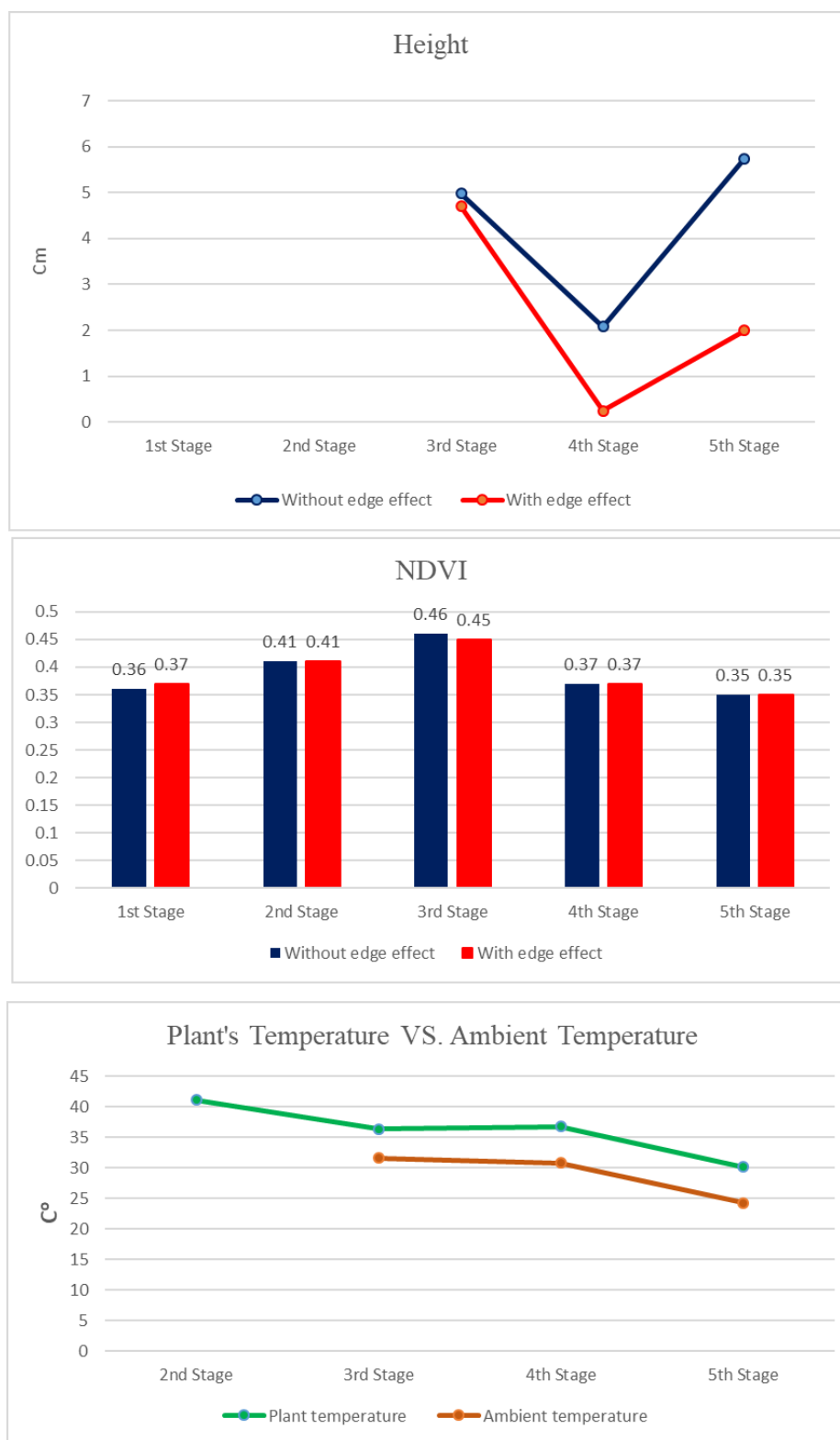


Figure F- 12: Variation of NDVI, height, temperature, ambient temperature and humidity of plot #17.46 during summer 2018



**F4. Analyzing growth of the plot #14.44 (Selected randomly from HA2 rep2 genotype)**



*Figure F- 13: Plot #14.44 on June 19, 2018(Seedling Status)*



*Figure F- 14: Plot #14.44 on June 29, 2018 (Flowering Status)*





*Figure F- 15: Plot #14.44 on July 18, 2018 (End of Flowering Status)*

#### **F4.1. Summary of captured data for plot # 14.44 during summer 2018**

*Table F- 4: Variation of NDVI, height, temperature, ambient temperature and humidity of plot #14.44 during summer 2018*

Stage	Date	NDVI		Height (cm)		Temp(C°)		Ambient Temp (C°) Ref: Platform's weather station		Ambient Humidity (%) Ref: Platform's weather station	
		*	**	*	**	*	**	*	**	*	**
1 <sup>st</sup>	June 19, 2018	0.40	0.39	-	-	46.57	46.89	-	-	-	-
2 <sup>nd</sup>	June 29, 2018	0.48	0.48	-	-	38.21	38.59	-	-	-	-
3 <sup>rd</sup>	July 18, 2018	0.54	0.53	5.12	4.77	39.00	40.47	31.21	31.06	39.19	39.96
4 <sup>th</sup>	August 2, 2018	0.43	0.44	4.71	4.60	36.29	36.79	29.40	29.39	42.60	42.50
5 <sup>th</sup>	August 14, 2018	0.39	0.39	12.50	13.39	29.48	30.14	23.64	23.68	34.82	34.65

\*: Without edge-effect

\*\*: With edge-effect

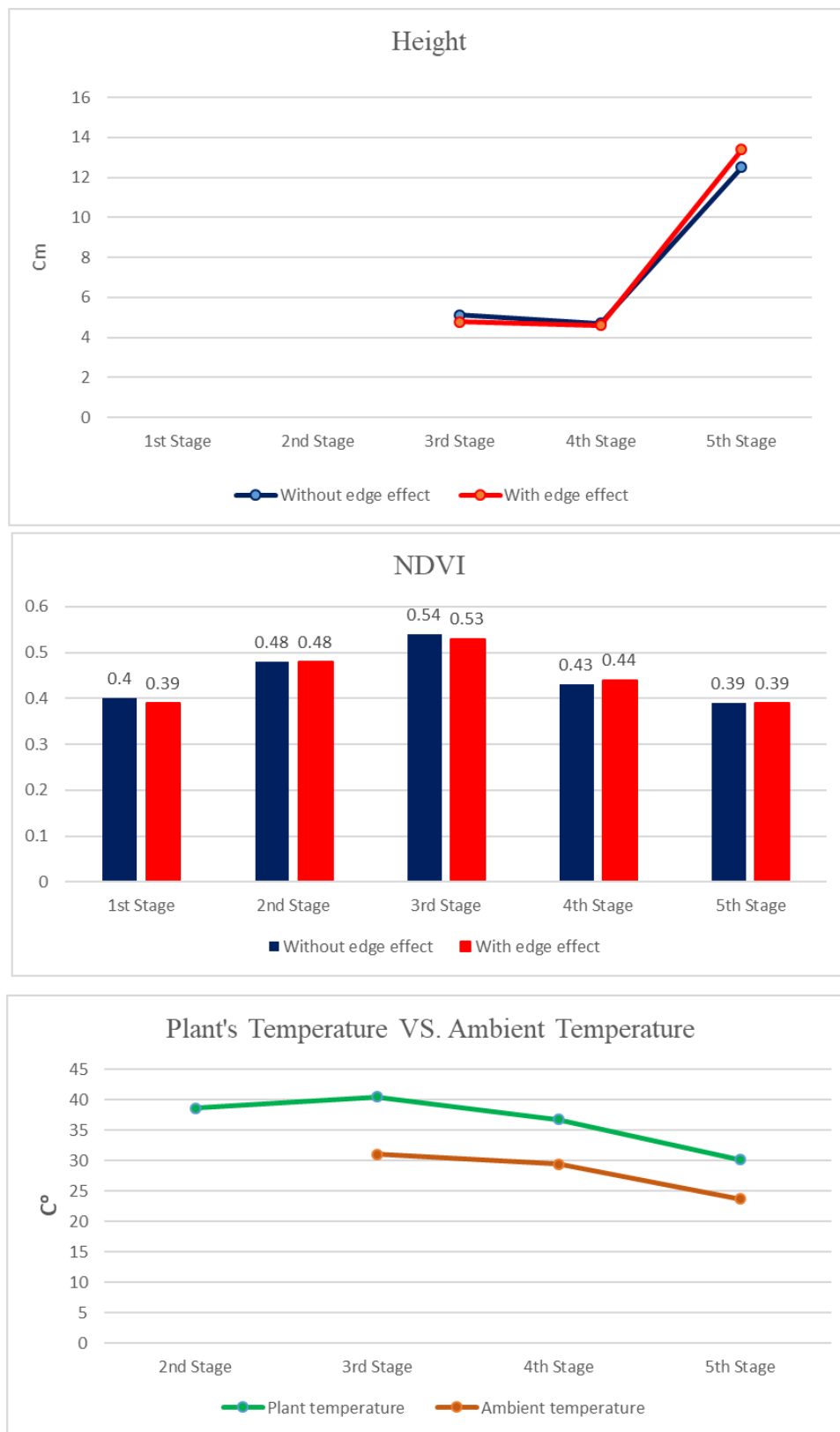


Figure F- 16: Variation of NDVI, height, temperature, ambient temperature and humidity of plot #14.44 during summer 2018



**F5. Analyzing growth of the plot #30.77 (Selected randomly from TC8 genotype)**



*Figure F- 17: Plot #30.77 on June 19, 2018 (Seedling Status)*



*Figure F- 18: Plot #30.77 on June 29, 2018 (Flowering Status)*





*Figure F- 19: Plot #30.77 on July 18, 2018 (End of Flowering Status)*



*Figure F- 20: Plot #30.77 on July 18, 2018 (End of Flowering Status)*



## F5.1. Summary of captured data for plot # 30.77 during summer 2018

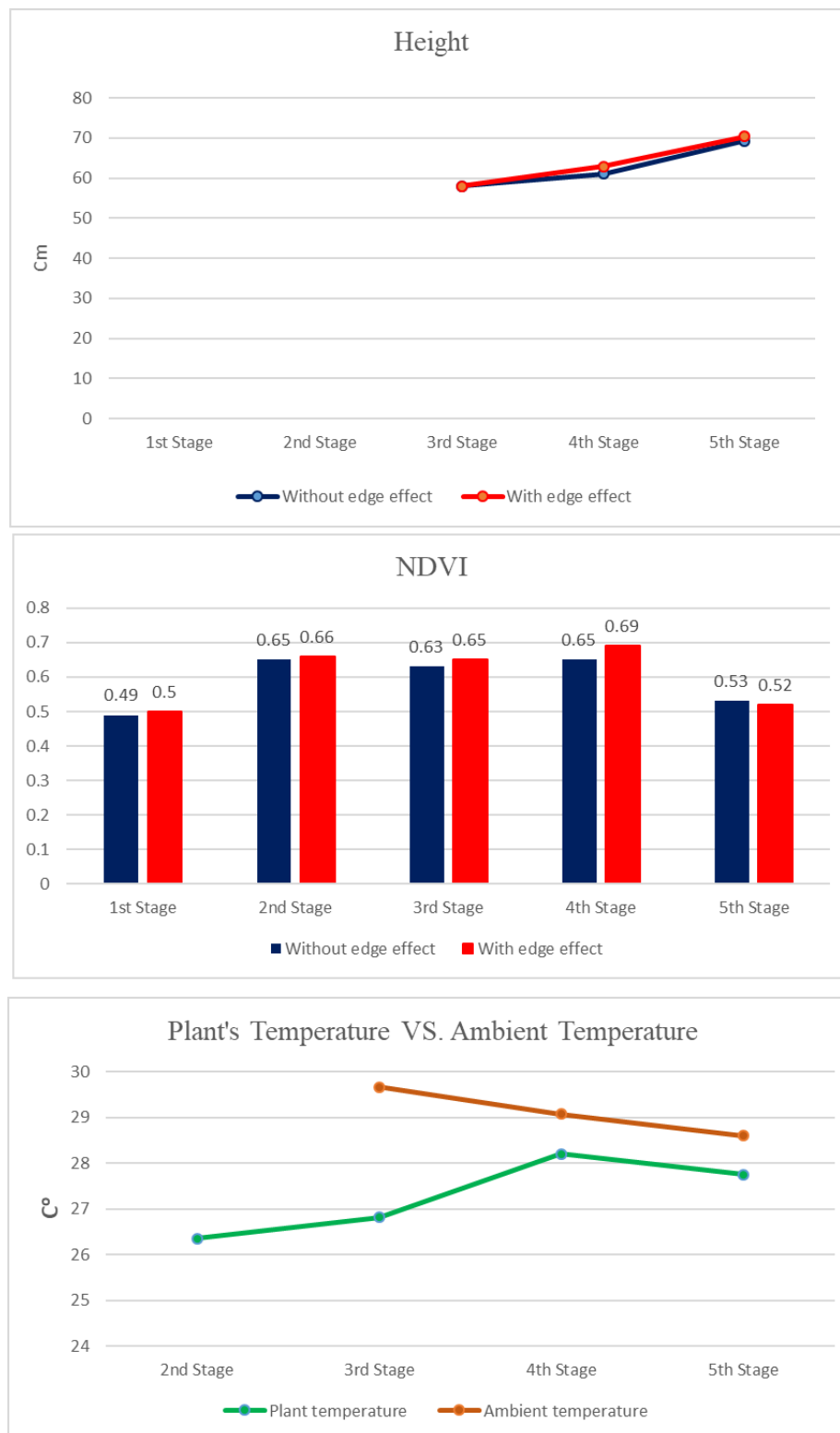


Figure F- 21: Variation of NDVI, height, temperature, ambient temperature and humidity of plot #30.77 during summer 2018

*Table F- 5: Variation of NDVI, height, temperature, ambient temperature and humidity of plot #30.77 during summer 2018*

Stage	Date	NDVI		Height (cm)		Temp(C°)		Ambient Temp (C°) Ref: Platform's weather station		Ambient Humidity (%) Ref: Platform's weather station	
		*	**	*	**	*	**	*	**	*	**
1 <sup>st</sup>	June 19, 2018	0.49	0.50	-	-	34.09	34.33	-	-	-	-
2 <sup>nd</sup>	June 29, 2018	0.65	0.66	-	-	26.32	26.35	-	-	-	-
3 <sup>rd</sup>	July 18, 2018	0.63	0.65	57.99	57.99	26.77	26.82	29.20	29.67	56.13	54.36
4 <sup>th</sup>	August 2, 2018	0.65	0.69	61.07	62.92	28.42	28.20	29.10	29.08	40.09	39.94
5 <sup>th</sup>	August 14, 2018	0.53	0.52	69.26	70.40	27.93	27.75	28.60	28.60	23.01	23.01

\*: Without edge-effect

\*\*: With edge-effect



## **APPENDIX G- Analyzing growth of canola plots over summer 2019**

This section provides obtained results from the collected data over summer 2019 and use of Pheno-VISDM3 for 6 different plots with diverse genotype.

### **G1. Analyzing growth of the plot #3.7 (Selected randomly from HA01 genotype)**



*Figure G- 1: Plot #3.7 on June 26, 2019 (Seedling Status)*



*Figure G- 2: Plot #3.7 on July 11, 2019 (Start of Flowering Status)*





*Figure G- 3: Plot #3.7 on July 31, 2019 (End of Flowering Status)*



*Figure G- 4: Plot #3.7 on August 15, 2019 (Start of Maturity Status)*





*Figure G- 5: Plot #3.7 on August 28, 2019 (End of Maturity Status)*

## G1.1. Summary of captured data for plot # 3.7 during summer 2019

*Table G- 1: Variation of NDVI, height, temperature, ambient temperature and humidity of plot #3.7 during summer 2019*

Stage	Date	NDVI		Height (cm)		Temp(C°)		Ambient Temp (C°) Ref: Platform's weather station		Ambient Humidity (%) Ref: Platform's weather station	
		*	**	*	**	*	**	*	**	*	**
1 <sup>st</sup>	26 June, 2019	0.50	0.50	-	-	22.49	22.80	22.80	22.40	42.72	42.72
2 <sup>nd</sup>	11 July, 2019	0.63	0.63	22.22	21.92	21.98	21.92	20.11	20.07	69.60	69.71
3 <sup>rd</sup>	13 July, 2019	0.49	0.49	97.96	97.99	23.25	23.20	22.40	22.48	71.01	70.73
4 <sup>th</sup>	15 August, 2019	0.64	0.64	75.27	74.86	23.85	24.07	21.97	21.98	55.84	55.95
5 <sup>th</sup>	28 August, 2019	0.64	0.64	73.49	74.08	18.36	18.33	18.25	18.25	61.37	61.45

\*: Without edge effect

\*\*: With edge effect

It should be mentioned that these variation numbers were calculated from average of measurements.

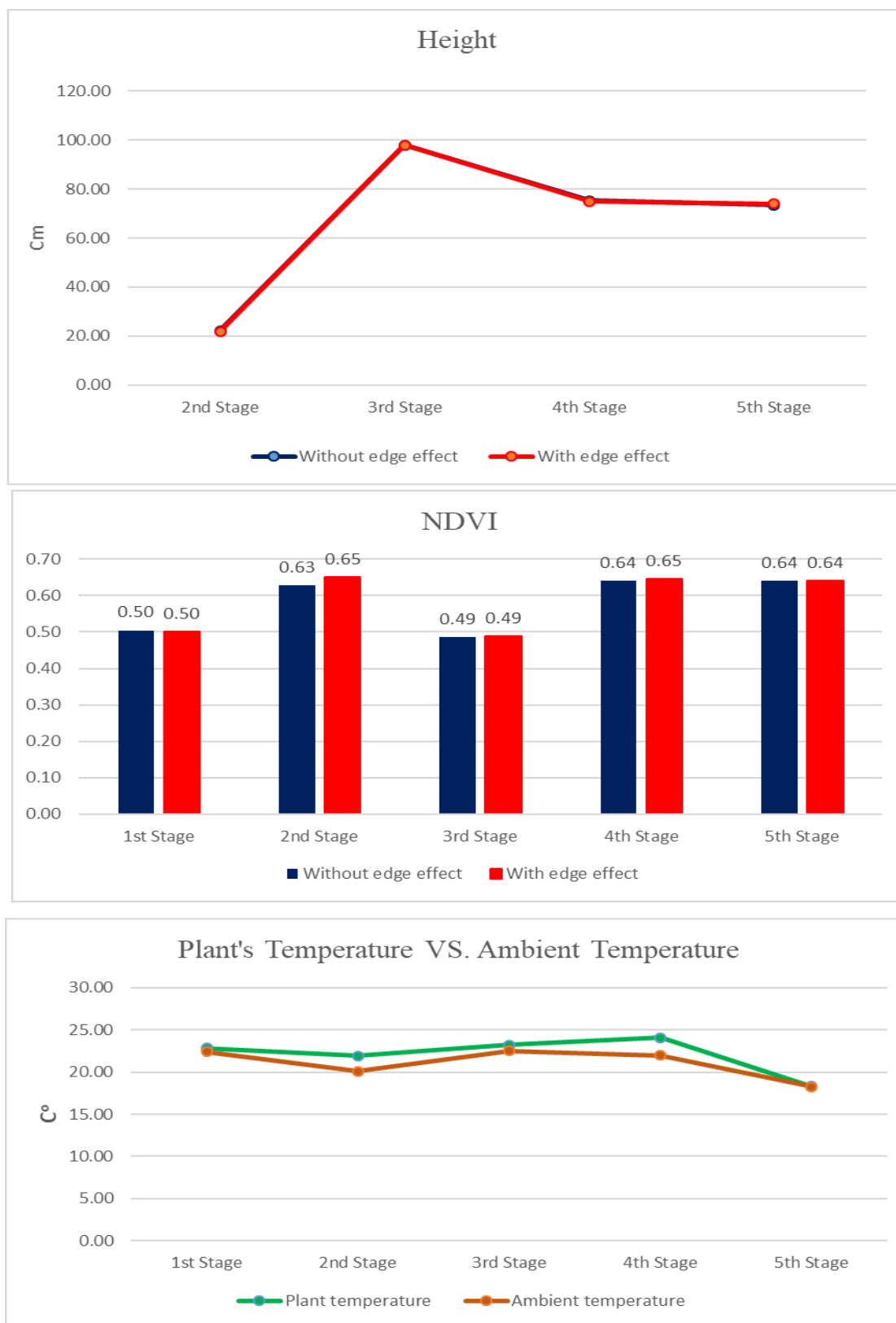


Figure G- 6: Variation of NDVI, height, temperature, ambient temperature and humidity of plot #3.7 during summer 2019



**G2. Analyzing the growth of plot #7.20 (Selected randomly from HA02 genotype)**



*Figure G- 7: Plot #7.20 on June 26, 2019 (Seedling Status)*



*Figure G- 8: Plot #7.20 on July 11, 2019 (Start of Flowering Status)*





*Figure G- 9: Plot #7.20 on July 31, 2019 (End of Flowering Status)*



*Figure G- 10: Plot #7.20 on August 15, 2019 (Start of Maturity Status)*





Figure G- 11: Plot #7.20 on August 28, 2019 (End of Maturity Status)

## G2.1. Summary of captured data for plot # 7.20 during summer 2019

Table G- 2: Variation of NDVI, height, temperature, ambient temperature and humidity of plot #7.20 during summer 2019

Stage	Date	NDVI		Height (cm)		Temp(C°)		Ambient Temp (C°) Ref: Platform's weather station		Ambient Humidity (%) Ref: Platform's weather station	
		*	**	*	**	*	**	*	**	*	**
1 <sup>st</sup>	26 June, 2019	0.46	0.51	-	-	30.93	30.70	24.02	24.01	40.09	40.09
2 <sup>nd</sup>	11 July, 2019	0.74	0.73	41.05	42.14	23.93	23.83	21.00	21.01	63.46	63.92
3 <sup>rd</sup>	13 July, 2019	0.66	0.66	100.94	102.31	23.35	23.39	22.86	22.83	64.76	64.84
4 <sup>th</sup>	15 August, 2019	0.72	0.73	84.51	85.17	25.49	25.25	23.21	23.23	52.30	52.28
5 <sup>th</sup>	28 August, 2019	0.66	0.68	72.47	73.62	18.62	18.61	19.46	19.47	56.78	56.77

\*: Without edge effect

\*\*: With edge effect



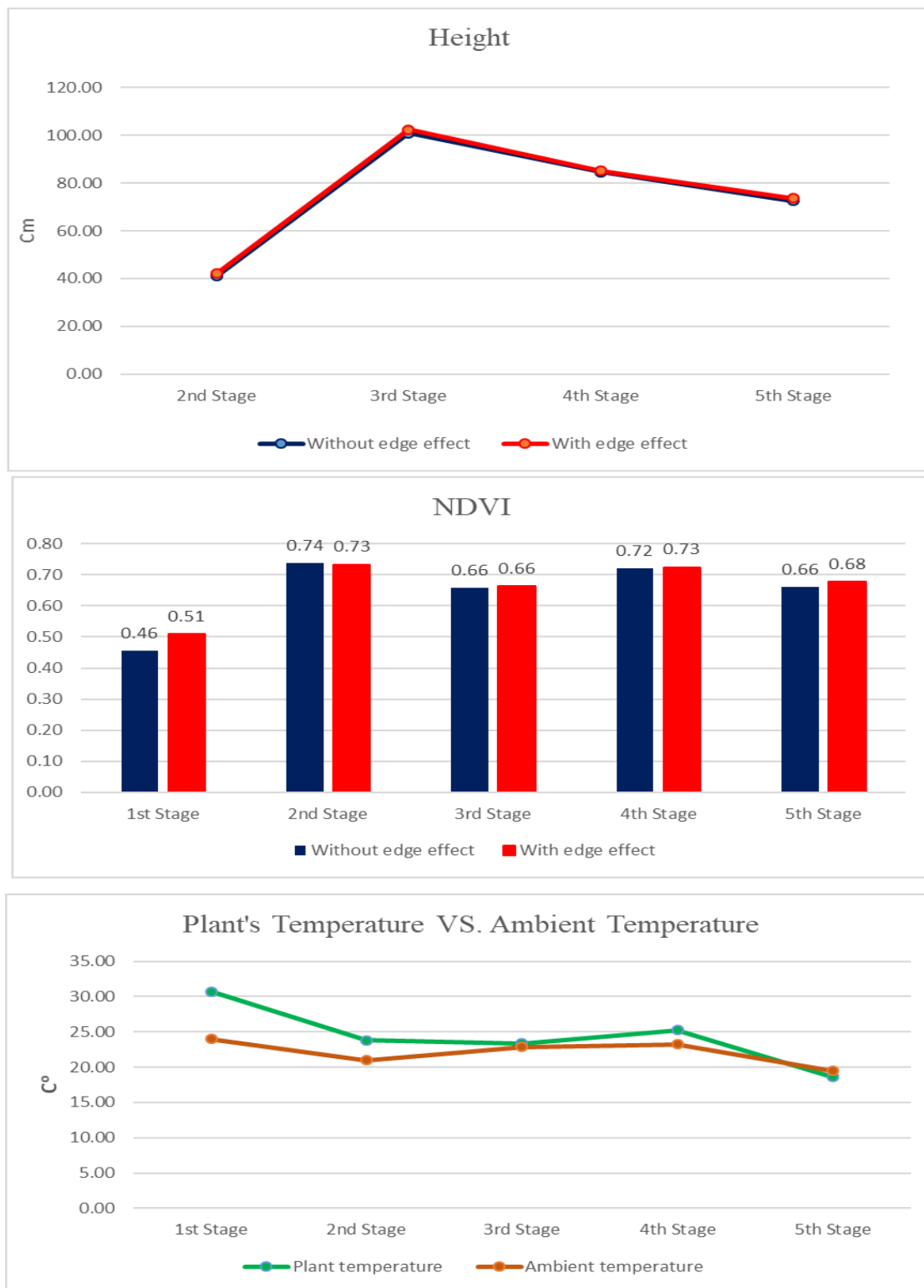


Figure G- 12: Variation of NDVI, height, temperature, ambient temperature and humidity of plot #7.20 during summer 2019

**G3. Analyzing the growth of the plot #10.3 (Selected randomly from HA03 genotype)**



*Figure G- 13: Plot #10.3 on June 26, 2019 (Seedling Status)*



*Figure G- 14: Plot #10.3 on July 11, 2019 (Start of Flowering Status)*





*Figure G- 15: Plot #10.3 on July 31, 2019 (End of Flowering Status)*



*Figure G- 16: Plot #10.3 on August 15, 2019 (Start of Maturity Status)*





*Figure G- 17: Plot #10.3 on August 28, 2019 (End of Maturity Status)*

### **G3.1. Summary of captured data for plot # 10.3 during summer 2019**

*Table G- 3: Variation of NDVI, height, temperature, ambient temperature and humidity of plot #10.3 during summer 2019*

Stage	Date	NDVI		Height (cm)		Temp(C°)		Ambient Temp (C°) Ref: Platform's weather station		Ambient Humidity (%) Ref: Platform's weather station	
		*	**	*	**	*	**	*	**	*	**
1 <sup>st</sup>	26 June, 2019	0.68	0.69	-	-	26.53	26.20	25.54	25.50	33.52	33.52
2 <sup>nd</sup>	11 July, 2019	0.67	0.66	55.62	54.68	24.23	24.37	21.62	21.62	63.57	63.60
3 <sup>rd</sup>	13 July, 2019	0.73	0.73	96.59	96.34	23.98	24.03	23.45	23.40	62.28	62.53
4 <sup>th</sup>	15 August, 2019	0.65	0.66	80.67	81.16	26.62	26.71	23.64	23.62	49.74	49.76
5 <sup>th</sup>	28 August, 2019	0.50	0.52	78.17	79.03	19.13	19.12	19.62	19.59	56.65	56.65

\*: Without edge effect

\*\*: With edge effect

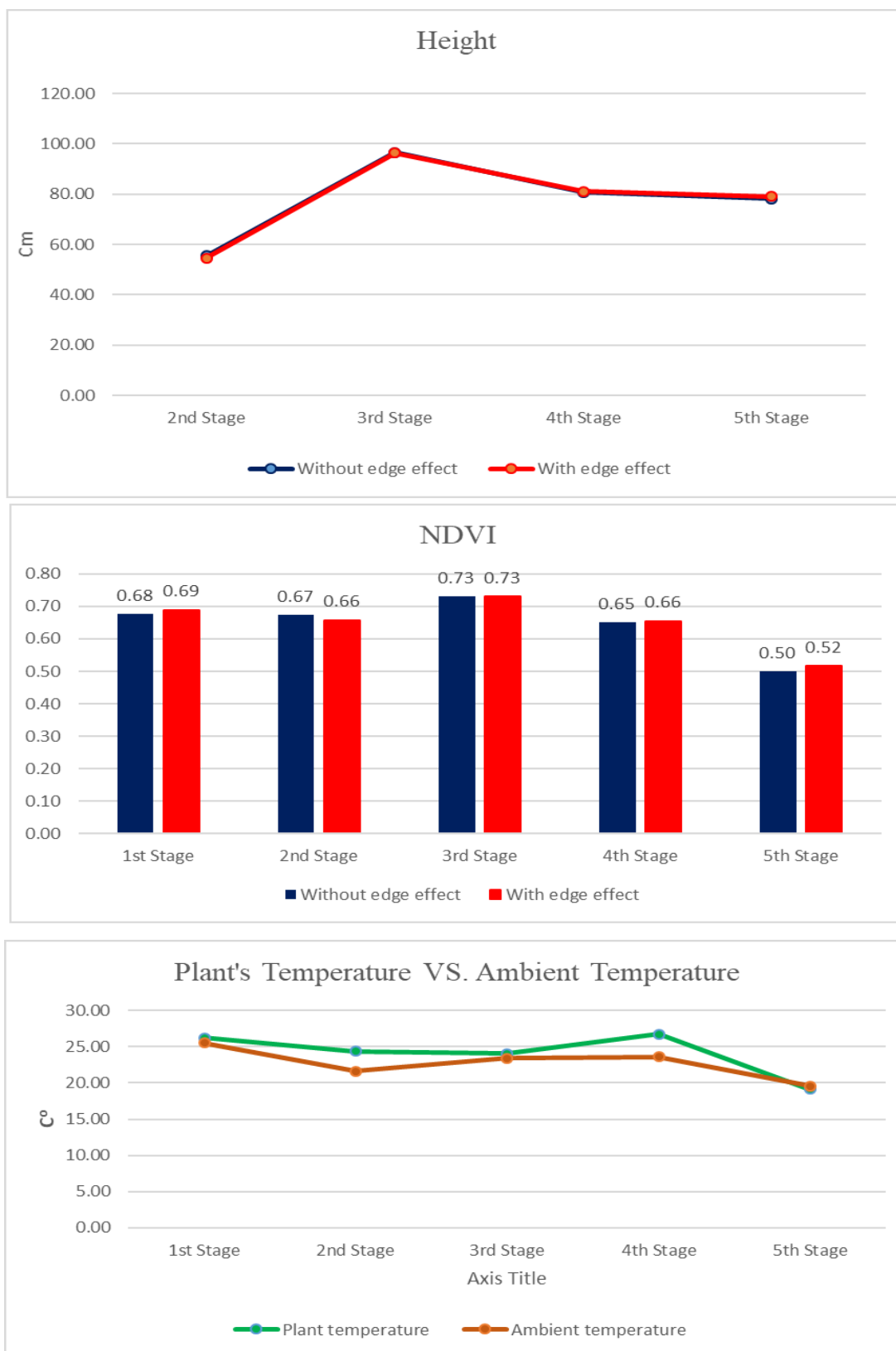


Figure G- 18: Variation of NDVI, height, temperature, ambient temperature and humidity of plot #10.3 during summer 2019



**G4. Analyzing the growth of the plot #14.30 (Selected randomly from PR-RST genotype)**



*Figure G- 19: Plot #14.30 on June 26, 2019 (Seedling Status)*



*Figure G- 20: Plot #14.30 on July 11, 2019 (Start of Flowering Status)*





*Figure G- 21: Plot #14.30 on July 31, 2019 (End of Flowering Status)*



*Figure G- 22: Plot #14.30 on August 15, 2019 (Start of Maturity Status)*





*Figure G- 23: Plot #14.30 on August 28, 2019 (End of Maturity Status)*

#### **G4.1. Summary of captured data for plot # 14.30 during summer 2019**

*Table G- 4: Variation of NDVI, height, temperature, ambient temperature and humidity of plot #14.30 during summer 2019*

Stage	Date	NDVI		Height (cm)		Temp(C°)		Ambient Temp (C°) Ref: Platform's weather station		Ambient Humidity (%) Ref: Platform's weather station	
		*	**	*	**	*	**	*	**	*	**
1 <sup>st</sup>	26 June, 2019	0.59	0.57	-	-	31.61	31.80	26.29	26.30	31.86	31.86
2 <sup>nd</sup>	11 July, 2019	0.66	0.65	56.82	57.27	23.86	20.52	21.95	21.98	61.82	61.72
3 <sup>rd</sup>	13 July, 2019	0.79	0.79	80.46	81.01	24.03	24.00	23.37	23.37	62.54	62.50
4 <sup>th</sup>	15 August, 2019	0.69	0.69	72.08	73.41	25.56	25.54	24.47	24.48	47.06	47.06
5 <sup>th</sup>	28 August, 2019	0.56	0.57	68.41	68.14	20.03	20.08	20.28	20.29	53.43	53.42

\*: Without edge effect

\*\*: With edge effect

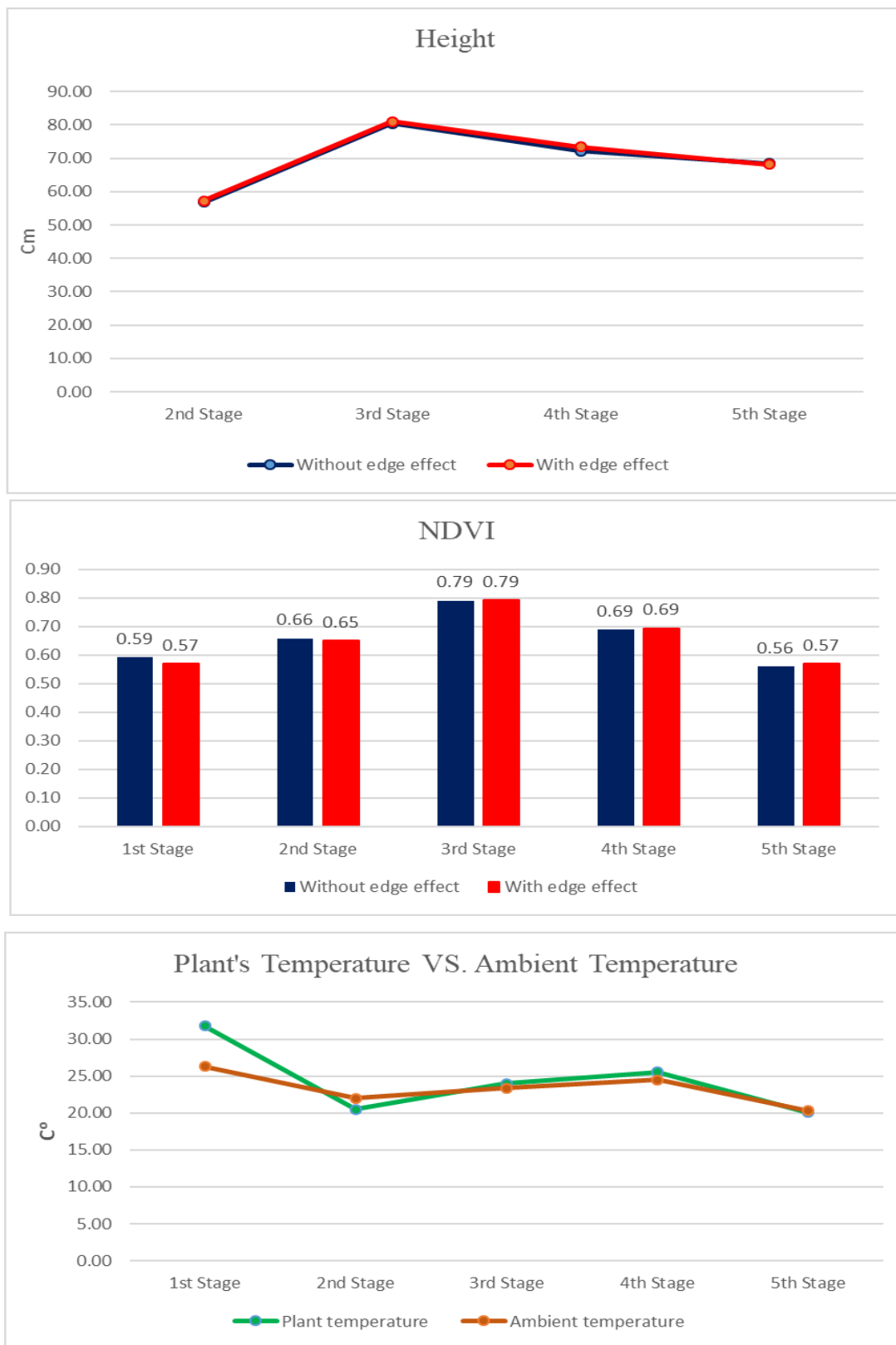


Figure G- 24: Variation of NDVI, height, temperature, ambient temperature and humidity of plot #14.30 during summer 2019



**G5. Analyzing the growth of the plot #16.2 (Selected randomly from PR-RST Extra genotype)**



*Figure G- 25: Plot #16.2 on June 26, 2019 (Seedling Status)*



*Figure G- 26: Plot #16.2 on July 11, 2019 (Start of Flowering Status)*





*Figure G- 27: Plot #16.2 on July 31, 2019 (End of Flowering Status)*



*Figure G- 28: Plot #16.2 on August 15, 2019 (Start of Maturity Status)*





*Figure G- 29: Plot #16.2 on August 28, 2019 (End of Maturity Status)*

## G5.1. Summary of captured data for plot # 16.2 during summer 2019

*Table G- 5: Variation of NDVI, height, temperature, ambient temperature and humidity of plot #16.2 during summer 2019*

Stage	Date	NDVI		Height (cm)		Temp(C°)		Ambient Temp (C°) Ref: Platform's weather station		Ambient Humidity (%) Ref: Platform's weather station	
		*	**	*	**	*	**	*	**	*	**
1 <sup>st</sup>	26 June, 2019	0.48	0.48	-	-	31.32	31.80	25.77	25.70	34.34	34.34
2 <sup>nd</sup>	11 July, 2019	0.74	0.73	33.48	32.63	23.56	28.61	21.74	21.72	64.17	64.30
3 <sup>rd</sup>	13 July, 2019	0.60	0.53	99.30	99.30	24.56	24.56	24.56	24.56	62.38	62.38
4 <sup>th</sup>	15 August, 2019	0.68	0.67	82.38	82.19	25.78	25.87	24.41	24.40	49.41	49.47
5 <sup>th</sup>	28 August, 2019	0.66	0.66	72.55	69.02	20.56	20.65	19.59	19.59	57.64	57.69

\*: Without edge effect

\*\*: With edge effect

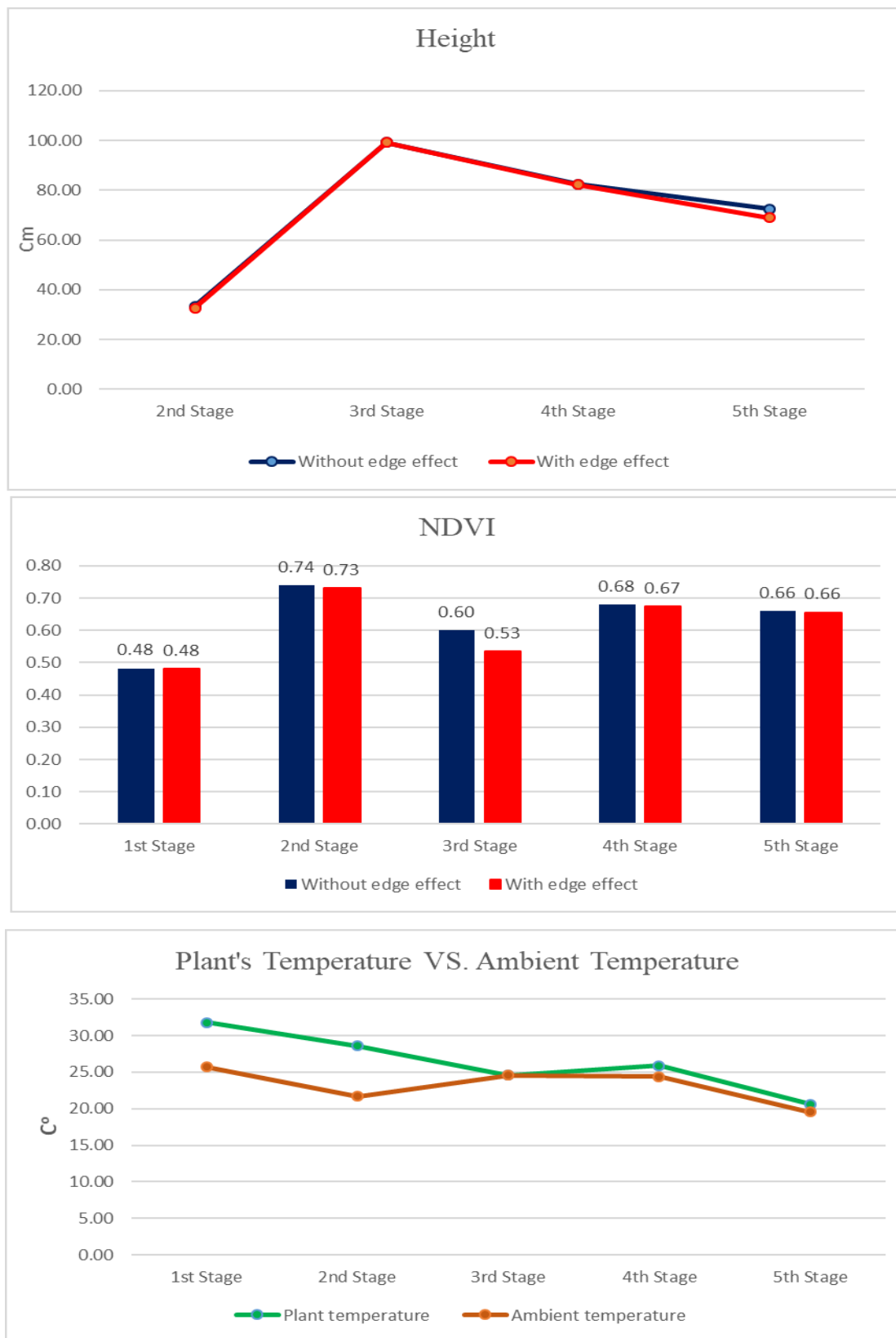


Figure G- 30: Variation of NDVI, height, temperature, ambient temperature and humidity of plot #16.2 during summer



**G6. Analyzing the growth of the plot #18.18 (Selected randomly from IM-RST genotype)**



*Figure G- 31: Plot #18.18 on June 26, 2019 (Seedling Status)*



*Figure G- 32: Plot #18.18 on July 11, 2019 (Start of Flowering Status)*





*Figure G- 33: Plot #18.18 on July 31, 2019 (End of Flowering Status)*



*Figure G- 34: Plot #18.18 on August 15, 2019 (Start of Maturity Status)*





*Figure G- 35: Plot #18.18 on August 28, 2019 (End of Maturity Status)*

## G6.1. Summary of captured data for plot # 16.2 during summer 2019

*Table G- 6: Variation of NDVI, height, temperature, ambient temperature and humidity of plot #18.18 during summer 2019*

Stage	Date	NDVI		Height (cm)		Temp(C°)		Ambient Temp (C°) Ref: Platform's weather station		Ambient Humidity (%) Ref: Platform's weather station	
		*	**	*	**	*	**	*	**	*	**
1 <sup>st</sup>	26 June, 2019	0.45	0.45	-	-	33.54	33.50	26.47	26.40	33.14	33.14
2 <sup>nd</sup>	11 July, 2019	0.74	0.74	36.04	36.04	25.74	25.30	21.77	21.77	60.34	60.35
3 <sup>rd</sup>	13 July, 2019	0.64	0.64	106.02	105.56	22.99	23.05	23.95	23.94	61.56	62.08
4 <sup>th</sup>	15 August, 2019	0.70	0.71	80.45	80.59	24.68	24.61	24.34	24.34	49.27	49.24
5 <sup>th</sup>	28 August, 2019	0.65	0.65	74.55	74.55	21.17	21.17	20.19	20.19	57.05	57.05

\*: Without edge effect

\*\*: With edge effect

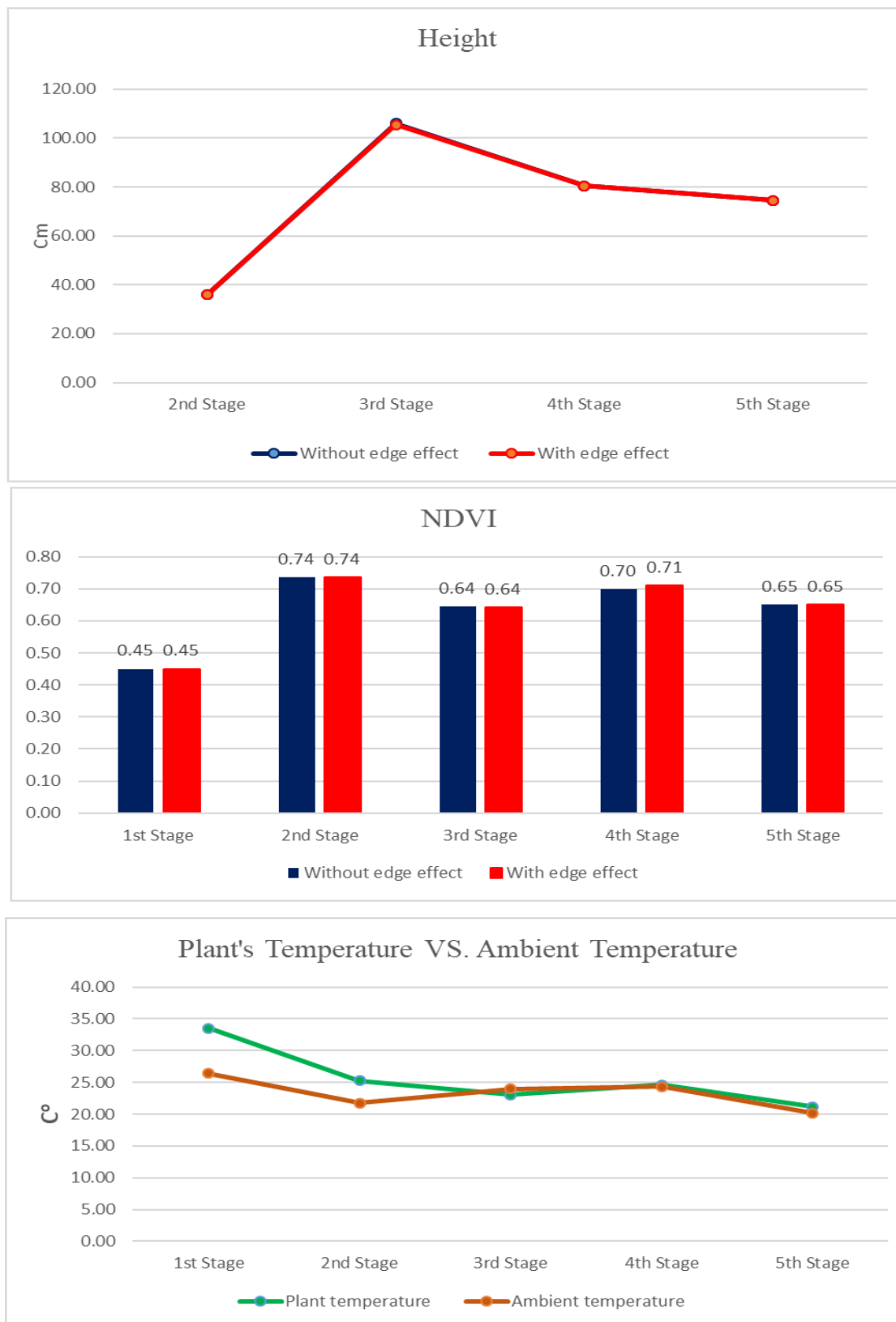


Figure G- 36: Variation of NDVI, height, temperature, ambient temperature and humidity of plot #18.18 during summer 2019



## APPENDIX H- Analyzing growth of wheat plots over summer 2018

This section provides obtained results from the collected data over summer 2018 and use of Pheno-VISDM2 for 6 different plots with diverse genotype.

### H1. Analyzing growth of the plot #108 (Selected randomly from genotype 18)



*Figure H- 1: Plot #108 on July 13, 2018 (Flowering Status)*



*Figure H- 2: Plot #108 on July 26, 2018 (End of Flowering Status)*





*Figure H- 3: Plot #108 on August 9, 2018 (Before Maturity Status)*

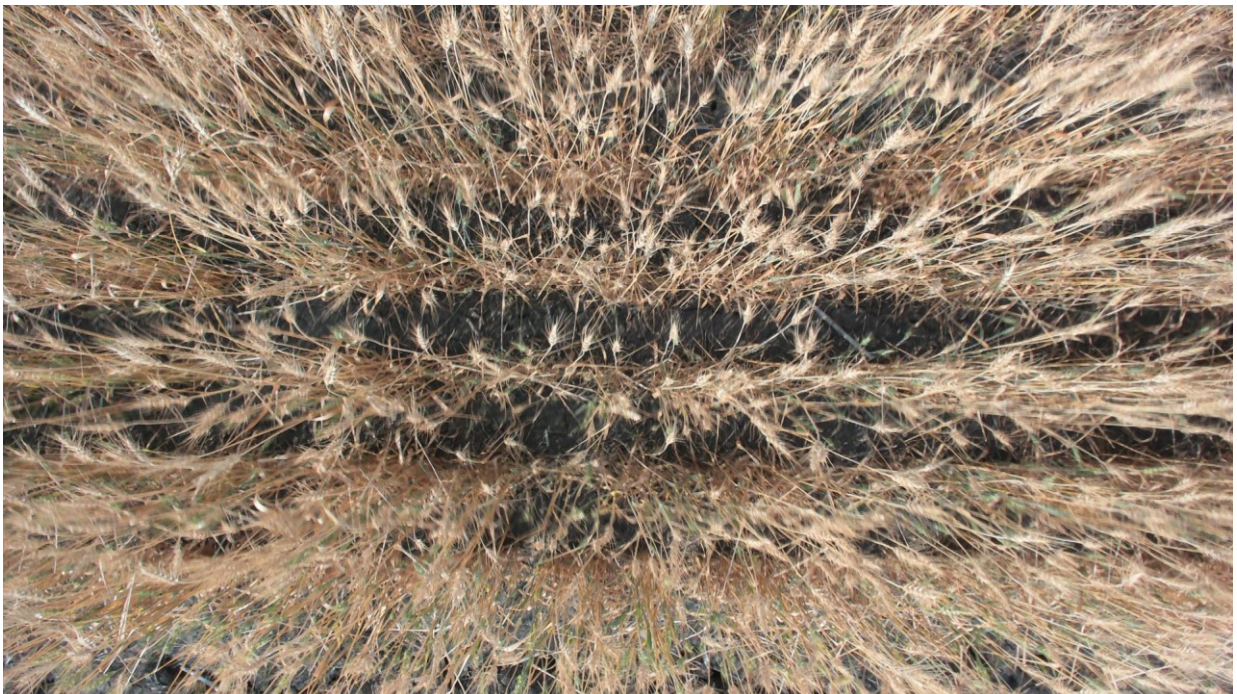


*Figure H- 4: Plot #108 on August 23, 2018 (Before Harvest Status)*



## H1.1. Summary of captured data for plot # 108 during summer 2018

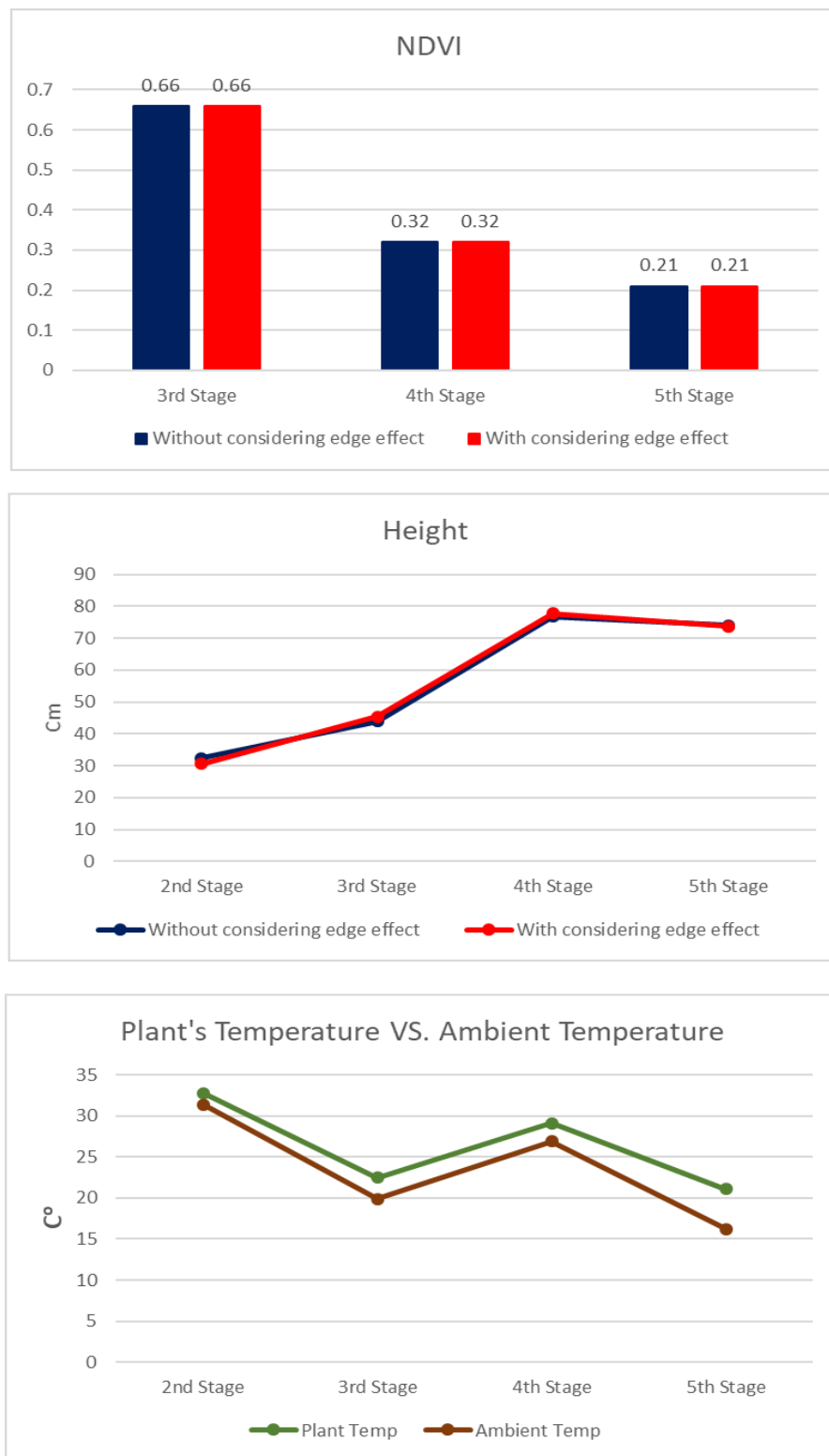


Figure H- 5: Variation of NDVI, height, temperature, ambient temperature and humidity of plot #108 during summer of 2018

*Table H- 1: Variation of NDVI, height, temperature, ambient temperature and humidity of plot #108 during summer of 2018*

Stage	Date	NDVI		Height (cm)		Temp(C°)		Ambient Temp (C°) Ref: Platform's weather station		Ambient Humidity (%) Ref: Platform's weather station	
		*	**	*	**	*	**	*	**	*	**
2 <sup>nd</sup>	June 13, 2018	-	-	32.3	30.6	32.7	32.8	31.4	31.4	56.1	56.2
3 <sup>rd</sup>	July 26, 2018	0.66	0.66	43.9	45.4	22.2	22.5	19.9	19.9	47.2	47.2
4 <sup>th</sup>	August 9, 2018	0.32	0.32	76.7	77.7	29.0	29.1	26.9	26.9	42.5	42.5
5 <sup>th</sup>	August 23, 2018	0.21	0.21	74.0	73.7	20.9	21.1	16.2	16.2	62.1	62.1

\*: Without edge effect

\*\*: With edge effect

## H2. Analyzing growth of the plot #112 (Selected randomly from genotype 8)



*Figure H- 6: Plot #112 on July 13, 2018 (Flowering Status)*





*Figure H- 7: Plot #112 on July 26, 2018 (End of Flowering Status)*



*Figure H- 8: Plot #112 on August 9, 2018 (Before Maturity Status)*





*Figure H- 9: Plot #112 on August 2018 (Before Harvest Status)*

## H2.1. Summary of captured data for plot # 112 during summer 2018

*Table H- 2: Variation of NDVI, height, temperature, ambient temperature and humidity of plot #112 during summer of 2018*

Stage	Date	NDVI		Height (cm)		Temp(C°)		Ambient Temp (C°) Ref: Platform's weather station		Ambient Humidity (%) Ref: Platform's weather station	
		*	**	*	**	*	**	*	**	*	**
2 <sup>nd</sup>	June 13, 2018	-	-	28.5	23.7	33.2	33.3	31.4	31.4	54.7	54.7
3 <sup>rd</sup>	July 26, 2018	0.58	0.57	51.8	54.9	22.4	22.9	19.9	19.9	48.6	48.4
4 <sup>th</sup>	August 9, 2018	0.36	0.37	76.4	76.8	29.1	29.9	26.9	26.9	41.4	41.5
5 <sup>th</sup>	August 23, 2018	0.17	0.17	70.7	72.0	21.5	21.7	16.1	16.1	62.4	62.4

\*: Without edge effect

\*\*: With edge effect



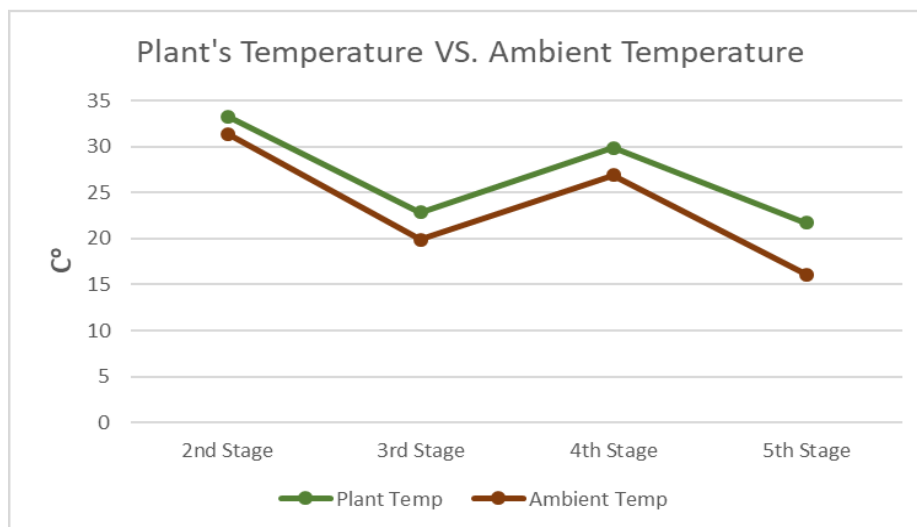
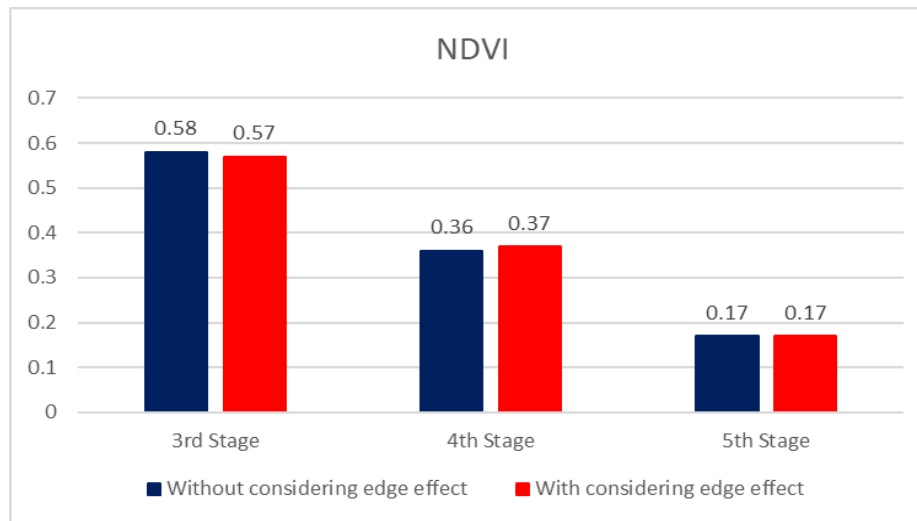


Figure H- 10: Variation of NDVI, height, temperature, ambient temperature and humidity of plot #112 during summer of 2018

### H3. Analyzing growth of the plot #175 (Selected randomly from genotype 45)



*Figure H- 11: Plot #175 on July 13, 2018 (Flowering Status)*



*Figure H- 12: Plot #175 on July 26, 2018 (End of Flowering Status)*





*Figure H- 13: Plot #175 on August 9, 2018 (Before Maturity Status)*

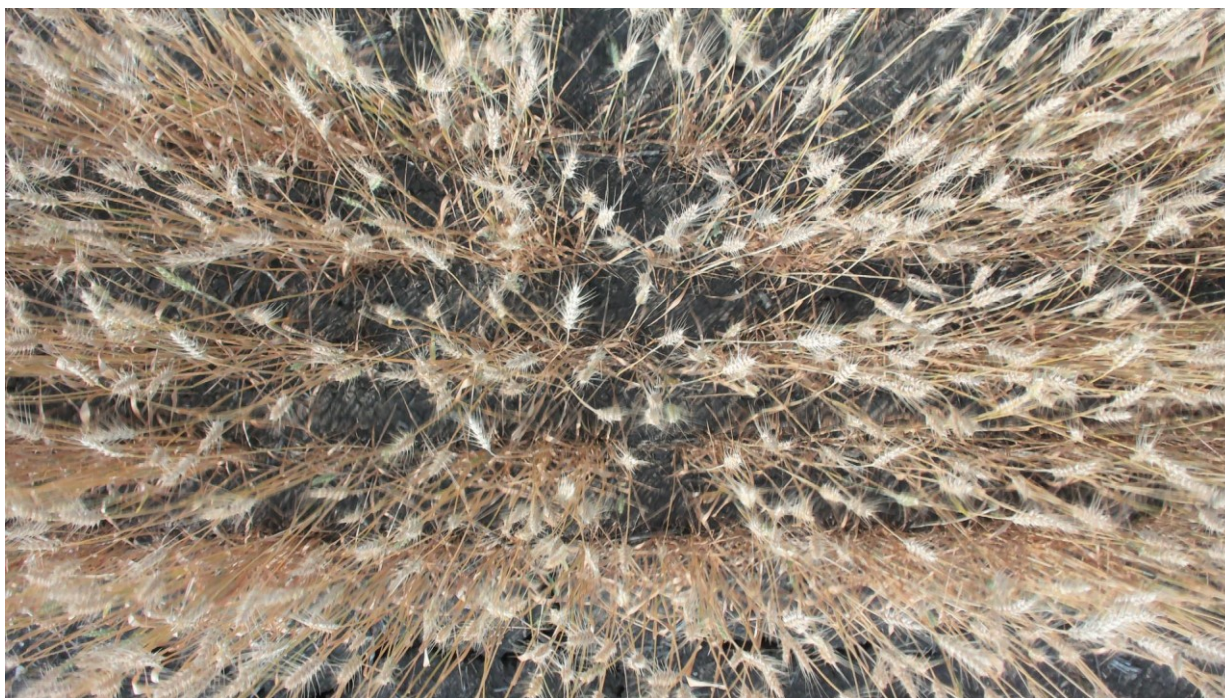


*Figure H- 14: Plot #175 on August 23, 2018 (Before Harvest Status)*

### H3.1. Summary of captured data for plot # 175 during summer 2018

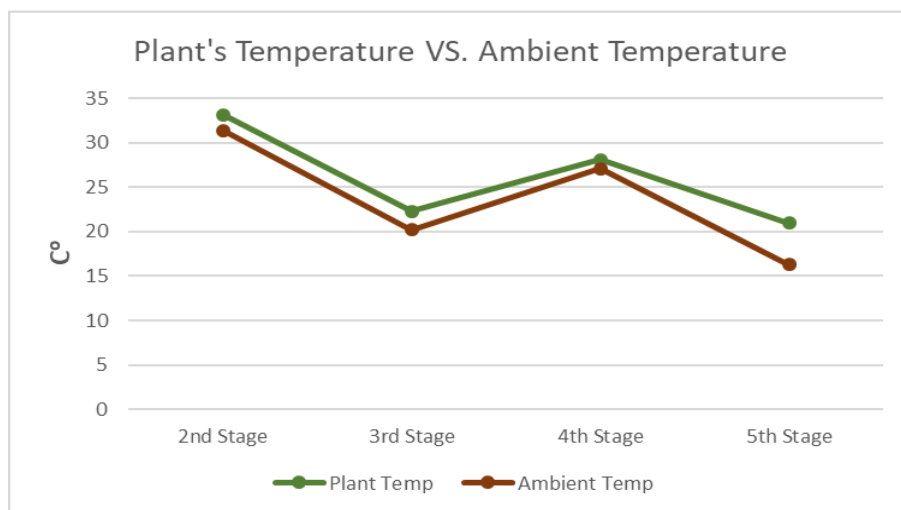
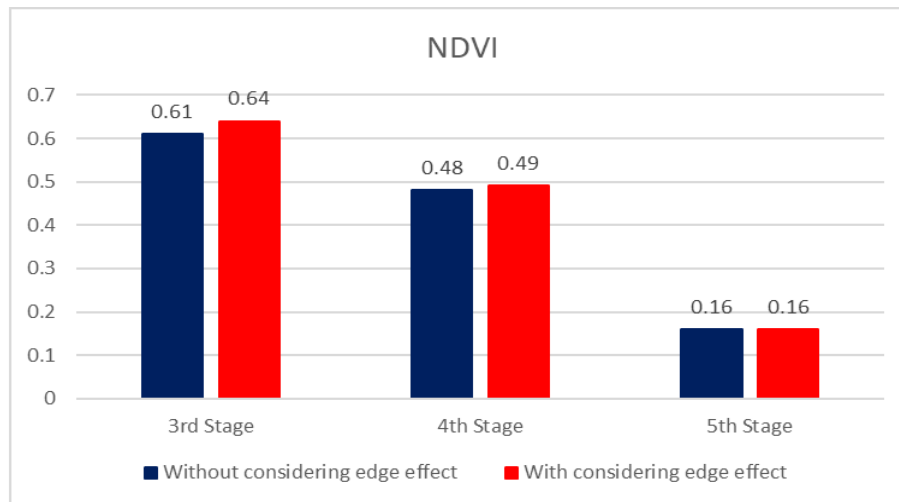




Figure H- 15: Variation of NDVI, height, temperature, ambient temperature and humidity of plot #175 during summer of 2018

Table H- 3: Variation of NDVI, height, temperature, ambient temperature and humidity of plot #175 during summer of 2018

Stage	Date	NDVI		Height (cm)		Temp(C°)		Ambient Temp (C°) Ref: Platform's weather station		Ambient Humidity (%) Ref: Platform's weather station	
		*	**	*	**	*	**	*	**	*	**
2 <sup>nd</sup>	June 13, 2018	-	-	29.9	28.1	32.9	33.2	31.4	31.4	54.4	54.4
3 <sup>rd</sup>	July 26, 2018	0.61	0.64	48.5	45.4	22.3	22.3	20.2	20.2	50.3	50.2
4 <sup>th</sup>	August 9, 2018	0.48	0.49	75.5	75.6	28.1	28.1	27.1	27.1	41.5	41.6
5 <sup>th</sup>	August 23, 2018	0.16	0.16	77.2	77.6	21.0	21.0	16.3	16.3	61.2	61.2

\*: Without edge effect

\*\* : With edge effect

#### H4. Analyzing growth of the plot #260 (Selected randomly from genotype 31)



Figure H- 16: Plot #260 on July 13, 2018 (Flowering Status)





*Figure H- 17: Plot #260 on July 26, 2018 (End of Flowering Status)*



*Figure H- 18: Plot #260 on August 9, 2018 (Before Maturity Status)*





*Figure H- 19: Plot #260 on August 23, 2018 (Before Harvest Status)*

#### H4.1. Summary of captured data for plot # 260 during summer 2018

*Table H- 4: Variation of NDVI, height, temperature, ambient temperature and humidity of plot #260 during summer of 2018*

Stage	Date	NDVI		Height (cm)		Temp(C°)		Ambient Temp (C°) Ref: Platform's weather station		Ambient Humidity (%) Ref: Platform's weather station	
		*	**	*	**	*	**	*	**	*	**
2 <sup>nd</sup>	June 13, 2018	-	-	35.1	33.3	30.9	30.9	31.2	31.2	56.2	56.4
3 <sup>rd</sup>	July 26, 2018	0.67	0.65	62.2	63.6	22.6	22.7	20.4	20.4	48.5	48.4
4 <sup>th</sup>	August 9, 2018	0.37	0.39	78.8	81.3	28.4	28.4	27.2	27.2	41.8	41.9
5 <sup>th</sup>	August 23, 2018	0.16	0.16	78.9	79.8	20.9	20.9	15.9	16.1	63.4	63.6

\*: Without edge effect

\*\*: With edge effect

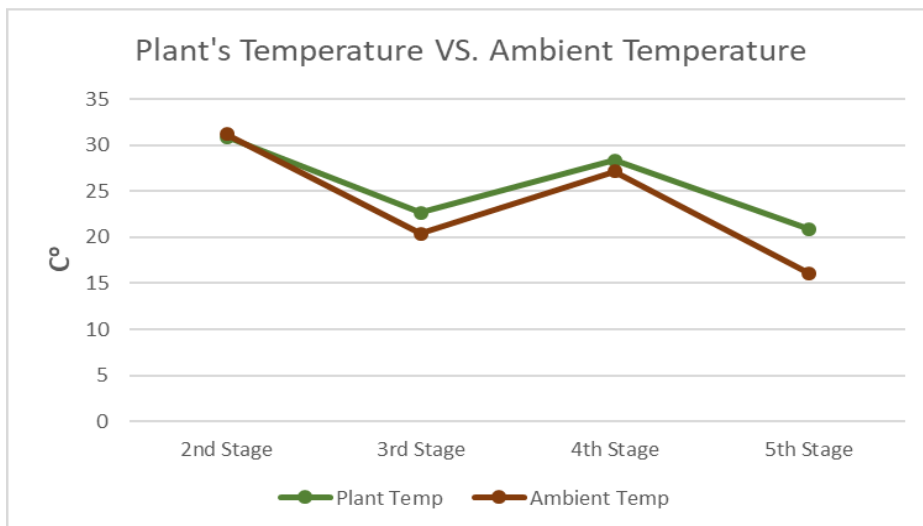
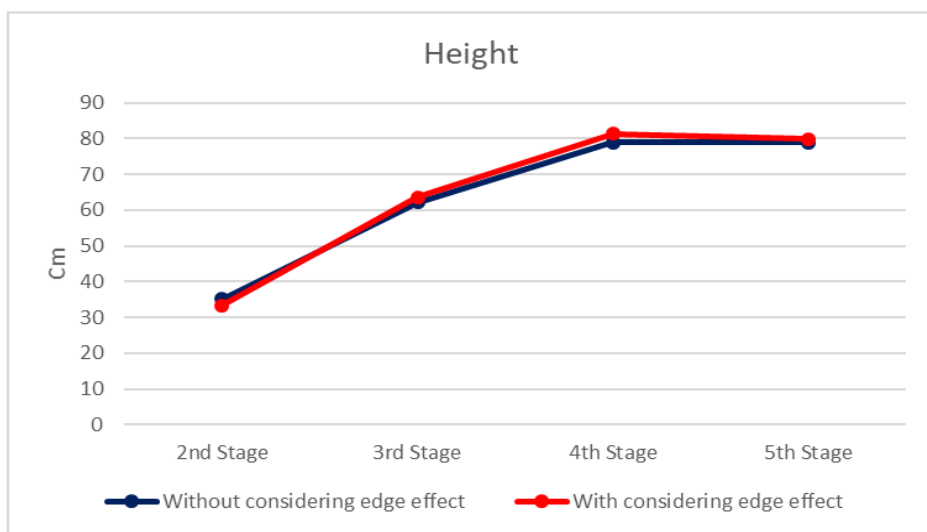
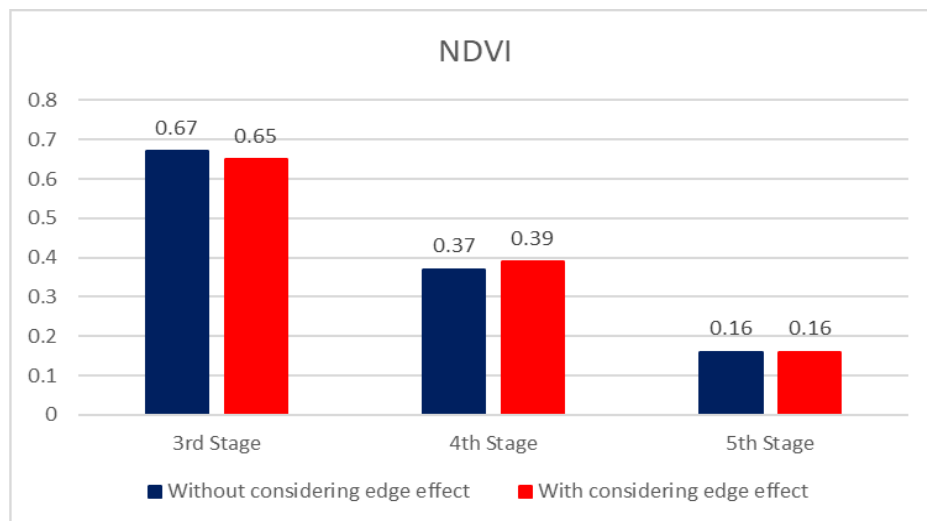


Figure H- 20: Variation of NDVI, height, temperature, ambient temperature and humidity of plot #260 during summer of 2018



## H5. Analyzing growth of the plot #333 (Selected randomly from genotype 51)



*Figure H- 21: Plot #333 on July 13, 2018 (Flowering Status)*

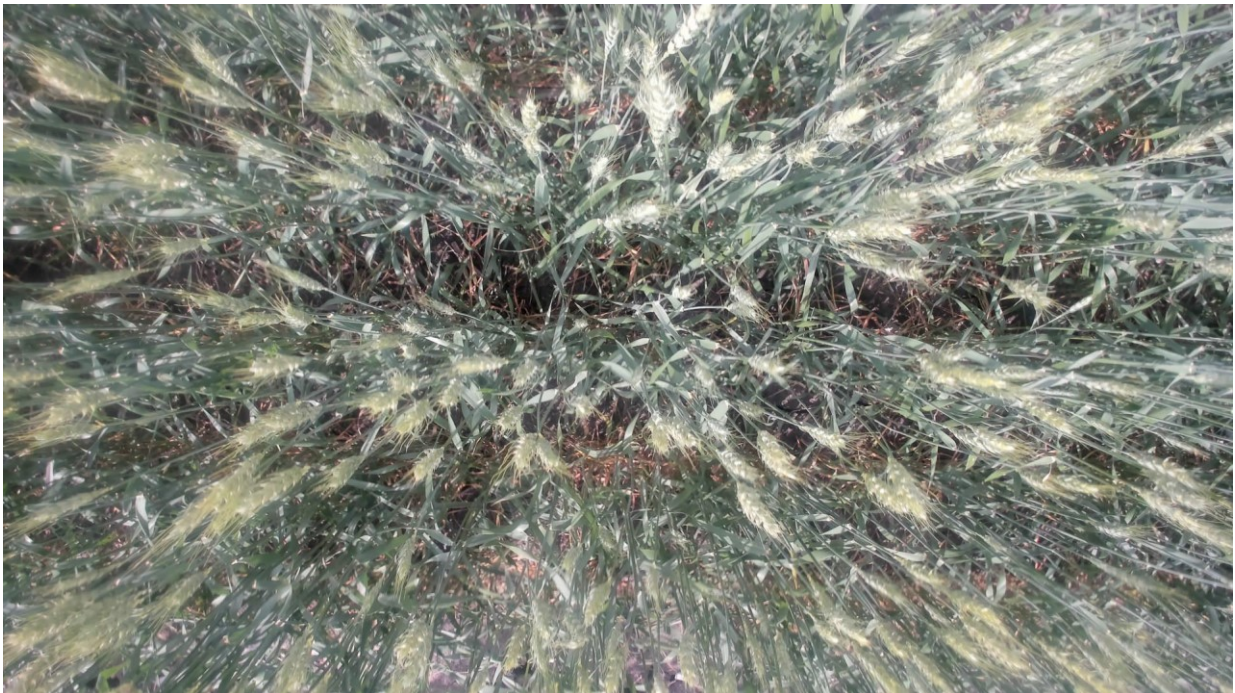


*Figure H- 22: Plot #333 on July 26, 2018 (End of Flowering Status)*



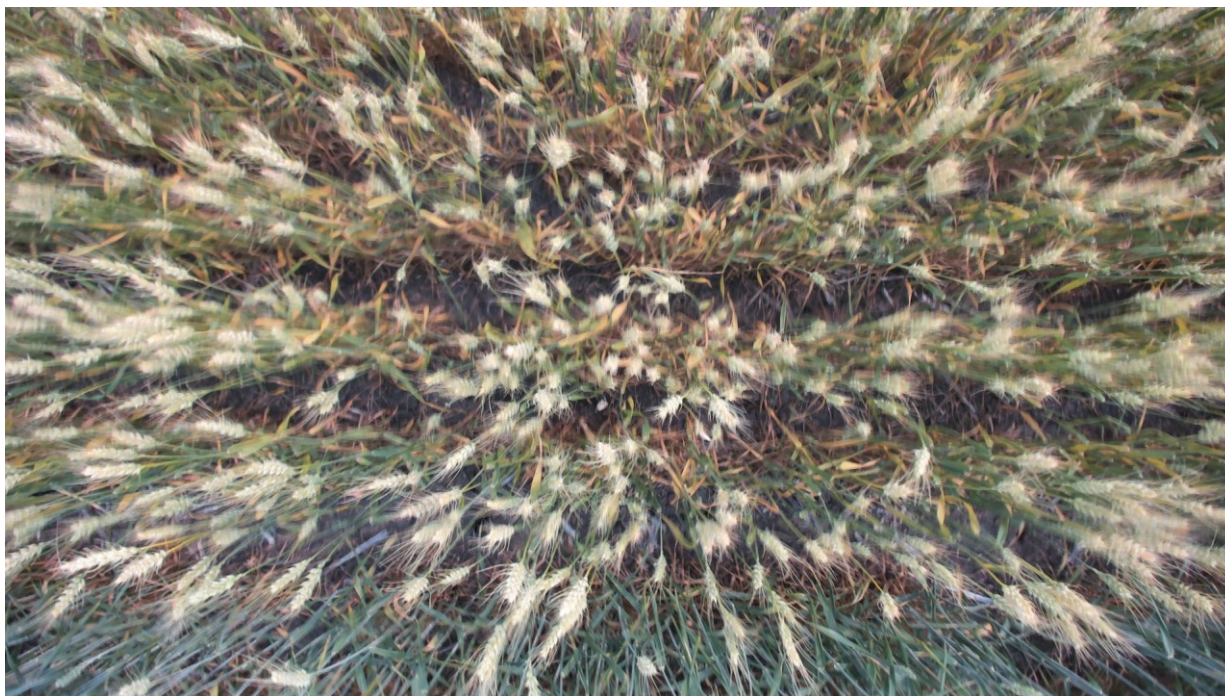


*Figure H- 23: Plot #333 on August 9, 2018 (Before Maturity Status)*



*Figure H- 24: Plot #333 on August 23, 2018 (Before Harvest Status)*

## H5. Summary of captured data for plot # 333 during summer 2018

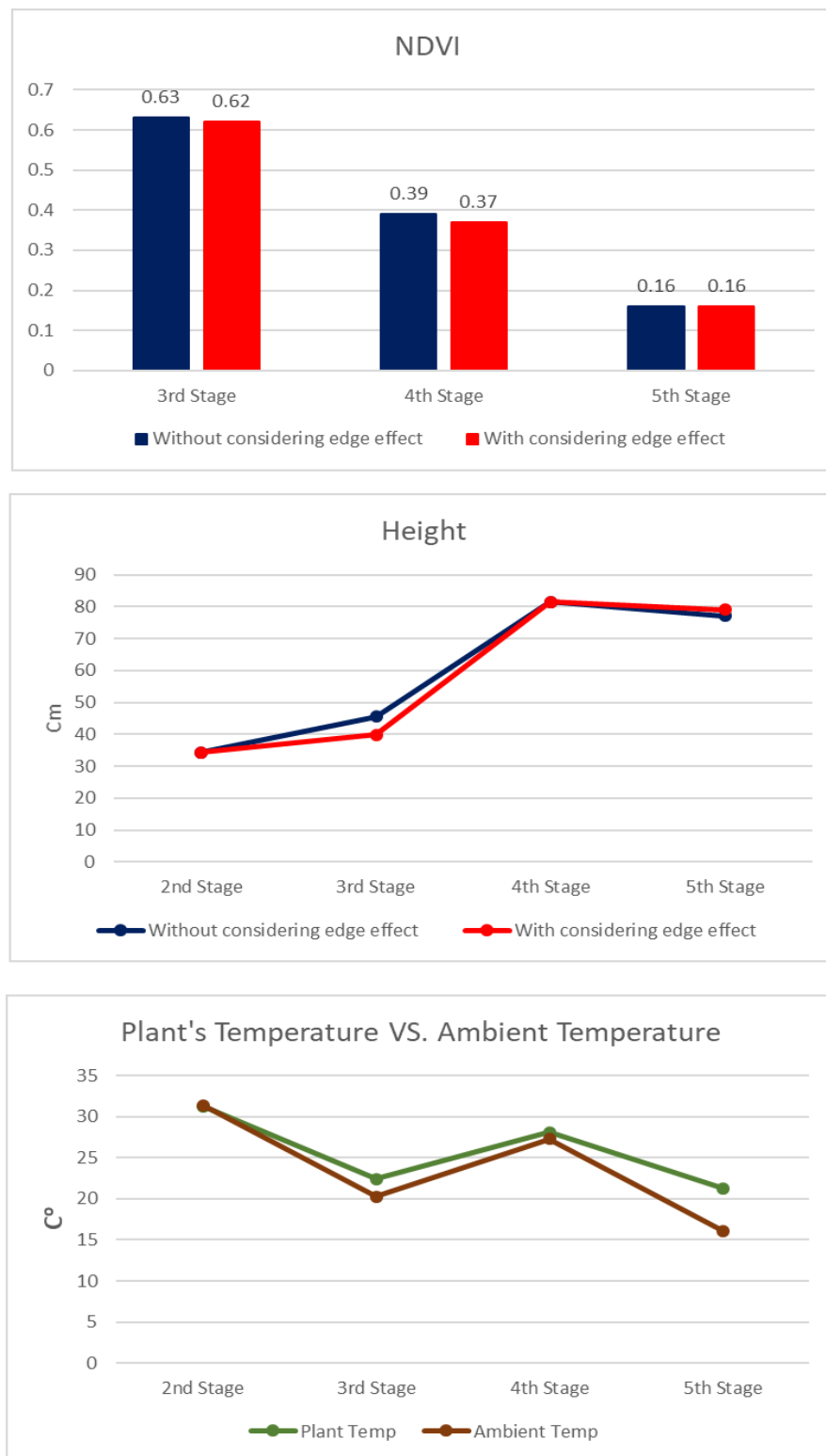


Figure H- 25: Variation of NDVI, height, temperature, ambient temperature and humidity of plot #333 during summer of 2018



Table H- 5: Variation of NDVI, height, temperature, ambient temperature and humidity of plot #333 during summer of 2018

Stage	Date	NDVI		Height (cm)		Temp(C°)		Ambient Temp (C°) Ref: Platform's weather station		Ambient Humidity (%) Ref: Platform's weather station	
		*	**	*	**	*	**	*	**	*	**
2 <sup>nd</sup>	June 13, 2018	-	-	34.3	34.3	31.2	31.3	31.4	31.4	54.3	54.1
3 <sup>rd</sup>	July 26, 2018	0.63	0.62	45.5	39.9	22.3	22.4	20.4	20.3	46.8	46.9
4 <sup>th</sup>	August 9, 2018	0.39	0.37	81.4	81.4	27.9	28.1	27.3	27.3	41.3	41.3
5 <sup>th</sup>	August 23, 2018	0.16	0.16	77.1	79.1	21.3	21.3	16.1	16.1	62.1	62.0

\*: Without edge effect

\*\*: With edge effect

## H6. Analyzing growth of the plot #373 (Selected randomly from genotype 72)

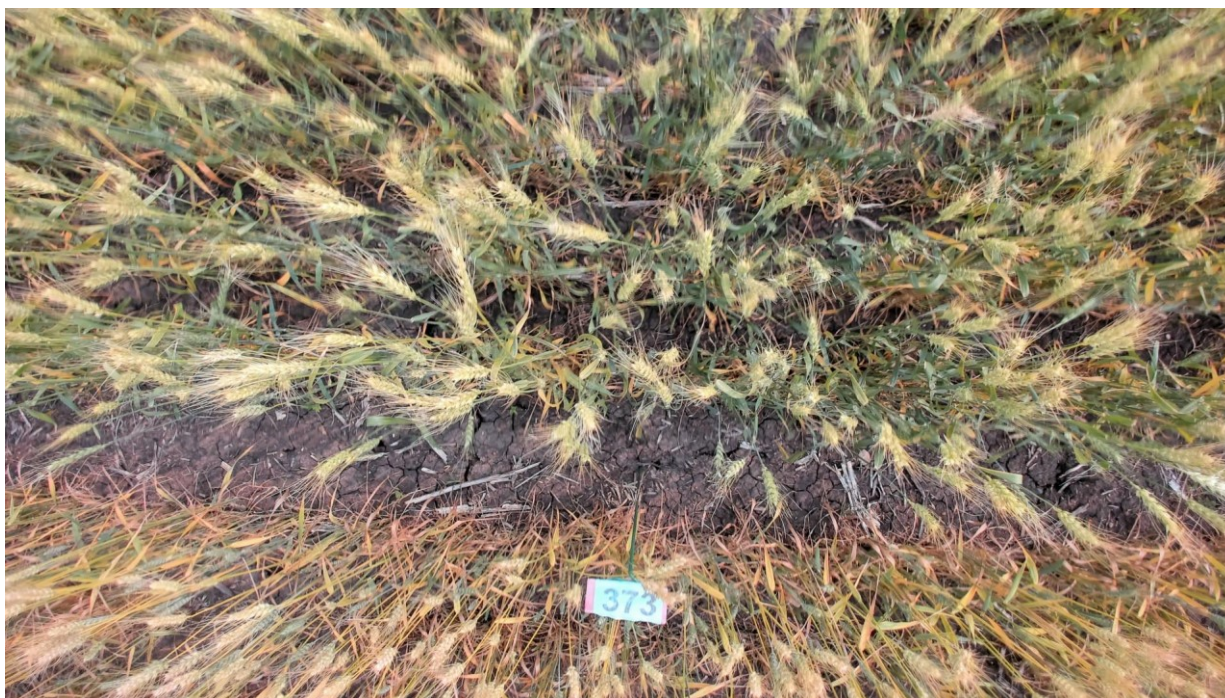


Figure H- 26: Plot #373 on July 13, 2018 (Flowering Status)





*Figure H- 27: Plot #373 on July 26, 2018 (End of Flowering Status)*



*Figure H- 28: Plot #373 on August 9, 2018 (Before Maturity Status)*





Figure H- 29: Plot #373 on August 23, 2018 (Before Harvest Status)

## H6.1. Summary of captured data for plot # 373 during summer 2018

Table H- 6: Variation of NDVI, height, temperature, ambient temperature and humidity of plot #373 during summer of 2018

Stage	Date	NDVI		Height (cm)		Temp(C°)		Ambient Temp (C°) Ref: Platform's weather station		Ambient Humidity (%) Ref: Platform's weather station	
		*	**	*	**	*	**	*	**	*	**
2 <sup>nd</sup>	June 13, 2018	-	-	36.0	35.3	32.6	32.8	31.4	31.4	52.0	52.0
3 <sup>rd</sup>	July 26, 2018	0.63	0.64	54.5	47.7	25.1	25.4	20.4	20.4	48.6	48.5
4 <sup>th</sup>	August 9, 2018	0.45	0.45	73.7	69.8	29.2	29.3	27.3	27.3	41.7	41.6
5 <sup>th</sup>	August 23, 2018	0.16	0.16	77.1	79.1	21.3	21.3	16.1	16.1	62.1	62.0

\*: Without edge effect

\*\*: With edge effect

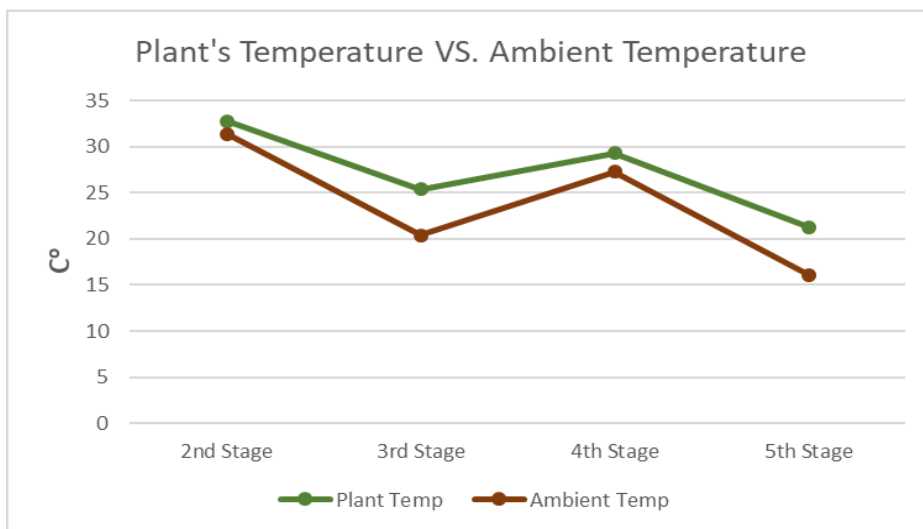
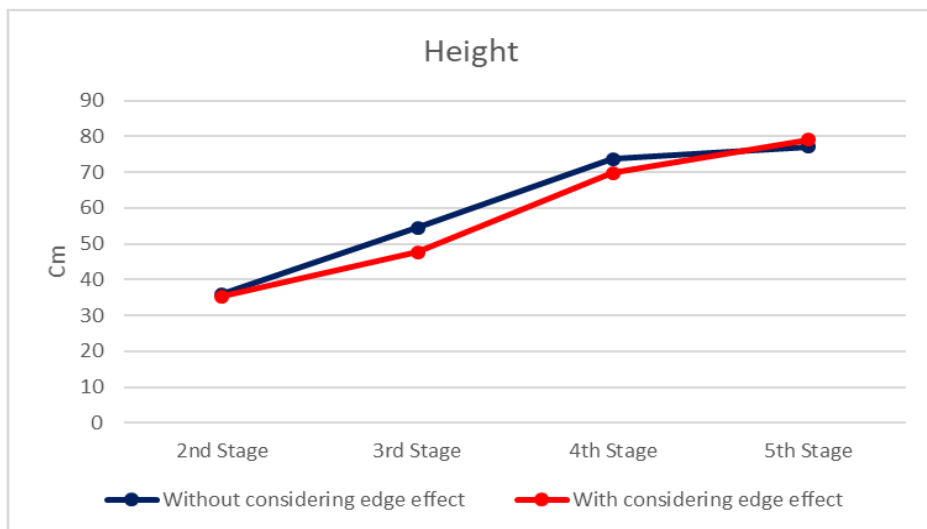
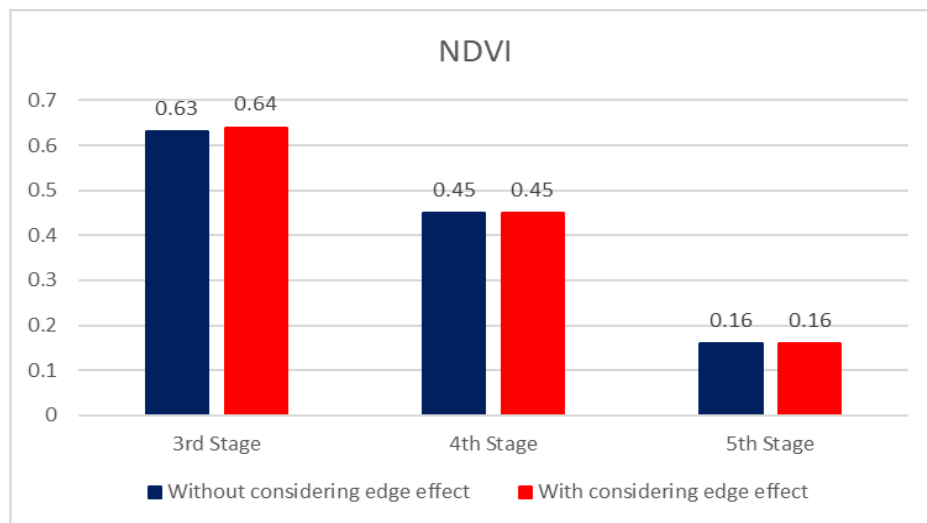


Figure H- 30: Variation of NDVI, height, temperature, ambient temperature and humidity of plot #373 during summer of 2018



## APPENDIX I- Analyzing growth of wheat plots over summer 2019

This section provides obtained results from the collected data over summer 2019 and use of Pheno-VISDM3 for 6 different plots with diverse genotype.

### I1. Analyzing growth of the plot #104 (Selected randomly from genotype 44)



*Figure I- 1: Plot #104 on July 23, 2019 (Flowering Status)*



*Figure I- 2: Plot #104 on August 1, 2019 (End of Flowering Status)*





*Figure I- 3: Plot #104 on August 20, 2019 (Before Maturity)*



*Figure I- 4: Plot #104 on September 17, 2019 (Before Harvest Status)*

## I1.1. Summary of captured data for plot # 104 during summer 2019

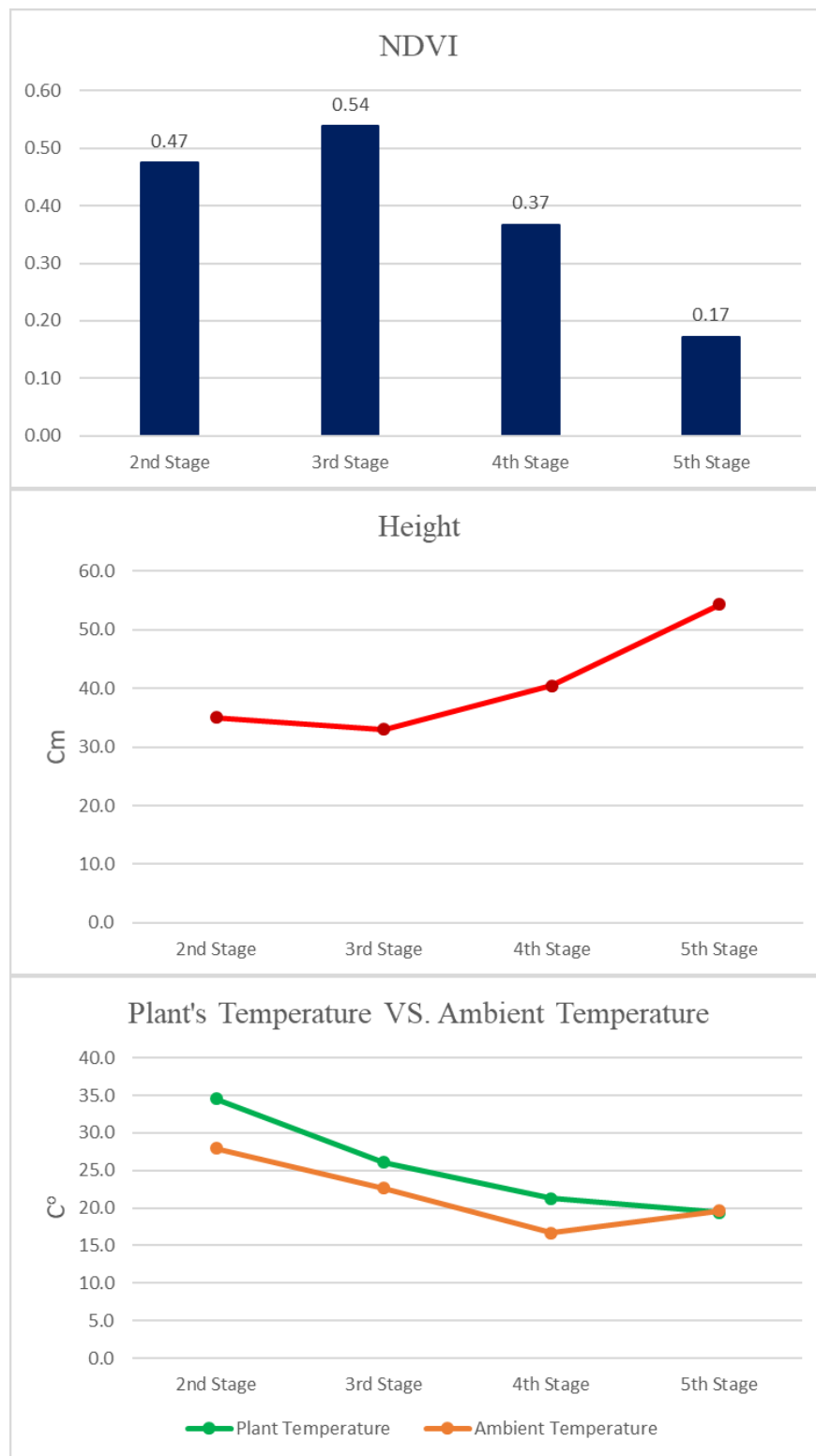


Figure I- 5: Variation of NDVI, height, temperature, ambient temperature and humidity of plot #104 during summer of 2019



*Table I- 1: Variation of NDVI, height, temperature, ambient temperature and humidity of plot #104 during summer of 2019*

Stage	Date	NDVI	Height (cm)	Temp p(C°)	Ambient Temp (C°) Ref: Platform's weather station	Ambient Humidity (%) Ref: Platform's weather station
2 <sup>nd</sup>	July 23, 2019	0.47	35.1	34.5	27.9	57.5
3 <sup>rd</sup>	August 1, 2019	0.54	33.0	26.0	22.6	73.5
4 <sup>th</sup>	August 20, 2019	0.37	40.4	21.3	16.6	54.8
5 <sup>th</sup>	September 17, 2019	0.17	54.3	19.4	19.6	66.2

## **I2. Analyzing growth of the plot #169 (Selected randomly from genotype 63)**



*Figure I- 6: Plot #169 on July 23, 2019 (Flowering Status)*





*Figure I- 7: Plot #169 on August 1, 2019 (End of Flowering Status)*



*Figure I- 8: Plot #169 on August 20, 2019 (Before Maturity)*





*Figure I- 9: Plot #169 on September 17, 2019 (Before Harvest Status)*

## I2.1. Summary of captured data for plot # 169 during summer 2019

*Table I- 2: Variation of NDVI, height, temperature, ambient temperature and humidity of plot #169 during summer of 2019*

Stage	Date	NDVI	Height (cm)	Temp (C°)	Ambient Temp (C°) Ref: Platform's weather station	Ambient Humidity (%) Ref: Platform's weather station
2 <sup>nd</sup>	July 23, 2019	0.73	46.4	28.6	28.0	55.8
3 <sup>rd</sup>	August 1, 2019	0.72	51.3	23.6	22.7	73.4
4 <sup>th</sup>	August 20, 2019	0.50	63.6	18.1	17.0	51.6
5 <sup>th</sup>	September 17, 2019	0.15	68.8	18.4	19.3	67.5

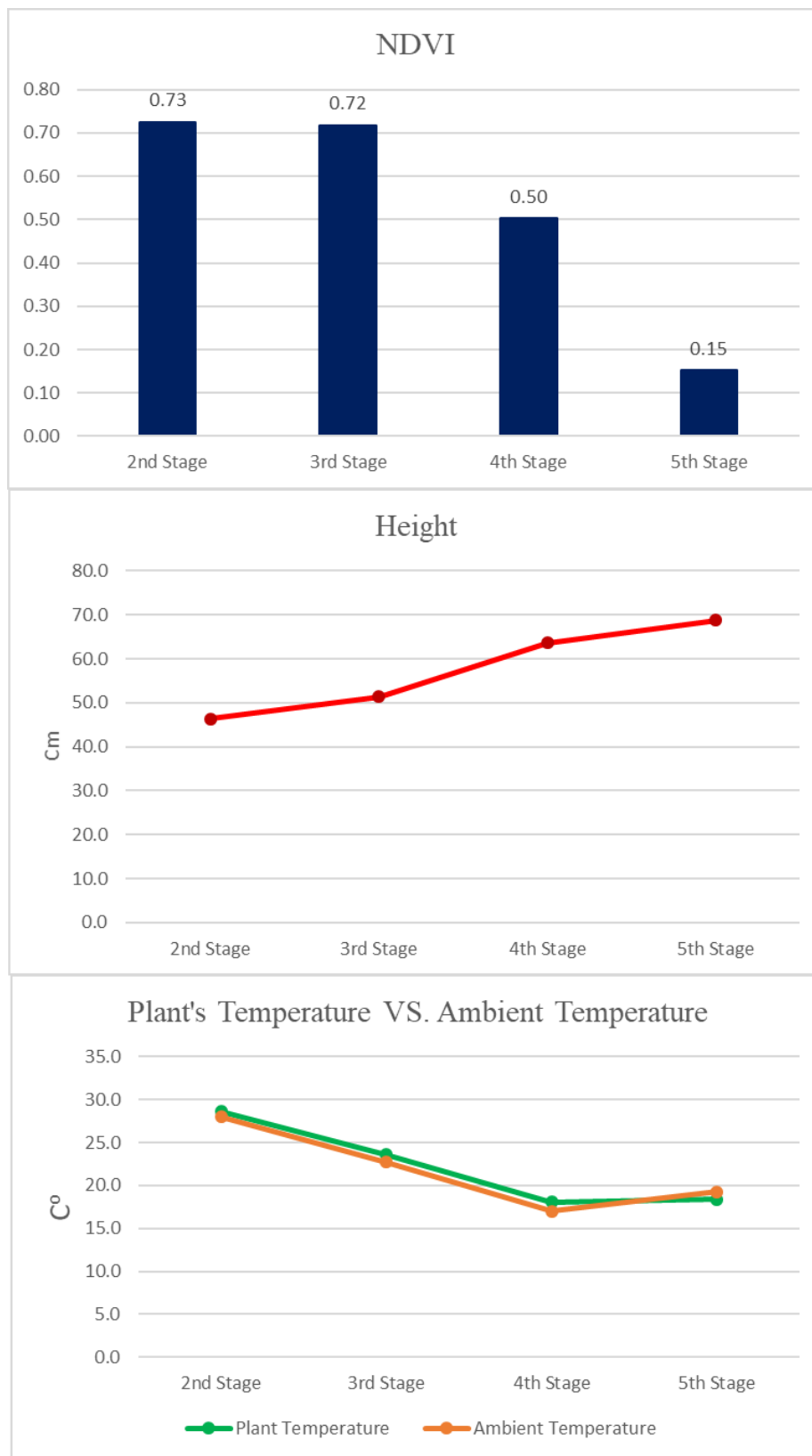


Figure I- 10: Variation of NDVI, height, temperature, ambient temperature and humidity of plot #169 during summer of 2019



### **I3. Analyzing growth of the plot #225 (Selected randomly from genotype 81)**



*Figure I- 11: Plot #225 on July 23, 2019 (Flowering Status)*



*Figure I- 12: Plot #225 on August 1, 2019 (End of Flowering Status)*





*Figure I- 13: Plot #225 on August 20, 2019 (Before Maturity)*



*Figure I- 14: Plot #225 on September 17, 2019 (Before Harvest Status)*



### I3.1. Summary of captured data for plot # 225 during summer 2019

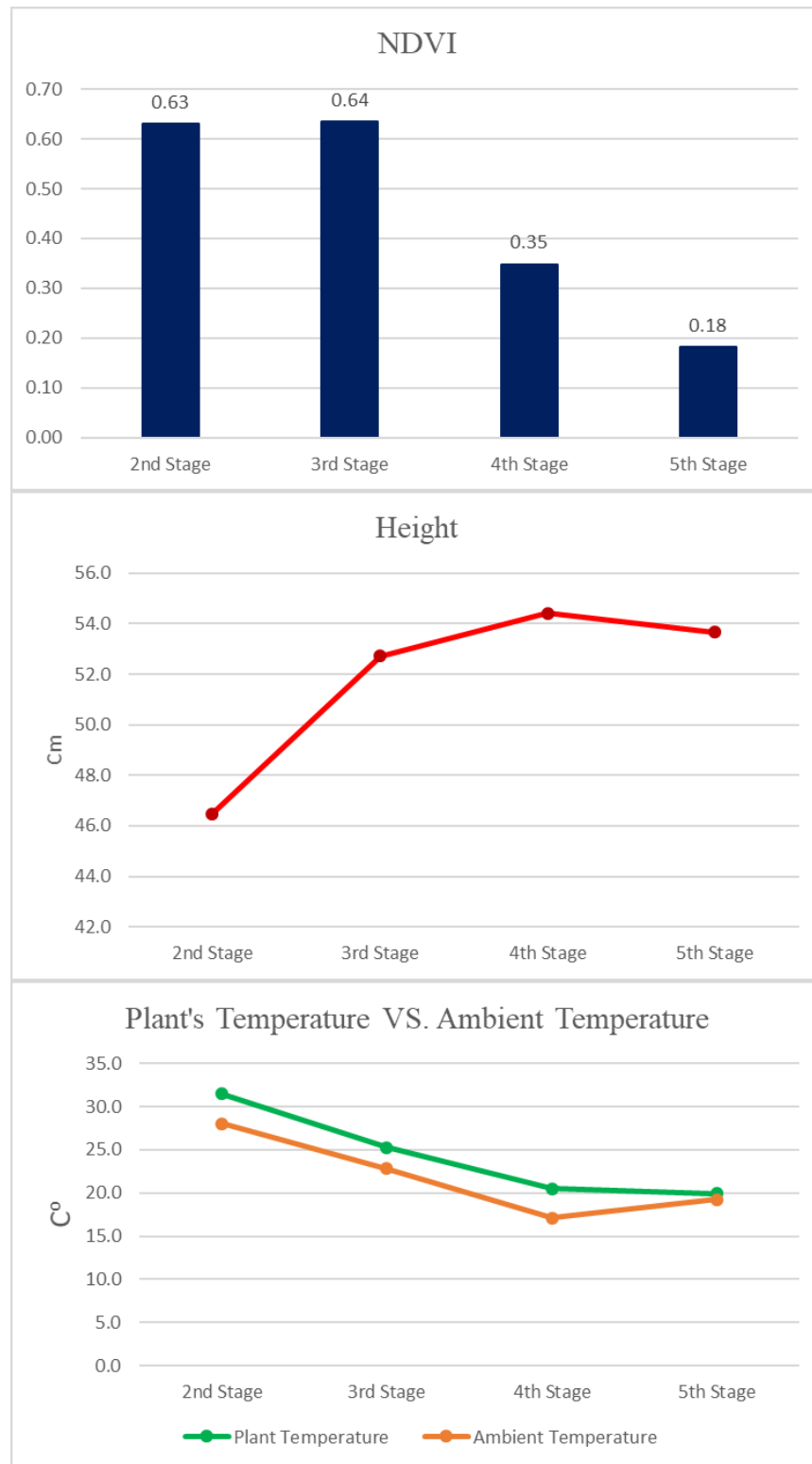


Figure I- 15: Variation of NDVI, height, temperature, ambient temperature and humidity of plot #225 during summer of 2019

*Table I- 3: Variation of NDVI, height, temperature, ambient temperature and humidity of plot #225 during summer of 2019*

Stage	Date	NDVI	Height (cm)	Temp p(C°)	Ambient Temp (C°) Ref: Platform's weather station	Ambient Humidity (%) Ref: Platform's weather station
2 <sup>nd</sup>	July 23, 2019	0.63	46.5	31.5	28.0	53.9
3 <sup>rd</sup>	August 1, 2019	0.64	52.7	25.3	22.8	75.1
4 <sup>th</sup>	August 20, 2019	0.35	54.4	20.5	17.1	52.3
5 <sup>th</sup>	September 17, 2019	0.18	53.7	19.9	19.2	67.3

#### **I4. Analyzing growth of the plot #264 (Selected randomly from genotype 11)**



*Figure I- 16: Plot #264 on July 23, 2019 (Flowering Status)*





*Figure I- 17: Plot #264 on August 1, 2019 (End of Flowering Status)*



*Figure I- 18: Plot #264 on August 20, 2019 (Before Maturity)*





*Figure I- 19: Plot #264 on September 17, 2019 (Before Harvest Status)*

## **I4.1. Summary of captured data for plot # 264 during summer 2019**

*Table I- 4: Variation of NDVI, height, temperature, ambient temperature and humidity of plot #264 during summer of 2019*

<b>Stage</b>	<b>Date</b>	<b>NDVI</b>	<b>Height (cm)</b>	<b>Temp p(C°)</b>	<b>Ambient Temp (C°) Ref: Platform's weather station</b>	<b>Ambient Humidity (%) Ref: Platform's weather station</b>
2 <sup>nd</sup>	July 23, 2019	0.59	42.5	31.5	28.1	52.6
3 <sup>rd</sup>	August 1, 2019	0.66	52.3	25.0	23.0	73.7
4 <sup>th</sup>	August 20, 2019	0.43	54.2	20.1	17.2	49.6
5 <sup>th</sup>	September 17, 2019	0.18	55.4	22.1	19.7	65.7



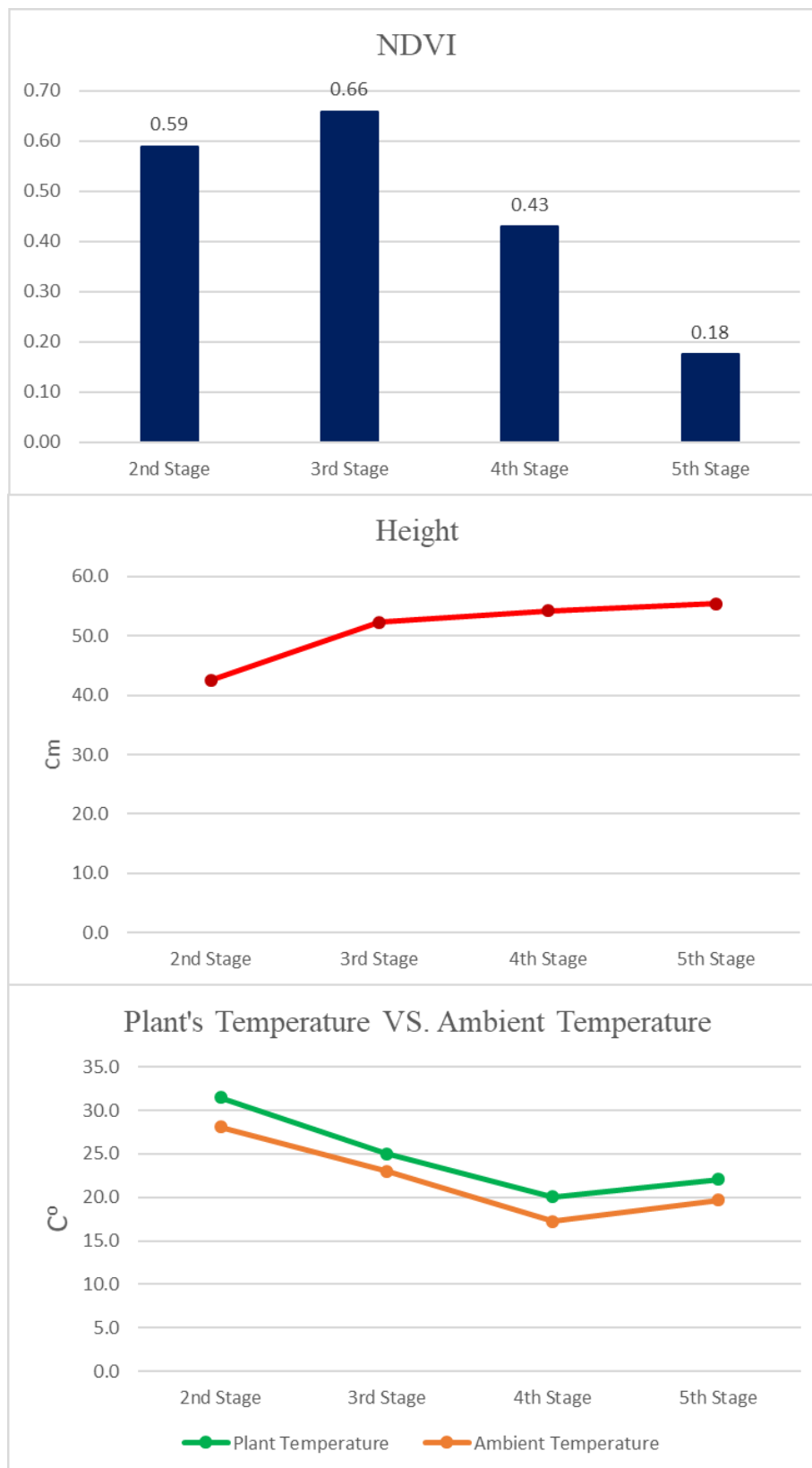


Figure I- 20: Variation of NDVI, height, temperature, ambient temperature and humidity of plot #264 during summer of 2019

**I5. Analyzing growth of the plot #321 (Selected randomly from genotype 27)**



*Figure I- 21: Plot #321 on July 23, 2019 (Flowering Status)*



*Figure I- 22: Plot #321 on August 1, 2019 (End of Flowering Status)*





*Figure I- 23: Plot #321 on August 20, 2019 (Before Maturity)*



*Figure I- 24: Plot #321 on September 17, 2019 (Before Harvest Status)*

## I5. Summary of captured data for plot # 325 during summer 2019

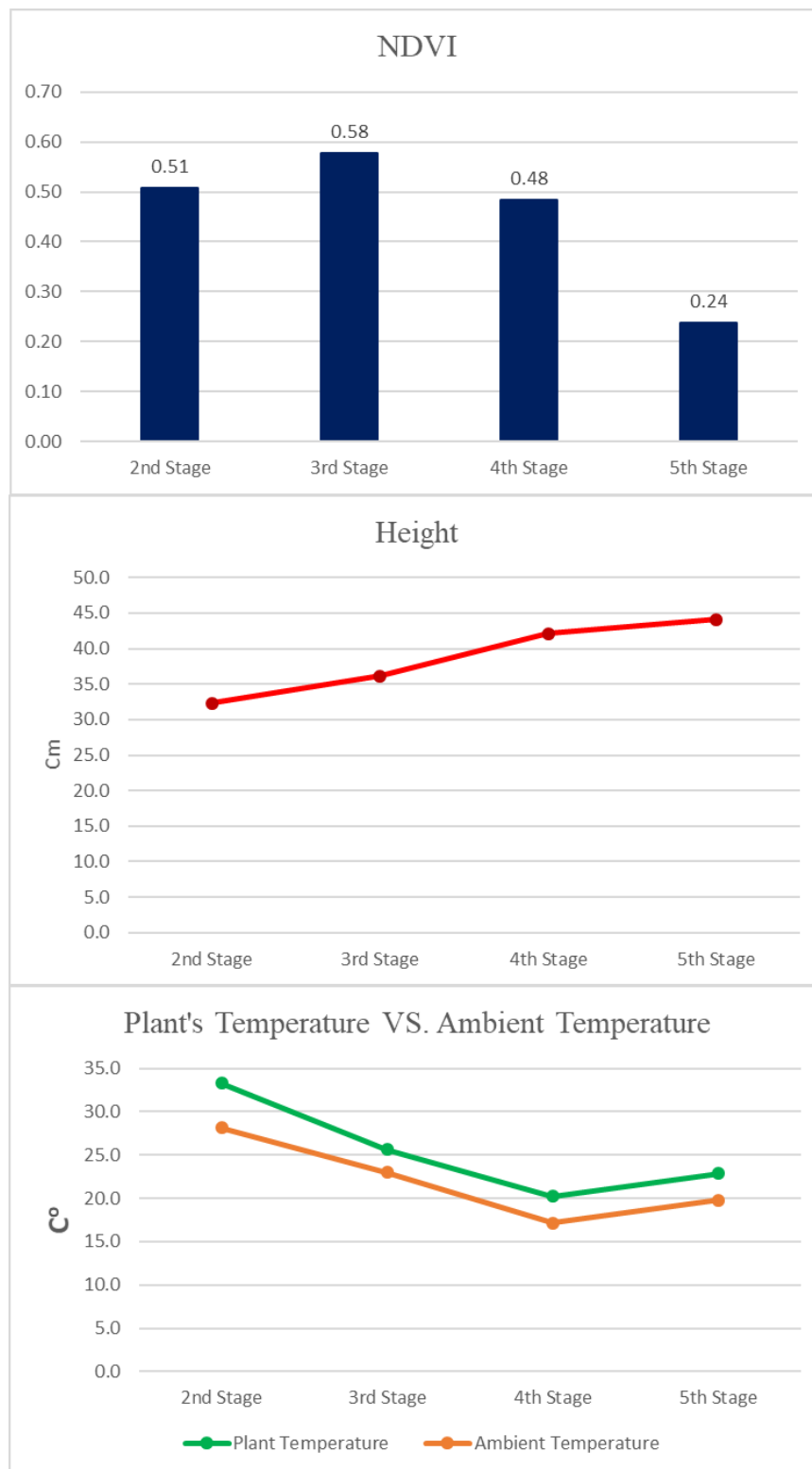


Figure I- 25: Variation of NDVI, height, temperature, ambient temperature and humidity of plot #321 during summer of 2019



*Table I- 5: Variation of NDVI, height, temperature, ambient temperature and humidity of plot #321 during summer of 2019*

Stage	Date	NDVI	Height (cm)	Temp p(C°)	Ambient Temp (C°) Ref: Platform's weather station	Ambient Humidity (%) Ref: Platform's weather station
2 <sup>nd</sup>	July 23, 2019	0.51	32.3	33.3	28.1	54.7
3 <sup>rd</sup>	August 1, 2019	0.58	36.1	25.6	23.0	73.4
4 <sup>th</sup>	August 20, 2019	0.48	42.1	20.2	17.2	51.8
5 <sup>th</sup>	September 17, 2019	0.24	44.1	22.9	19.8	66.1

## **I6. Analyzing growth of the plot #376 (Selected randomly from genotype 3)**



*Figure I- 26: Plot #376 on July 23, 2019 (Flowering Status)*





*Figure I- 27: Plot #376 on August 1, 2019 (End of Flowering Status)*



*Figure I- 28: Plot #376 on August 20, 2019 (Before Maturity)*





*Figure I- 29: Plot #376 on September 17, 2019 (Before Harvest Status)*

## I6.1. Summary of captured data for plot # 376 during summer 2019

*Table I- 6: Variation of NDVI, height, temperature, ambient temperature and humidity of plot #376 during summer of 2019*

Stage	Date	NDVI	Height (cm)	Temp p(C°)	Ambient Temp (C°) Ref: Platform's weather station	Ambient Humidity (%) Ref: Platform's weather station
2 <sup>nd</sup>	July 23, 2019	0.54	33.2	32.7	28.2	54.2
3 <sup>rd</sup>	August 1, 2019	0.61	42.5	24.3	23.0	71.5
4 <sup>th</sup>	August 20, 2019	0.50	50.6	20.5	17.0	53.0
5 <sup>th</sup>	September 17, 2019	0.21	56.2	22.8	20.1	64.9

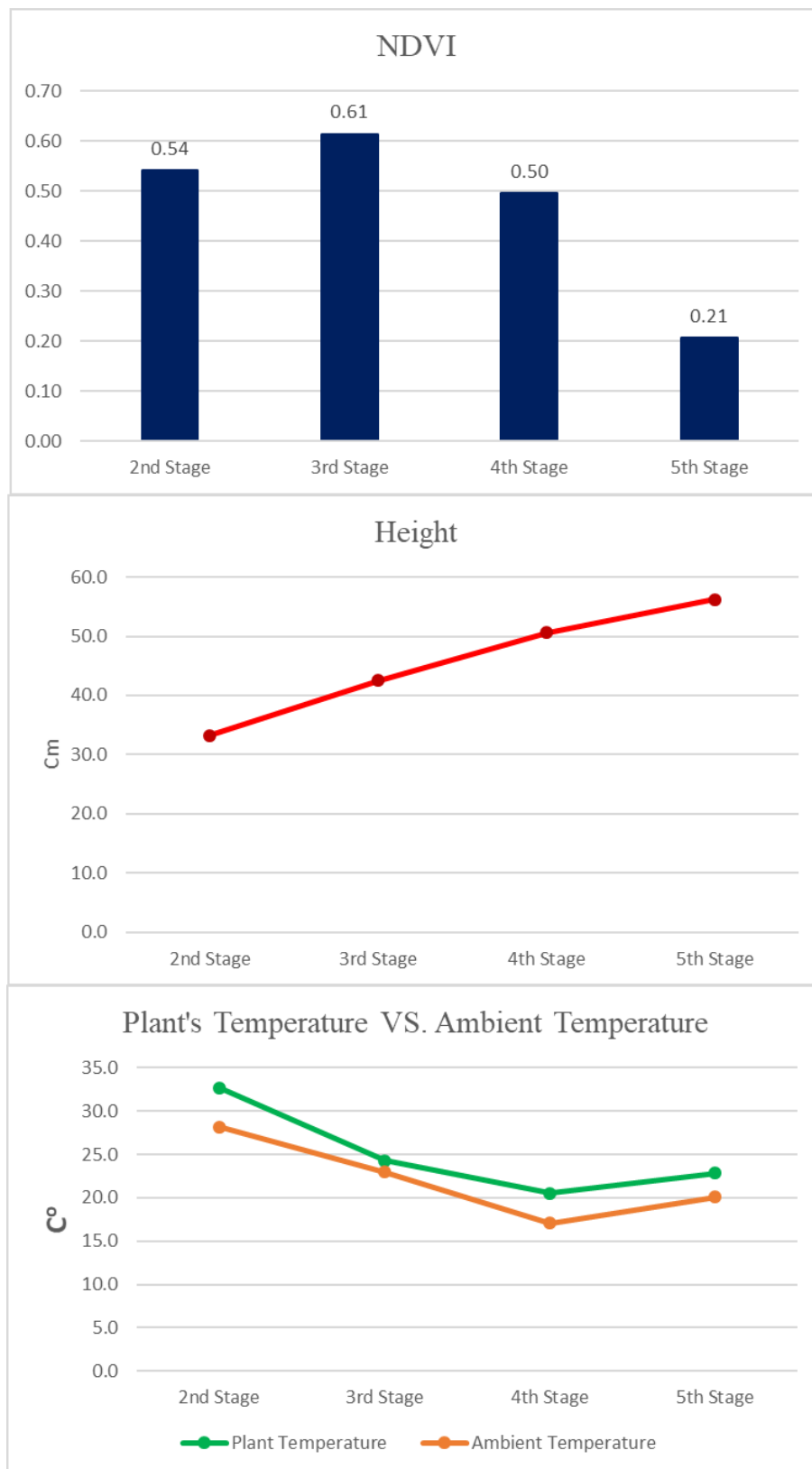


Figure I- 30: Variation of NDVI, height, temperature, ambient temperature and humidity of plot #376 during summer of 2019